UCLouvain

epl

École polytechnique de Louvain

Electromechanical device for measuring passive stiffness and viscosity of human finger

Towards a quantitative evaluation of spasticity

Author: **Donatien Doumont**

Supervisors: **Benoît Herman, Bruno Dehez**

Reader: **Gaëtan Stoquart**

Academic year 2020–2021

Master [120] in Electro-mechanical Engineering

Abstract

This master's thesis intends to design a device capable of measuring finger joint's passive stiffness and viscosity or also called passive musculo-articular stiffness (PMAS). This electromechanical device aims to generate passive oscillations to a finger's joint and measure its passive resistance at different frequencies. This device based on a method developed by Lehmann and Detrembleur allows to distinguish the passive stiffness and the viscosity from the global impedance, enabling an objective and quantified measurement of PMAS. This quantification method may provide a better understanding of neurological disorders such as spasticity and therefore provide better treatments.

This project was launched by the *Louvain Bionics* in 2019 and has already been the subject of a Master thesis in 2020. Previous works in *UCLouvain* have already been conducted to assess PMAS. Two machines were designed, one to assess the ankle joint and the other to assess the wrist joint. Some aspects of this thesis's prototype are largely inspired from the wrist device.

The thesis follows a typical design methodology. In the first step, the context is presented. This includes anatomical and biomechanical considerations of the finger, a description of spasticity and of the quantification method of PMAS, and lastly a review of similar PMAS measuring devices. In the second step, as a result of the functional requirements built in collaboration with clinicians, conceptual designs and comparative studies are produced to generate a fitted solution to the problem. The third step characterizes the prototyping step. It involves an optimized sizing of the actuation, sensory system and mechanical transmission, a complete electrical schematic and CAD on *Solidworks*, and finally, future assessments of the prototype.
Construction of the prototype has been initiated, but first assessments of the measurement's precision are yet to be established.

Abstract in french

L'intention de ce mémoire est de concevoir un dispositif capable de mesurer la raideur passive et la viscosité articulaire des doigts ou raideur passive musculo-articulaire (PMAS).

Ce dispositif électromécanique permet de générer une oscillation imposée à une articulation de doigt et d'ainsi mesurer sa résistance passive à différentes fréquence. Ce dispositif basé sur une méthode développée par Lehmann et Detrembleur permet de distinguer la raideur et la viscosité de l'impédance totale, rendant possible une mesure objective et quantifiée de la PMAS. Cette méthode de quantification pourrait fournir une meilleure compréhension de troubles neurologiques telle que la spasticité et ainsi fournir de meilleurs traitements.

Ce projet a été lancé par le *Louvain Bionics* en 2019 et fut le sujet d'un mémoire en 2020. De précédents travaux ont déjà été conduits pour évaluer la PMAS au sein de l'*UCLouvain*. Deux machines ont été conçues, la première permettant d'évaluer l'articulation de la cheville et la deuxième pour l'évaluation de l'articulation du poignet. Plusieurs aspects du prototype de ce mémoire ont été grandement inspirés par la machine poignet.

Ce mémoire suit une méthodologie typique de conception. Dans la première étape, le contexte est présenté. Cela inclut des considérations anatomiques et biomécaniques des doigts, une description de la spasticité et de la méthode de quantification Detrembleur, et enfin une revue de machines de mesure similaires permettant une évaluation de la PMAS. Dans la seconde étape, à la suite d'exigences fonctionnelles établies en collaboration avec des cliniciens, des conceptions conceptuelles et des études comparatives ont été produites pour générer une solution adaptée au problème. La troisième étape caractérise l'étape de prototypage. Elle implique un dimensionnement optimisé de l'actionnement moteur, du système de capteurs et de la transmission mécanique, une installation électrique complète et un modèle CAO sur *Solidworks*, et enfin, des perspectives futures du prototype.
La construction du prototype a été lancée, mais de premières évaluations de la mesure doivent encore être établies.

First and foremost, I would like to express my deepest gratitude to my supervisors, PhD. Benoît Herman and PhD. Bruno Dehez, for their availability, feedback and guidance throughout this year's work. This master thesis could not have been completed without their insightful advises and continuous involvement.

I also wish to express my sincere appreciation to PhD. Gaëtan Stoquart, PhD. Christine Detrembleur and PhD. student Anh Phong Nguyen from NMSK, who provided their medical expertise in order to guide my work, and to Messrs. Frank Hesbois, Thierry Daras, Vincent Musette and Antoine Bietlot for their technical support.

Finally, a thousand thanks to my girlfriend who spellchecked this manuscript, friends and family who supported and helped me from the start.
A big thanks to each of you.

Table of contents

1 Context & objectives

1.1 Anatomical and biomechanical considerations . . . 1
1.1.1 Structure of the hand's musculoskeletal system . . . 1
1.1.2 Modeling of joint articular units . . . 4
1.1.3 Mechanical joint impedance . . . 6
1.2 Spasticity . . . 10
1.2.1 Definition . . . 10
1.2.2 Spasticity's impact . . . 11
1.2.3 Qualitative and semi-quantitative evaluation . . . 12
1.2.4 Spasticity management . . . 13
1.3 Review of PMAS measuring devices . . . 14
1.4 Detrembleur's method of PMAS measurement . . . 23
1.5 Thesis objectives . . . 27

2 Conceptual design

2.1 Functional requirements . . . 29
2.2 Search for solutions . . . 34
2.2.1 Movement generation review . . . 34
2.2.2 Measurement review . . . 38
2.2.3 Morphological solutions graphs . . . 40
2.3 Comparative studies . . . 44
2.3.1 Four bar drive *versus* direct drive . . . 44
2.3.2 Kinematic comparison of finger's driving system . . . 45

3 Prototype

3.1 Kinematic consideration . . . 47
3.2 Actuation, sensing and control . . . 51
3.2.1 Motor selection . . . 51
3.2.2 Electrical installation . . . 54
3.2.3 Control connective settings . . . 57

3.3 Detailed design 59
3.3.1 Structure assembly 61
3.3.2 Electrical assembly 62
3.3.3 Motor and four bar assembly 63
3.3.4 Column sensor assembly 67
3.3.5 Finger interface assembly 70
3.4 Final Assessment 72

A Appendix : explanations
A.1 Fourier transform ii
A.2 Possible improvement of Detrembleur's method iv
A.3 Robotran analysis v
A.4 Other articles vi
A.5 Material mechanical dimensioning and properties viii

B Appendix : figures and code
B.1 Computer code xi
B.2 Additional design documents xiv
B.3 Clinical aspects xx
B.4 Wrist PMAS device xxx

C Appendix : technical doc
C.1 Drawings of machined pieces xxxii
C.2 Drawings of 3d printed pieces xxxvii
C.3 Datasheets xlviii
C.3.1 Actuator sensing and control datasheet xlix
C.3.2 Mechanical datasheet lxvii

List of Figures

1 Stages of a design. ii
2 Hand and finger bones [6]. 2
3 Lateral view of the finger tendon insertions [11]. 4
4 Frame of finger joint motion at the MCP [12]. 4
5 Model of muscle tendon unit. 5
6 Planar Couette flow [22]. 7
7 Diagram of a linear spring damper oscillator system. 8
8 The stretch reflex arc [30]. 10
9 Hammer tap illustration. 11
10 Spastic posture of the hand. 11
11 Apparatus of Wright and Johns [41] 14
12 Rack's cat EOD : Came mechanism apparatus used for a cat by [44]. 15
13 Crank rod mechanism apparatus for the human elbow joint in [45] using a free oscillation technique. 16
14 Rack's thumb EOD. 18
15 Ankle's EOD of [15]. 19
16 Side view of Unsworth's arthrograph. 19
17 Ankle's EOD of [16]. 20
18 (a) Device and (b) Results of Esteki and Mansour [49]. 21
19 Ankle's EOD of [40]. 22
20 Schematic of Detrembleur's method. 23
21 Schematic : Evaluation of the passive stiffness and viscosity after Fourier separation. 25
22 Viscous and elastic torque components at a given frequency. 26
23 Functional requirement part 1. 30
24 Functional requirement part 2. 31
25 Resistance of the mechanism and MCP finger joint. 33
26 Slider-crank mechanism kinematic representation[53]. 34
27 Slider crank deviation from pure sinewave with parameter λ. 35
28 Came morphological graph. 36
29 Four bar linkage schematic 1. 36

30 Four bar linkage schematic 2. 36
31 Encoder disk schematic of incremental and absolute encoder 38
32 Morphological graphs of binding system to finger. 42
33 Morphological graphs of the device's different configuration possibilities. 43
34 Two types of kinematic of eccentric arm. 46
35 Four bar dimension optimization 49
36 Robotran analysis : fitted sinewave 49
37 Overall kinematic diagram. 50
38 Load definition for motor selection 51
39 Speed-torque diagram. 52
40 Electrical schematic. 54
41 Diagram of the control loop applied on the motor. 55
42 Global overview of the device assembly (CAD). 60
43 Structure (CAD). 61
44 Electric level. 62
45 Robotran analysis : reaction forces at the motor bearing at maximum load. 63
46 Motor assembly section view(CAD). 64
47 Motor assembly (CAD). 66
48 Higher front view of the column assembly (CAD). 67
49 Column sensor assembly (CAD). 69
50 Eccentric arm (CAD). 70
51 Finger interface assembly (CAD). 71
52 Prototype building process. 74
53 Fourier series. ii
54 Post processing update iv
55 Wrist EOD results for two patients. iv
56 Graphical description of the multibody system (MBS) on the editor MBsysPad. . . v
57 Schematic diagram of experimental apparatus. vi
58 (a) Kuo et al.'s finger EOD. (b) Experimental data on the whole pROM. vii
59 Stress-strain diagram. ix
60 Conceptual design of the master thesis by [5] xiv
61 Planned timeline for the Master's thesis. xiv
62 Objective tree. xv
63 Optimization of the coupler bar length with 20deg amplitude peak-to-peak. xvi

64 Position transducer type and characteristics [57]. xvi
65 Illustration of torque measurement type given its location in kinematic chain. . . . xvii
66 Finger interface (CAD) : Inertial oscillating system measured by the torque meter. . xviii
67 Global prototype views (CAD) : left and right, front and back view. xix
68 Anterior view of muscles of the right wrist joint (a) Superficial view [58]. xx
69 Anterior view of muscles of the right wrist joint (b) Intermediate view [58]. . . . xxi
70 Anterior view of muscles of the right wrist joint (c) Deep view [58]. xxii
71 Posterior view of muscles of the right wrist joint (a) Superficial view in french annotations [58]. xxiii
72 Posterior view of muscles of the right wrist joint (b) Deep view in french annotations [58]. xxiv
73 Intrinsic muscles of the hand. xxv
74 Three-level connection model of muscles which links the digit motion during each finger movement [9]. xxvi
75 Modified Ashworth table [59]. xxvii
76 Modified Tardieu table [60]. xxvii
77 Forces relationships in five types of stiffness in Wright and Johns [42]. xxviii
78 Apparatus of Bäcklund and Tiselius [43]. xxviii
79 Joint capsule complex structure [61]. xxix
80 Structure of a skeletal muscle [62]. xxix
81 Wrist EOD. xxx

List of Tables

1 Pre-dimensioning data 31
2 Comparative table between four bar and direct drive solutions. 44
3 Four bar mechanism dimensions. 49
4 Characteristic and specification of the EC 45 flat 80w motor. 53
5 Characteristic and specification of the *Futek* Model TRS605 - 5Nm torque meter. 56
6 Characteristics and specification of the AHS36B-BDAC004096 absolute encoder. 56
7 Main components in the electrical circuitry. 58
8 Device's global dimensions 59

9 Material mechanical properties. viii
10 Comparative of EC motor *Maxon*. xiv

Nomenclature

Mathematical symbol

η	Viscosity	$[\mathrm{Nm.(rad/s)^{-1}}]$
κ	Passive stiffness	$[\mathrm{Nm.rad^{-1}}]$
I	Inertia	$[\mathrm{g.cm^2}]$
ϵ	Strain	[m]

Abbreviation

ADC	Analog-to-digital converter
CE	Contractile element
CLC	Capsule-ligament complex
CNS	Central nervous system
DC	Direct current
DIP	Distal interphalangeal joint
DoF	Degree of freedom
EC	Electronic commutation
EMG	Electromyography
EOD	Electromechanical oscillation device
FPGA	Field programming gate array
FS	Full scale *or* span
FT	Fourier transform
MCP	Metacarpophalangeal joint
MSK	Musculoskeletal system
MTU	Muscle-Tendon Unit
PE	Parallel element
PIP	Proximal interphalangeal joint
PMAS	Passive musculo-articular stiffness
pROM	passive range of motion
PWM	Pulse-width modulation
RMS	Root mean square
SE	Series element
SRA	Stretch reflex activity
SSI	Serial synchronous interface
SSI	Synchronous serial interface
UMN	Upper motor neuron

Introduction

SPASTICITY affects 12 million people around the world. Three-quarters of the multiple sclerosis patient population suffers from spasticity and 30% to 80% of post stroke patients have disabling spasticity [1],[2]. A recent epidemiology forecast reports that the total prevalence of spastic patient cases will increase in the next ten years [3]. This shows the importance of studying this condition.
Without a careful, precise and personalized evaluation, the spacticity can not be considered as properly treated. If qualitative evaluations are commonly used, they displayed lack of precision and subjective factors in their measurements. In this regard, the famous Lord Kelvin once declared : *"When you can measure what you are speaking about, and express it in numbers, you know something about it... when you cannot express it in numbers, your knowledge is of a meager and unsatisfactory kind"*. If this judgement is rather extreme, it highlights the fundamental objectives of measuring instruments.

It is in this context that the *Louvain Bionics* financed and launched a multi-disciplinary project aiming to study the effectiveness of shock wave therapy on fingers flexor muscles.
The *Louvain Bionics* is a research center created in 2014, promoting collaborative research thanks to close interconnections with *UCLouvain*'s hospital network and technological plateforms. The latter involves the *CREDEM* plateform which is a part of the institute of mechanics, material and civil engineering (*IMMC*) of *UCLouvain* and the *openHub* plateform.

This master thesis is involved in the first step of this project i.e. the design and manufacturing of an electromechanical device capable of assessing passive stiffness and viscosity of the human finger. Multiple other works in *UCLouvain* were conducted in previous years, including an ankle device in 1998 and a wrist device in 2017 designed by Christine Detrem-

bleur and Benoît Herman (see Fig. 19 and Fig. 81). In the continuity of this, two Master thesis were conducted by Amandine Apamon and then, by Jordan Corbisier [4],[5]. The subject of this Master thesis aims to finish the drafted conceptual design and produce a valid prototyping solution. Depending on the conceptual design outcomes, the device could mimic some aspects of the wrist PMAS device created in *UCLouvain*.

The methodology followed is a standard rationalized method to design a solution for a given problem. It sometimes requires to rethink some concepts, adapt the design or to be improved by iterative procedures at any time in the process. Hence, the manuscript is not chronologically written. The global pattern used for the design can be modeled as Fig. 1.

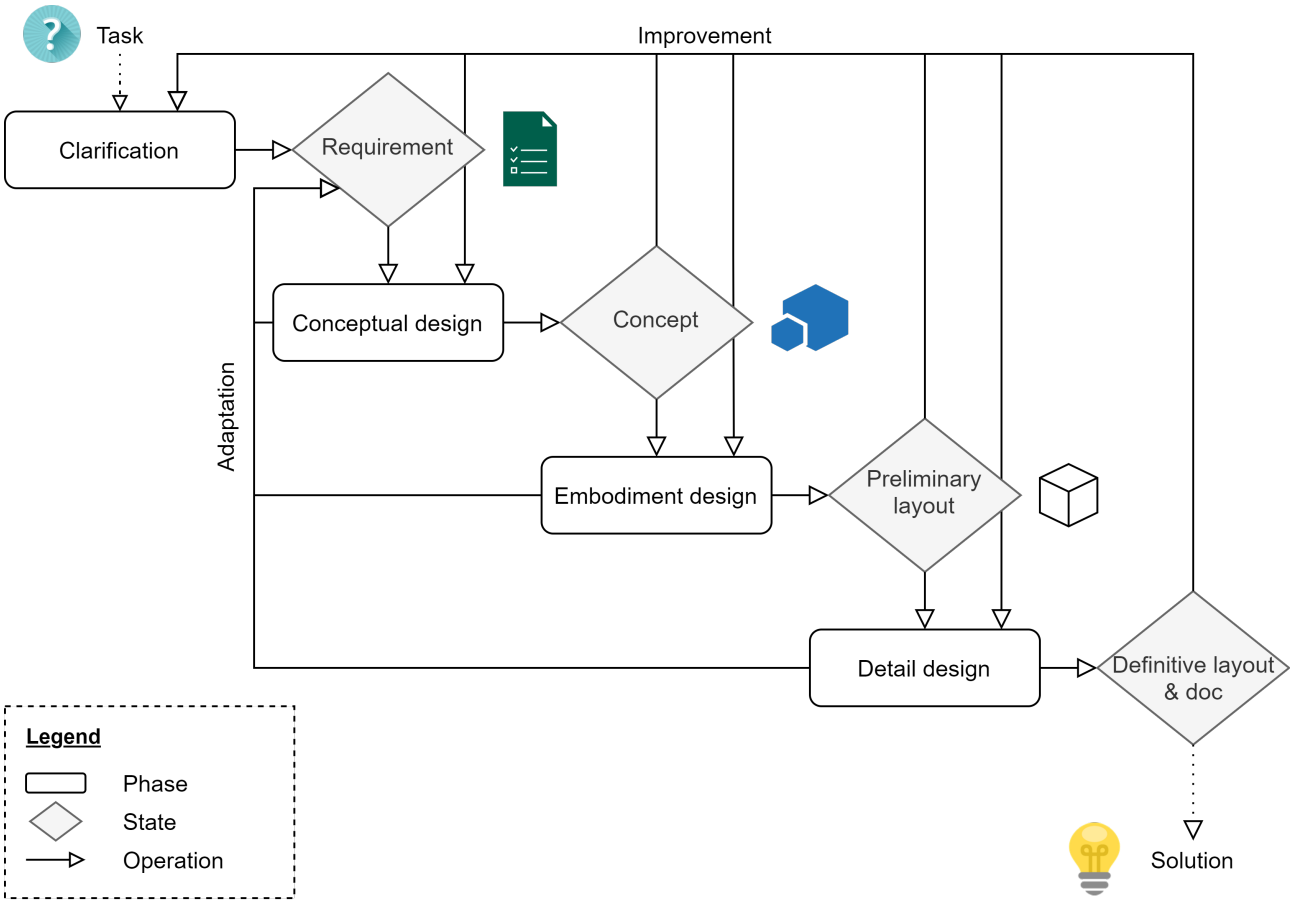


Fig. 1: Stages of a design.

The manuscript's plan is divided in three chapters :

The **first chapter** concerns the context and objectives of this piece of work. It involves anatomical and biomechanical considerations where I detail the structure of the hand, how

to model a finger joint and define terminologies related to this piece of work. It is followed by a description of spasticity and by a review of some particular passive musculoarticular stiffness (PMAS) measuring devices. The last sections of the first chapter details the method used to assess PMAS and the thesis objectives.

The **second chapter** concerns conceptual designs used in order to generate solutions for the functional requirements. This chapter is composed of comparative studies that allow us to choose the best fitted solution to the problem.

The **third chapter** concerns the prototyping step. It is composed of an optimized mechanical bar transmission, a description of the electrical circuit and the sizing of the components involved in the detailed design. Finally, I conclude this piece of work by a final assessment, involving considerations about the prototype and possible future perspectives.

1 Context & objectives

In this chapter, context and objectives of the Master's thesis are clarified. The first section aims to describe the structure on which the measurement of passive musculoarticular stiffness is made and how a joint can be modeled. In the next sections, spasticity is defined, a review of different PMAS measuring is drawn, and the method in order to measure PMAS is described. Finally, this chapter is concluded by the thesis' objectives.

1.1 Anatomical and biomechanical considerations

The forearm and the hand are a locus of a complex system of muscles and tendons. They are actioned in a coordinated way to achieve functional movements, such as precision grip (pinched grip) to be able to pick a pen and write for example.
This section describes (in a non-exhaustive way) the structure of the musculoskeletal system of the hand and identifies the sources of joint resistance.

1.1.1 Structure of the hand's musculoskeletal system

This organ system gives humans the ability to move using their muscular and skeletal systems. It provides form, support, stability and movement to the body.

Bones The stucture of the hand is provided by bones. It is composed of 27 bones as depicted in Fig. 2 which are subdivided in the following three categories.

- The forearm articulates with the hand bones at the junction of the wrist and is constituted of 8 **carpals** called Scaphoid, Lunate, Triquetrum, Pisiform (the smallest one and hidden by the Triquetrum in figure), Trapezoid, Capitate and Hamate.
- The wrist connects to 5 **metacarpals**, which are the largest bones of the hand and are numbered from 1 to 5 starting at the thumb.

- Finally 14 **phalanges** provide the structure of the fingers: 5 proximals, 4 intermediates (not present in the thumb) and 5 distals.

Joints Also known as *articulations*, joints are defined as an area of junction between two or more bones [7]. From bottom to top, finger joints are named:

- Metacarpophalangeal (MCP) joints, at the junction of metacarpals and proximal phalanges.
- Proximal interphalangeal (PIP) joints, located between proximal phalanges and middle phalanges.
- Distal interphalangeal (DIP) joints, between the middle and distal phalanges.



Fig. 2: Hand and finger bones [6].

Ligaments Bones are connected to one another via dense bands of fibrous connective tissues, ligaments. They provide joint passive stabilization at rest and during normal pROM. They also guide and limit the joint's pROM under tensile load.

Muscle-tendon units Tendons are similar in their composition since they are also made of connective collagenous tissues. This gives them *viscoelastic* properties. However they have a different job, tendons connect muscles to bones. They transmit the active force from muscles to bones and thus play an active part in limb motion. When muscles contract, they pull on the joint's bones via the tendons attached to them, exactly as a mass is pulled via a string in pulley mechanisms. Thus there exist two antagonistic types of muscle : the flexor and the extensor. These are respectively responsible for bending and extending limbs around a joint.[1].

[1]In order to actuate a revolute joint in robotics (only joints present in mother nature), there is only need for one actuator (electromechanical, pneumatic, hydraulic,...). In biology, joints are over-actuated i.e. more

Skeletal muscle features the following functional characteristics :

- Excitability : faculty to acknowledge a stimulus and react in consequence.
- Contractibility : specific to muscular tissues, it is the ability to contract in reaction to a stimulus.
- Elasticity : ability to extend and to take back its initial state after a stretch. It is an intrinsic property of the muscle. It provides a smooth transmission of tension from muscles to bones.
- Plasticity : ability of modifying its structure. For example sprinters possess more "fast-twitch[2]" muscular fibers (or type II fibers) than "slow-twitch" (or type I) which are more resistant to fatigue and predominant in marathoners [8].
- Extensibility : ability to be extended, which can be elastic or plastic.

The major part of muscles acting on the 2^{nd} to 4^{th} fingers are located outside the hand in the forearm or the arm and named **extrinsic muscles** (see Figs. 68 to 72 in Appendix B). Each finger is multitendoned, with three muscle-tendons involved according to Schieber [9] (see Fig. 74). Concerning only flexing movements, two muscles play the major role in finger flexing movements, flexor digitorum profundus and flexor digitorum superficialis.

The muscles that lie in the hand are called **intrinsic muscles** (by opposition to the external ones) and are depicted in Fig. 73. Lumbrical muscles are especially important in the flexing movement at the MCP and extension movement at the PIP and DIP [10].

Joint capsule complex Another component of the MSK system of a finger joint is the joint capsule complex or CLC. It is a complex around the joint composed of a synovial layer and a fibrous layer (Fig. 79). In addition to muscle-tendon units, this complex also provides resistance to motion, typically through its ligaments.

actuators than degrees of freedom (DOF) but allow to perform other functions. In humans, contracting both a flexor and an extensor muscle can create more impedance at the joint. Hence the joint becomes stiffer, which can be needed in daily situations. This concept of "local intelligence" is called embodiment in the robotic and artificial intelligence area.

[2]Fast-twitch fibers produce fast contractions that fatigue quickly.

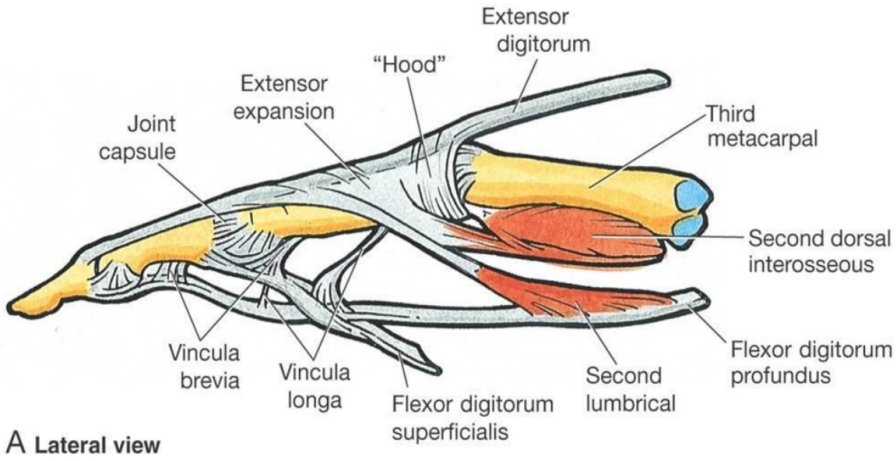


Fig. 3: Lateral view of the finger tendon insertions [11].

1.1.2 Modeling of joint articular units

The joint's motion has to be defined. Fig. 4 shows the reference frame used to measure finger motion at the MCP. The angle zero is positioned at the line which intercepts the wrist joint and MCP joint. The neutral position, or sometimes also referred to as equilibrium position, is defined as the angular position at which the smallest passive moment in flexion occurs.

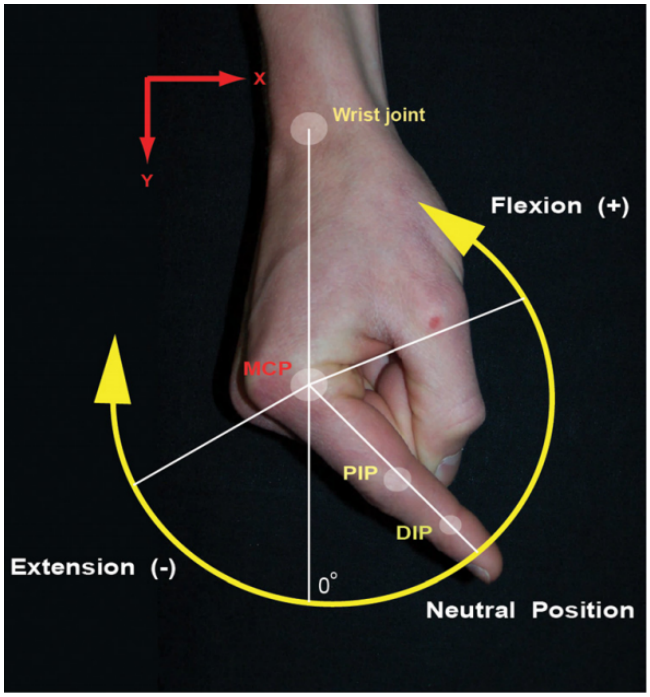


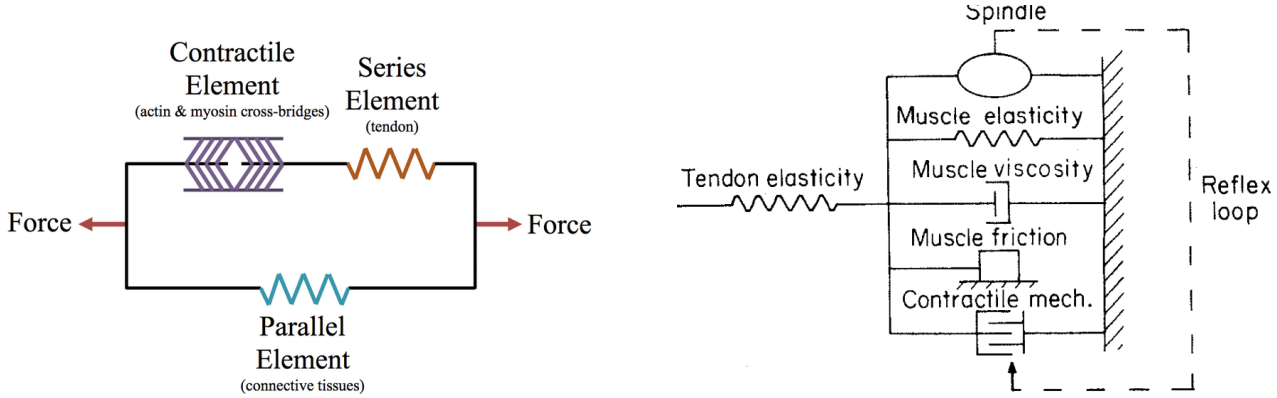
Fig. 4: Frame of finger joint motion at the MCP [12].

Factors that prevent a joint to go towards its extreme positions result from intra-articular and extra-articular factors. The former one includes capsule ligaments and cartilage. The latter includes flesh and passive tension in muscles and tendons.

As mentioned, ligaments and tendons exhibit viscoelastic properties together with muscles. Hill in 1938, proposed a three-element muscle tendon model that has since been largely used. It is composed of a contractile element and two passive elements, one in series and the other in parallel.

- The contractile element (CE) models the active part of the muscle. It freely extends in case of external forces applied to it and is capable of shortening when activated. It is identified as the "sliding actin and myosin filaments and the forces being the result of numerous active cross-bridges between them" (Martins et al. [14]).
- The series element (SE) can be represented as a nonlinear spring arranged in series with CE. It allows a rapid change in the muscle state and provides an energy storing mechanism. It is associated with the intrinsic elasticity of the CE composition ([14]).
- The parallel element (PE) can also be represented as a nonlinear spring and is parallel to CE and SE. It is responsible for the passive behavior of the muscle when it is stretched by external forces. It is identified as the elasticity of connective tissues and sarcolema (see Fig. 80 in Appendix B).

In studies on PMAS and active muscular activities, Rack in 1983 and Lehmann in 1989 used a similar model to the one depicted in Fig. 5b. Additionally to non neural mechanisms i.e. the *intrinsic* stiffness or PMAS, this model takes into account neural mechanisms, hence the changes in muscle activation due to reflex mechanisms.



(a) Hill three-element MTU model [17].

(b) Diagrammatic representation of tendon, muscle and stretch reflex [16].

Fig. 5: Model of muscle tendon unit.

It is tricky to clearly identify parts attributable to each of the components of a joint resistance within such an intertwined system. Concerning the elastic component, Kuo and Deshpande

[18] are interested in finding whether the MTU plays the major part in the joint PMAS. It's outcome using this same famous Hill-type model suggests that less than fifty percent of the total passive moment is attributable to the MTU and the "rest" to CLC.
With respect to the muscle-tendon unit alone, Latash and Zatsiorsky [19] consider that human tendons and ligaments contribute more to "passive resistance of joints to motion while relaxed muscle fibers show relatively low resistance to stretch". Since the MTU is built in a parallel way, its deformation in a relaxed state of the muscle mainly induces deformation of the muscle.

Moreover, each of the joints are not only triggered by a single flexor/extensor MTU group. As stated in Muscolino et al. [11] whenever a muscle (or its tendon) crosses a finger joint, it mobilizes it even if its tendon insertion is not placed on this joint. This coupling makes it more complex to identify a single muscle involvement in motion resistance.
In Fig. 3, one can observe that DIP joints (for fingers 2 to 4) are only bent by the deep flexor tendons, which is not the case for PIP and MCP joints that are also bent by superficial ones [9]. However it is safe to admit that MCP joints are essentially flexed by superficial flexor tendons.

As it is stated in Latz et al. [20], the wrist position has an influence on the MCP joint PMAS. It is quite understandable since tendons from extrinsic muscles are pulled when the wrist is either flexed or extended.

1.1.3 Mechanical joint impedance

Rheology is the branch of physics that deals with deformation and flow of materials. It is applied here to human joints and motion resisting forces.
The mechanical impedance in biomechanics represents the relationship between deformation (kinematics) and resulting dynamics i.e. forces/torques in human limbs/joints (Chino and Takahashi [21]). Impedance modulation is a fundamental mechanism to describe how humans physically interact with the external environment. This impedance is composed of the effective mass, inertia, damping and stiffness.

- **Stiffness** is related to the concept of *elasticity*. Chino and Takahashi write "*stiffness [...] is a mechanical measure of a material's elasticity*". The elastic modulus or young modulus is defined as Eqn. (1.1). It is described as the mechanical resistance of a material being

stretched when stress is applied to it.

$$\delta \triangleq \frac{stress}{strain} \tag{1.1}$$

In a first-order linear approximation to the real response of a spring, according to Hooke's law, one can describe stiffness as the constant factor linking the force F_s needed to elongate (resp. compress) a linear spring to a certain length Δx. Similarly, torsion spring is the equivalent angular form, as formulated mathematically in Eqn. (1.2).

$$k \triangleq \frac{F_{lin,spring}}{\Delta x} \text{ and } \kappa \triangleq \frac{\tau_{tors,spring}}{\Delta \theta} \tag{1.2}$$

In a more general manner, continuous elastic materials (like rubber or even steel bars) are expressed by a similar linear relationship between stress tensor $\boldsymbol{\sigma}$ (analogous to the force) and strain tensor $\boldsymbol{\varepsilon}$ (analogous to the displacement). This results in the stiffness tensor $\mathbf{c}$ given in Eqn. (1.3).

$$\boldsymbol{\sigma} = \mathbf{c}\boldsymbol{\varepsilon} \iff \sigma_{ij} = \sum_{k=1}^{3}\sum_{l=1}^{3} c_{ijkl}\varepsilon_{kl} \tag{1.3}$$

The modeled joints have a stiffness component that is meant to represent a physical torsion spring with units $\mathrm{Nm.rad}^{-1}$.

- **Viscosity** is widely used in fluid mechanics to describe the resistance τ_{shear} of a fluid that is deformed at a given rate $\frac{\partial u}{\partial y}$ or shear rate. In this manner, the *dynamic viscosity*[3], according to Newton's law, is defined Eqn. (1.4) for a situation such as depicted in Fig. 6 which can be written as Eqn. (1.5) for a 3-dimensional flow in tensor form.

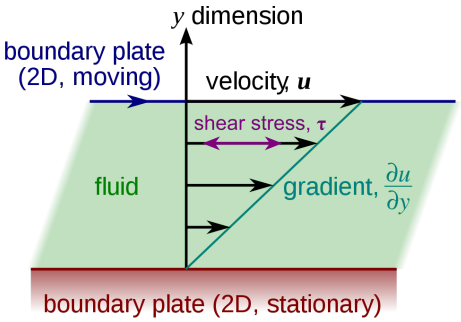


Fig. 6: Planar Couette flow [22].

$$\mu = \frac{\tau_{shear}}{\frac{\partial u}{\partial y}} \qquad [Pa.s] \; or \; [N.s/m^2] \tag{1.4}$$

$$\tau_{ij} = \sum_{k}\sum_{l} \mu_{ijkl}\frac{\partial v_k}{\partial r_l} \tag{1.5}$$

[3] Another definition of viscosity is the *kinematic viscosity*, which is defined as $\nu = \frac{\mu}{\rho}$. It describes the same phenomenon but has different units.

Newton's law can also be written to set the relationship between a stress in a viscous material and a subjected strain variation in time (Eqn. (1.6)). The dynamic viscosity can be expressed as Pa.s or $(N/m^2).s$ units.

$$\sigma = \eta \left(\frac{\partial}{\partial t} \right) \varepsilon = \eta \dot{\varepsilon} \iff \eta = \frac{\sigma}{\dot{\varepsilon}} \tag{1.6}$$

Hence the concept of viscosity describes the **linear relation between an imposed constraint to a viscous material and velocity of deformation**.

Damping is a more general concept linked to viscosity. It is the effect of the reduction in amplitude of oscillations by irreversibly dissipating energy within an oscillatory mechanism. Damping models contain empirical constants that describe dissipation through, for example, viscosity, coefficient of friction, or material losses in solids (Akay and Carcaterra [23]).

One can illustrate a damped linear harmonic system through a simple spring-damper system with only three components as Fig. 7. In order to move the mass at a given position x_1, an external force has to counteract the damper force proportionally to the body velocity. In this case, the coefficient is called a viscous damping coefficient (Eqn. (1.7)).

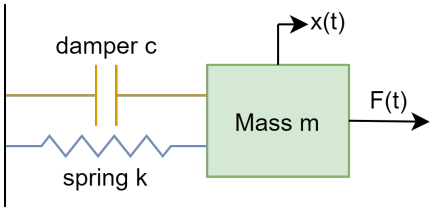


Fig. 7: Diagram of a linear spring damper oscillator system.

$$F_{damper}(t) = c\frac{dx(t)}{dt} \tag{1.7}$$

$$F(t) = m\frac{d^2x(t)}{dt^2} + c\frac{dx(t)}{dt} + kx(t) \tag{1.8}$$

Some authors criticize the use of viscosity when applied to the study of human movements. Zatsiorsky [24] found at least 11 meanings in scientific literature for *"muscle and joint viscosity"* in 1997. Latash and Zatsiorsky [25] recommend to use the term viscosity only in accordance with the SI metric system, and the term *velocity-dependent resistance* to describe the resistance proportional to velocity (measured in $N.(m/s)^{-1}$) to avoid misunderstanding.

However in a matter of consistency and clarity with the other works in *UCLouvain*, "viscosity" will be used to describe this "velocity-dependent resistance" coefficient. Since it is applied to a rotational motion, there units are $Nm.(rad/s)^{-1}$.

- **Moment of inertia or rotational inertia** can be described in a informal way as the resistance of a physical object to change its angular velocity. Formally, it is defined as the ratio of the net angular momentum L to its angular velocity ω (Eqn. (1.9)) and calculated for a three dimensional body Q at a point P as Eqn. (1.10). It depends on the mass distribution and the body's axis of rotation. A well known interpretation of this phenomenon is the spinning skater that changes its rotational inertia when its arms are brought back to its center of rotation.

$$I = \frac{L}{\omega} \tag{1.9}$$

$$I_P = \iiint_Q \rho(x,y,z)\|\mathbf{r}\|^2 \, dV = \begin{bmatrix} I_{xx} & I_{xy} & I_{xz} \\ I_{yx} & I_{yy} & I_{yz} \\ I_{zx} & I_{zy} & I_{zz} \end{bmatrix} \tag{1.10}$$

The passive model used in this thesis consists of a constant average stiffness and a constant viscosity. This model has to be used in a limited range of limb motion. According to Mizrahi [26], linear models fail to predict the true dynamics of physiological joint impedance and must be treated as a non linear phenomenon for the whole RoM.

It is a damped linear oscillator model in the form of a differential equation as following :

$$M(t) = I\frac{d^2\theta(t)}{dt^2} + C\frac{d\theta(t)}{dt} + K\,\theta(t) \tag{1.11}$$

And so the whole apparatus impedance can be expressed as a second degree transfer function in the Laplace domain (Eqn. (1.12)).

$$G(s) = \frac{M}{\theta}(s) = \frac{1}{Is^2 + Cs + K} \tag{1.12}$$

1.2 Spasticity

1.2.1 Definition

The pathophysiologic basis of spasticity is not completely understood and it is often misused and overused because there is no unanimous definition. Elia et al. [27] describe the spasticity as "[a motor disorder] characterized by a **velocity-dependent** increase in [myotatic] stretch reflex activity (SRA)". It is one of the types of muscle overactivity that may affect subjects with damages to the central nervous system (CNS) or with a pyramidal system lesion. It can be seen as a secondary effect of many conditions, notably head injury, spinal cord injury, stroke, cerebral palsy, multiple sclerosis and so forth (Thompson et al. [28]). In a more general manner, the word spasticity is clinically used to describe a constellation of symptoms, including increased resistance to passive movement, increase of phasic-SRA, clonus and flexor/extensor spasms (Gelber and Jeffery [29]).

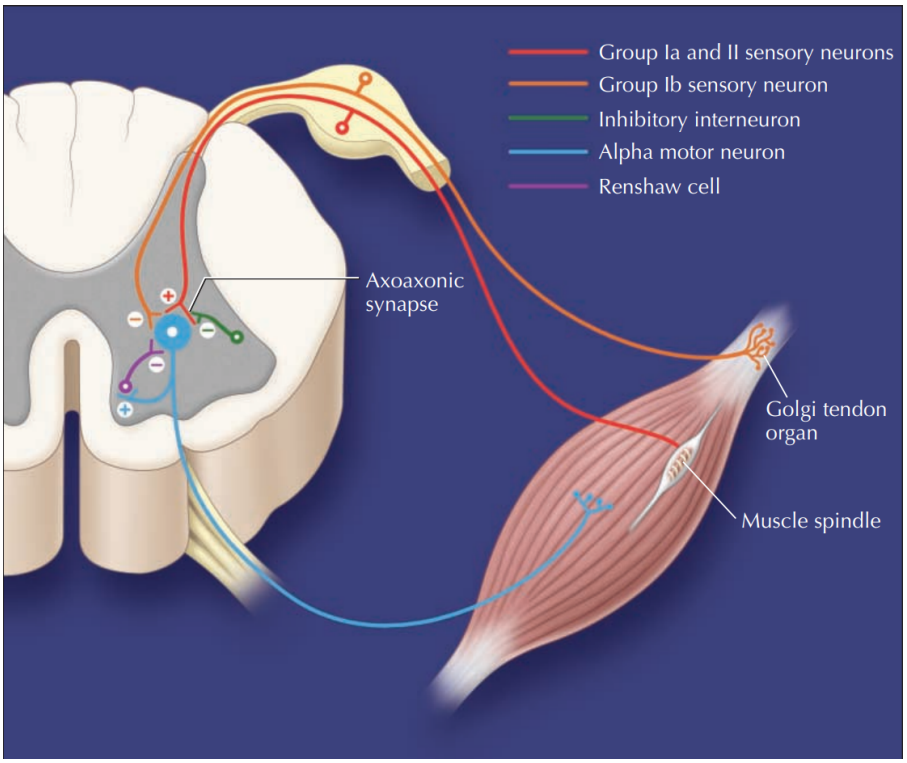


Fig. 8: The stretch reflex arc [30].

In order to understand how spasticity exhibits these physiological symptoms, it is important to clarify what constitutes stretch reflex circuit pathways.
In normal conditions, the brain and muscle act in harmony to keep a certain muscle tension, to counteract forces coming from the environment or to perform activities.

More precisely, as shown in Fig. 8, in response to physical deformations sensed by muscle spindles, afferent nerve fibers send signals from muscles to the brain. It then transmits them back via efferent motor neurons to the muscles - in this case alpha motor neuron - to control motion. The modulated brain signal says how much the muscle contracts or relaxes (Reid [31]).
In these pathways, there are numerous excitatory and inhibitory modulatory synaptic influences. If imbalances in this modulation occur it could result in hyperexcitability of the stretch reflex arc. This is what spasticity constitutes (Satkunam [30]). It is a neurological condition affecting upper motor neurons (UMN) which can alter the net inhibition of peripheral nerves in the affected region where the CNS is damaged. As a result, a hyperexcitability of the myotatic reflex pathways is observed and leads to a velocity-dependence resistant to motion.

One could note that the well known hammer tap on the knee is a way to visualize hyperexcitability of a SRA as illustrated in Fig. 9. Besides, it is even used to assess the absence or presence of spasticity ([16]).



Fig. 9: Illustration of a hammer knee tap on a subject suffering from hyperexcitability [32].



Fig. 10: Typical spastic posture of the hand : flexion of the wrist and clenched finger flexion [33].

Spasticity is **elective**. In the upper limb, most impacted muscles are the adductor, flexor, and pronator. This results in spastic subjects having their arm alongside their trunk, with flexed elbow, wrist, and fingers, and their palm facing downwards [34].

1.2.2 Spasticity's impact

Spasticity is a multi-faceted syndrome and it may accompany paresis. In addition to hyperexcitability, Dietz and Berger [35] hypothesize that spasticity is also responsible for increases in muscle tone - basically the feeling of resistance in joints to an imposed movements - appearing

with relatively mature spasticity (more than 1 year). Indeed, this hyperexcitability of SRA is often associated with increases of rigidity or hypertonia[4]. Fibrous contractures within muscles or in periarticular tissues produce an increased resistance to passive muscle stretch and thus are one of the cause of increased muscle tone [28]. Moreover, the shortening of the MTU is also an expression of spasticity. These mechanical changes in muscle properties contribute to abnormal postures as seen in Fig. 10.

On one hand, spasticity is source of harmful effects. It causes discomfort, spasmodic episodes can be annoying and painful, it may interfere with physical activities and also has an emotional impact on self image or motivation [28].
On the other hand, in presence of UMN lesions, spasticity can be useful in some situations. It could provide posture and tone, allowing a person to stand when muscle weakness would not otherwise allow it [28]. In this light, management of spasticity for subjects must focus on the subject's goals and functions.

1.2.3 Qualitative and semi-quantitative evaluation

Clinical evaluation is usually performed by the assessment of pROM. The Modified Ashworth scale and Modified Tardieu scale are commonly used to classify the severity of hyperresistance.

- **Modified Ashworth scale** ranges from 0 representing no increase in muscle tone to 5, in which affected part(s) are rigid in flexion or extension (Fig. 75 in Appendix B).
- **Modified Tardieu scale** ranges from 0 to 4 and assesses the joint with different speeds (Fig. 76 in Appendix B).

These scaling evaluations do not need instrumental requirements and are easy to use. However, they are still subjective factors. An evaluation can differ from one physiotherapist/ doctor to another. In addition, neural and non-neural components are not distinguishable[36]. In spite of that, the validity and reliability of these scales have been disputed [37], [38]. For instance, a scale of 5 in the modified Ashworth scale means a completely rigid joint i.e. the limb is not able to move around the evaluated joint. Hence, it can not claim to assess spasticity since it is in conflict with its definition, it is a velocity-dependent condition and thus, can

[4]Defined as a condition involving too much muscle tone. Spasticity is a particular case of hypertonia, dystonia is another one involving involuntary sustained or intermittent muscle contractions or rigidity. According to Gelber and Jeffery [29], spasticity must be differentiated from rigidity. Where both include involuntary increases in muscle tone, rigidity is defined only as an increase in muscle tone **at rest**.

only evaluate rigidity.
Other methods such as the pendulum test are also used to assess spasticity by putting the knee in motion and measuring multiple parameters.

Spasticity unequally affects people of different ages but also the region, scope and maturity of the lesion [29]. Furthermore, the measurement of passive musculoarticular components are also influenced by several other factors like temperature, time of day, history of previous pathologies or immobilization [39]. Hence, in order to make experimental assessments of spasticity, it is required to have a controlled environment with a rigorous experimental procedure to normalize the data.

1.2.4 Spasticity management

It is not possible - strictly speaking - to treat spasticity since it results from a damaged UMN. However there are possibilities to mask in a certain degree its negative symptoms.
It is only after a rigorous clinical analysis and evaluation of the conditions and their impacts that an appropriate selection of the treatment can be done.
The treatment must consider drug therapies, surgery, orthosis and physiotherapy. One of the most commonly used drug is the intrathecal baclofen which is a type of chemical nerve block. The latter being one of the studied treatments used with the ankle EOD of Detrembleur and Plaghki [40] in *UCLouvain*.
Extracorporeal Shock Wave therapy (ESWT) is also a way of improving spasticity through physical modalities. It is a rather new treatment that delivers high pressurized sonic pulses to injured soft tissues. The mode of action of this non invasive technique is poorly known.

1.3 Review of PMAS measuring devices

Literature provides quantitative results on passive musculoarticular stiffness (PMAS) of various nature of joints. In this regard, the apparatus described in this section exhibits different architectures. In this review, I am only interested in apparatus designed to provide sinusoidal imposed movements to joints, which constitute the basis of the quantification method used for the design of this thesis' device. This review is not complete, it is there to give insights and inspiration for the design step.
The binding system for the excited joint is not of particular interest for this work as soon as it is dependent on the joint type and method of quantification.
Literature investigates movements of different amplitude and frequency. In some articles, the subject is even asked to maintain active tension to spot typical features. I am choosing to keep some of the outcomes on the influence of stretch reflex activities (SRA).
A lot of the earliest PMAS measuring devices only give schematic representations, which brings limited understanding of its real design.

Wright and Johns's finger EOD In earlier scientific papers written in 1960 and 1961 by Wright and Johns [41], it was observed that little has been done to quantify PMAS in human joints. It was one of the first studies to present a method capable of roughly estimating joint impedance at small frequencies. Qualitatively, it was considered that five types of different stiffness could model the intrinsic impedance of finger joints: elastic, viscous, inertial, frictional and plastic.

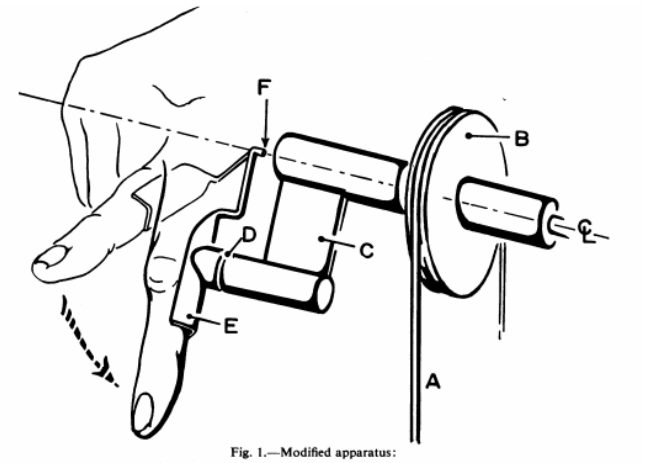


Fig. 1.—Modified apparatus:
A. Cable driven sinusoidally by a crank.
B. Pulley converting motion to sinusoidal rotation.
C. Lever transmitting torque to finger and on which strain gauges are bonded.
D. Swivel.
E. Finger holder.
F. Centre indicator.

Fig. 11: Apparatus of Wright and Johns [41] .

The measurement was made on the MCP joint of the second finger and carried out under large amplitudes of sinusoidal movements. Two types of motions were investigated in order to generate the movement: a pendulum and a motor driven mechanism. Since the later allows a wider range of possible frequencies, the motor was kept.
In order to record the dynamical response of the finger i.e. the torque in this context, a strain gauge was placed at the lever (see Fig. 11).

In addition to a dynamical study, a transient study was conducted. The goal was to find the relative weight of elasticity in the global impedance (or stiffness[5]).
This paper states that the major component of joint stiffness is the elastic one and that - what it calls - plastic stiffness[6] is significant. According to the paper, frictional, inertial and viscous stiffness are negligible in the experiment's range of frequencies i.e. 3 Hz max.
Bäcklund and Tiselius [43] in 1967 reused the same type of apparatus (but rather simplified) as described by Wright and Johns and perform an amplitude of 60° in either direction from 35° of finger flexion which gives an average PMAS over a wider pROM.

Following a similar approach, Rack et al. extensively studied dynamical responses of human joints (or more generally mammalian joints). They designed multiple apparatus to measure forces generated in cats from the hip joint in [44] and humans from the elbow [45], from the thumb's interphalangeal joint [46] and from the ankle [15].

Rack's cat EOD In 1966 they are interested in finding the effects of tetanized[7] mammalian muscle energy dissipation during imposed sinusoidal stretching in [44]. With the assumption that muscles play the major part of the PMAS.
It is assumed that the passive tension produced by muscles can be separated into only two components: elasticity (energy conservative) and viscosity (energy dissipative). But they stated that muscle properties cannot be modeled in the full joint range through a linear model.
The apparatus depicted in Fig. 12 uses a came mechanism shaped as an eccentric

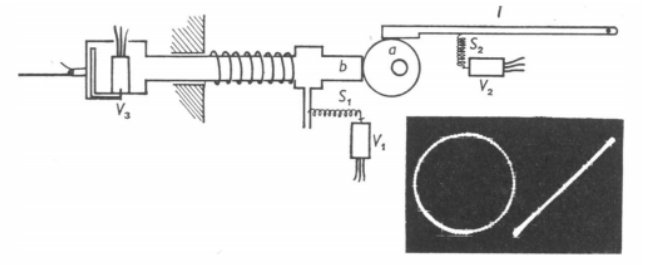


Fig. 12: Came mechanism apparatus used for a cat by [44]: Rotation of the eccentric (a) causes a horizontal movement of the bolt (b) which is communicated to the muscle through a myograph containing transducer valve (V_3). Movement of the bolt is recorded by the valve (V_1) which measures tension in the spring (S_1). Velocity of movement of the bolt is measured by valve (V_2) which records tension in the spring (S_2); the spring (S_2) is stretched by movement of the lever (l) which is arranged to move at 90° to the movement of the bolt. *Inset.* Velocity-tension figure (left), and length-tension figure (right).

[5] One can note that in these scientific papers, they use the term stiffness. It is not to be understood in a strict engineer definition. Indeed, in a strict sense, stiffness is a component of the *elasticity tensor* as explained in a previous paragraph. They interpret the viscous stiffness (with unit $Nm.rad^{-1}$) as the stiffness in quadrature to the elastic stiffness with the same unit.

[6] Component that can be interpreted as a spring attached to a frictional element. See Fig. 77 in Appendix B for the interpretation of the different components.

[7] A tetanic contraction is a sustained muscle contraction evoked when the motor nerve that innervates a skeletal muscle emits action potentials at a very high rate [47].

wheel. It produces a horizontal beam to follow its circumference, transforming a rotary motion into a linear motion.
Very small amplitudes of sinusoidal stretch movements were conducted (0.7 to 3.8 mm peak-to-peak) and amplitude changes were made possible by the use of different eccentrics. By using a force transducer at the end of the beam, it can measure tension.
It is important to notice that two combinations of a spring attached to a force transducer (S1/V1 and S2/V2) were used in order to find the length and velocity, due to less reliable sensors at the time [8]. Although elegant, this technique does not provide precise measurements of velocity if the motion of the eccentric depends on the mechanical precision and strong assumptions.
Rack expresses the tension as Fourier series and, in this manner, is able to identify components in phase and in quadrature with movement. Further explanations of this method are given in Section 1.4. According to Rack, elastic and viscous properties of muscle vary with both frequency and amplitude of oscillation. Viscous stiffness resistance being velocity dependent, the frequency of oscillation is increased.

Rack's elbow EOD In 1974, the elbow joint's apparatus (Fig. 13) was designed with a crank rod mechanism to assess PMAS using a *free-oscillation technique*.
It is driven by a highly inertial fly-wheel (i.e. crank here) actuated by a motor until it reaches the desired speed and is freed (hence measurements are made through a whole range of frequencies). It allows to study work transfers between the fly-wheel and the limb. On the other hand, the decrease of the crank speed is completely uncontrolled. Precise measurement at a given frequency is not possible.

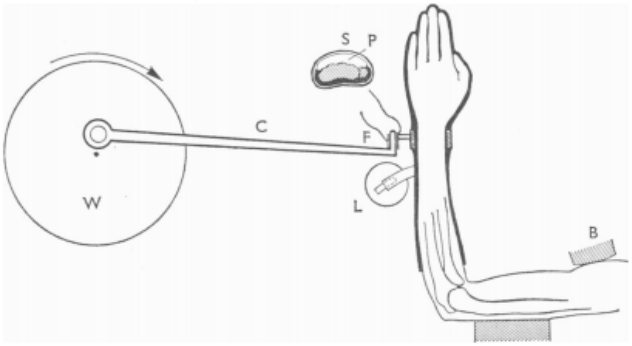


Fig. 13: Crank rod mechanism apparatus [45]. The fly-wheel (W) rotates, and the crank (C) drives the wrist through a sinusoidal movement. The forearm and hand were held in a close fitting mould by a canvas sheath (S) and pneumatic bag (P). The end of the crank carried a force transducer (F). A photo-electric position transducer(L) measured the mould position.

In order to produce the closest sinusoidal function possible, the ratio between the eccentric pin of the crank and the length of the rod must be "large". In the paper, dimensions are 5mm and 450mm respectively giving a ratio of 90, which is sufficient to have a negligible departure

[8] Indeed with the knowledge of the spring constant, it is straightforward to identify length through Hooke's law equation : $F_{spring} = k * \chi$

from a pure sinewave according to the authors. A statement considered in Section 2.2.1.
The elbow was positioned at a neutral angle of 90deg and the arm was restrained to only perform flexion-extension movements.
The apparatus is not designed to provide PMAS measurements on both arms.
The subject is instructed to maintain a constant mean flexing force against the crank attached to the wrist with the help of a displaying meter system. So there is an active contribution in the measurement attributable to the subject and that may lead to uncertainty [16].

This study shows an interest in the reflex pathway mechanism of muscles and tries to understand how much SRA is involved in the results. They study the influence of timing, amplitude and mean force exerted by the subject. They observe - what they designate as - "negative frictional" properties during small oscillations (1-2 mm peak-to-peak) at 8 to 12 Hz. According to the authors, it is attributable to the delay of the stretch arc, creating an activity assisting the movement i.e. negative viscosity rather than a simple "positive viscosity" attributable to muscle viscoelastic intrinsic properties.
Finally, they observed that SRA was more present in greater exerted flexing force of the subject.

Rack's thumb EOD Latter on in 1982, a similar apparatus was designed in order to assess PMAS of the thumb's DIP joint. The thumb is attached thanks to a mold, several turns of rubber strips and then firmly attached to a lever with a spring to ensure coupling at all times. Moreover a *plaster-of-Paris* mould[9] encloses the other fingers, the palm of the hand, and the forearm. This custom made prosthesis-like mechanism does not allow for a large population range of subjects. This design certainly can not provide reproducible results.
At the sensing level, a u-shaped beryllium-copper force transducer is placed between the fly wheel and the lever of the thumb. A homemade encoder with 400 holes drilled in the flywheel activated by a photo-diode is used in order to measure its angular position.
Once again, the subject is asked to maintain a flexing force of 0.75Nm which is about 10% of the maximal force (so he is focused on doing this task with a value displayed in front of him) which is here of course smaller than for the elbow's EOD. Amplitudes of 1.4deg and 5.1deg (resp. 24mrad and 89mrad) are exerted at 13.5 and 3.5hz. The frequency gradually decreases but the flywheel is always driven to keep control over the frequency. It takes into account, in

[9] Molding material made by mixing a powder with water and letting it dry for about 10 minutes.

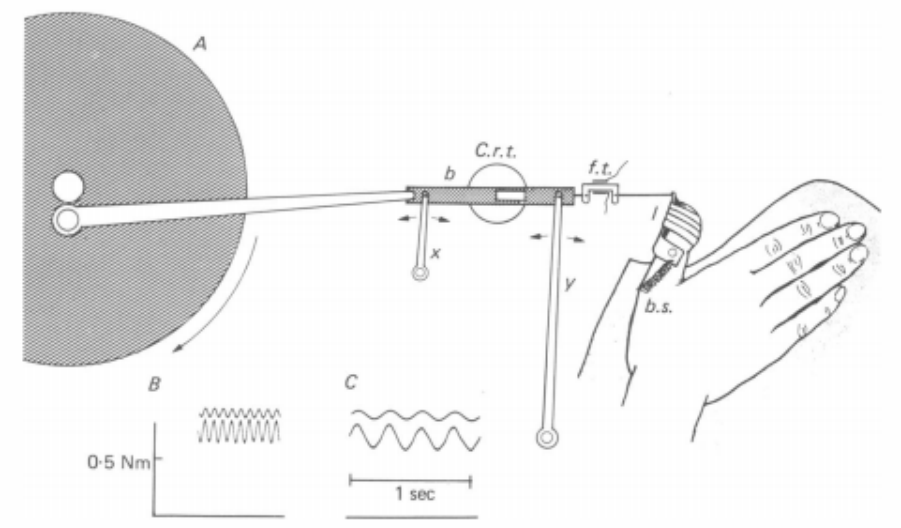


Fig. 14: Rack's thumb EOD : Rotation of the fly-wheel acts through an eccentrically mounted driving pin and a crank to cause a reciprocating sinusoidal movement of the b bar.

its method, some contaminants of a second order function added to Eqn. (1.14).

$$p(t) = a \cdot sin(\omega t) + b \cdot cos(\omega t) + \left[c + d \cdot t + e \cdot t^2\right] \tag{1.13}$$

Evans et al.'s ankle EOD In 1983 Evans et al. [15] used electromyographical tools to record the muscular activity of subjects during sinusoidal movements. The particular interest in combining EMG with EOD is to tell how much delay is present in SRA and its amplitude response. The EMG amplitude was clearly correlated with the amplitude of movement, but in a non linear way. Moreover saturation occurs with larger amplitudes of movement. EMG measurements are limited to local samplings of action potential of muscle unit fibers [16]. Once again for this device, subjects are asked to perform a mean flexing force to trigger reflex responses. In contrast, for relaxed limbs, at the beginning of the experiment, there was none or very little reflex response, even to large and fast sinusoidal movements. Potentiometer and strain gauge are used in the resisting force and EMG recording.

Unsworth et al.'s finger arthrograph Arthrograph machines are devices with only a quasi-static measurement method[10] to assess the stiffness, but it broadens significant insights about the human-machine interface. Unsworth et al. [48] designed the arthrograph in Fig. 16. It is configured with the driving assembly placed beneath the hand. It has a certain modularity to adapt to subject's hand morphology. It allows to evaluate varying sizes of hands thanks to

[10]The goal is to have a negligible inertial effect and negligible SRA but still fast enough not to hinder subject relaxation during the measurement of passive stiffness.

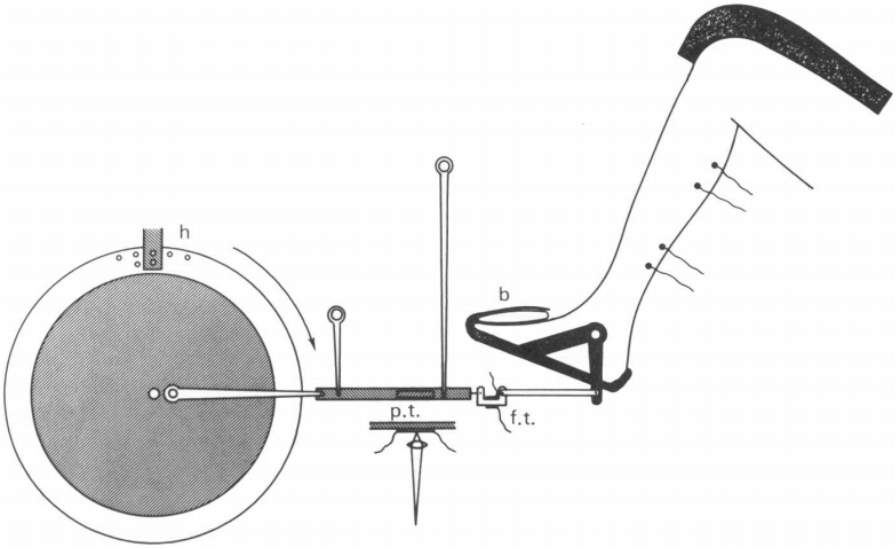


Fig. 15: Ankle's EOD of [15].

the variable driving arm height and different finger width with a v-shaped tightening system for the finger. Moreover they use a leather thumb support to leave the finger free to move without hindrance and a cylindrical frame to grasp. They call attention to the machine's comfortability.

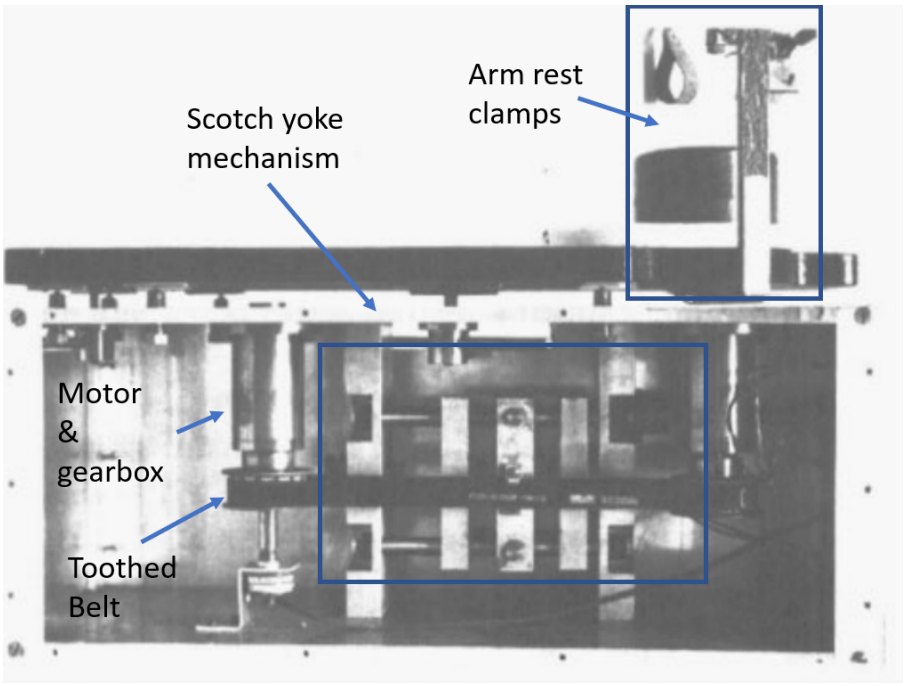


Fig. 16: Side view of Unsworth's arthrograph with panels removed to show scotch yoke mechanism, drive assembly and arm rest clamps [48].

Lehmann's ankle EOD Based on - amongst others - the work of Rack et al., Lehmann designed an EOD for the ankle to provide quantitative measurements of spasticity in 1989. Rack's mathematical model is reconsidered, procedure and findings are reinvestigated. The schematic representation of Lehmann's system can be seen in Fig. 17.
A 1/2hp (372W) brushed DC-motor driven crank mechanism allows the creation of an oscillation of 5deg amplitude ($\pm$ 2.5deg) around the neutral position of the ankle, from 3 to 12hz in random sequence frequency and a sampling rate of 500hz. A torque and a displacement transducer are placed on both sides of the shaft surrounding the foot plate.
An accuracy validation of the equipment was performed. Two torsional springs of different stiffness were used to resist footplate movements.

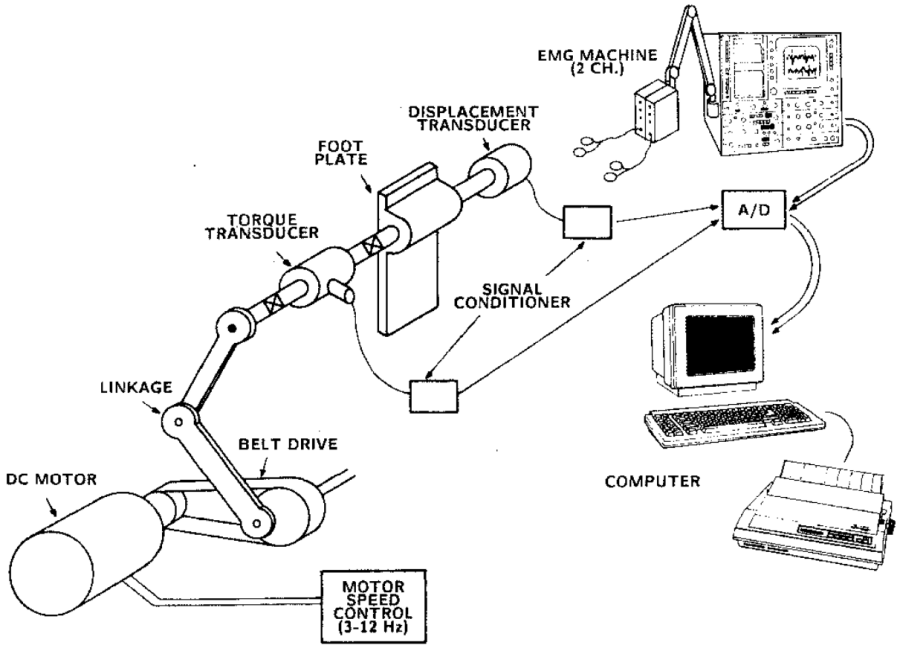
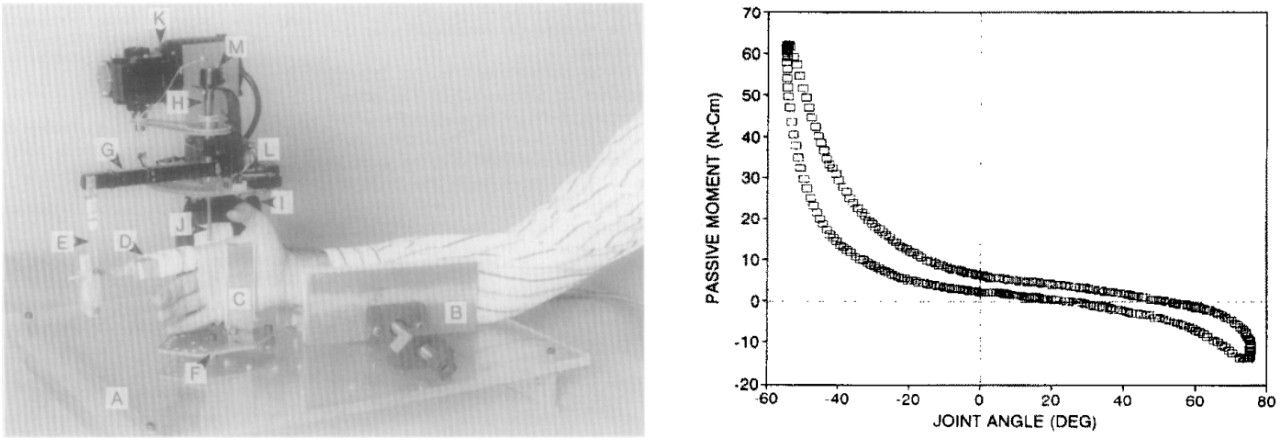


Fig. 17: Ankle's EOD of [16].

In this method, the global inertia and friction of the machine is taken into account, which was not the case in Rack's work. One can observe in Eqn. (1.14) that even in small amplitudes of movement, the mass' importance (or inertia) on the dynamics evolves in a quadratic manner. Its reshaped model is described in Section 1.4. Once again, they used EMG data with surface electrodes in addition to its mechanical measurement apparatus. The method does not rely on voluntary contraction, which according to Lehmann [16] increases the uncertainty on what is quantified, because the "quantitative relationship between increase in reflex response, and change in passive properties" is unknown. The active component in the model Fig. 5b is influenced by five parameters : gain, latency, phase shift, natural frequency, and damping

ratio, and is represented by a low pass system function. This model was compared to experimental measurements after parameters were tuned in order to fit it.
In order to assess the PMAS, without the active component, chemical nerve block procedures were used with *Lidocaine*. Hence PMAS of spastic and healthy subjects can be compared.

Esteki and Mansour's finger EOD This device does not use Lehmann's method, the velocity is very small (0.05 to 1.29rad.s^{-1}) and measurements are made over a large pROM. From the design Fig. 18a, results in Fig. 18b show the passive moment created from a 60°-extension to 80°-flexion of the second finger MCP joint. One can observe that a range of about 60° around -10deg to 50deg joint angle can be attributed to a constant passive stiffness.
This device pays special attention to the positioning and immobilisation of the forearm [B]



(a) (b)

Fig. 18: (a) Device and (b) Results of Esteki and Mansour [49].

and the palm of the hand [C], and an indicator [J] helps to position the MCP joint with the device's axis of rotation.

Detrembleur and Plaghki's finger EOD In 2000, Detrembleur and Plaghki [40] designed an EOD device following the same method as Lehmann [16] in order to provide objective and quantitative measures of PMAS and thus be able to assess the effects of baclofen.
A four bar mechanism is used to produce a sinusoidal movement out of a constant motor driven speed. Ten oscillation frequencies are operated by means of 1hz-increments. Fig. 19 shows the device with the description of each mechanical element that composes it.
The machine has been subjected to a review in the frame of a master thesis [50] in order to update it. For instance, the goniometer which compels to calibrate the machine after each measurement, is advised to be replaced by an absolute encoder.

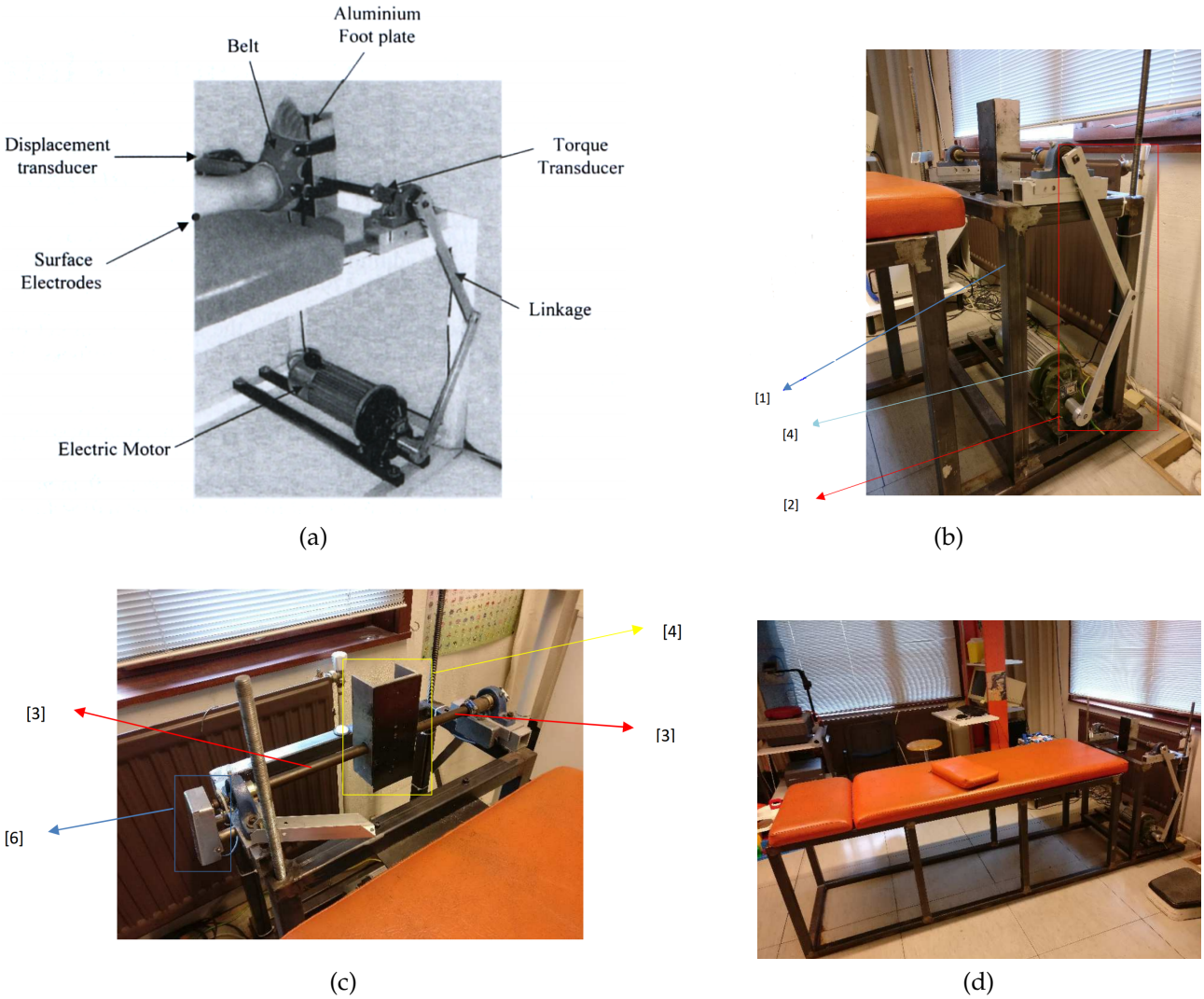


Fig. 19: Ankle's EOD of [40]. [1] structure, [2] four bar mechanism, [3] shaft, [4] dc motor, [5] strain gauge sensor and [6] a goniometer.

1.4 Detrembleur's method of PMAS measurement

In this section, the method based on Rack and adapted by Lehmann, and Detrembleur and Plaghki is described. This method aims to measure the passive musculo-articular stiffness (PMAS) of a distal joint by imposing a sinusoidal movement to a limb at multiple frequencies. Rack writes: "The non-linear behaviour of striated muscles presents an obstacle to the investigation of its properties, but this can be partly overcome by the use of sinusoidal stretching, since it is then possible to separate the tension that develops in two components [...]".
Sinusoidal movements are well understood methods of analysis, easy to generate and provide more repeatable and controllable stimulation [16]. A repeating movement has the advantage of making it possible to measure force over a number of similar cycles, and separate the relevant force changes from other random fluctuations, in contrast to other mechanical stimuli like ramp waveforms.
In Fig. 20, a schematic depicts Detrembleur's method.

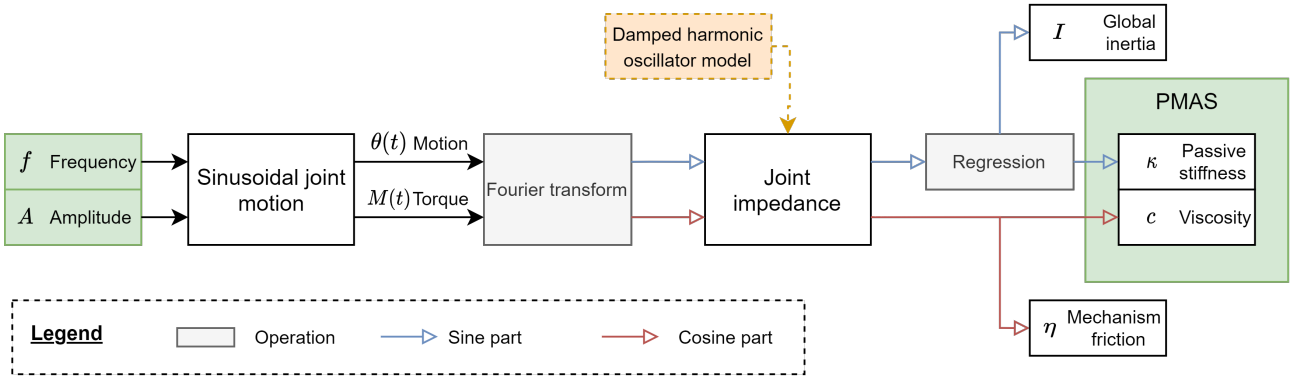


Fig. 20: Schematic of Detrembleur's method.

First, the apparatus has to produce a pure sinewave function to a distal joint. Two choices have to be made 1) range of frequency and 2) amplitude of oscillations. These two choices have to be made while considering the type of joint assessed. Ditroilo et al. [51] writes that the main concern for this type of method is the assumption of linearity of the system modeled as a damped harmonic oscillator. But over a limited pROM, this assumption stands [39].

One can differentiate the movement to find its rotational velocity and acceleration :

$$\begin{aligned}\theta(t) &= A \cdot \sin(2\pi f t) = A \cdot \sin(2\pi f t + 0)\\ \frac{d}{dt}\theta(t) &= A \cdot \omega \cdot \cos(2\pi f t) = A \cdot \omega \cdot \sin(2\pi f t + \pi/2)\\ \frac{d^2}{dt^2}\theta(t) &= -A \cdot \omega^2 \cdot \sin(2\pi f t) = A \cdot \omega^2 \cdot \sin(2\pi f t + \pi)\end{aligned}$$

In Section 1.1.3, components that constitute the impedance are described and, through a sinusoidal movement, the torque becomes as Eqn. (1.14).

$$M(t) = A \cdot \underbrace{(\kappa - I\omega^2)}_{A_1} \cdot \sin(2\pi f t) + A \cdot \underbrace{\omega(\eta + f_r)}_{A_2} \cdot \cos(2\pi f t) \tag{1.14}$$

Where

- M(t) is the measured torque created by the imposed movement $\theta(t)$.
- K represents the finger's passive stiffness κ. It is in phase with movement.
- I is the finger's global inertia and the mechanism. It is in opposition of phase to movement.
- C is the "damping coefficient" that comprises the finger's viscosity η and internal friction in the mechanism is denoted by f_r. It is quadrature to movement.

A Fourier transform on this torque allows to separate the in-phase/opposition A_1 of phase component with the movement (inertia and stiffness i.e. sine part here) and the ones who quadrature with it A_2 (viscosity and friction i.e. cosine part here). To see this, it is important to clearly understand how this transformation works. A quick description that pictures it is available in Appendix A.1.

With the assumption of an impedance model restricted to small amplitudes of ideal sinusoidal motion of a joint, only fundamental components should appear in the frequency domain. In reality, some non-idealities can interfere in the measurement method. Thus, only the amplitude at the fundamental frequency is kept in the impedance. All the other harmonics are discarded from subsequent analysis.

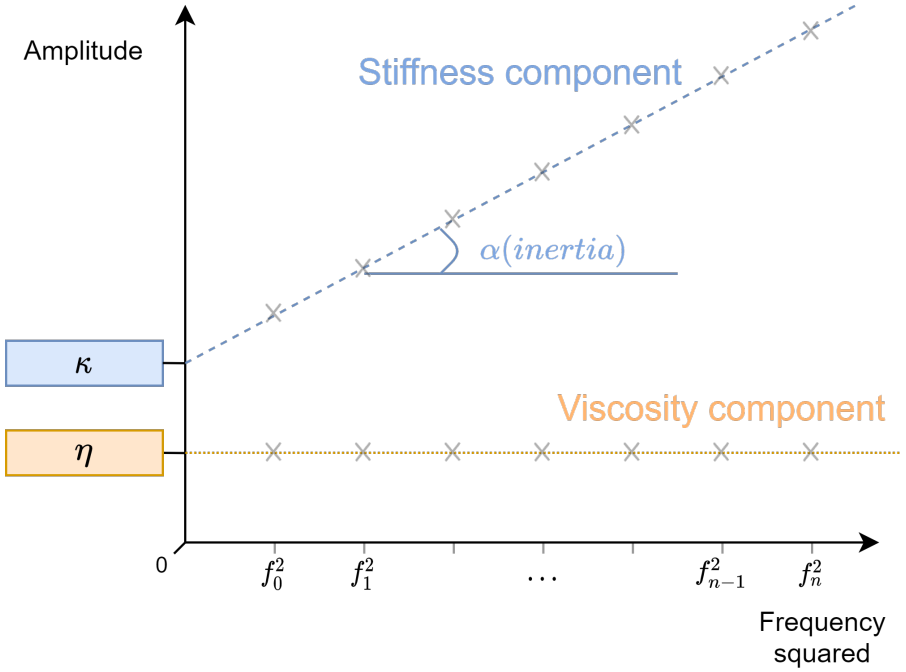


Fig. 21: Schematic : Evaluation of the passive stiffness and viscosity after Fourier separation.

The final step is the identification of the passive stiffness and viscosity. In order to do that, two components in the impedance have to be cleared out.

(i) **Friction** in the mechanical system has to be known. A "no-load" experiment can unravel friction by identifying the quadrature component in the impedance. So the only interest here is the "cosine part" of the imposed movement.

(ii) Influence of **inertia** can be cleared out with a linear regression over all frequencies of oscillation to the y-axis. Indeed, the only component influenced by frequency in this model for the "sine part" is the passive stiffness. Fig. 21 shows the result of the last step.

In fact, the steeper the slope is, the more problematic the "noise" becomes in the linear regression to find the stiffness. The inaccuracies or errors on stiffness dk for a given parallel translation i.e. offset error of the linear regression ξ and slope angle ϕ are given in Eqn. (1.15).

$$dk = \frac{\xi}{\cos(\phi)} \tag{1.15}$$

So, if the slope tends to be horizontal then $dk = \xi$ and if the slope tends to a vertical line then $dk \longrightarrow \infty$.

A *Nyquist diagram* or *phase diagram* is often used in literature as a convenient way to represent PMAS as vectors in frequency functions (Fig. 22). They are called joint stiffness vectors. Some features can be obtained through these vectors such as, the global shape or the path length. The latter being a good candidate in order to discriminate spastic and healthy groups in [16].

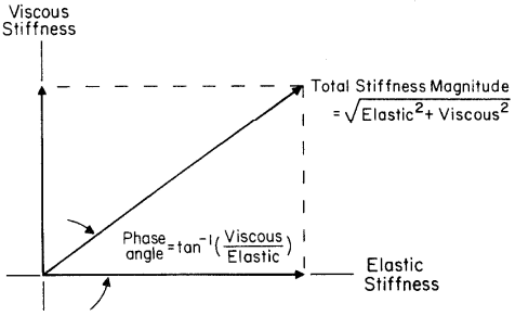


Fig. 22: Viscous and elastic torque components at a given frequency.

A possible improvement of the method is given in Appendix A.2 and needs to be examined.

1.5 Thesis objectives

The goal of this Master's thesis is to design and build an electromechanical device which can measure passive stiffness and viscosity of human fingers using Detrembleur's method. My job is to review the work of the previous Master's thesis [5] and to base my design on it.
The targeted populations are healthy subjects and people suffering from spasticity. It is intended to be used in a clinical institute under the supervision of qualified users. Given the medical nature of the device, the proximity of relatively fast movement of some parts of the machine calls for a high interest in the subject's security.
The method of Detrembleur does not aim to measure a "functional action" type movement as it is. It is designed to measure PMAS through a single joint excitation. But, the pinched action for example, essentially involves the MCP joint motion.

Through meetings with clinicians, objectives were clarified (Fig. 62 in Appendix B). Typically, to sense the choice of finger joints the machine has to measure. **Polyvalence** in the measurements of finger joint is keyword. Polyvalence of the type of finger joint, of the finger type, in the adaptation to the subject's morphology and finally to be able to take measures on both hand.

(i) The thumb is excluded. It is different from other finger types because of the fact that it is mostly moved by intrinsic muscles and that the primary axis of rotation of the thumb is not even close to coincide with other finger types. They are numerous added difficulties to consider when assessing the thumb.

(ii) Multiple fingers collectively moved to assess PMAS is not interesting for clinicians, it would be more difficult to spot relative involvement of fingers.

(iii) Individual assessment but for different fingers are more interesting. For a subject suffering from spasticity, given spastic posture, some fingers could be easier to measure then others.

(iv) A different type of joint assessment inside a finger is interesting. As mentioned in Section 1.1.2, MTU involvement in PMAS for DIP and MCP joints are supposedly quite distinctive.

(v) Finally, motor disorder is not always exhibited in both arms. Limiting the evaluation of spasticity to only one hand would therefore decrease the number of statistical data in

half for ulterior studies.

The goal using this device would be to firstly, identify normative values of PMAS in healthy subjects (normalized given the age, height, morphology and sex [39]). Secondly, to provide quantitative and objective data establishing the validity of a treatment "against" spasticity. And finally, the ultimate goal would be to use this machine in order to generate a diagnosis based on normative values.

Given the conclusion resulting from the conceptual design, the solution could be to mimic some features of the existing wrist device and apply it to this device.

2 Conceptual design

AFTER clarifying the context, the model on which the machine has to be built and the objectives of the thesis, there is a clear and concrete foundation to build on.
Based on the objective tree, built in collaboration with clinicians, a more descriptive and practical listing is drawn: the functional requirements.

2.1 Functional requirements

This step allows the establishment of all of the requirements and constraints the device needs to fulfill.
The two main functions are the PMAS measurements based on Detrembleur's method and the offer of finger measurement polyvalence. From there, multiple functional requirements are drawn and can be seen in Fig. 23. If the motion that needs to be performed by the finger is known, the resistance to it still has to be assessed. This is described in the next paragraphs.
Thanks to the past experiences of the two other machines assessing PMAS of human joints in *UCLouvain*, it is possible to estimate the order of precision needed for the angular position sensor and torque sensor. The most recent apparatus, the "wrist EOD" adapted by B.Herman and C.Detrembleur, has an angular coder precision of 0.8° [39].
The device's life cycle is obviously to be maximized. The number of revolutions made by a typical experimental procedure (in Fig. 38a) is approximately 700. To this day, the number of subjects that used the machine is about 2000. Hence, the order of revolutions is evaluated to more than $\mathcal{O}$ (10^6).
Concerning the constraint imposed, the security of the subject is paramount. Disengagement of the finger at any time must be allowed and restriction of the amplitude of movement by the actuator must set. It was observed that in every study on PMAS, the subject had to be

relaxed in order to have reproducible measures, hence the device must be comfortable and not disturbing or frightening.

The machine will possibly be transported in different establishments, which means it has to be able to go though doors and to be connected to any ordinary electrical supply.

The price limit is evaluated according to the founding granted to PhD G. Stoquart by the *Louvain Bionics*.

Author: Donatien Doumont	Specifications : **Electromechanical device for measuring passive stiffness and viscosity of human finger**	date: 13/02/20 version : 5
Context :	Design and building of a device in the frame of engineer master thesis. The device must be capable of measuring the human stiffness of fingers for a spastic patient as well as healthy one. The idea behind is to fulfill the lack of precision that current methods display for the measure of spasticity. The goal of this device is to put in motion fingers joints in order to retrieve their stiffness and viscosity. Ideally the latter has to be measured for two joints fingers which are mostly activated by 2 differents kind of muscles. The method to uncover the PMAS is the one used by PhD. Detrembleur based on angular position measure and torque measure over time for a joint sinewave movement.	
origin	**Main Functions** MF1 Measure PMAS based on Detrembleur s method. MF2 Offer polyvalence of measure.	
	Functional Requirement (FR)	**Criteria and levels**
D.D./B.H.	FR1 Measure joint(s) angular position	1.1 Resolution : level equivalent to the wrist EOD.
D.D./B.H.	FR2 Measure joint(s) torque	2.1 Resolution : level equivalent to the wrist EOD. 2.2 Range : 2.5 Nm<
B.H./B.H.	FR3 Generation of the movement	3.1 Amplitude : [+-10°, +-15°, +-20°] to stay in the linear range of the stiffness of joint. 3.2 Sinusoïdality level : % asymmetry, % sharp shape. 3.3 Frequency range : 3 to 15 Hz.
	FR4 Finger joint adaptation	4.1 Adapted to MCP joint. 4.2 Adapted to DIP joint. 4.3 Rigid system to avoid discomfort of patient during movement. 4.4 Adapted to different morphologies. 4.5 Adapted to multiple finger type. 4.6 Ambidextrous measurement. 4.7 Neutral position adjustement.

Fig. 23: Functional requirement part 1.

origin	**Constraints**	**Constraint Requirement (CR)**	**Criteria and levels**
B.H./D.D.	C1 Security	CR 1.1 No pain or harm for the patient	1.1.1 Disengagement of the fingers. 1.1.2 Restriction of amplitude of movement.
D.D.	C2 Comfort	CR 2.1 Noise	2.1 <+ 60 dB (limite of tiresome)
		CR 2.2 Comfortable tightening system for the patient	
C.D.	C3 Transportablity	CR 3.1 Land on table	
		CR 3.2 Go through doors	3.2 <630 mm of larger
D.D.	C4 Electical supply	CR 4.1 Voltage supply	4.1 230 V
B.H.	C5 Cost	CR 5.1 Budget	5.1 <5000 euro (TVA incl.)

Fig. 24: Functional requirement part 2.

Torque evaluation This describe the simulation of the resistant torque produced by the finger in the worst case, in order to give a certain level for the technical functions. Hence certain types of torque sensors or motors can be eliminated in the search of solutions. Data for these evaluations are listed in Table 1.

- Maximum amplitude and frequency of sinusoidal motion are chosen.
- Total inertia is assumed to be composed of the finger's inertia, taken at the MCP joint (worst case), and of a steel shaft that is supposed to represent the system. It is also assumed that the finger and the shaft are both straight cylinders. Thanks to anthropological studies [52], the dimensions of the largest finger are selected. The mechanism's inertia is neglected in this pre-dimensioning evaluation, which is a reasonable assumption given the results in Section 3.2.1 for the four bar mechanism.

Symbol	Value	Units
A_{p-p}	40	deg
Freq	15	Hz
κ	0.6	$Nm.rad^{-1}$
η	0.06	$Nm.(rad/s)^{-1}$
ρ_f	1170	$kg.m^{-3}$
L_f	11.52	cm
D_f	2.5	cm
ρ_{steel}	7860	$kg.m^{-3}$
L_s	12.5	cm
D_s	1	cm

Table 1: Pre-dimensioning data

It is computed in Eqs. (2.1) to (2.3).

$$\begin{aligned} I_{finger} &= I_{cyl,x} + m \cdot \left(\frac{L}{2}\right)^2 \\ &= m \cdot \left(\frac{D^2}{16} + \frac{L^2}{12} + \frac{L^2}{4}\right) \end{aligned} \tag{2.1}$$

$$I_{shaft} = I_{cyl,z} = \frac{M}{2} \cdot \frac{D^2}{4} \tag{2.2}$$

Where

$$m_{cyl} = \rho \cdot \pi \left(\frac{D}{2}\right)^2 \cdot L \tag{2.3}$$

Hence, the total inertia is $I_{tot} = I_{finger} + I_{shaft} \simeq 3200 g.cm^2$.
This inertia is very high. It is used in order to have an upper bound of torque to measure. The measured inertia in [12] is far smaller. It is about 750 g.cm^2.

- The passive stiffness and viscosity of the finger at the MCP are determined thanks to the works of [41] and [16]. Lehmann [16] states that spastic subjects joints are approximately twice the value of healthy subjects. Hence the maximum values of κ and η are taken and given in Table 1.
- The mechanism's friction is neglected, as the mechanism has the objective of limiting this component as much as possible in the measured torque.
- Gravity is also neglected, as the motion is made in the transverse plane of the hand around the z-axis.

With these assumptions, the results are depicted in Fig. 25[11] and maximum torque produced at 15Hz is about :

$$\boxed{M_{max}^{finger} \simeq 2200\, mNm}$$

[11] Fig. 25 does not intend to represent an experiment that will be conducted to assess PMAS. The speed profile can be seen in Fig. 38a.

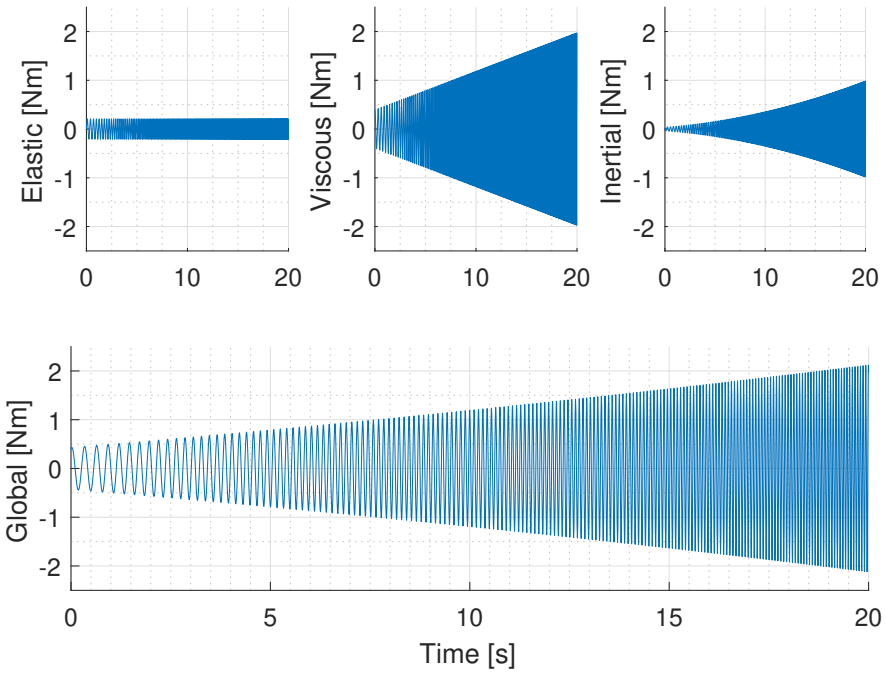


Fig. 25: Resistance of the mechanism and MCP finger joint : simulated behaviour for a progressive increase of velocity from 3 Hz to 15 Hz.

2.2 Search for solutions

The most critical technical functions to be performed by this machine are the measurement of joint(s), angular position (FR1) and measurement of joint(s) torque (FR2). The previous Master's thesis [5] considers a wide number of possible mechanisms and sensory applications in order to be used with Detrembleur's method with typical evaluation criteria : simplicity, compacity, fiability, precision and ergonomy. I consider, here, a subset of them.
The key words to keep in mind when searching the best adapted solution for a design problem are summed up in the following sentence : "*Simple is beautiful*".

2.2.1 Movement generation review

The electromechanical device will use an electrical type of actuator. Hence, the actuator provides a rotational motion. Rotary-to-rotary mechanisms seem to be better suited for this application, since the goal is a rotating motion. Displacement of any kind can be converted into rotary to linear and inversely but it would, for example, ultimately result in additional inaccuracies through mechanical backlash. Let's recall that high precision is needed for the generation of movement in order to keep the linear assumption of the method.

Rotary to linear mechanism A quick reminder of some of these types of mechanisms are given, such as the crank mechanism, rack and pinion and lead screw driver.

- Crank-rod or slider-crank mechanism : It is a rotary to linear movement mechanism. It is composed of 2 moving bars and a slider constrained by a bearing block. Given the slider race needed by the requirements, as described in Fig. 27, λ must be maximised depending on the available space. The kinematic made by this mechanism is given in Eqn. (2.4).

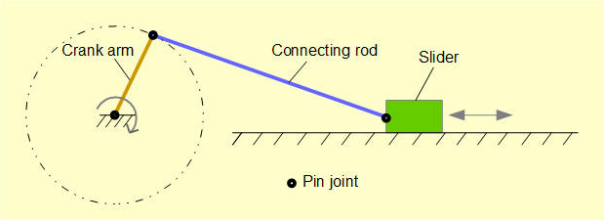
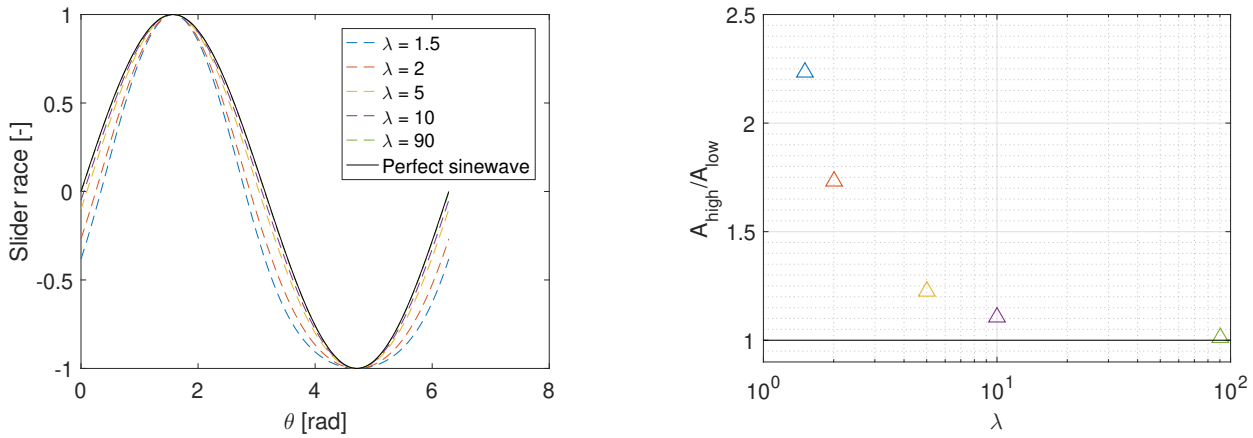


Fig. 26: Slider-crank mechanism kinematic representation[53].

$$X = R \cdot \left(\sin(\theta) + \sqrt{\lambda^2 - \cos^2(\theta)} \right) \tag{2.4}$$

Where L is the rod length, R is the crank radius, θ the crank angle and λ[12] is the ratio $\frac{L}{R}$.

[12]This parameter is used to express the deviation from a pure sinewave, but others could have been used e.g. RMS error on slope. The study only aims to interpret the influence of λ on the sinewave deviation.



(a) (b)

Fig. 27: Slider crank deviation from pure sinewave function with parameter λ : (b) shows the deviation of amplitude from x-axis symmetry versus λ.

- Rack and pinion mechanism : It uses a gear wheel and rack that moves linearly according to the wheel rotation where the actuation is located. It is at the software level (meaning at the control level of the actuator) that the change of amplitude results without any mechanical intervention, but physical securities are needed. [13]. Small amplitude of movement combined with backlash limits the precision of movement.

- Lead screw driver : Once again, the rotary motion of the actuation is transformed in a linear one through a helical path i.e. the thread of the rod. It is rather compact and can be used in large load applications.
  It can provide high precision of movement, but it is suited for slow application. Moreover, it induces more friction compared to others. Once again, the amplitude of sinusoidal movement is done at the software level and physical safety is needed.

Direct drive The most obvious choice is the direct drive of a sinusoidal waveform from the actuator. As soon as the feedback command is smooth and fast enough for 15 Hz. It is an unconstrained movement. This solution, which involves no gearhead, is avoided because of the possible backlash involved (creates hysteresis in the motion). Furthermore, given the torque requirements, the motor must be "torqueful".

Came mechanism Came mechanisms are widely used in automatic machineries, instruments and steering controls. They generate diversified and complicated types of motion with

[13] It is also possible to induce a rotary motion with a curved track.

simple and compact systems.
A cylindrical shape of came, as in Fig. 28, can transform a circular motion into a sinusoidal one.
The precision depends on the manufacturing process. They are more suitable for low speed and low torque applications. It can be worn out and induces noise.

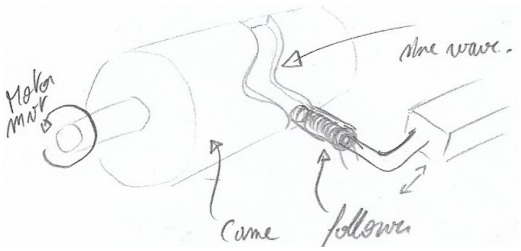


Fig. 28: Came morphological graph.

Four bar mechanism A schematic of this mechanism is given in Fig. 29. It is a restricted movement. Given the length of the bar, this mechanism can produce different kinds of movements. The Grashof theorem [54] states that there exists at least one link which can fully revolve in respect to the other three links if

$$l + s \leqslant p + q \tag{2.5}$$

and none of the four links can make a full revolution if

$$l + s > p + q \tag{2.6}$$

Where the links length are ranged as

$$l > p \geqslant q > s.$$

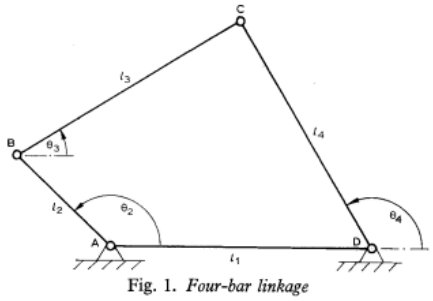


Fig. 29: Four bar linkage schematic 1.

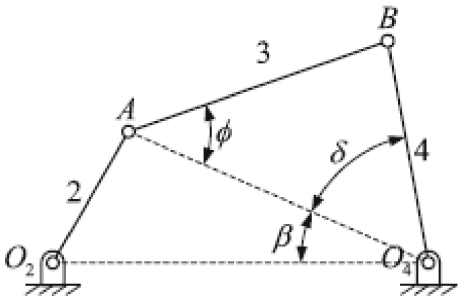


Fig. 30: Four bar linkage schematic 2.

In the next section, the bar 2 will be called the crank, bar 3 the coupler and bar 4 the follower. In order to have a crank - pendulum configuration, Eqn. (2.5) must be satisfied and if so, an angle θ_{in} produced by the actuator (θ_2 in figure) creates a rotary movement θ_{out} (θ_4 in figure)

as given in Eqs. (2.7) to (2.11).

$$\overline{O_4A} = \sqrt{l_1^2 + l_2^2 - l_1 \cdot l_2 \cdot \cos(\theta_{in})} \tag{2.7}$$

$$\beta = \arcsin\left(\frac{l_2 \cdot \sin(\theta_{in})}{\overline{O_4A}}\right) \tag{2.8}$$

$$\phi = \arccos\left(\frac{l_3^2 + \overline{O_4A}^2 - l_4^2}{2 \cdot l_3 \cdot \overline{O_4A}}\right) \tag{2.9}$$

$$\delta = \arcsin\left(\frac{l_3 \cdot \sin(\phi)}{l_4}\right) \tag{2.10}$$

$$\theta_{out} = 180° - (\beta + \delta) \tag{2.11}$$

This mechanism has the advantage of having a minimum number of pieces in movement to create a rotary quasi sinusoidal motion by actuating it with constant speed. It is intrinsically limited in its amplitude and consequently imposes a manual intervention for amplitude adjustment.
Optimizations of the bar are available in Section 3.1.

Outcome on possible mechanisms Functional requirements are expected to generate a rotary sinusoidal motion over more than 1 million motion cycles. Rotary to linear mechanisms, which would require an additional system to transform the motion, are rejected and the came mechanism is not suited for this application.

This result agrees with what was found in the previous thesis [5]. The four bar and direct drive are kept. One of these two solutions must still be selected. This demands pushing the comparison a little bit further in the dimensioning step. This is done in Section 2.3.1.

2.2.2 Measurement review

The functional requirements ask for a measurement method to sense the finger's resistance and motion. Given the range of frequency, the type of transducer must be rather robust to vibrations.

Angular position measurement Angular motion can be measured by various transducers which are listed in Fig. 64 in Appendix B. Encoders are the most widely used in medical and robotic applications. These are digital sensors. Either magnetic technology using hall effects are used or optical ones including photoelectric transducers are.

- Incremental encoder called **relative encoder** works in respect to a starting (and an ending) position (see Fig. 31 on the left). In other words, a "homing routine" is needed to establish a known referenced position from the start at each activation of the power. They only need two bands of holes and two (to three) transducers, which makes them simpler then their absolute counterparts.
- Coded position sensors called **absolute encoder** on the other hand are designed to know its position at any time without initialization procedures, to know its absolute position (see Fig. 31 on the right). They provide binary coded words that are directly translated through specific code. They need $\log_2 N$ bands of holes and as much transducers where N is the number of bits. They typically cost twice as much as relative ones.

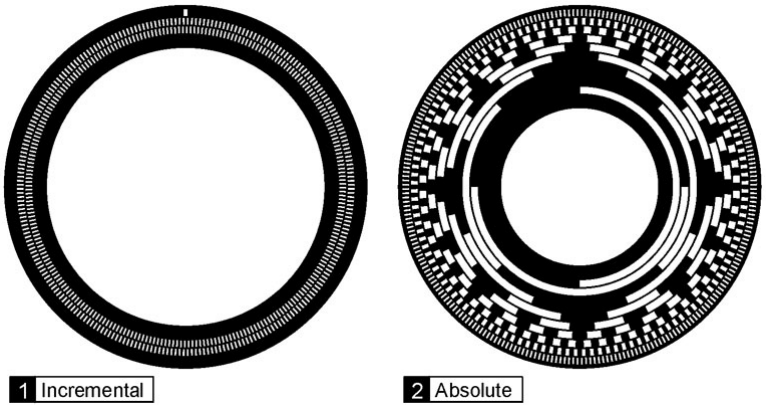


Fig. 31: Encoder disk schematic of incremental and absolute encoder which consists of a black disk and cut holes in between.

A 12-bit resolution for instance, has a precision (least significant bit) of

$$LSB_{WEIGHT} = 360° \div 2^{12} \simeq 0.09 \left[\frac{°}{bit}\right]$$

Torque measurement The simplest solution with a rotary motion is to directly measure the torque produced by the finger. There are two types of measurements that can be made depending on the sensor's location : 1) before the actuator or after the load, a reaction torque[14] is measured or 2) if the measurement is made in the mechanical chain, a rotary torque is measured (see Fig. 65 in Appendix B). There exists two main types of torque transducers : non-contact and contact torque sensors. There are multiple non-contact designs and technologies but essentially, either optic or magnetic are used to make the bridge from the rotor and the stator, just like electronically commutated motors.
Force/torque sensors are made of an elastic body, which undergoes strains/deformations under the force's action to be measured.
Strain gauges are resistive sensors that measure mechanical deformations, there are called impedimetric sensors. They provide long-term stability, wide temperature-range operation, and more importantly, they are immune to vibrations when compared to other technologies. The rotor is composed of multiple strain gauges to measure deformation of the rotating shaft, also called torsion bar. Subjected to deformation, strain gauge responds with electrical changes in resistance as Eqn. (2.12). The signal is then conditioned and torque can be recorded through an electrical signal in volts, proportionally to deformation.

$$\frac{\Delta R}{R} = S_e \, \epsilon \tag{2.12}$$

Where S_e is the sensitivity of the strain gauge.
The working principle with contact designs is the same, but the coupling between the rotor and stator is done through contact brushes.

Force sensors could also be used to record the torque, but it would add unnecessary complex systems into the mechanism. For example, the fingertip force could be recorded as it was done in [49] and [12]. But it would bring more inertia in the mechanism and added compliance, which would decrease the precision of the method as explained in the next section.
Solutions involving force sensors are excluded.

Outcome For the angular position measure, the absolute encoder is selected. Today's coded position sensors have definitely enough resolution and are preferred in order to forget about a homing routine.
For this application, the torque meter placed closest to the finger is called in order to have the

[14] Reaction torque is the force that acts on an object when it is not free to rotate.

smallest inertia attributable to the mechanism. Depending on the type of kinematic used to put the finger in motion, a reaction torque or a rotary torque will be measured.

2.2.3 Morphological solutions graphs

The objective is to generate alternative solutions involving the main functions and their functional requirements to find the one best suited for the problem.

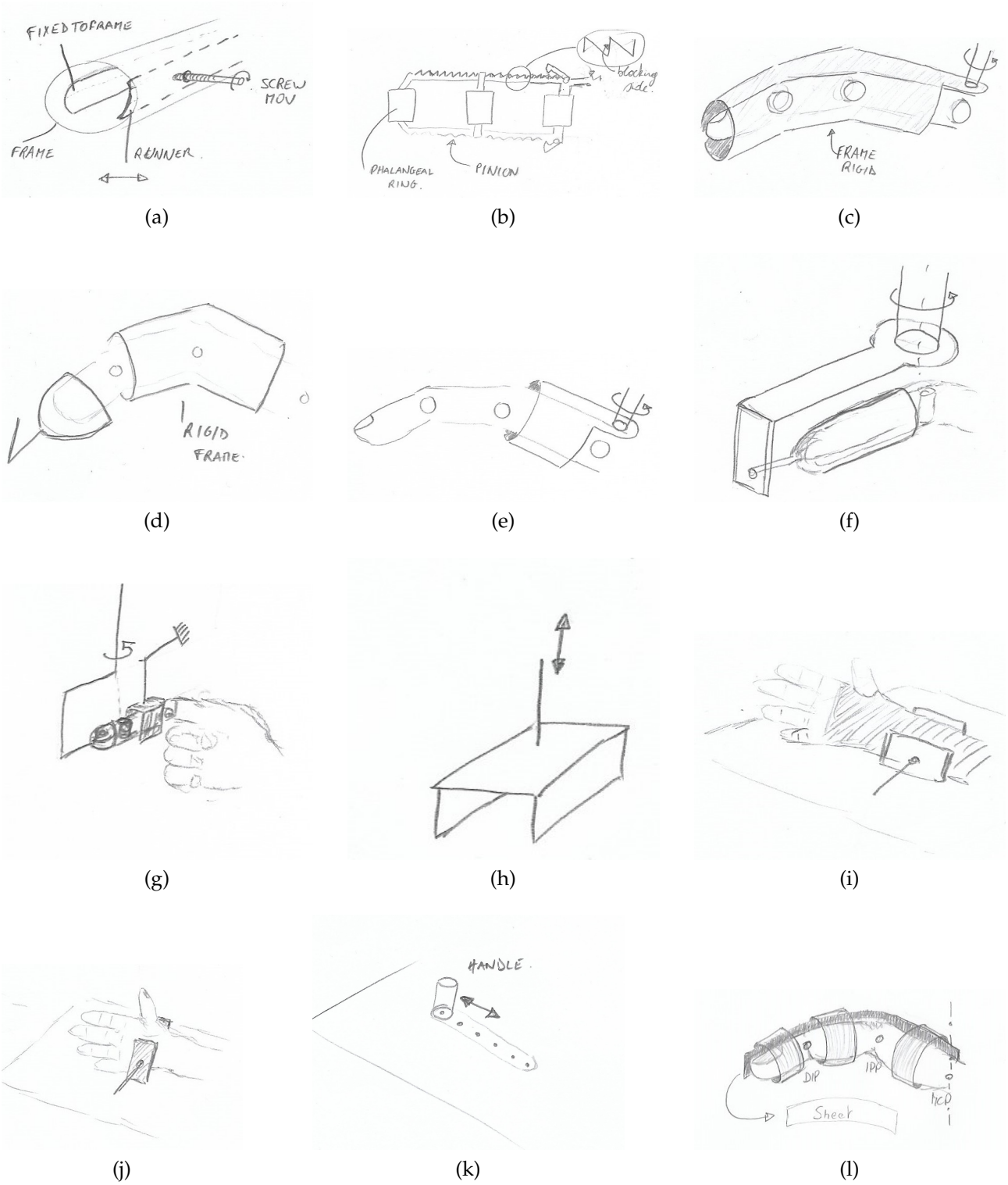
Binding system The finger's binding system must be rigid. In case of MCP measurement, only the first phalange needs to be bound with the system in order to put the finger in motion (Fig. 32e). But this configuration is uncomfortable for the subject if the rest of the finger is able to move, especially at high frequencies. Hence a rigid frame surrounding the finger is preferred.
The frame can be modeled to take the finger's shape at rest or straightened.
It is also necessary to somehow fix the hand. It can take the shape of a gripping handle (Fig. 32k). However, the coupling occurring between fingers could hinder the measurements or even produce unwanted voluntary forces to the assessed fingers.
A system where the hand's palm is clamped (Fig. 32j) seems to be better suited for this kind of measurement. This is what is done in the device of Kuo et al. [12].
As mentioned, the wrist has an influence on the resistance of the MCP. Hence, the subject's arm should be able to move freely in order to be able to set its own neutral position.

A binding system involving a metal sheet (with ferromagnetic properties) attached with velcro tape at each phalange is also conceptualized in Fig. 32l. The idea is to give the liberty to the subject to disengage its finger from the mechanism (cfr. constraint requirement). With magnets housed in the driving arm, the coupling can be made.

Overall configuration Fig. 33 shows different imagined device configurations. The biggest issues with these graphs come from the fact that inertia is proportional to the distance squared from the axis of rotation. An arm that clamps the finger at the front of it (such as in Kuo et al. [12]), does not represent a suitable solution. Furthermore, compliance of the arm could undermine the measurement.
The solutions in Figs. 33h to 33j with the driven arm which is offset from the finger side, drastically reduces the inertia of the mechanism and with it, the compliance inherent to the arm. Of course, an arm parallel to the driving finger is required in these cases.

For these solutions, two kinds of mechanical assembly locations are imagined. The configuration called "beneath" and the "above" configuration.
The first one has the advantage of giving an open visual space. The subject's hand is completely visible to him/her at any time. On the other hand, this configuration required a lot of space beneath the subject's hand. Thus, it is not assured that the machine could simply be placed on a table. It could result in an uncomfortable position of the subject's arm.
The "above" configuration consists of an actuation assembly located above the finger's interface[15].
The system must adapt to different types of finger joints i.e. MCP and DIP of different fingers (FR4). The solution with rail offers a very easy configurable choice of the finger to measure. Adding a rail to both of these configurations is possible.

[15]It is the region where the machine's mechanism comes in contact with the subject's finger.



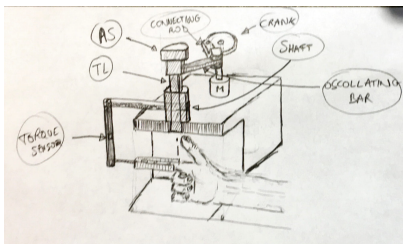
(a) (b) (c)

(d) (e) (f)

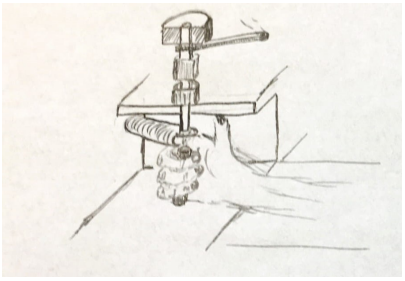
(g) (h) (i)

(j) (k) (l)

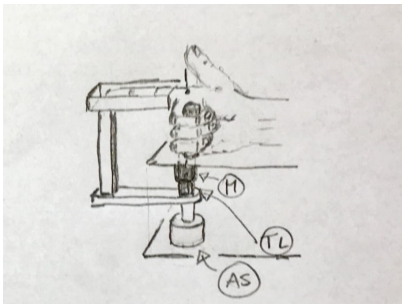
Fig. 32: Morphological graphs of binding system to finger.



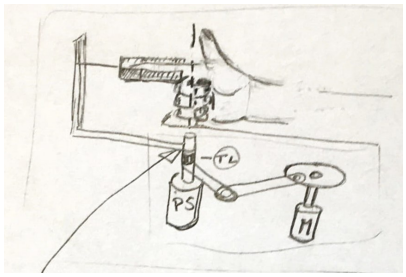
(a)



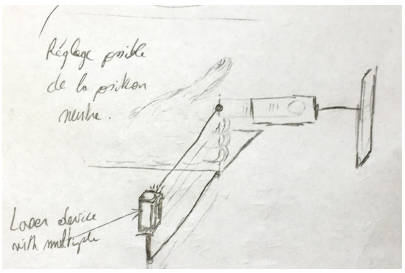
(b)



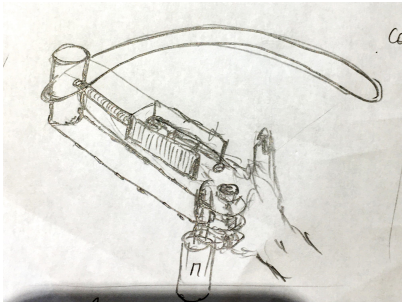
(c)



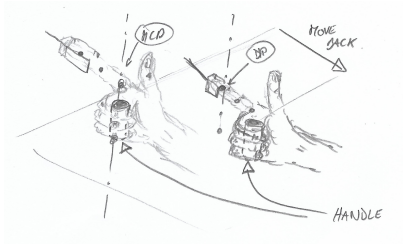
(d)



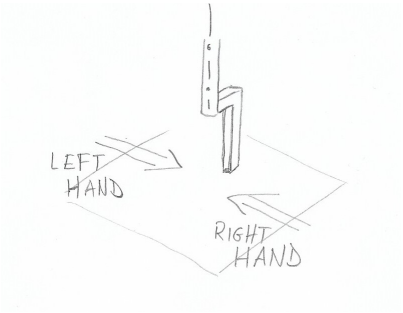
(e)



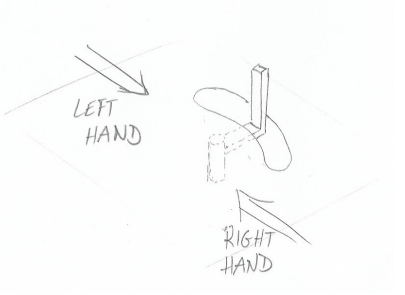
(f)



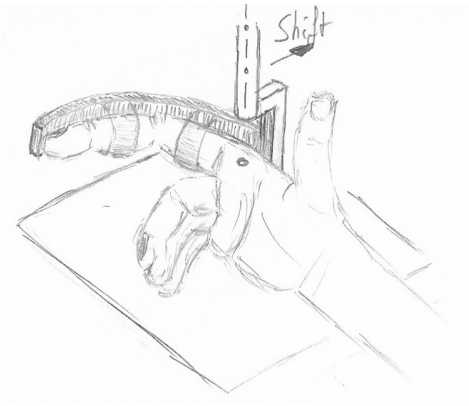
(g)



(h)



(i)



(j)

Fig. 33: Morphological graphs of the device's different configuration possibilities : (a) (Above config.) Section view with front driven arm. (b) (Above config.) Section view of a direct MCP driving. (c) (beneath config.) Direct driving (d) (beneath config.) Four bar driving. (e) Laser used to position the hand. (f) (beneath config.) Front driven arm with an arc-shaped gap. (g) Front driven arm adjustment to DIP and MCP measurements. (h)-(j) Above and beneath config. of shifted shaft.

2.3 Comparative studies

2.3.1 Four bar drive *versus* direct drive

As mentioned in previous sections, the four bar mechanism and direct drive mechanism are shortlisted for the movement generation. In order to find the one best suited, it is necessary to enter into prototyping details. The motor and control requirements for both configurations, amongst others, need to be investigated.

In Table 2 informations relative to security criteria, sinusoidal movement precision and adjustment, overall cost and homing routine requirements are gathered.

Criteria		Four bar drive		Direct drive	
Security	**/5**	- Amplitude constrained by design	**5**	- Motor oversizing prohibited - Mechanical constraint needed - Added soft/hardware limitation for torque - Smallest number of moving parts	**2**
Sinusoidal motion	**/3**	- Mechanical change of amplitude - Very close to perfect sinewave - Driven at constant velocity	**2**	- Software change of amplitude - Motor encoder needed - Commutation with FOC needed	**2**
Cost	**/2**	- Speed servo controller sufficient - Added number of mechanical parts for the mechanism	**2**	- High torque capacity motor required - Position servo controller required - Added security units of hardware	**1**
Homing routine	**/1**	- Not necessary even with relative encoder	**1**	- Required with relative encoder	**0**
Total :		10		5	

Table 2: Comparative table between four bar and direct drive solutions.

Four bar drive

The four bar drive mechanically constraints the amplitude of the output motion, which ensures that the finger will never be moved outside a safe space. Precautions must still be taken so that the subject is able to withdraw its hand from the mechanism.
Adjustment of amplitude for the movement must be changed by the user manually at the crank level. By using appropriate tools, manual changes enclosed in safe areas can on the contrary, be better suited than software changes for the user.
An optimization on the bar dimension of the 4-bar allows to create a practically pure sinewave with RMS error of $\mathcal{O}$ (10^{-3} degree) (Section 3.1).
A classic homing routine with end-stop sensors is not necessary, even with relative encoders.

With only one period of motion activated, minimum and maximum positions can be retrieved and kept in memory.
A constant velocity driven motor will carry less constrains to it.

Direct drive

Motor abilities in case of direct drive mechanisms must be set to a minimum. The motor can not be oversized. In the event of a failure of any kind, the security of the subject must be assured and special attention must be given to this mechanism. Torque limitation at the hardware via limitations of supply current in the controller and software level in accordance to the amplitude of the movement (torque is a function of amplitude of motion). Furthermore, mechanical constraints such as end-stop sensors must be added to avoid overshoot of amplitude in case of failure and shut off of the actuation.
Nevertheless, this mechanism involves the smallest number of mechanical parts in motion possible.
More precise control mechanisms must be involved. A brushless motor with N pair of poles has a resolution for position control of 360°/(6*N) thanks to six different signal combinations per revolution. Meaning that a 7.5deg of accuracy can be expected with a 8-poles motor, which is certainly not sufficient. Hence, an encoder dedicated to the motor positioning is necessary.
Moreover, an expert from *mdp Maxon France* advised to use a more advanced commutation principle than the classic block commutation. Sinusoidal commutation using field-oriented control provides more precise positioning and allows for the cancellation of torque ripple. In conclusion, more expensive electronics are required.

Outcome This study's outcome is clear, a solution involving a **four bar drive** is more favorable for this application.
This finding facilitates the prototyping step. Indeed, the design can mimic some aspects of the wrist PMAS device created in *UCLouvain*. Especially at the control level, the computer program will essentially be the same.

2.3.2 Kinematic comparison of finger's driving system

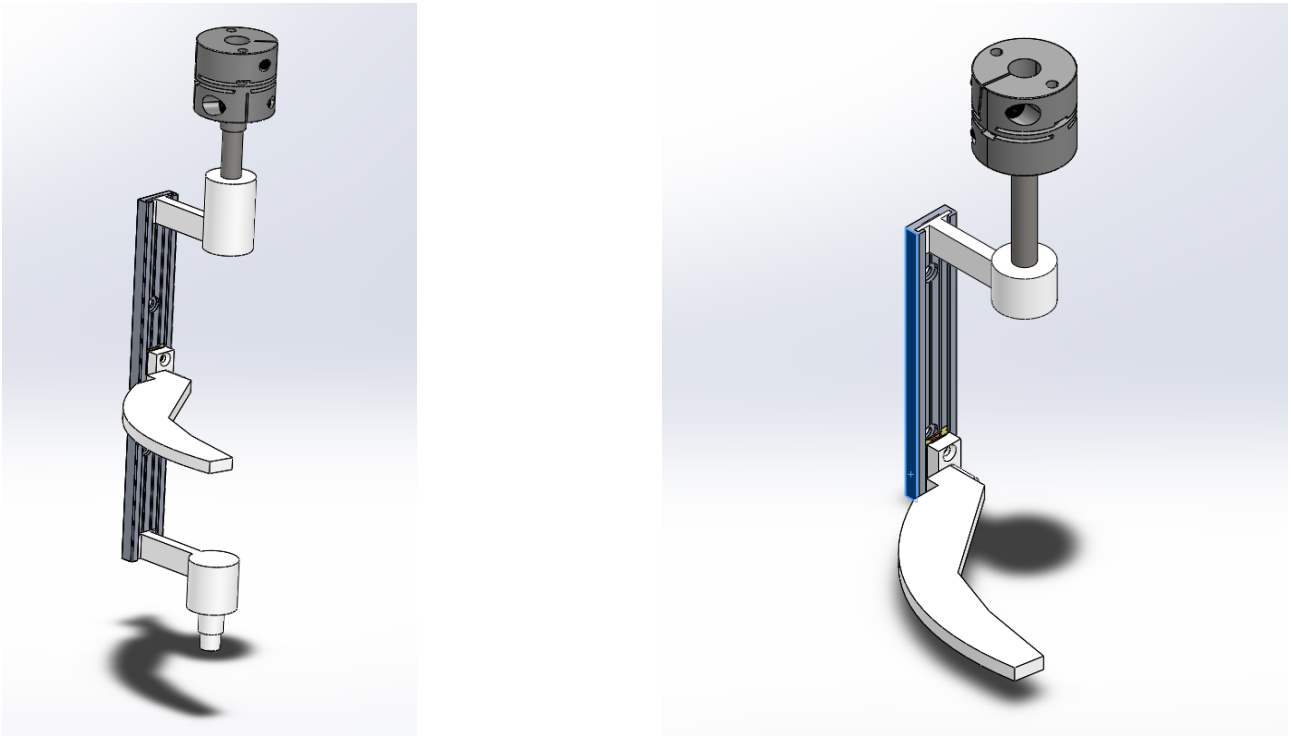
For the shifted shaft and finger driving arm, two different kinematics are studied. The first one in Fig. 34a is composed of a rail, which is maintained by two pivots at both ends. With this configuration, the lower pivot does not experience any force. Indeed, the principal stress

component of the column assembly, is torsion. In addition, this configuration adds more inertia to the mechanism.

The second one, also composed of a rail, is only sustained by an upper pivot. The second is the best option but still needs to be improved. This is done in Section 3.3.5. This requires the use of a torque meter that measures a rotary torque.

These two solutions involve a driving finger arm that can slide freely along a rail. This feature is really interesting in the machine's design. It allows for the functional requirement to be met (FR4).

Furthermore, the finger arm can rotate around the horizontal. This allows the assessment of finger joints from the right hand or the left hand.



(a) (b)

Fig. 34: Two types of eccentric arm kinematics : (a) Version with 2 spaced pivots (b) Version in cantilever.

3 Prototype

In this chapter, the prototype is described. The first section aimed to find the optimized bar dimensions for the four bar mechanism. A procedural method is established. In the following section, the motor and sensors are selected and the electrical installation is depicted. I concluded this chapter with the detailed design of the prototype and its final assessments.

3.1 Kinematic consideration

In this section, the procedures used in order to optimize the bar dimensions and the global kinematic diagram are detailed.

In the previous Master's thesis [5], the bar dimensions were deduced to minimized "fast return" motion. This parameter is not the best choice to fit a sinewave. It only makes sure that the same amount of time is used for the clockwise and anti-clockwise motion at the output angle.
The level of the fast return mechanism is defined with the Q symbol as Eqn. (3.1) (β is given in Fig. 30).

$$Q = \frac{180° + \beta}{180° - \beta} \tag{3.1}$$

This optimization is multi-dimensioned, meaning that four elements need to be found and optimized. I am choosing to discriminate through a mean squared error between a fitted true sinewave, with the output angular position and with the output angular acceleration.
The sinewave function (Eqn. (3.2)) that is used, is fitted knowing the maximum and minimum angles made by the four bar and to find the "best fit" through a delay that minimizes the RMS

error (code in Appendix B.1).

$$x_{fit} = A \cdot \sin\left(\theta_{in}(t) + \phi\right) + C \tag{3.2}$$

Where

$$\begin{cases} A &= max(\theta_{out}) - min(\theta_{out})/2 \\ \phi &= min(RMS(x_{fit} - \theta_{out})) \\ C &= max(\theta_{out}) + min(\theta_{out})/2 \end{cases}$$

The bar dimensions are chosen using the following procedure :

1. First the length of bar 1 (or more exactly the distance between the two pivots) has to be placed given the device's overall dimensions. The length needs to be as large as possible.

2. The follower (bar 4) needs to be small, as seen in Fig. 35b. just like the crank mechanism where the parameter λ had to be maximized, the fraction between bar 1 and bar 4 also has to be.

3. The crank (bar 2) dimension is directly dependent on the length of the follower and the amplitude of required oscillating movements at the output angle. Indeed, with a small approximation, length of the crank is found with Eqn. (3.3). In reality, the amplitude is a little larger by making this approximation, but this is not an issue. As soon as the amplitude is known, the accuracy is not that important for the precision of the method.

$$L_2 \simeq L_4 \cdot \sin\left(A\right) \tag{3.3}$$

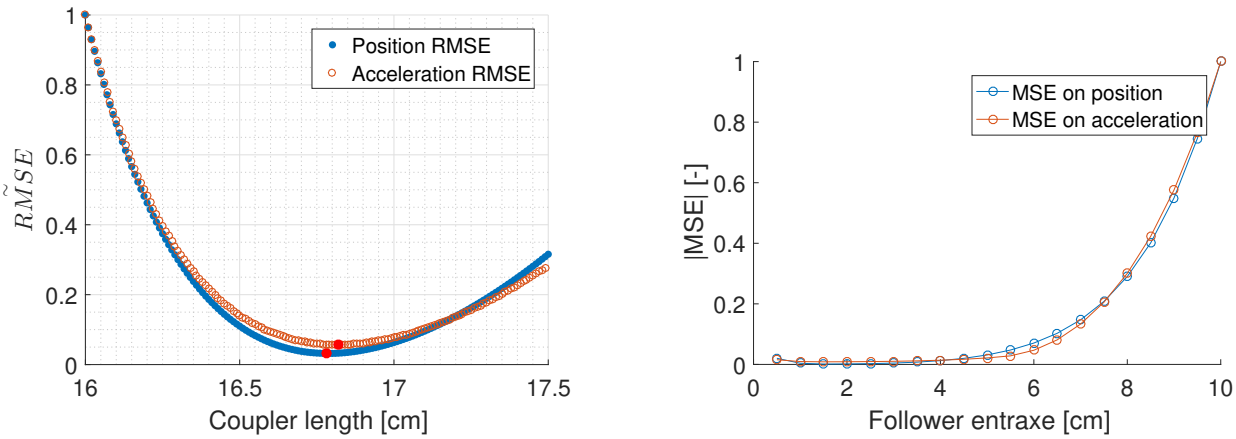
4. The coupler (bar 3) length is the one optimized given the length of the other. Two types of optimizations are done. One on the RMSE between the output angular position and the fitted sinewave, and the other between the latter and the output angular acceleration. They both give very similar coupler lengths (Table 3).

This procedure to find the best dimension for the bar is done for the three different required amplitudes.

$$\boxed{Bar\,3 = 16.85cm} \tag{3.4}$$

Ideally, different coupler lengths should be used for each amplitude in addition to a crank length adjustment. However, the results are very close, as seen in Table 3. By making a

trade-off between all of them, the RMSE is, at it's worst, less than an 0.035 degree, which is perfectly acceptable with the coupler dimension in Eqn. (3.4).



(a) (b)

Fig. 35: Four bar dimension optimization of (a) the coupler bar length and (b) the follower bar length with 20deg amplitude peak-to-peak according to the normalized RMSE.

	Amplitude			Units
	+-10°	+-15°	+-20°	
Bar 1		18		cm
Bar 2	0.69	1.04	1.37	cm
Bar 3	16.78	16.83	16.88	cm
	16.82	16.89	16.98	cm
Bar 4		4		cm
RMSE	1.32	8.34	33.82	mdeg

Table 3: Four bar mechanism dimensions.

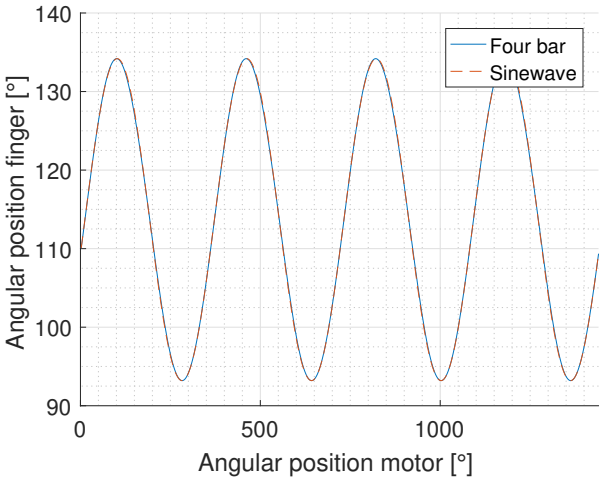


Fig. 36: Robotran analysis : angular position of the chosen bar length of the four bar versus a fitted pure sinewave.

More optimization results can be found in Table 3. Furthermore, an analysis is also conducted on *Robotran* as the first validation of the four bar and can be found in Appendix A.3. The results are given in Fig. 36.

The overall kinematic diagram can be found in Fig. 37. It is composed of the motor (M), encoder and torque meter (T.M.). Elastic couplings are used to connect each unit. Two standard ball bearings are used for each shaft, to carry radial loads.
The finger interface part has improved comparatively to the kinematic comparison in Section 2.3.2 and its detailed components are found in Section 3.3.5.

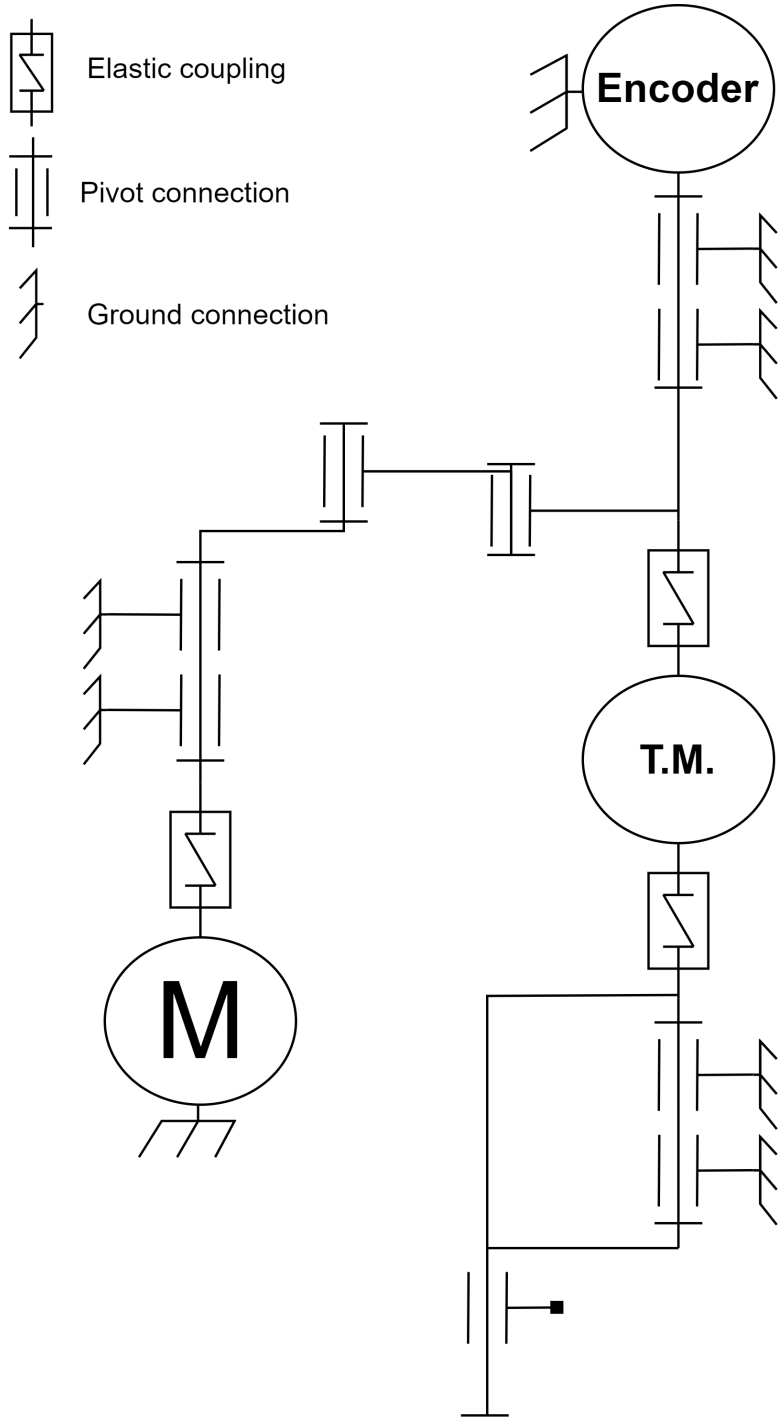


Fig. 37: Overall kinematic diagram.

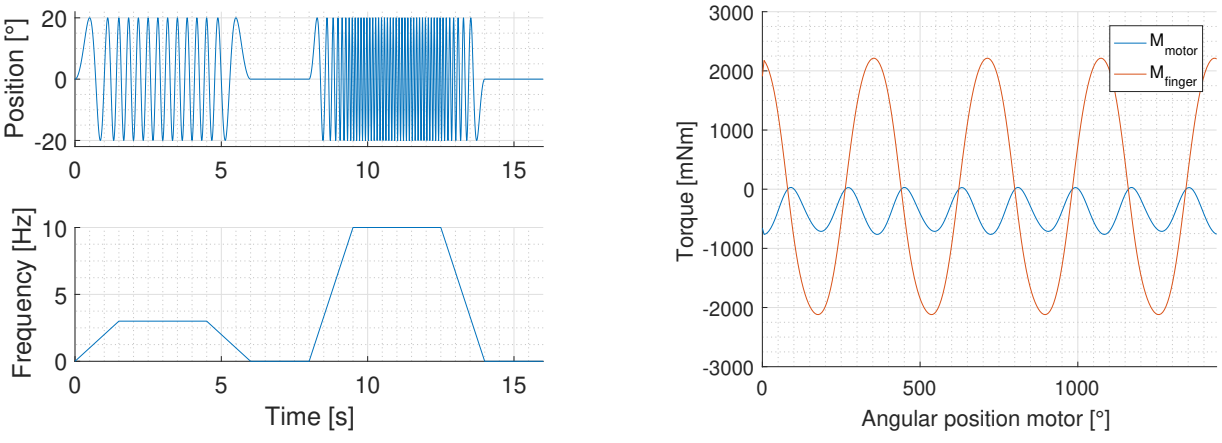
3.2 Actuation, sensing and control

The electrical installation and computer control code are completely taken from the wrist device and simply adapted to the required actuation and sensor. Further more, the range of frequency is extended for this finger device from 12Hz to 15Hz given the type of joint moved.

3.2.1 Motor selection

The following procedure is the one suggested by *Maxon* group in order to select a motor of their catalog. Given the number of required cycles (million ones) and it's quite modest price, electrically commutated (EC) - also named brushless - motors are preferred over brushed ones. Indeed, the brushed motor has an expectancy of 1000 hours compared to 10.000 hours for EC motors, where it is the ball bearings that limit the service life.
The selection method here is a *direct* method, meaning that from a load requirement, an actuator is chosen.

1. **Load definition** : First of all, the speed profile has to be determined along with the RMS and peak values of the torque over a typical evaluation.



(a) (b)

Fig. 38: Load definition : (a) *MATLAB* analysis : typical speed profile for 3Hz and 10Hz. (b) *Robotran* analysis : torque at $\pm$ 20° amplitude and 3Hz.

The speed profile in Fig. 38a is evaluated given the measure already done by the ankle EOD. Indeed, it goes through a constant acceleration during approximately 1.5sec, reaches the required frequency, decelerates during 1.5sec and then 2sec of relaxation. Small positive torque of about 5mNm can be seen in the load study of Fig. 38b, meaning that there are moments where the motor must brake[16].

[16]This observation is even more accurate by taking into account non idealities of human joint resistance.

$$M_{RMS} = \sqrt{\frac{1}{\Delta T}\sum_{i=1}^{N} t_i \cdot M_i^2} \tag{3.5}$$

As explained in Section 2.1, the inertia is evaluated for the larger existing finger and subjects as spastic as possible. In case of a spastic patient, it makes sense to lower the amplitude of oscillation and restrict it to $\pm$ 15deg for the motor selection. Indeed, the pROM is smaller for spastic subjects [55]. The evaluation of the root's mean square for a whole experimentation (see Eqn. (3.5)), with frequencies ranging from 3 Hz to 15 Hz according to the speed profile in Fig. 38a at 30 deg peak-to-peak and peak torque at 15 Hz gives:

$$\boxed{M_{RMS}^{motor} \simeq 110\,Nm} \qquad \boxed{M_{peak,\,15\,Hz}^{motor} \simeq 450\,mNm} \qquad \boxed{N_{max}^{motor} = 900\,rpm}$$

2. **Gearhead selection** : In this particular application, gearhead is prohibited to avoid backlash, as already mentioned.

3. **Motor selection** : The selection of the motor can be drawn in a speed-torque diagram. In this diagram, the line is characterized by the no-load speed n_0, stall torque M_H and of course the gradient of the curve $\Delta n / \Delta M$.
   In a thermal point of view, the temperature rises in the winding are the most critical parameters to consider. From this, one can draw the continuous operation allowed by the motor on the left of the vertical line that defines the nominal torque. On the right, only short term operations are allowed.

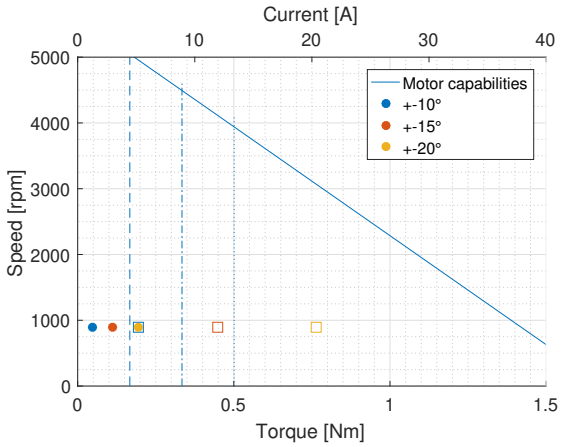


Fig. 39: Speed-torque diagram. Motor abilities : the solid line is the speed-torque line, it is the locus of nominal voltage applied to the motor depending on torque; the dashed line is the RMS torque value of the motor (dotted line is M_{RMS}x2 and dash-dot is M_{RMS}x3). Load : dots represent the RMS value and squares represent the peak value at 15Hz.

The rule is the following: with M_{nom} the nominal torque of the motor and Δt the approximate duration at which the motor can sustain this load.

$$\text{(i)}\ M_L = M_{nom}x2 \longrightarrow \Delta t \simeq 5\tau_w.$$

$$\text{(ii)}\ M_L = M_{nom}x2.5 \longrightarrow \Delta t \simeq \tau_w.$$

$$\text{(iii)}\ M_L = M_{nom}x3 \longrightarrow \Delta t \simeq 0.6\tau_w.$$

Multiple motors are admissible in the *Maxon* catalog. Each of the product lines from *Maxon* have there own characteristics that can be found in Table 10. The line EC flat seems to better meet the specifications, given their high nominal torque capabilities. Moreover, at this stage of the mechanical assembly, the inertia does not have to be minimized. The torque meter measures the torque from its output side. Hence, the inertial components at its input are not relevant.
It is advised to stay in a limited range of power. In case of unexpected events, the abilities of the motor must be limited.

Name	Value	Units
Power	80	W
Nominal voltage	24	V
Nominal torque	167	mNm
Speed constant	236	rpm/V
Torque constant	40.4	mNm/A
No load current	270	mA
No load speed	5600	rpm
Max radial load	15.1	N
Thermal time constant winding	34	s
Inertia	181	g.cm^2

Table 4: Characteristic and specification of the EC 45 flat 80w motor.

The brushless slotted windings DC motor EC 45 flat 80w is selected. Its specifications are listed in Table 4 and the speed-torque curve in Fig. 39. It is an 8-magnetic pole pairs flat design motor equipped with an MILE encoder (inductive encoder).

The peak torque is easily attainable by the motor and the RMS value is below the nominal torque of the motor. The peak current is computed through Eqn. (3.6) and is equal to 11.4A. In addition to the motor, this value must be attainable by the speed controller and by the power supply.
The peak torque also influences the voltage. Eqn. (3.7) gives the voltage depending on the characteristic point in the speed-torque diagram. Voltage at peak torque at 15Hz is about

13.5V.

$$I_{mot} = I_0 + k_M \cdot M_{motor} \tag{3.6}$$

$$U_{mot} = \frac{n0_{theor}}{k_n} \tag{3.7}$$

Where

$$n0_{theor} = N_{motor} + \Delta n / \Delta M \cdot M_{motor}$$

3.2.2 Electrical installation

The electrical circuit schematic is depicted in Fig. 40 and the main components are listed in Table 7. It is the same electrical configuration that has been used for the wrist device.
It is composed of 3 main blocks : power supply and emergency block, controller block and the actuation and sensor block.

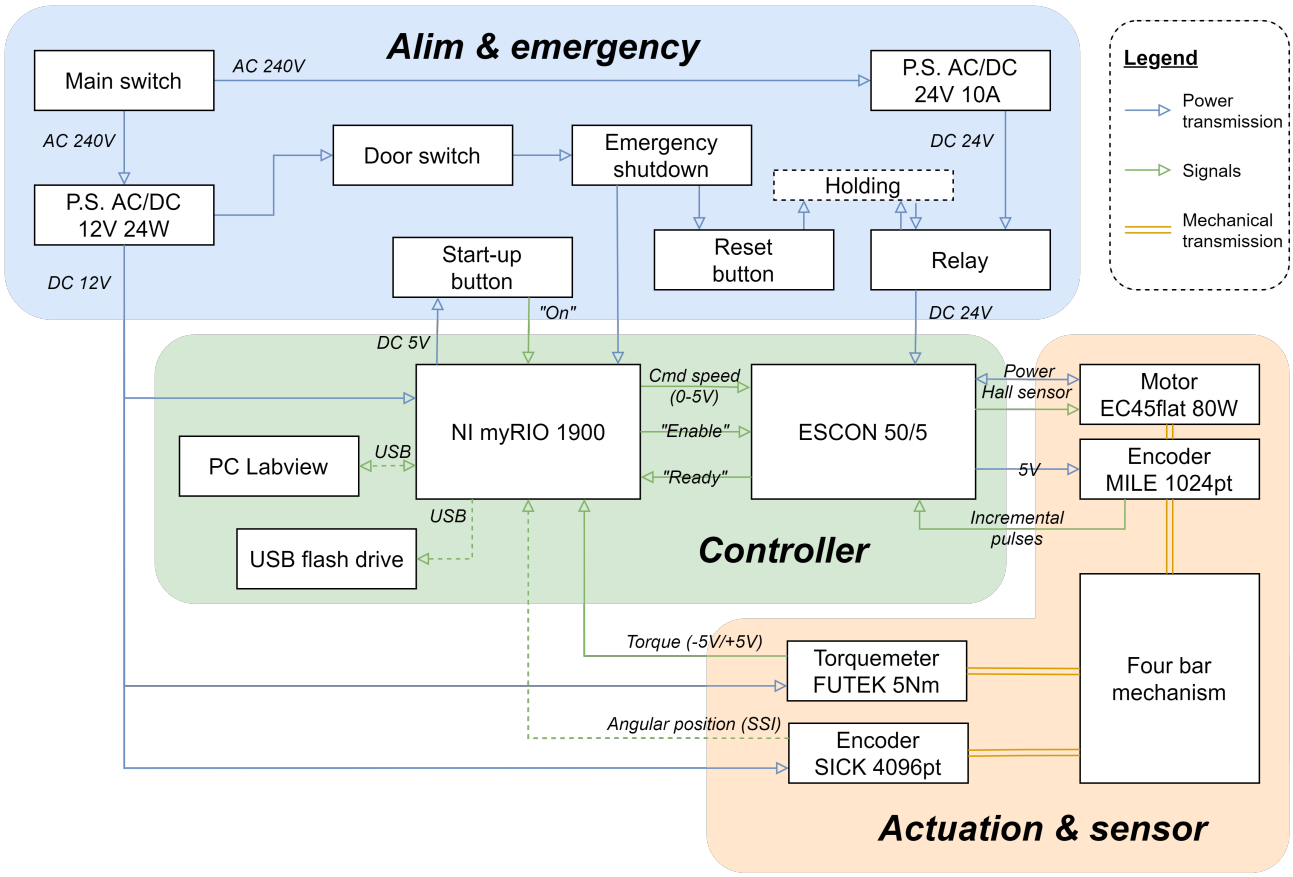


Fig. 40: Electrical schematic.

In this circuit, two power supply units are used, allowing a decoupling between the *myRIO* and sensors with the servo controller and the motor.
When the door is open, the machine will never operate, the servo controller is not supplied thanks to the relay.
The brain of the device i.e. *NI myRIO 1900* dialogues with the computer through a *LabVIEW* software interface. The embedded device is started by means of physical buttons accessible to the users.

As soon as the servo controller *ESCON* is ready, it sends a signal to the *myRIO* that enables the card. The speed command is then sent to the speed control card that translates it into PWM signals in order to generate the motion of the motor. The motor possesses six hall sensors that communicate the rotor position back to the electronic commutation of the ESCON.

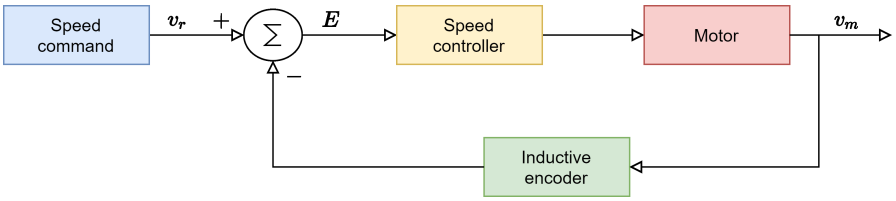


Fig. 41: Diagram of the control loop applied on the motor.

The encoder directly connected to the motor also communicates to the card to give incremental pulses informations. This control loop is depicted in Fig. 41.
Two sensors connected to the mechanism are supplied by the 12V power supply. An analog signal representing the torque signal is transmitted by the *FUTEK* torque meter. In parallel, a digital signal representing the angular position is transmitted in SSI communication by the *SICK* encoder.

One can see in Fig. 38b, in the motor study, that there are moments where the motor must brake. The current generated by this phenomenon causes the controller *ESCON* to disconnect itself. Hence, a capacity put in parallel allows to absorb the energy to resolve this problem. In contrast, adding the capacity delays the shut down of the device in case of an emergency stop.

At the end of the measurement, the computer code from the *myRIO* exports the result in ".txt" files into the USB flash drive connected to the machine.

Torque meter selection The torque meter needs to be able to acquire torque produced by the finger, from a range of 0 to 2200mNm. The combined error of the torque meter present in the wrist's EOD is 1% over the rated output (*Sensy* 62200 - 75Nm).

The chosen torque meter is the *Futek* Model TRS605 - 5Nm with specifications listed in Table 5 (datasheet in Appendix C.3). It is a non-contact shaft-to-shaft rotary torque sensor with an encoder.

Unfortunately its encoder provides low resolution hence, it can not be used to sense the rotary motion to be used for the quantification method.

The bearing of the torque meter has an approximate durability of 10.000 hours.

The combined error is about $\pm 0.3\%$ of rated output (30mV).

Name	Value	Units
Rated output	± 5	V
Non linearity	± 0.1	%
Hysteresis	± 0.2	%
Rotational speed	7.000	rpm
Encoder pulses per revolution	360	pt
Calibration of Conformance	12	V
Inertia	15	gcm^2

Table 5: Characteristic and specification of the *Futek* Model TRS605 - 5Nm torque meter.

Absolute encoder selection For the wrist EOD, the resolution was 4096pt, which is coded in a 12-bit long word. The encoder should be capable of communicating in SSI, which facilitates the adaptation with the computer code in *LabVIEW*. From the *SICK* catalogue, the Model AHS36B-BDAC004096 is chosen with specifications listed in Table 6 (datasheet in Appendix C.3).

Name	Value	Units
Number of steps per revolution	4.096	pt
Single turn		
Error limits	0.35	deg
Type of coding	Gray code	-
Communication interface	SSI	-
Inertia	15	gcm^2

Table 6: Characteristics and specification of the AHS36B-BDAC004096 absolute encoder.

Other electrical component The power units are selected from the type of nominal voltage required by 1) the motor and speed controller card and 2) by the *myRIO*.

Hence a 24V and 12V respectively are selected. The other electrical components are :

(i) The main switch to supply the supply unit in AC 240V;

(ii) The door switch is a roller plunger limit switch that is normally open, meaning that the internal switch is open when the door is closed;

(iii) Push buttons for emergency and to start the experiment;

(iv) The relay which plays the protecting role in the circuit to stop feeding the actuator during emergency events.

(v) A capacity when the motor enters in a generator phase.

(vi) A LED screen is also used to display information about the experiment and communicates in SPI.

(vii) A laser (not in the schematic) is also used to precisely position the hand in order to make sure that the measured joint axis coincides with the machine's axis of rotation.

3.2.3 Control connective settings

The *NI-myRIO 1900* is composed of a processor dualcore ARM Cortex-A9 and a FPGA of Xilink that communicates through SPI. It features UART lines in addition to analog and digital IN/OUT (of respectively $\pm$10V, 0-5 V and 0-3.3 V). On the FPGA, other buses can be used such as Serial Peripheral Interface Bus (SPI), I2C, PWM and quadrature encoder input on the DIO line. The device also possess internal status LED that must be visible from outside the machine at all times.
The torque meter provides a $\pm$5V signal, this 10 volts signal can only enter in the Mini System Port (MSP) connector C which can measure up to $\pm$10V input differential signals. Unfortunately, its absolute accuracy is about $\pm$200mV which lowers the precision of the measure. It is partially explained by the analog-to-digital converter.
Finally, the encoder is connected to the device through one of the DIO as well as the LED screen which communicates via the SPI bus from the FPGA via multipurpose DIO channels.

Component	Reference
myRIO	NI myRIO-1900
Power supply 24 V	Power supply unit - TRIO-PS-2G/1AC/24DC/10 - 2903149
Power supply 12 V	Switch Mode DIN Rail Panel Mount Power Supply, 55W, 12V dc/ 4.6A
Relay	TeSys K LP1K 3 Pole Contactor, 3NO, 12 A, 5.5 kW, 12 V dc Coil, Screw Terminal
Door switch	IP67 Positive Break, Snap Action Limit Switch, Roller Plunger, Plastic, NO/NC, 240V
Speed controller card	ESCON 50/5
Motor	BLDC-Motor - EC45fl. BL Y 80W KL 1WE A K 673030 Inductive Encoder - ENC MILE 1024IMP 2K
Torque meter	TRS605, 5 N-m, Non-Contact Shaft to Shaft Rotary Torque Sensor w/ Encoder, 10mm Shaft, 12 Pin Binder Receptacle, 09-0331-90-12
Encoder	Absolute encoders AHS36B-BDAC004096, 1075904
Screen	LCD1602 RGB Backlight Module

Table 7: Main components in the electrical circuitry.

3.3 Detailed design

In the prototyping step, this part is essential to improve the details of the prototype. The description of the assembly is given, component's choices justified and pieces subjected to *significant* stress are studied to assess their structural mechanical resistance.

The device is configured in a multi-level arrangement in Fig. 42. A true scaled human hand is placed in order to perceive the real volume of the device. The device's global dimensions are given in Table 8.

Name	Value	Units
Length	35	cm
Width	25	cm
Height	50	cm

Table 8: Device's global dimensions

For a clearer description, the device is subdivided into five assemblies. They are named : structure assembly, electrical assembly, motor and four bar assembly, column sensor assembly and finally the finger interface assembly.

Most of this machine's parts come from the company *Misumi* that proposes a large catalog of mechanical components and with whom *UCLouvain* has good relations. These parts specifications are available in Appendix C.3.2. The other parts are either 3d printed or manufactured inside the CREDEM plateform of *UCLouvain*. The 3d printed parts are composed of Onyx. This composite based material features a very good mechanical resistance. In addition, parts can be filled with aluminium fiber as reinforcement principle. As for the machined parts, aluminium 6060 is used. The properties of materials used for the prototype are listed in Table 9.
The drawings of the machined parts (or retouched ones) and 3d parts are given respectively in Appendix C.1 and Appendix C.2.

The mechanical resistance is evaluated with the *von Mises* yield criterion that assesses whether the material stays in an elastic range of stress which is described in Appendix A.5.

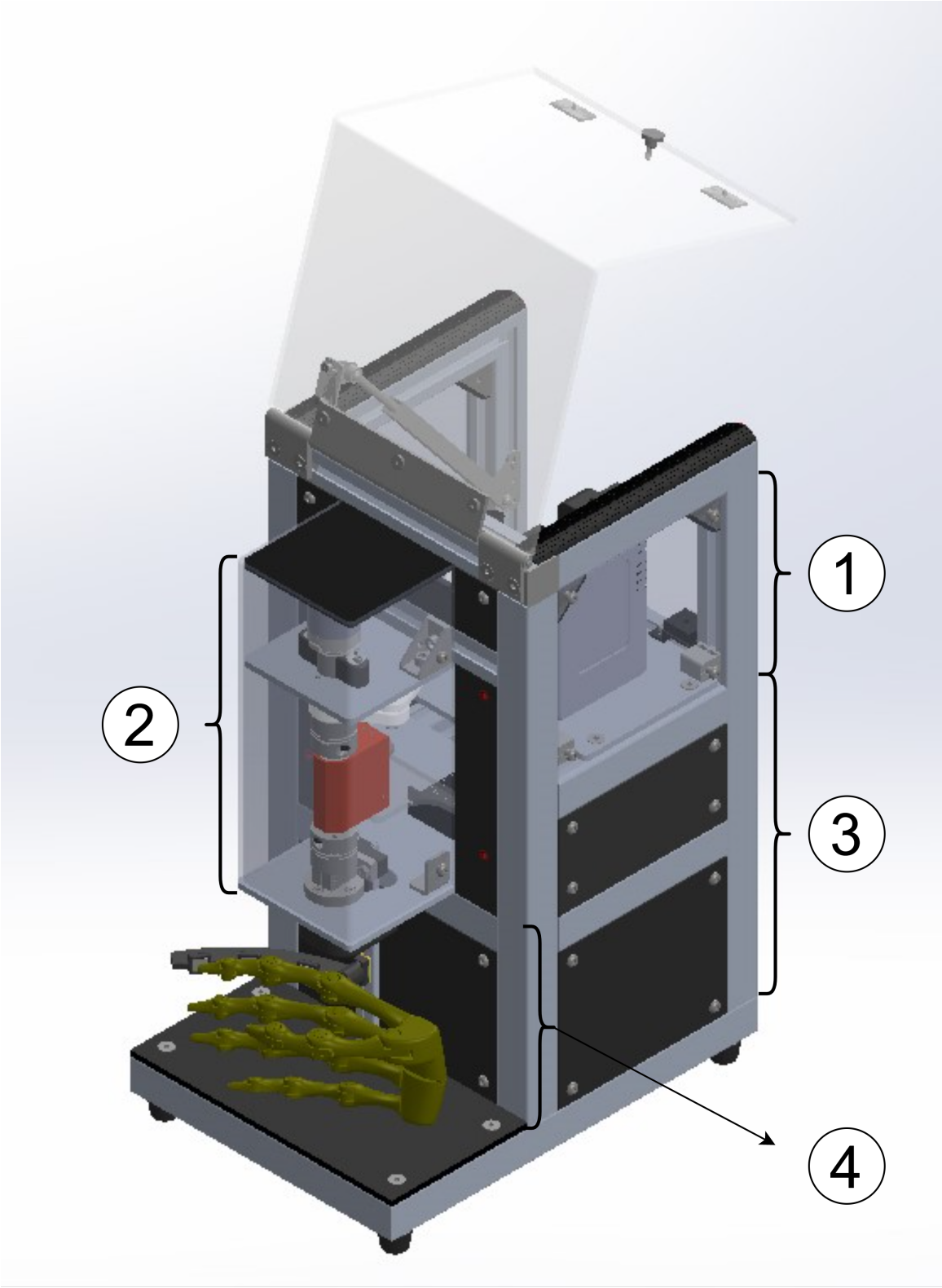


Fig. 42: Global CAD overview : 1) Four bar and control stage. 2) Column assembly stage. 3) Electrical stages. 4) Finger interface.

3.3.1 Structure assembly

The structure can be seen in Fig. 43. The frame of the structure is composed of squared aluminium extrusion bars that ensure a robust frame, are easy to assemble and very versatile units.
It is composed of transparent (in acrylic) and opaque (in polyacetal) panels that cover the openings left by the bars. The first and second stages who have no interest in being seen from outside are covered by dark panels. The stage where the motor assembly, four bar, *myRIO* and column assembly are, are covered by a transparent medium.
Polyacetal plates are also used at the finger interface to lay the hand on it and at the electrical stage. This type of material is used in a large variety of applications, from the automotive industry to electronics.

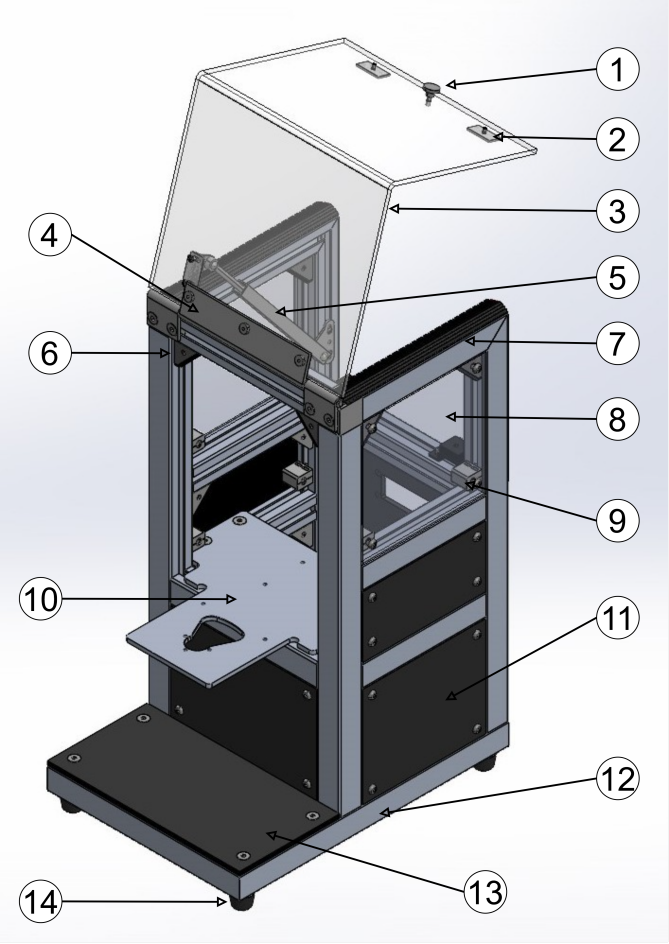


Fig. 43: Structure (CAD) : 1) Doorknob. 2) Door magnet. 3) Door. 4) Hinges. 5) Spring stays. 6) Bracket support for aluminium bar. 7) Bar covers. 8) Side panels (transparent). 9) Panels support brackets. 10) Plate of sensor column assembly. 11) Side panels (opaque). 12) Aluminium extrusion bars. 13) Hand support plate. 14) Anti-vibrations feet.

The load on it will never exceed more than 10kg and yielding strength is 110MPa = 11000N.mm^{-2} as given in Table 9 in Appendix A.5

The aluminium plate used to support the column assembly is positioned against the vertical front bars in addition to countersunk screws that are positioned in the other horizontal axis.

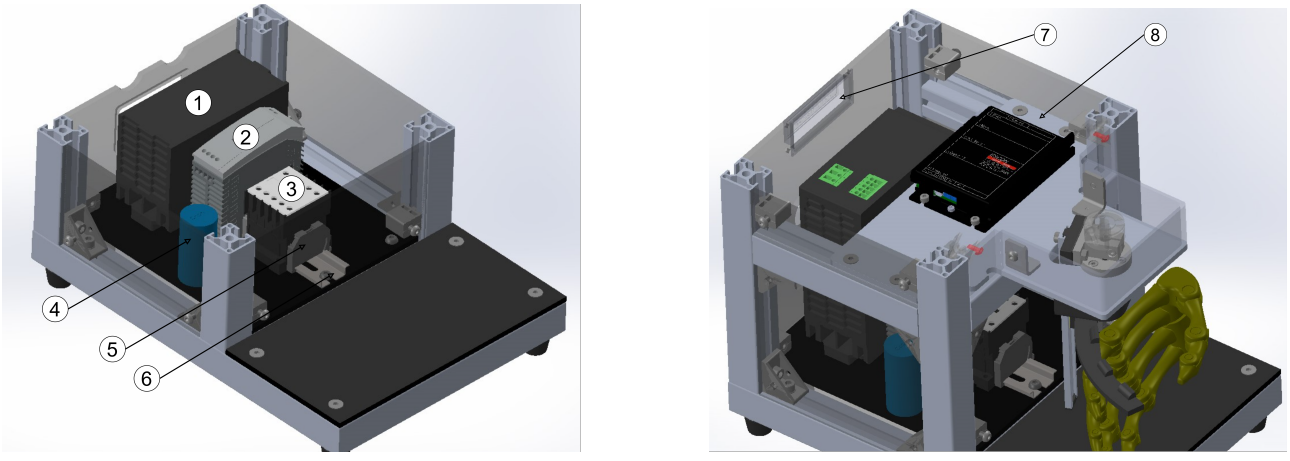
The door is composed of a L-shaped acrylic transparent panel that opens on the last stage of the structure. A "spring stays" helps opening the door and magnets are used to ensure the door stays closed.

The stays is attached to the frame of the structure at one end and to the door on the other. The placement of the spring stays has two DOF. It needs to be able to sustain the door when opened and can not induce the opening of the door when closed. The placement of the stays results in the fact that it is able to easily sustain the door when opened and furthermore, it helps to maintain the door closed[17]. The *MatLAB* code from which the end positions of the stays were computed, is available in Appendix B.1.
The frame sits on four anti-vibration feet that dampen some of the vibrations caused by the mechanism.

3.3.2 Electrical assembly

The electrical assembly is mostly gathered and placed on the lowest stages. On the first one, the two supply units and the relay are placed in series on a rail (rail din). They are fixed on the rail thanks to screwless end stop mountings (Wago). The rail is fixed directly on the structure. On the second one, only the speed controller is placed and fixed on the aluminium plate. The electric cables from the first stage can easily be accessed from the second one since the aluminium plate extends only on half of the box.
The back panel supports the LED screen, main switch and USB connector.

The supply units are the machine's heaviest components. The machine is configured in a multi-staged manner, in order to keep a low center of mass of the machine, to stabilize it. This stage is completely closed from outside and not visible thanks to opaque side panels.



(a) (b)

Fig. 44: Electric level : 1) Power supply 24V. 2) Power supply 12v. 3) Relays. 4) Capacity. 5) Screwless end stop for rail mouting. 6) Rail din for electrical mounting. 7) LED screen. 8) ESCON controller.

[17] Indeed, the lever arm is located so that the lever pushes the door against the frame.

3.3.3 Motor and four bar assembly

The factor that will determine the shape of the assembly, is whether the bearing from the motor can sustain the load. The *Robotran* analysis in Appendix A.3 is also used to assess whether the bearing present in the motor can withstand the reaction forces. Fig. 45 shows that the maximum force present is about 60N. Given the datasheet in Appendix C, the maximum radial load is 15.1N, hence the need for additional bearings to withstand present forces. The selected ball bearings have a basic dynamic load rating of more than 1000N (Appendix C.3).

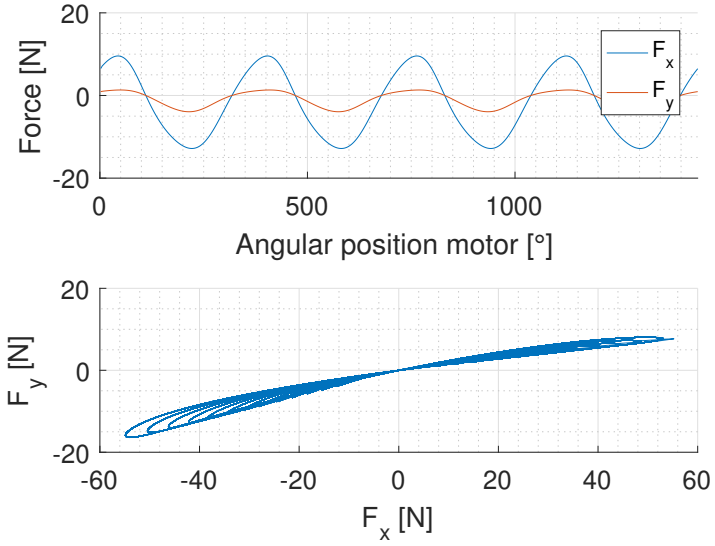


Fig. 45: Robotran analysis : reaction forces at the motor bearing at maximum load.

The shaft from the motor is not long enough, an additional shaft is used between the motor and the crank.
Care to use minimum height was taken in order to limit the shear constraints being caused by the four bar. A double bearing carter with adjacent bearings is used and the crank height is minimized.

Motor side The motor is fixed to a 3d-printed plate, which is fixed to an aluminium plate via three hexagonal supports. The motor shaft is coupled to the additional motor shaft via elastic shaft couplings. An elastic one is used in case of misalignment from two shafts axis of rotation. The latter is placed against a bearing spacer, itself placed against the inner ring of the lower bearing.

- **Motor shaft dimensioning** It is subjected to torsion and maximum torsion stress is given in Eqn. (3.8). The shaft is made of steel, hence an equivalent stress of $\sigma_{eq} =$

$7.8N.mm^2$ is only 0.03% of σ_Y.

$$\tau_{torsion} = \frac{16M^{motor}}{\pi D^3} = \frac{16 \cdot 24650}{\pi \cdot 8^3} = 4.5N.mm^{-1} \tag{3.8}$$

Furthermore, the allowable torque for the elastic coupling at the motor interface is 1.3Nm, which is acceptable.

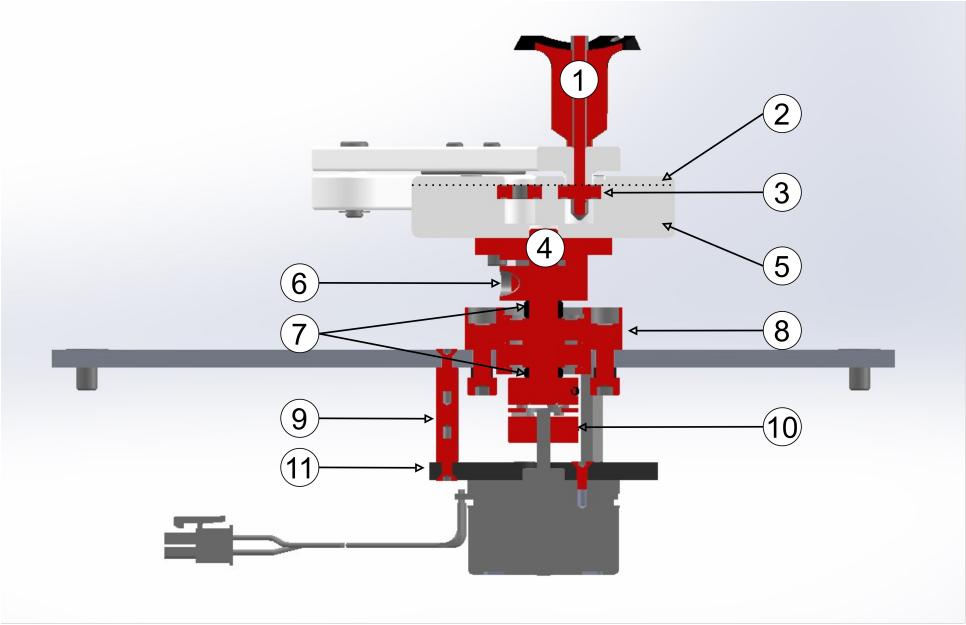


Fig. 46: Motor assembly section view : 1) Ball lock pins. 2) Crank cap. 3) Bearing. 4) Motor shaft. 5) Crank body. 6) Flanged shaft support. 7) Bearing spacer. 8) Double bearing 9) Hexagonal rod. 10) Elastic coupling 4/8. 11) Motor lower plate.

Four bar side The crank is coupled to the shaft via a flanged shaft support. The support is also placed against a bearing spacer.
The crank is designed with three bearing housings. These bearings are drowned and kept inside thanks to a crank cover (cap). The idea is to be able to choose the amplitude of oscillation. In order to do that quickly and efficiently, a system involving a ball lock pins is designed. The plunger is housed and kept in the gap thanks to its ball lock. When the button is pushed, the ball lock is released. It can then be placed at another crank gap. The crank's different bearings are designated by engraved text on the cap. The pins is slipped and placed against the coupler (bar 2) and the latter shoulders against the bearing.

- **Follower dimensioning** The flexion stress applied to the follower bar is found in

Eqn. (3.9).

$$\sigma_f = \frac{M^{finger}}{I/y} = \frac{2200}{11520/12} = 2.3N.mm^{-2} \tag{3.9}$$

Where I is the inertia of the rectangular section and y is the distance from the neutral fiber(b = width of the bar and h = height of the bar).

$$I = \frac{h \cdot b^3}{12} = \frac{10 \cdot 24^3}{12} = 11520mm^{-4} \ \& \ y = \frac{24}{2} = 12mm$$

One can verify that the shear force from the force found with *Robotran* is similar to the force found with the hypothesis that the follower bar is approximately perpendicular to the coupler (Eqn. (3.10)). Then, the shear constraint is found in Eqn. (3.11).

$$F_{shear} \simeq \frac{M^{finger}_{peak}}{L_4} = \frac{2200}{40} = 55N \tag{3.10}$$

$$\tau_{shear} = \frac{F_{shear}}{A_{L4}} = \frac{55}{10 \cdot 24} = 0.23N.mm^{-2} \tag{3.11}$$

Hence, $\sigma_{eq} = 2.33N.mm^{-2}$ which is 0.05% of σ_Y.

- **Coupler dimensioning** By action-reaction, the force acting there is about 55N. The principal constraint for the bar is compression. Once again, with the perpendicular hypothesis, the flexion component is null. This bar is reinforced with fiberglass, which features high strength, nearly equal to 6061-T6 Aluminum.

$$\sigma_{comp} = \frac{F_{comp}}{A_{L3}} = \frac{55}{7 \cdot 24} = 0.33N.mm^{-2} \tag{3.12}$$

The critical buckling force is computed in Eqn. (3.13), the value is nowhere near the peak value made by the finger resistance in the four bar mechanism.

$$F_{crit} = \frac{\pi^2 \cdot E \cdot I}{L_e} = \frac{\pi^2 \cdot 3.10^3 \cdot \frac{24 \cdot 7^3}{12}}{168.5} = 1450kN \tag{3.13}$$

With L_e equalled to the length of the bar L because the two ends are attached with the rotation joint, E the Young modulus of the Onyx material. The inertia is the minimum inertia of the bar section.
The equivalent stress $\sigma_{eq} \simeq \sigma_{comp}$ is <0.01% of σ_Y.

- **Crank dimensioning** The principal constraints acting on the bar are a shear stress and

torsion constraint. Obviously, the constraints come from the resisting torque of the joint finger. The peak torque of the motor was computed in Section 3.2.1, as well as the forces at the pivot. The crank constraints are transmitted to the shaft support (in steel) to which it is fastened.

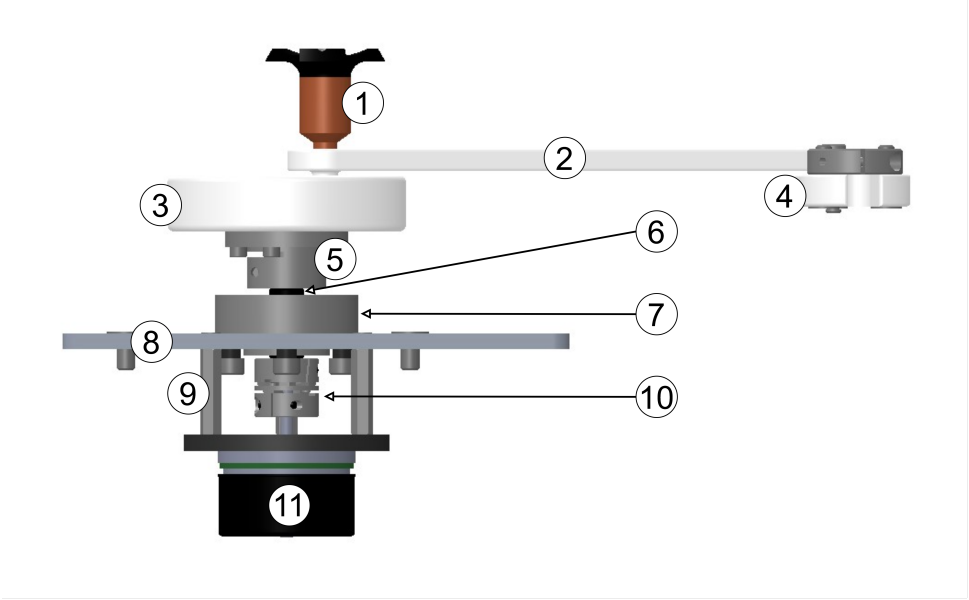


Fig. 47: Motor assembly (CAD) : 1) Ball lock pins. 2) Four bar coupler bar. 3) Four bar crank. 4) Four bar follower. 5) Flanged shaft support. 6) Bearing spacer. 7) Double bearing. 8) Motor higher plate. 9) Hexagonal rod. 10) Elastic coupling 4/8. 11) EC-motor.

This stage includes the *myRIO*. It is mounted directly to the extrude bar structure with a 3d printed part (called myRIO mount). This mount allows to easily connect inputs and outputs on the *myRIO* and still have a clear vision of the myRIO's led. Furthermore, it is rather well dissociated from the four bar area on the same level.

3.3.4 Column sensor assembly

This assembly is composed of the encoder, the follower of the four bar and the torque meter. This assembly is described in Fig. 49.
One can make the assumption that twist's angle of the shafts included in the assembly, is null. This is true as soon as the angle of twist is less than a 1mdeg in Eqn. (3.14).

$$\theta_{twist} = \frac{M^{finger} \cdot L}{J \cdot G} = \frac{2200 \cdot 200}{\frac{\pi}{32} 8^4 \cdot 190e5} = 0.001892° \tag{3.14}$$

Where $J = D^4\pi/32$ is the moment of inertia of a plane cylinder.
With this assumption and a proper clamping through the coupling units, the encoder measures the same angular motion than the imposed motion of the finger.

Encoder side The higher components of the column sensor assembly is the encoder and its mounting facilities. A front view is given in Fig. 48.
The encoder plate is made of aluminium 6061 and machined according to the drawing in Appendix C.1. It is attached to an extrude bar via two brackets (Appendix C.3.2) and directly beneath the plate with a countersunk screw. By rotating the bearing carter, the plate is kept close to the follower bar, which transmits the torque.
Therefore, in this configuration, the encoder needs to be mounted with spacer mountings (3d printed).

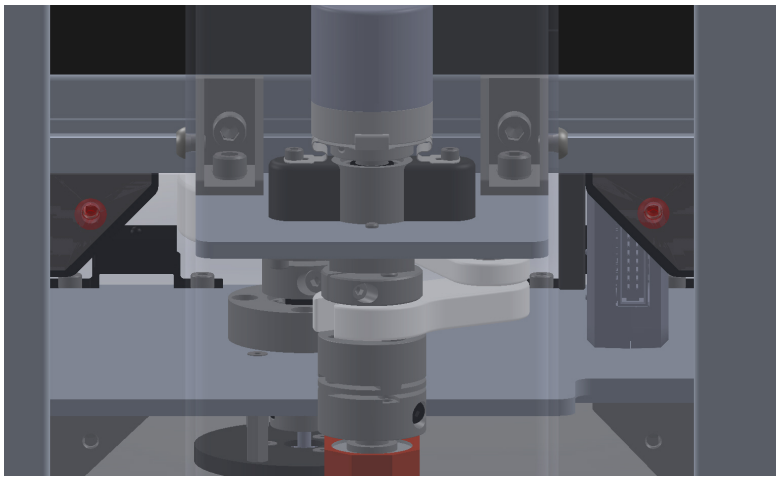


Fig. 48: Higher front view of the column assembly (CAD).

- **Encoder shaft dimensioning** The maximum torsion stress encountered by the steel shaft is :

$$\tau_{torsion} = \frac{16M}{\pi D^3} = \frac{16 \cdot 2200}{\pi \cdot 10^3} = 11.2N.mm^{-2} \tag{3.15}$$

The equivalent stress $\sigma_{eq} \simeq 19.39N.mm^{-2}$ is <0.08% of σ_Y.

Torque meter side The follower bar is coupled with a shaft collar to ensure a tight steel to steel coupling with the encoder shaft. The collar goes in contact with a bearing spacer.
Behind the follower bar, once again, an elastic coupling for shaft-to-shaft coupling is used. The allowable torque for the elastic coupling at the motor interface is 5Nm, which is acceptable. The torque meter is left floating in the axial direction. The only mounting part is a plate that makes sure the stator part of the torque meter does not rotate around its axis (due to friction between the torque meter's shaft and its bearings).
The second coupling is the same except that it couples a 10mm-shaft diameter with a 8mm-shaft diameter. It rests on a shaft support that constitutes the shifted rail for the finger driving arm.
Finally, the last parts of the column assembly are the bearing spacer and a double bearing carter.

- **Finger shaft dimensioning** The maximum torsion stress encountered by the steel shaft is :

$$\tau_{torsion} = \frac{16M}{\pi D^3} = \frac{16 \cdot 2200}{\pi \cdot 8^3} = 21.9N.mm^{-2} \tag{3.16}$$

The equivalent stress $\sigma_{eq} \simeq 37.93N.mm^{-2}$ is <0.15% of σ_Y.

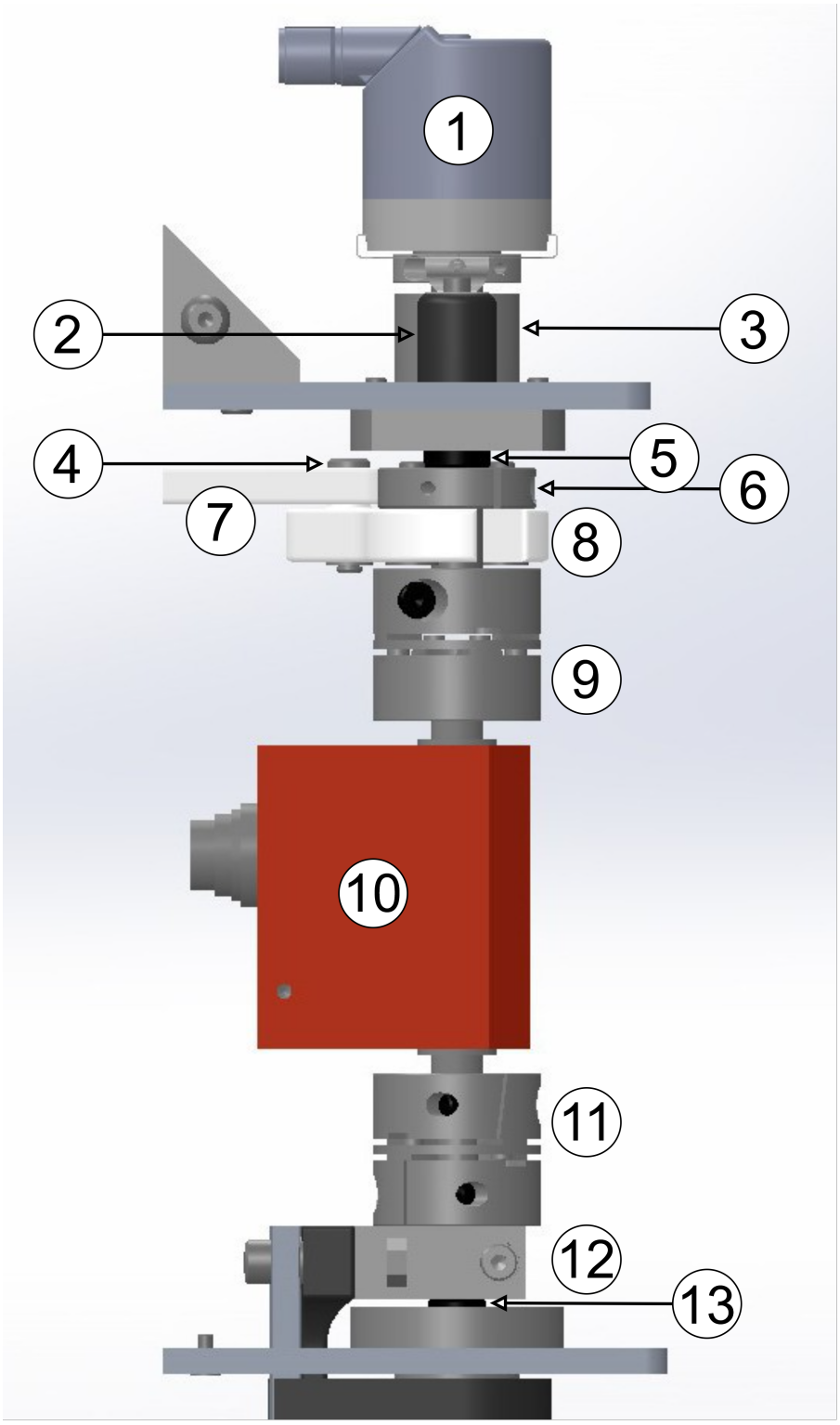


Fig. 49: Column sensor assembly : 1) Absolute encoder. 2) Encoder mounting. 3) Double bearing. 4) Flanged pivot + ring. 5) Bearing spacer. 6) Shaft collar. 7) Four bar coupler bar. 8) Four bar follower bar. 9) Elastic coupling 10/10. 10) Torque meter. 11) Elastic coupler 10/8. 12) T-shaped shaft support. 13) Bearing spacer.

3.3.5 Finger interface assembly

This part of the device delimits the location where the mechanism is in contact with the subject. The mountings to the shaft are designed in order to induce the smallest torsion constraints possible to the rail by adding limited inertia to the mechanism. Two shaft supports are chosen. They must exhibit a low mass given the inertia constraint of the measurement method, hence aluminium is preferred over steel material.
A bone shaped part (3d printed) is placed between the rail and the shaft support to couple them. The rail is encased in the bone part and screwed to the shaft support.
As already explained, the rail allows to choose the type of finger assessed and to have a system that is adapted to any size of hand [52].

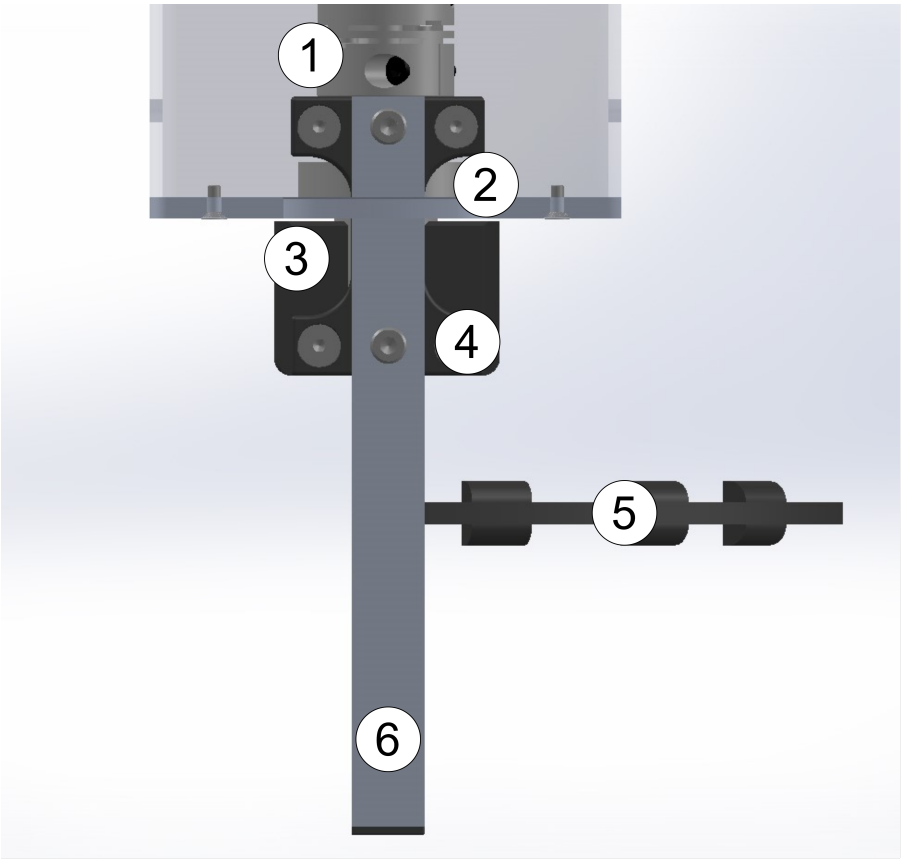


Fig. 50: Eccentric arm (CAD): 1) Elastic coupling of the shaft. 2) Double bearing. 3) Cover of the shaft support. 4) Support for the rail. 5) Finger driving arm. 6) Finger rail.

As already discussed, the binding system for the finger needs to be rigid. Furthermore, the oscillation needs to be done around the equilibrium position of the finger (cfr. Section 1.1.2). This is done by using an appropriate shape of the finger driving arm already curved. From the previous thesis [5], this value is about 40deg.
If wrist position influences MCP measurement, the question of whether the finger needs to

be straight (0° for both joints IPP and DIP) or curved (neutral position for both joints), has to be investigated[18].

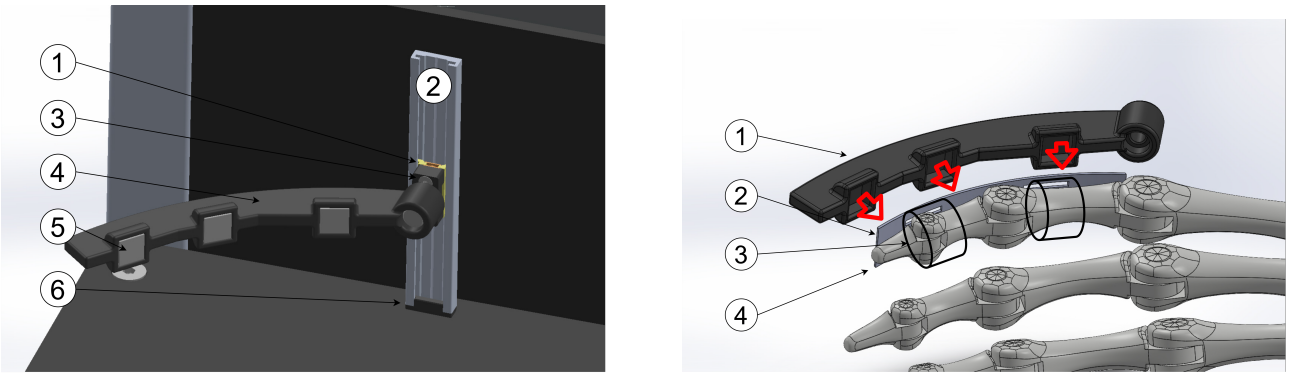
The finger driving arm is composed of three magnets that ensure a coupling with the finger. This type of coupling is used as an easy and effective strategy for disengagement. By binding the external side of the finger to a ferromagnetic sheet of metal, the coupling is made. Disengagement is facilitated by applying a shear force (perpendicular to the magnet axis). Shear load of magnet is approximately 15% of axial load. The metal sheet can be fastened to the finger via *Velcro* strips.

- **Magnet dimensioning** : For a maximum torque of 2200mNm, only the magnet's force in the middle of the first phalange should be about 100N, at the second 41 N and the distal 31N. With a neodymium magnet.

  With three drowned magnets in the finger driving arm, the attraction force reported at the MCP is :

$$\vec{M}_{magnet} = \sum_{i=1}^{3} \vec{d} \times \vec{F}_{magnet} = 18.6 \cdot (80 + 60 + 25) = 3069 mNm$$

  Hence, a coefficient of security (in the worst case) of about 1.4 ensures that the finger driving arm and the finger will stay together at any time.



(a) Finger interface (CAD): 1) Slider of the rail. 2) Rail. 3) Slider attachment. 4) Finger driving arm. 5) Finger coupling magnet. 6) Rail stop end.

(b) Finger binding and coupling to device (CAD): 1) Finger driving arm. 2) Metal sheet with slots. 3) Velcro strips. 4) Oscillating finger.

Fig. 51: Finger interface assembly (CAD).

The inertia found for the whole rotating system (Fig. 66) from the torque meter's base with *Solidworks* is about 1800g.cm^2.

[18]No studies were found.

3.4 Final Assessment

The purpose of this thesis was to design and build an electromechanical device capable of measuring passive stiffness and viscosity of the human finger.
After exploring designs of various experimental apparatus and conceptual designs of previous thesis, after having generated and compared solutions, a prototype was created.
The design of the prototype meets the requirements. The prototype's features include :

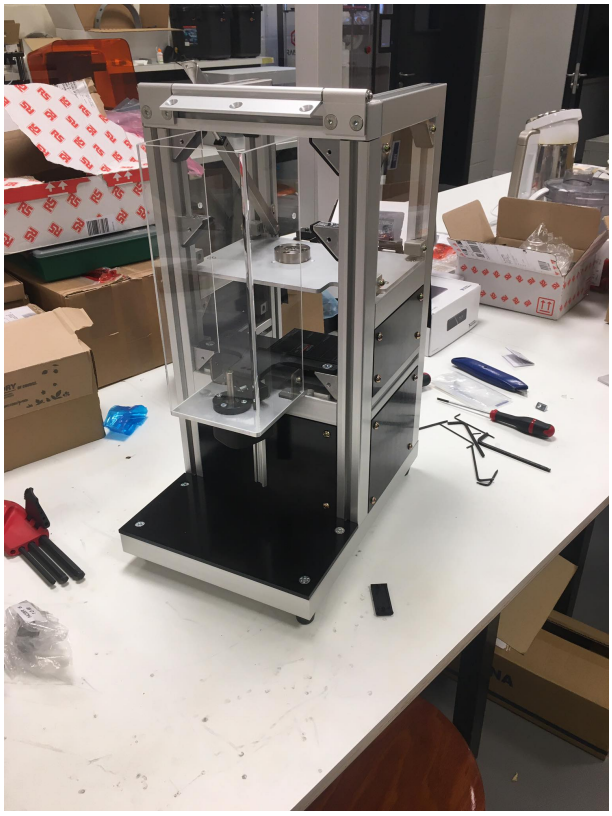
- ✔ Strong, completely closed and transportable device that can be used in any establishment supplied in electricity.
- ✔ An easy, fast and safe amplitude adjustment.
- ✔ Adaptable to any hand or finger size and can be used for both hands.
- ✔ Possible assessment of the 2nd to 4th finger.
- ✔ Visible mechanical assembly for maintenance check.
- ✔ Precise sinusoidal motion.
- ✔ Precise angular and torque measurements adapted to high spastic subject's fingers.
- ✔ Easy finger disengagement and opened view of the subject's finger at any time.
- ✔ Constrained motion.

The prototype is not completely assembled. Some pieces from the prototype still have to be delivered at this time. Still, the global structure is completed and can be seen in Fig. 52.

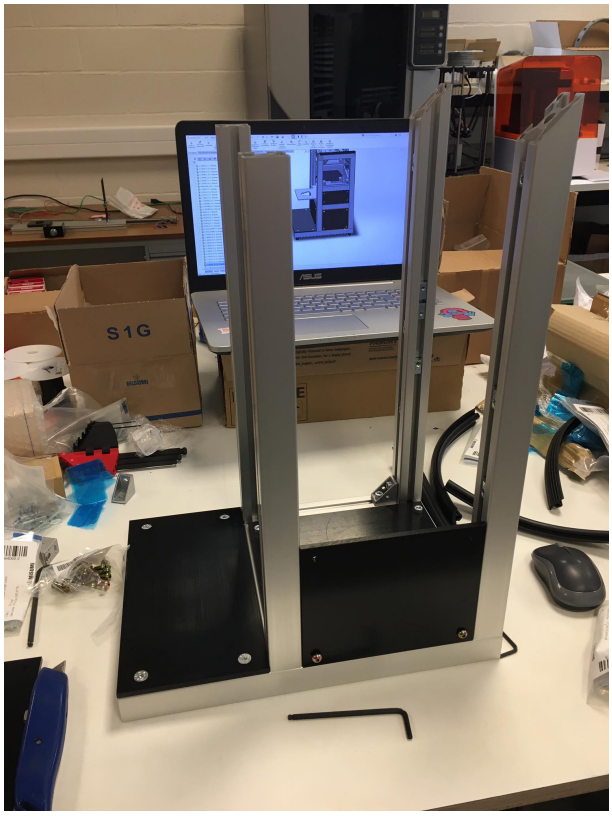
This manuscript is focused on the MCP joint measurement. Since the MCP joint resistance is higher (more inertial), actuators and the sensory system are dimensioned according to the worst possible case.
Further work would be to design a finger interface system in order to adapt DIP measurements in addition to the MCP one. This essentially includes the design of a finger driving arm and finger attachment.
In order to match the neutral position of the subject with the neutral position of the mechanism, two or more types of finger driving arms should be printed.

The design of the hand's fixation was left at the conceptual design step. A palm fixation should be considered.
Furthermore, the computer code from the wrist device still needs to be adapted to components' changes and to the frequency range's extension (from 3-12Hz to 3-15Hz).

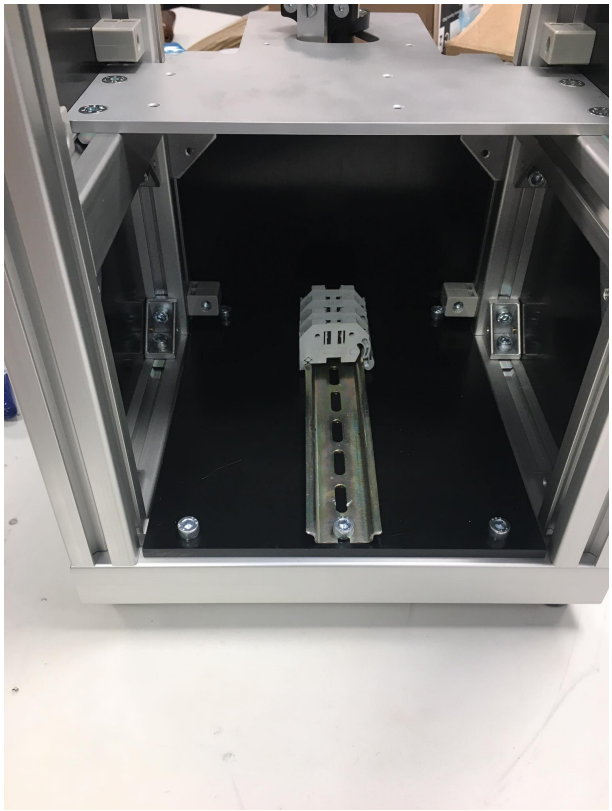
First future assessment of the prototype A first assessment to evaluate the effectiveness of the design, would consist of placing a pure elastic element at the finger interface. The output stiffness given by the prototype should give the same value as the elastic element's stiffness. On the other hand, assessment of the machine's viscosity precision is more difficult to make via a viscous standard. A viscosimeter works by inducing vibrations in a viscous standard, with orders of amplitude way smaller than the prototype's amplitude. Fortunately there is a way to bypass this, by indirectly assessing the viscosity. Using the pure elastic element, one can verify that the measured viscosity is null at all frequencies of oscillation.



(a)



(b)



(c)



(d)

Fig. 52: Prototype building process.

Research paper reference

[1] R. Gold, "Multiple sclerosis spasticity epidemiology – key publications," Expert Review of Neurotherapeutics, vol. 13, no. sup2, pp. 45–46, 2013. DOI: 10.1586/14737175.2013.865874. eprint: https://doi.org/10.1586/14737175.2013.865874. [Online]. Available: https://doi.org/10.1586/14737175.2013.865874.

[2] C.-L. Kuo and G.-C. Hu, "Post-stroke spasticity: A review of epidemiology, pathophysiology, and treatments," International Journal of Gerontology, vol. 12, no. 4, pp. 280–284, 2018, ISSN: 1873-9598. DOI: https://doi.org/10.1016/j.ijge.2018.05.005. [Online]. Available: https://www.sciencedirect.com/science/article/pii/S1873959818300073.

[3] "Spasticity - epidemiology forecast to 2030," Feb. 2021, ID: 4471032, p. 77.

[4] C. Apamon et al., "Conception et dimensionnement de dispositifs expérimentaux de mesure pour la recherche clinique," 2017.

[5] J. Corbisier et al., "Dispositif pour mesurer la raideur passive élastique et visqueuse des doigts humains," 2020. [Online]. Available: http://hdl.handle.net/2078.1/thesis:26482.

[9] M. Schieber, "Muscular production of individuated finger movements: The roles of extrinsic finger muscles," The Journal of neuroscience, vol. 15, Jan. 1995. DOI: https://doi.org/10.1523/JNEUROSCI.15-01-00284.1995.

[12] P.-H. Kuo et al., "Design and Performance of a Motor-Driven Mechanism to Conduct Experiments With the Human Index Finger," Journal of Mechanisms and Robotics, vol. 7, no. 3, Aug. 2015, 031010, ISSN: 1942-4302. DOI: 10.1115/1.4028639. eprint: https://asmedigitalcollection.asme.org/mechanismsrobotics/article-pdf/7/3/031010/6252946/jmr_007_03_031010.pdf. [Online]. Available: https://doi.org/10.1115/1.4028639.

[13] A. V. Hill, "The heat of shortening and the dynamic constants of muscle," Proceedings of the Royal Society of London. Series B - Biological Sciences, vol. 126, no. 843, pp. 136–195, 1938. DOI: 10.1098/rspb.1938.0050. [Online]. Available: https://royalsocietypublishing.org/doi/abs/10.1098/rspb.1938.0050.

[14] J. Martins et al., "A numerical model of passive and active behavior of skeletal muscles," Computer Methods in Applied Mechanics and Engineering, vol. 151, no. 3, pp. 419–433, 1998, Containing papers presented at the Symposium on Advances in Computational Mechanics, ISSN: 0045-7825. DOI: https://doi.org/10.1016/S0045-7825(97)00162-X. [Online]. Available: https://www.sciencedirect.com/science/article/pii/S004578259700162X.

[15] C. Evans et al., "Response of the normal human ankle joint to imposed sinusoidal movements," The Journal of Physiology, vol. 344, Mar. 1983.

[16] J. Lehmann, "Spasticity: Quantitative measurements as a basis for assessing effectiveness of therapeutic intervention," Archives of Physical Medicine and Rehabilitation, vol. 70(1), pp. 6–15, 1989.

[18] P.-H. Kuo and A. D. Deshpande, "Muscle-tendon units provide limited contributions to the passive stiffness of the index finger metacarpophalangeal joint," Journal of Biomechanics, vol. 45, no. 15, pp. 2531–2538, 2012, ISSN: 0021-9290. DOI: https://doi.org/10.1016/j.jbiomech.2012.07.034. [Online]. Available: https://www.sciencedirect.com/science/article/pii/S0021929012004666.

[20] D. Latz et al., "Influence of wrist position on the metacarpophalangeal joint motion of the index through small finger," HAND, vol. 14, no. 2, pp. 259–263, 2019, PMID: 29072491. DOI: 10.1177/1558944717736823. eprint: https://doi.org/10.1177/1558944717736823. [Online]. Available: https://doi.org/10.1177/1558944717736823.

[21] K. Chino and H. Takahashi, "The association of muscle and tendon elasticity with passive joint stiffness: In vivo measurements using ultrasound shear wave elastography," Clinical Biomechanics, vol. 30, no. 10, pp. 1230–1235, 2015, ISSN: 0268-0033. DOI: https://doi.org/10.1016/j.clinbiomech.2015.07.014. [Online]. Available: https://www.sciencedirect.com/science/article/pii/S0268003315002119.

[24] V. M. Zatsiorsky, "On muscle and joint viscosity," Motor Control, vol. 1, pp. 299–3095, Feb. 1997. DOI: 10.1123/mcj.1.4.299. [Online]. Available: https://www.researchgate.net/publication/306043716_On_Muscle_and_Joint_Viscosity.

[26] J. Mizrahi, "Mechanical impedance and its relations to motor control, limb dynamics, and motion biomechanics," Canadian Medical Association Journal, vol. 169(11),

pp. 1173–1179, 2015. [Online]. Available: https://www.cmaj.ca/content/169/11/1173.

[27] A. Elia et al., "Clinical trials of botulinum toxin in adult spasticity," Botulinum Toxin, vol. 69, pp. 148–158, 2009.

[28] A. J. Thompson et al., " clinical management of spasticity ," Journal of Neurology, Neurosurgery & Psychiatry, vol. 76, no. 4, pp. 459–463, 2005, ISSN: 0022-3050. DOI: 10.1136/jnnp.2004.035972. eprint: https://jnnp.bmj.com/content/76/4/459.full.pdf. [Online]. Available: https://jnnp.bmj.com/content/76/4/459.

[30] L. E. Satkunam, "Rehabilitation medicine: Management of adult spasticity," Canadian Medical Association Journal, vol. 169(11), pp. 1173–1179, 2003. [Online]. Available: https://www.cmaj.ca/content/169/11/1173.

[35] V. Dietz and W. Berger, "Normal and impaired regulation of muscle stiffness in gait: A new hypothesis about muscle hypertonia," Experimental Neurology, vol. 79, Mar. 1983. [Online]. Available: https://www.sciencedirect.com/science/article/abs/pii/0014488683900328?via%5C%3Dihub.

[36] M.-A. Haustrate et al., "Validation of an electromechanical oscillation device (eod) in the assessment of upper limb hyper-resistance in stroke patients," 2021.

[37] J. Fleuren et al., "Stop using the ashworth scale for the assessment of spasticity," Journal of Neurology, Neurosurgery, and Psychiatry, vol. 81, 2010. DOI: http://dx.doi.org/10.1136/jnnp.2009.177071.

[38] S. M. Aloraini et al., "Assessment of spasticity after stroke using clinical measures: A systematic review," Disability and rehabilitation, vol. 37, no. 25, pp. 2313–2323, 2015, ISSN: 0963-8288. DOI: 10.3109/09638288.2015.1014933. [Online]. Available: https://doi.org/10.3109/09638288.2015.1014933.

[39] A. P. Nguyen et al., "Effect of age and body size on the wrist's viscoelasticity in healhty participants from 3 to 90 years old and reliability assessment," Frontiers in Sports and Active Living, vol. 2, Apr. 2020. [Online]. Available: https://www.frontiersin.org/articles/10.3389/fspor.2020.00023/full.

[40] C. Detrembleur and L. Plaghki, "Quantitative assessment of intrathecally administered baclofen in spasticity," Archives of Physical Medicine and Rehabilitation, vol. 81, 2000. [Online]. Available: https://www.sciencedirect.com/science/article/abs/pii/S0003999300900716.

[41] V. Wright and R. J. Johns, "Observations on the measurement of joint stiffness," Arthritis & Rheumatism, vol. 3, Aug. 1960. [Online]. Available: https://onlinelibrary.wiley.com/doi/abs/10.1002/art.1780030406.

[42] ——, "Quantitative and qualitative analysis of joint stiffness in normal subjects and in patient with connective tissue diseases," Arthritis & Rheumatism, vol. 20, 1961.

[43] L. Bäcklund and P. Tiselius, "Objective measurement of joint stiffness in rheumatoid arthritis," Acta Rheumatologica Scandinavica, vol. 13, 1967. [Online]. Available: https://doi.org/10.3109/rhe1.1967.13.issue-1-4.23.

[44] P. M. H. Rack, "The behaviour of a mammalian muscle during sinusoidal stretching," The Journal of Physiology, vol. 183, Mar. 1966. [Online]. Available: https://physoc.onlinelibrary.wiley.com/doi/abs/10.1113/jphysiol.1966.sp007848.

[45] G. C. Joyce et al., "The forces generated at the human elbow joint in response to imposed sinusoidal movements of the forearm," The Journal of Physiology, vol. 240, Jan. 1974.

[46] T. I. H. Brown et al., "Forces generated at the thumb interphalangeal joint during imposed sinusoidal movements," The Journal of Physiology, vol. 332, Jan. 1982.

[48] A. Unsworth et al., "Measurement of stiffness in the metacarpophalangeal joint: The arthrograph," Clinical Physics and Physiological Measurement, vol. 3, no. 4, pp. 273–281, Nov. 1982. DOI: 10.1088/0143-0815/3/4/003. [Online]. Available: https://doi.org/10.1088/0143-0815/3/4/003.

[49] A. Esteki and J. Mansour, "An experimentally based nonlinear viscoelastic model of joint passive moment," Journal of biomechanics, vol. 29(4), pp. 443–450, Apr. 1996. DOI: 10.1016/0021-9290(95)00081-x..

[50] L. Maes et al., "Conception et dimensionnement d'une machine de mesure de la raideur passive de la cheville," 2017.

[51] M. Ditroilo et al., "Assessing musculo-articular stiffness using freee oscillations," Sports Med, vol. 41(12), pp. 1019–1032, 2011.

[52] T. M. Greiner, "Hand anthropometry of u.s. army personnel," 1991.

[54] W.-T. Chang et al., "A note on grashof's theorem," Journal of Marine Science and Technology, vol. 13(4), pp. 239–248, 2005, ISSN: 10232796. [Online]. Available: https://www.mendeley.com/catalogue/b3b1cb6b-edc3-36ed-a96f-bed8235002fe/.

[55] D. J. Twist, "Effects of a Wrapping Technique on Passive Range of Motion in a Spastic Upper Extremity," Physical Therapy, vol. 65, no. 3, pp. 299–304, Mar. 1985, ISSN: 0031-9023. DOI: 10.1093/ptj/65.3.299. eprint: https://academic.oup.com/ptj/article-pdf/65/3/299/10757453/ptj0299.pdf. [Online]. Available: https://doi.org/10.1093/ptj/65.3.299.

[56] J. Noth et al., "Long latency reflex force of human finger muscles in response to imposed sinusoidal movements," Exp Brain Res, vol. 55, Aug. 1984. DOI: https://doi.org/10.1007/BF00237282. [Online]. Available: https://link.springer.com/article/10.1007/BF00237282.

Book reference

[3] "Spasticity - epidemiology forecast to 2030," Feb. 2021, ID: 4471032, p. 77.

[11] J. E. Muscolino et al., "Les muscles : Action et palpations," in. Issy-les-Moulineaux-France: Elsevier Masson SAS, May 2013, ch. 7, ISBN: 9782294728334. [Online]. Available: https://www.elsevier-masson.fr/les-muscles-actions-et-palpation-9782294728334.html.

[19] M. L. Latash and V. M. Zatsiorsky, "5 - muscle tone," in Biomechanics and Motor Control, M. L. Latash and V. M. Zatsiorsky, Eds., San Diego: Academic Press, 2016, pp. 85–98, ISBN: 978-0-12-800384-8. DOI: https://doi.org/10.1016/B978-0-12-800384-8.00005-3. [Online]. Available: https://www.sciencedirect.com/science/article/pii/B9780128003848000053.

[23] A. Akay and A. Carcaterra, "Damping mechanism," in Active and Passive Vibration Control of Structures, P. Hagedorn and G. Spelsberg-Korspeter, Eds., CISM International Center for Mechanical Sciences, 2014, pp. 259–299.

[25] M. L. Latash and V. M. Zatsiorsky, "3 - velocity-dependent resistance," in Biomechanics and Motor Control, M. L. Latash and V. M. Zatsiorsky, Eds., San Diego: Academic Press, 2016, pp. 49–62, ISBN: 978-0-12-800384-8. DOI: https://doi.org/10.1016/B978-0-12-800384-8.00003-X. [Online]. Available: https://www.sciencedirect.com/science/article/pii/B978012800384800003X.

[29] D. A. Gelber and D. R. Jeffery, Clinical Evaluation and Management of Spasticity. New York: Springer science+, 2002.

Other reference

[3] "Spasticity - epidemiology forecast to 2030," Feb. 2021, ID: 4471032, p. 77.

[6] Froedtert, Ed., Hand and finger injuries and conditions. [Online]. Available: https://www.froedtert.com/hand/conditions/hand-fingers.

[7] T. F. D. by Farlex, Ed., Joint, The Free Dictionary by Farlex. [Online]. Available: https://medical-dictionary.thefreedictionary.com/joint.

[8] J. Hoefs, Sprinter vs. marathoner, livestrong.com, Ed., Jun. 2019. [Online]. Available: https://www.livestrong.com/article/429810-sprinter-vs-marathoner/.

[10] G. Sendic, Lumbrical muscles of the hand, kenhub.com, Ed. [Online]. Available: https://www.kenhub.com/en/library/anatomy/lumbrical-muscles-of-the-hand.

[17] N. Battista, Schematic diagram of the 3-element hill model of muscle contraction, Researchgate, Ed. [Online]. Available: https://www.researchgate.net/figure/Schematic-diagram-of-the-3-Element-Hill-model-of-muscle-contraction-containing-a_fig10_309425139.

[22] Wikipedia, Viscosity. [Online]. Available: https://en.wikipedia.org/wiki/Viscosity.

[31] P. Reid, Spasticity, T. S. H. at the Neurological Institute of New York, Ed., 2020. [Online]. Available: https://www.columbiaspine.org/condition/spasticity/.

[32] Humour à l'hopital. [Online]. Available: https://condor022.skyrock.com/3049102801-ahahah-HUMOUR-ahahah-l-hopital.html.

[33] Botox, Ed., Clinical presentation of adult spasticity, 2020. [Online]. Available: https://www.botoxmedical.com/FocalSpasticity/PatientIdentification.

[34] D. C. Leclercq, What is spasticity, spastic-hand.com, Ed.

[47] Wikipedia, Tetanic contraction. [Online]. Available: https://en.wikipedia.org/wiki/Tetanic_contraction.

[53] alistaistutorials.co.uk, Ed., Crank mechanism kinematics : Classic analysis. [Online]. Available: http://alistairstutorials.co.uk/tutorial13.html.

[57] directindustry.com, Ed., Choosing the right position sensor. [Online]. Available: https://guide.directindustry.com/choosing-the-right-position-sensor/#4.

[58] M. Key, Ed., Muscles of the forearm and hand. [Online]. Available: https://musculoskeletalkey.com/7-muscles-of-the-forearm-and-hand/.

[59] F. Bauch and H. Steinberg, Eds., Ashworth table. [Online]. Available: https://www.semanticscholar.org/paper/A-Review-%5C%3A-The-Validity-and-Reliability-of-the-as-a-Bauch-Steinberg/aac2976b83964df77646c38137c6143fcdd658b6.

[60] C. Hughes and I. Howard, Eds., Tardieu table. [Online]. Available: https://www.semanticscholar.org/paper/Spasticity-management-in-multiple-sclerosis.-Hughes-Howard/b89d9ac856c0b950f62e9ed3c5ae3b5232abe295.

[61] Musculoskeletal. [Online]. Available: https://s3.amazonaws.com/classconnection/893/flashcards/7930893/jpg/synovial_joint-13ea15b7a286fa1aae6-14CCCF539D7416E08D9.jpg.

[62] C. M, Muscles, a powerful organ - everything you need to know, SciFITence, Ed. [Online]. Available: http://scifitence.com/wp-content/uploads/2020/04/structure-of-skeletal-muscle-1.png.

Appendix

A Appendix : explanations

A.1 Fourier transform

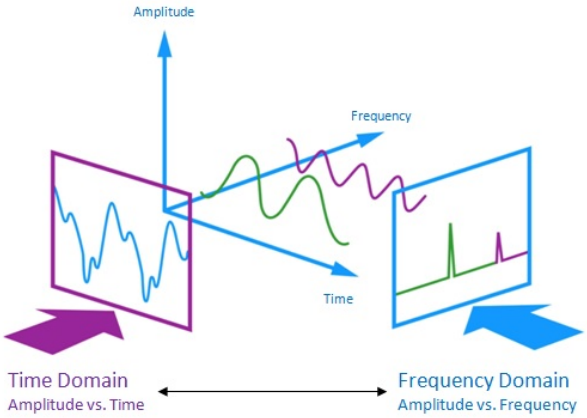
Every differentiable function on an interval P can be approximated by a **Fourier series**. It is an approximation of the original function using a sum of weighted periodical functions as defined in Eqn. (A.1).

$$s_N(x) = \frac{a_0}{2} + \sum_{n=1}^{N} \left(a_n \cdot \cos\left(\frac{2\pi}{P} nx\right) + b_n \cdot \sin\left(\frac{2\pi}{P} nx\right) \right) \tag{A.1}$$

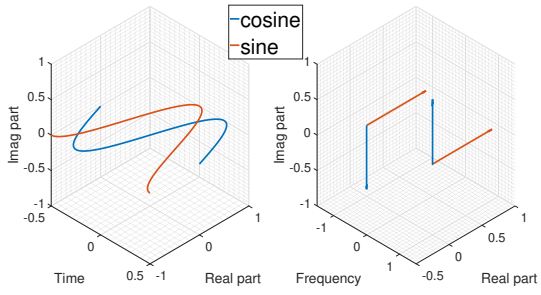
$$a_n = \frac{2}{P} \int_P s(x) \cdot \cos\left(\frac{2\pi}{P} nx\right) dx \tag{A.2}$$

$$b_n = \frac{2}{P} \int_P s(x) \cdot \sin\left(\frac{2\pi}{P} nx\right) dx \tag{A.3}$$

With these periodic functions, the n^{th} harmonics $\sin\left(2\pi x \frac{n}{P}\right)$ and $\cos\left(2\pi x \frac{n}{P}\right)$ have their own amplitudes a_n and b_n respectively (see Eqn. (A.2) and Eqn. (A.3)).
It is also sometimes convenient to represent a signal in the frequency domain, which can be done using a Fourier transform (FT). Basically, every harmonic amplitude (a_n,b_n) of the Fourier series is plotted versus its frequency or harmonic (see Fig. 53a).



(a) Fourier transform construction.



(b) Complex plane representation of sine and cosine function.

Fig. 53: Fourier series.

The sine and cosine function have the particularities of being at a 90° phase shift from one another in the complex plane. In other words, the FT of a cosine function is in phase with the real axis and the FT of a sine function is in phase with the imaginary axis (see Fig. 53b). Broken down in this manner, one can recognize that each of the harmonics have a component. In practice a *Fast Fourier Transform FFT* algorithm is used. It is essentially the same but it computes the same results in only $\mathcal{O}(n \log(n))$ steps in contrast to a $\mathcal{O}(n^2)$ complexity.

A.2 Possible improvement of Detrembleur's method

A further improvement of the method to be studied, would be to isolate the action of the extensor and the flexor from the whole amplitude. The idea behind this, resides in the fact that the wrist's device (Fig. 81) depicts significantly different torque patterns as seen in Fig. 55. Furthermore Kuo and Hu [2] state that spasticity is more often found in the flexor muscles of the upper limb (fingers, wrist, and elbow flexors). It is then interesting to investigate the different PMAS results that could be obtained for, respectively, the flexion and extension motion.

Decomposition of these two parts around the neutral position of the finger and reconstruction of two separate sinewaves is something to be investigated.

The steps involved in the post processing of the data are given in Fig. 54.

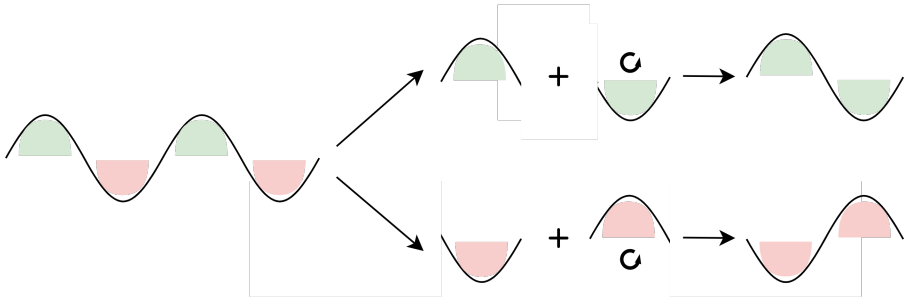


Fig. 54: Post processing of the torque meter signal by two successive steps: (1) Sinewave decomposition and 180° rotation of the odd part of the signal decomposed, (2) Sinewave reconstruction. In this manner, one can supposedly decorate the action of antagonistic muscles.

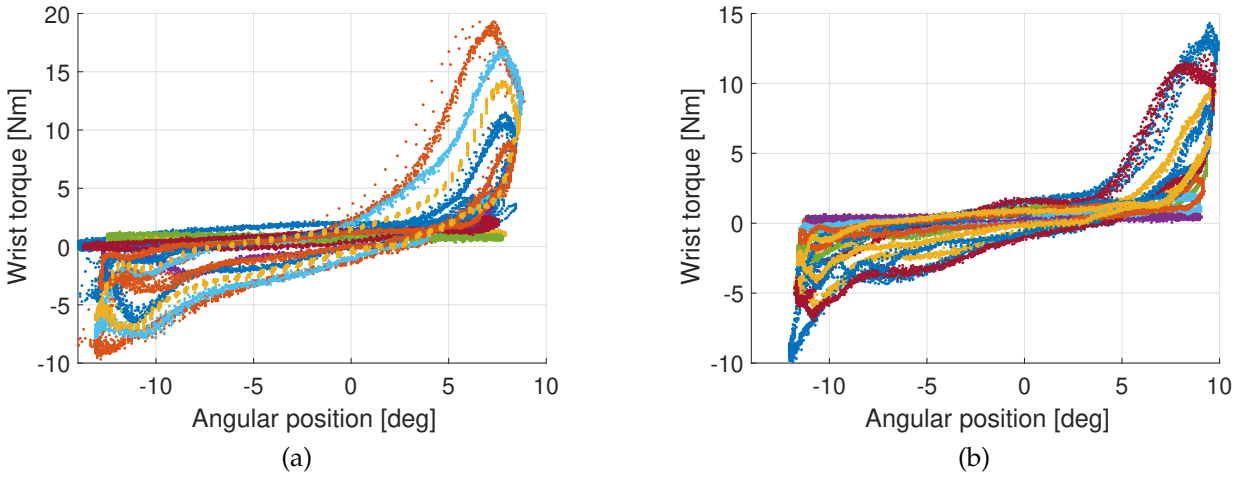


Fig. 55: Wrist EOD results for two patients.

A.3 Robotran analysis

Robotran is a multibody software based on a symbolic generation of equations. It is used to validated the kinematics and dynamics of the four bar mechanism (Fig. 56).
It is composed of 3 bodies and 8 joints (7 revolute joints and a ball[19]). Joints {q1, q2, q5, q6} are fictive prismatic joints that are blocked. They are used to give a DoF in the x and y direction and hence have to be able to assess the x and y forces acting on the bearing located at joint q3 and q7.

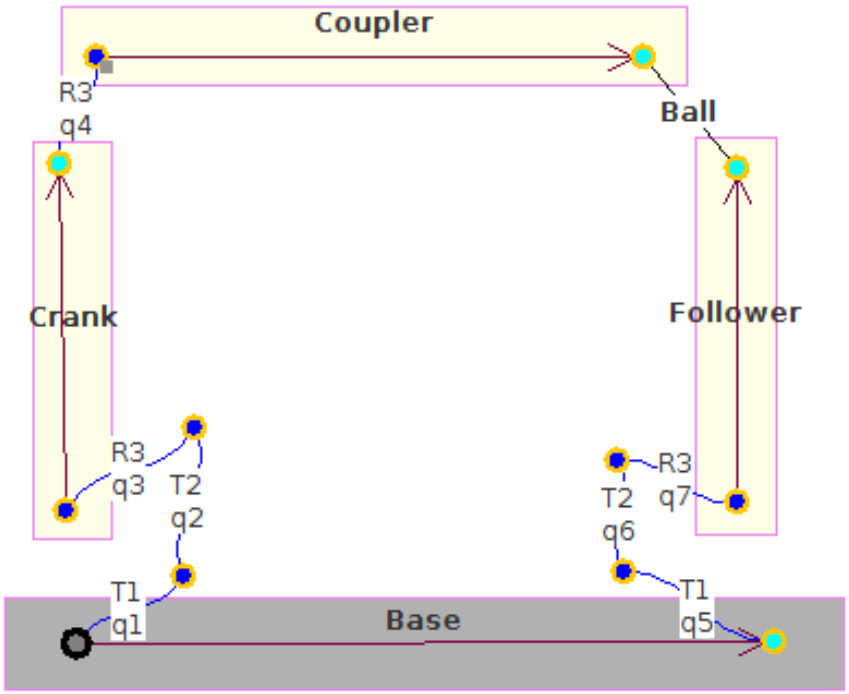


Fig. 56: Graphical description of the multibody system (MBS) on the editor MBsysPad.

A constant rotational velocity is imposed on q3 where the motor is placed (driven joint) and a torsional resistance is applied on q7 following Section 2.1 where the finger is being moved. The torque applied uses the same values as the ones listed in Table 1 and the speed ranges from 3 to 15 Hz at joint q3.

[19] Ideal element necessary in order to close the kinematic loop

A.4 Other articles

Noth et al.'s finger EOD Noth et al. [56] designed a finger-EOD with EMG recording which intended to find the gain and latency of reflex response. They found that two reflex arcs where to be distinguished. A faster one (around 37ms) would indicate a monosynaptic arc and a long latency one, 25ms later, which could result from more complex mechanisms. This machine also requires a constant torque to be maintained by the subject's finger. The frequency of the imposed movement goes with a range of 3 to 16Hz on a short amplitude 1° peak to peak. The linearity of the correction procedure for the stretcher system was verified using passive inertial and elastic loads. Relaxation is monitored with EMG.

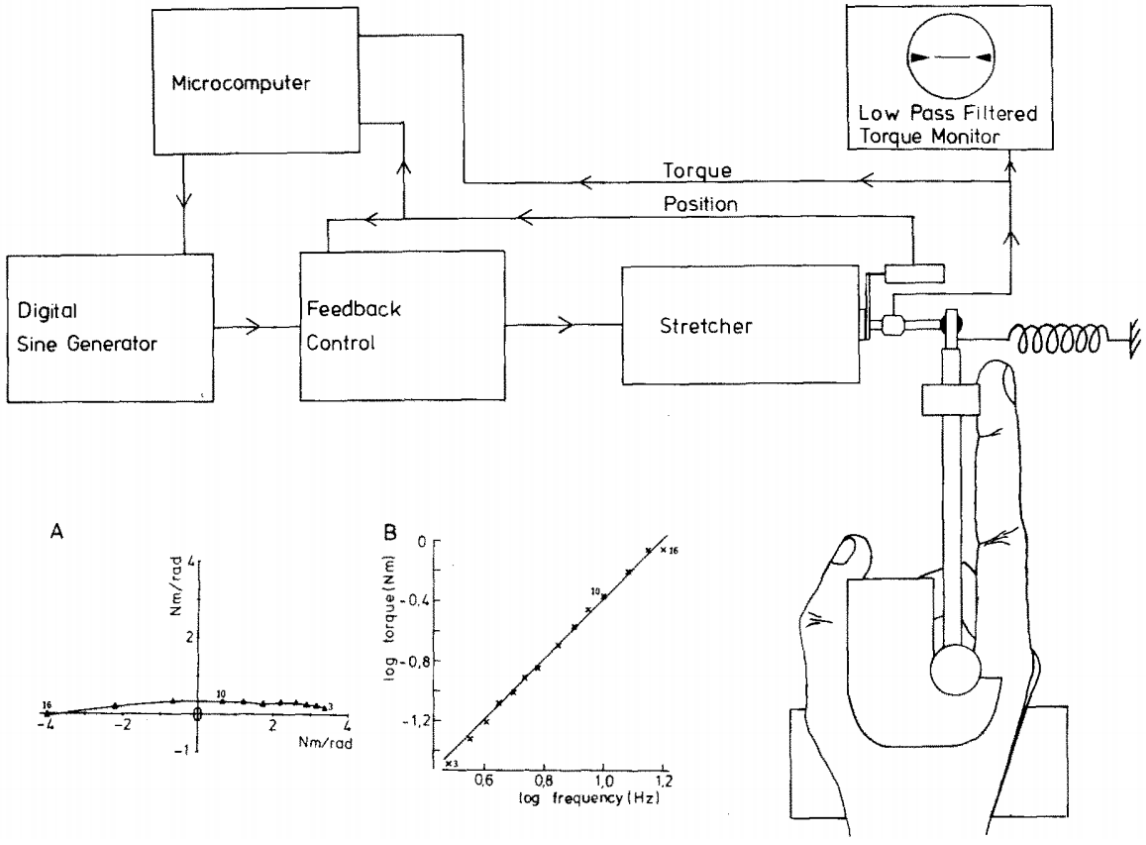
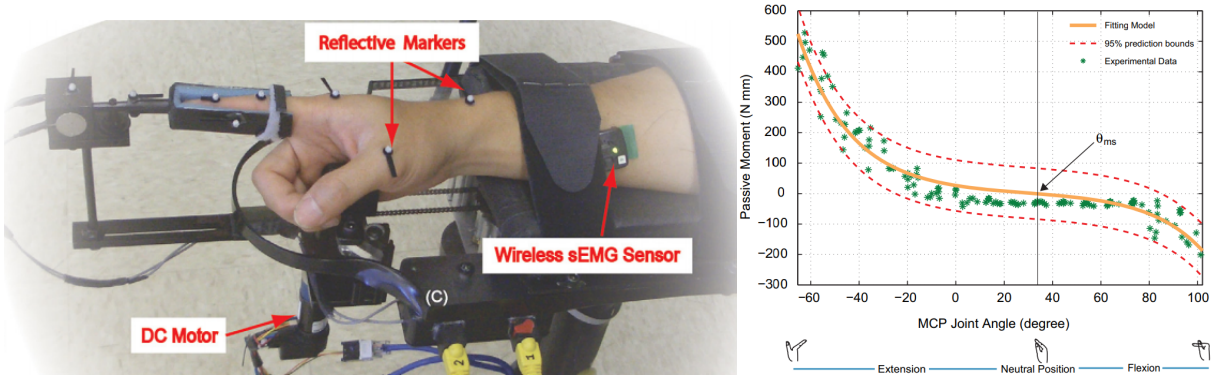


Fig. 57: Schematic diagram of experimental apparatus.

Kuo et al.'s finger EOD This configuration is quite new. The actuator assembly, as well as the sensor assembly are placed below the finger interface. An adjustable driving arm allows to test different sizes of index fingers.

The design objective of this device is to better understand the behaviour of hands in grasping

and manipulation tasks. And from this, enhance the behaviour of robotic hands.



(a) (b)

Fig. 58: (a) Kuo et al.'s finger EOD. (b) Experimental data on the whole pROM.

A.5 Material mechanical dimensioning and properties

The material that was chosen to verify the von Mises yield criterion states that the material remains elastic if the equivalent stress tensor is lesser then the admissible stress i.e. the yield stress σ_Y. Beyond that, the deformation enters the plastic state.

$$\sigma_{eq} < \sigma_Y \tag{A.4}$$

For an infinitesimal volume, the criterion is defined by ;

$$\sigma_{eq} = \sqrt{\frac{1}{2}\left[(\sigma_{11} - \sigma_{22})^2 + (\sigma_{22} - \sigma_{33})^2 + (\sigma_{33} - \sigma_{11})^2\right] + 3\left(\sigma_{12}^2 + \sigma_{23}^2 + \sigma_{13}^2\right)} \tag{A.5}$$

And simplify as ;

$$\sigma_{eq} = \sqrt{\sigma^2 + 3\tau^2} \tag{A.6}$$

Where σ is the sum of traction, compression and flexion constraints and τ is the sum of torsion and shear stress.

The mechanical properties of the materials used are summarized in Table 9.

Material	Mass density ($g.cm^{-3}$)	Young modulus (GPa)	Yield strength (MPa)	Tensile strength (MPa)
Polyacetal	1.34-1.43	2.5-5	48.6 - 72.4	60-89.6
Acrylic	1.18	2.4-3.17	28.6-70.2	60-89.6
Onyx	1.2	3	40	37
Aluminium alloy 6061	2.7	70-80	277	310
EN 1.1191 steel	7.85	190	246	493

Table 9: Material mechanical properties.

1. Young modulus is the slope of the curve in the elastic region.
2. Yield strength - Yield stress is the stress level at the point where the material begins to have permanent deformation at the point of plastic deformation.
3. Tensile strength is the maximum tensile load a material can withstand prior to fracture.

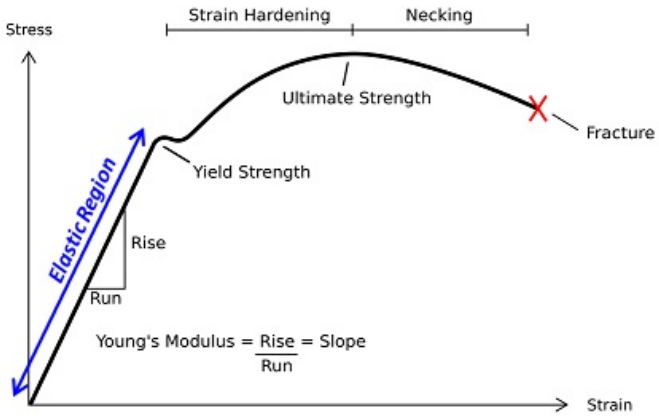


Fig. (1): stress-strain diagram

Fig. 59: Stress-strain diagram.

B Appendix : figures and code

B.1 Computer code

```
function [theta_out_sinewave, mse_sinewave] = sinusparfait(theta_in, theta_out,
    acc)
    theta_out_max = max(theta_out);
    theta_out_min = min(theta_out);
    theta_out_amplitude = theta_out_max - theta_out_min;
    theta_out_offset = theta_out_min + theta_out_amplitude/2;
    delay_init = theta_in(find(theta_out>theta_out_offset,1));

    % the "acc" argument in the function is used to fit the acceleration
    function which is not in phase with the position function
    %
    if acc == 1
        delay_init = theta_in(find(theta_out>theta_out_offset,1)) -90;
    end

    boundary = 20; % deg
    % Changing the delay to find the best sinewave approximation
    delay_list = delay_init - boundary : 0.05 : delay_init + boundary;
    mse_delay_list = [];
    for delay = delay_list
        theta_out_sinewave = theta_out_offset + (theta_out_amplitude/2) * ...
        sind(theta_in - delay);
        erreur = theta_out_sinewave - theta_out; %degree
        mse_delay = mean(erreur.^2);
        mse_delay_list = [mse_delay_list, mse_delay];
    end
    %best within 0.1 deg delay
    [mse_sinewave, idx] = min(mse_delay_list);

    % delay corresponding to the smallest error within the boundary
    delay_min = delay_list(idx);
    theta_out_sinewave = theta_out_offset + (theta_out_amplitude/2) * ...
        sind(theta_in - delay_min);
end
```

Matlab code : sinusparfait.m

```
%%
% D. Doumont
% June 2021
%
% The axis chosen, mass and center of mass of the door are taken from
% the CAD of the door FingerOscillatorV5.SLDASM
% Magnet and spring stays forces and dimensions are taken from MISUMI
% datasheet with ref : HMEN-T and STYSP170.
%
close all;
clear all;
%% Data
g = 9.81;
% Spring stays
F_dmin = 68.6;  %force at minimum contraction in N
F_dmax = 31.4;  %force at minimum contraction in N
d1 = (20+20)*1e-3;   %distance from the extrude in y-axis
d2 = (30+5)*1e-3;   %distance from the door in z-axis
L_dmin = 175*1e-3;   %distance from the door in z-axis
% Magnet
Fa = 29.4;       %single magnet force of attraction in N
L3 = 15*1e-3;   %length in y-axis from the bottom vertical side of the door
% Door
m = 643 * 1e-3;          %mass
CM = [0, 168.41, 54.49]* 1e-3; %center of mass

H = 200*1e-3;            %height
B = 220*1e-3;            %length
%% Computation
syms x1 x2
assume(x1,'real'); assume(x2,'real')
eq1 = (H - (x1+d2))^2 + (B - (x2+d1))^2 - L_dmin^2 == 0;
alpha = atan((H-(x1+d2))/(B-(x2+d1)));
eq2 = F_dmin*(sin(alpha)*x2 - cos(alpha)*d2) - m*g * (CM(2)) - 2*Fa * (H-L3) ==
    0;
eqn = [eq1, eq2]; vars = [x1,x2];
[solL1_magnet,solL2_magnet] =  vpasolve(eqn,vars);

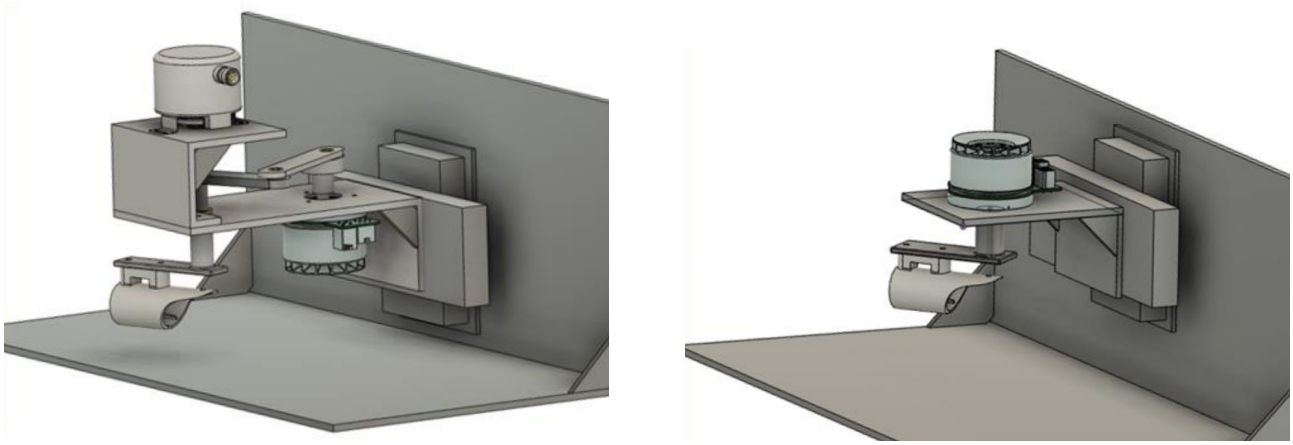
eq2 = F_dmin*(sin(alpha)*x2 - cos(alpha)*d2) - m*g * (CM(2)) == 0;
eqn = [eq1, eq2]; vars = [x1,x2];
```

```
[solL1,solL2] =  vpasolve(eqn,vars);

% Config chosen
solL2_2 = 40.25*1e-3;
%solL1_2 = 120*1e-3;
eq = (H-(x1+d2))^2 + (B-(solL2_2+d1))^2 - L_dmin^2 == 0;
[solL1_2] =  vpasolve(eq,x1,[0,B]);
%config at 0 deg : if the force is negative, the etais help to close the door.
L_dmin = sqrt((H-(solL1_2+d2))^2 + (B-(solL2_2+d1))^2);
alpha = atan((H-(solL1_2+d2))/(B-(solL2_2+d1)));
F_req_0 =  m*g * (CM(2))/(sin(alpha)*solL2_2 - cos(alpha)*d2);
%config at 90 deg
L_dmax = sqrt((B-d1-d2)^2 + (H+solL2_2-solL1_2)^2);
alpha = atan((H+solL2_2-solL1_2))/(B-(d1+d2));
F_req_90 =  m*g * CM(3)/(sin(alpha)*d2 + cos(alpha)*solL2_2);
%% Results
fprintf('Stays position for static force equilibrium\n')
fprintf('--> Sustain mass when closed: L1 = %1.1fmm & L2 = %1.1fmm\n',...
    solL1*1e3, solL2*1e3)
fprintf('--> Sustain mass and magnets when closed: L1 = %1.1fmm & L2 = %1.1fmm\n
    ',...
    solL1_magnet*1e3, solL2_magnet*1e3)
fprintf('Etais position chosen :\n')
fprintf('--> L1 = %1.1fmm & L2 = %1.1fmm \n',solL1_2*1e3, solL2_2*1e3)
fprintf('--> L_dmin(0deg) = %1.1fmm & L_dmax(90deg) = %1.1fmm\n',L_dmin*1e3,
    L_dmax*1e3)
fprintf('--> Force of stays for equilibrium:  F(0deg) = %1.1fN & F(90deg) = %1.1
    fN\n',...
    F_req_0, F_req_90)
```

Matlab code : EtaisValidation.m

B.2 Additional design documents



(a) (b)

Fig. 60: Conceptual design of the master thesis by [5]

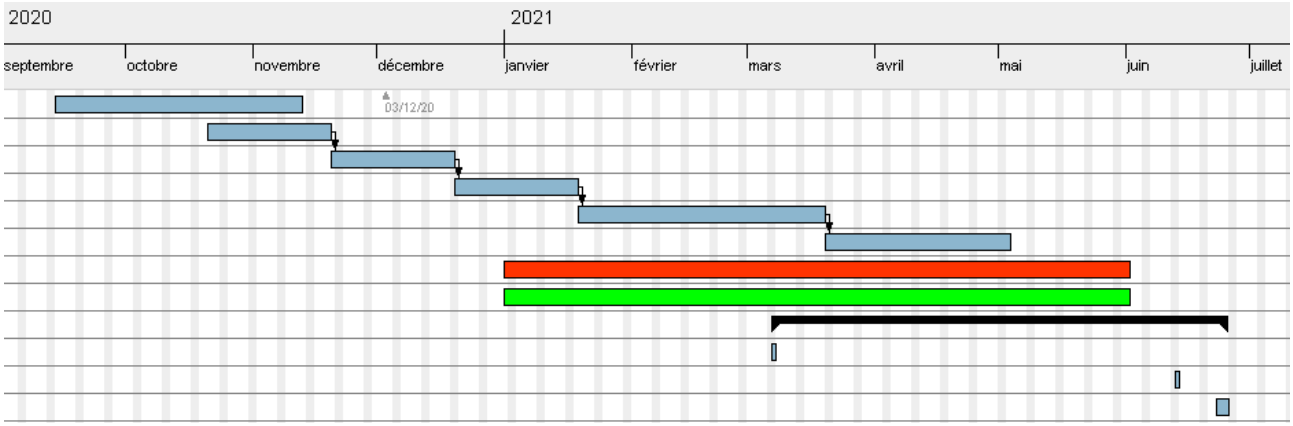


Fig. 61: Planned timeline for the Master's thesis.

Design principles		
Coreless winding : High speed Low torque Low vibration No cogging torque	***ECX SPEED*** High speed applications >10 000 rpm ***EC-max*** Maximum perf-to-price ratio No suitable for high power	***EC 4-pole*** Idea is to provide the highest power possible
Slotted windings : Limited speed (due to magnetic sat.) High torque Possible cogging	***EC-i / ECX TORQUE*** Very dynamic motor with fast acceleration	***EC flat*** Very high torque capability thanks to a large rotor diameter but flat at attractive price Good solution in limited space

Table 10: Comparative of EC motor *Maxon*.

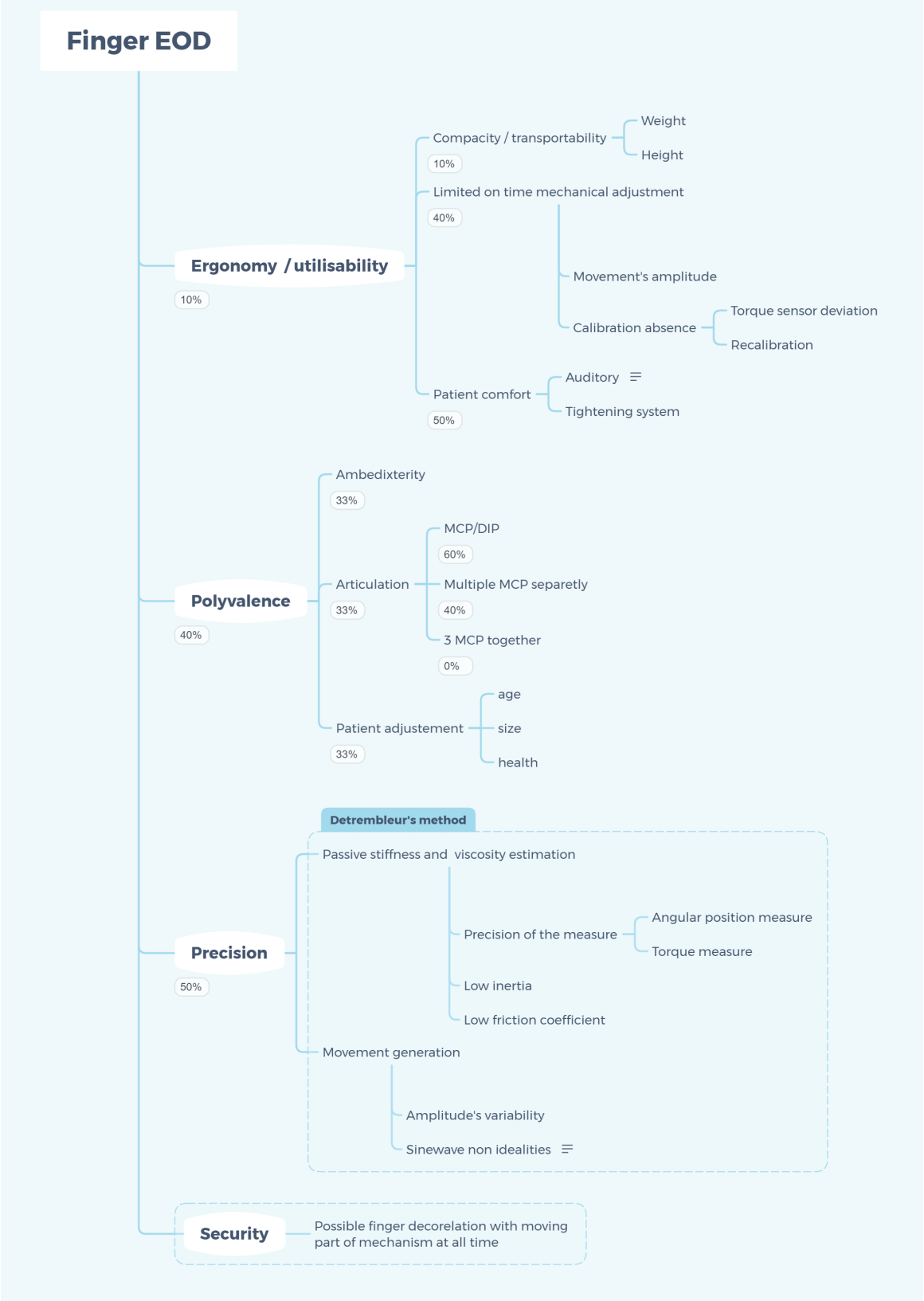


Fig. 62: Objective tree.

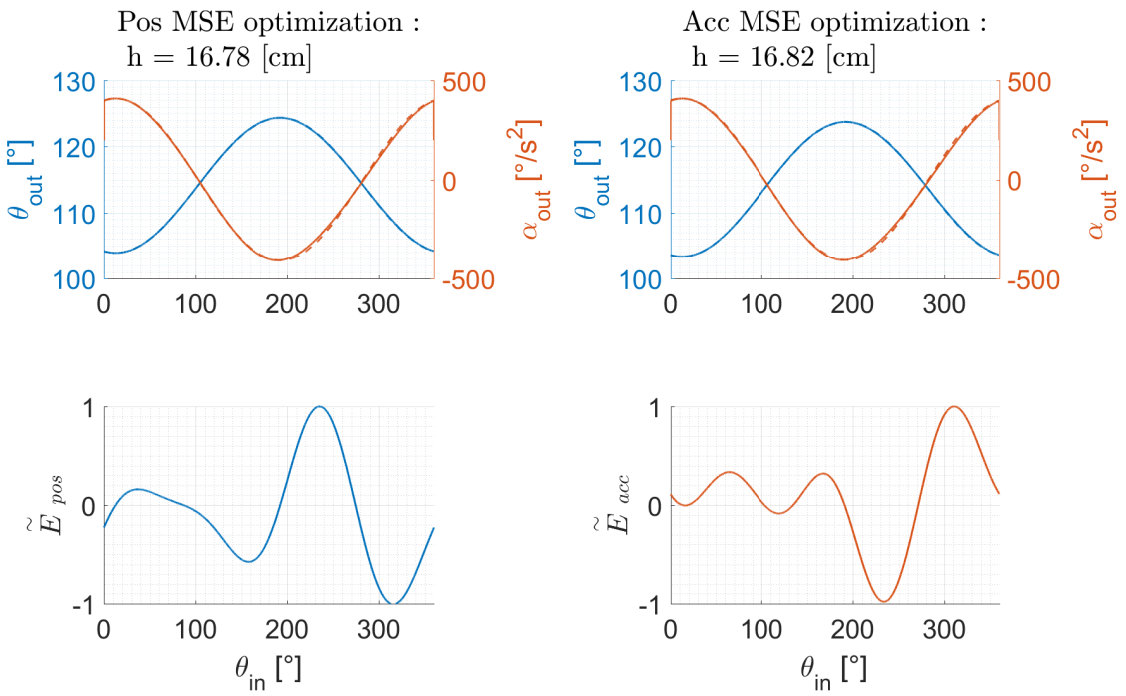


Fig. 63: Optimization of the coupler bar length with 20deg amplitude peak-to-peak. The dashed line is the four bar output angle and the solid one is the fitted sinewave. In blue is the angular position and in orange is the angular acceleration. The two plots on the bottom show the normalized error depending on the position of the first bar (crank).

TYPE OF SENSOR	NON-CONTACT	ADVANTAGES	DISADVANTAGES	NOTES
Potentiometric		• High accuracy • Inexpensive	• High wear and tear • Sensitive to dust • Sensitive to extreme temperatures	• Linear or angular sensor
LVDT or **RVDT**		• High accuracy • Heavy duty • Low sensitivity to harsh environments	• Quite expensive • Bulky and heavy	• RVDT: rotation limited to 40° more or less
Optical		• High accuracy • High resolution	• Fragile • Sensitive to dust • Sensitive to extreme temperatures	• More expensive than a magnetic sensor
Magnetic Hall effect	X	• Heavy duty • Low sensitivity to liquid	• Sensitive to impact • Disrupted by magnetic materials and electrical wires • Hysteresis	
Magnetostrictive	X	• Heavy duty • Accurate for long lengths	• Sensitive to temperature changes • Lack of accuracy for short lengths • Quite expensive	

Fig. 64: Position transducer type and characteristics [57].

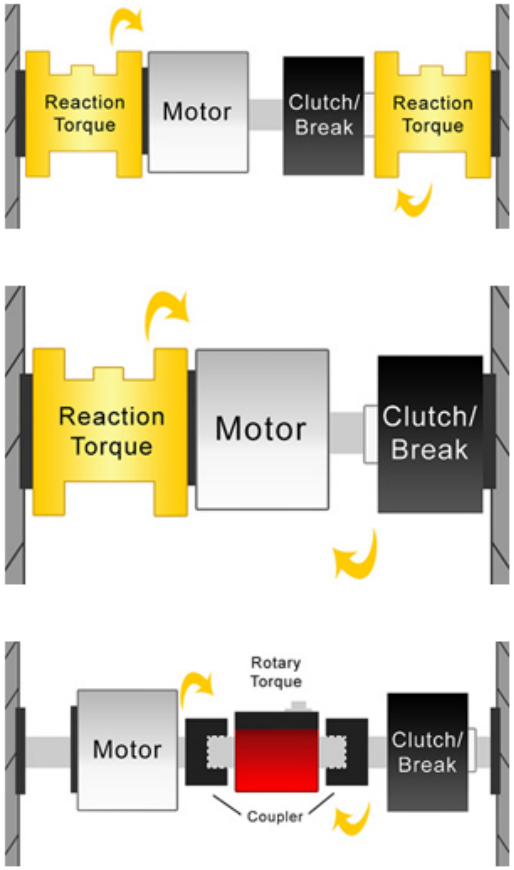


Fig. 65: Illustration of torque measurement type given its location in kinematic chain.

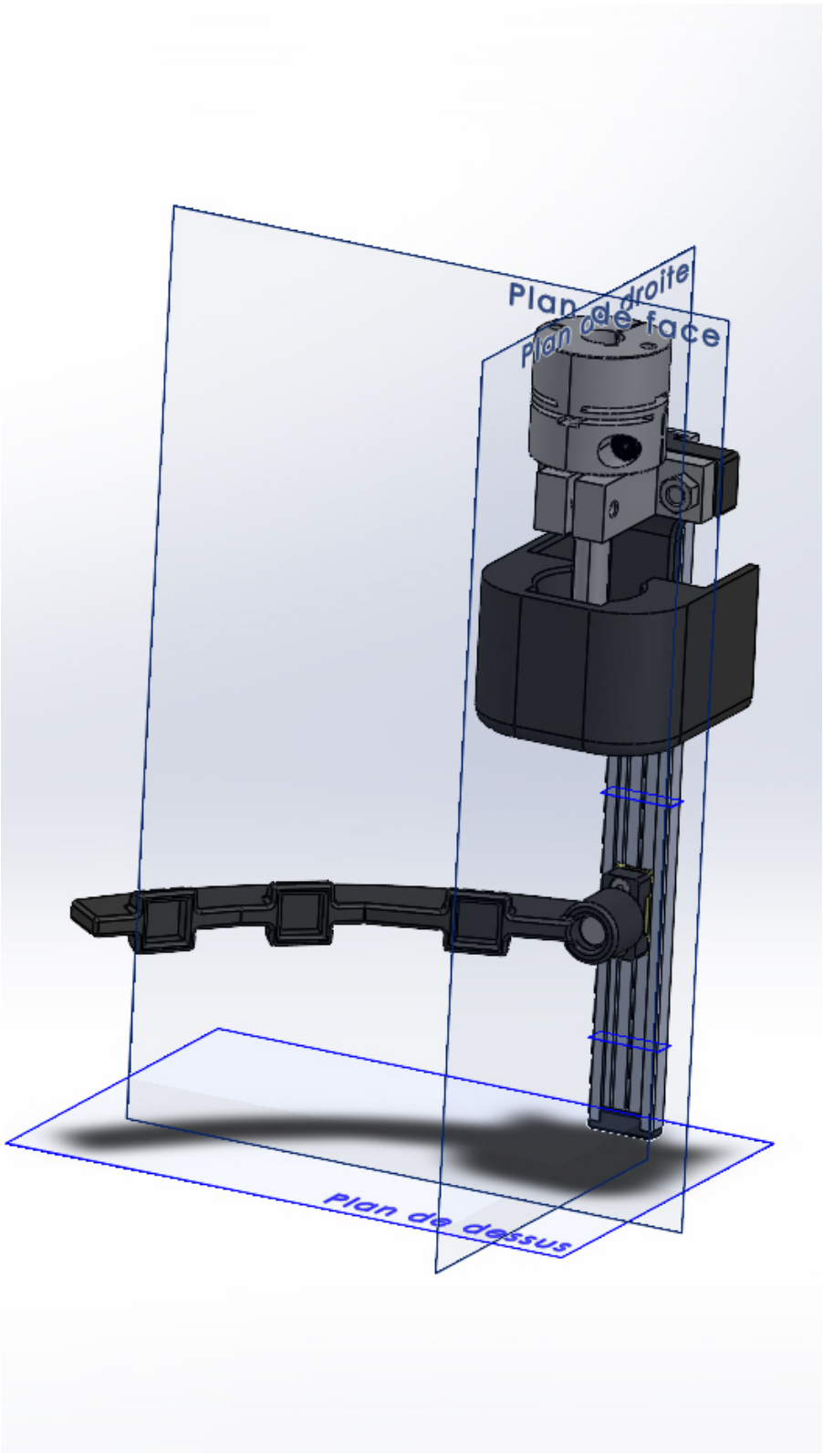
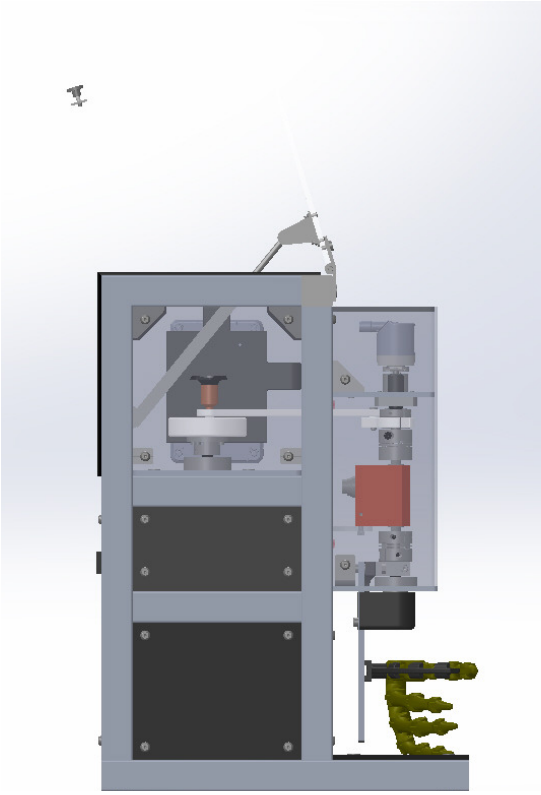
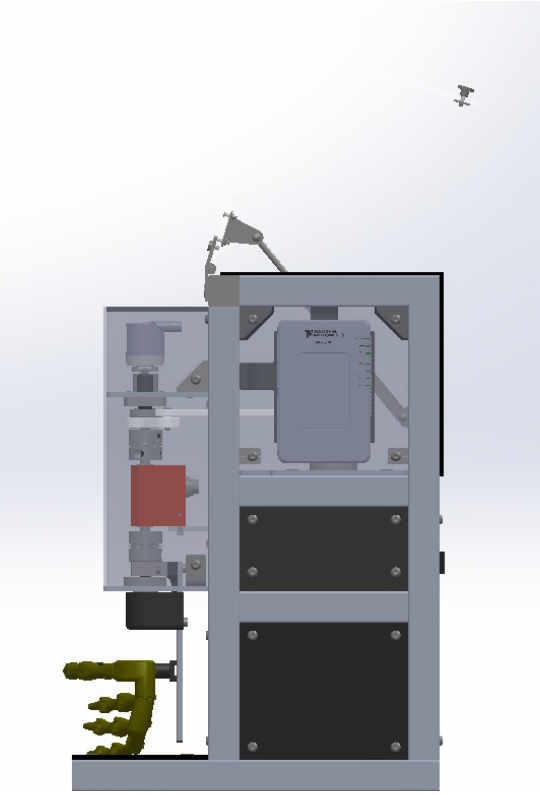


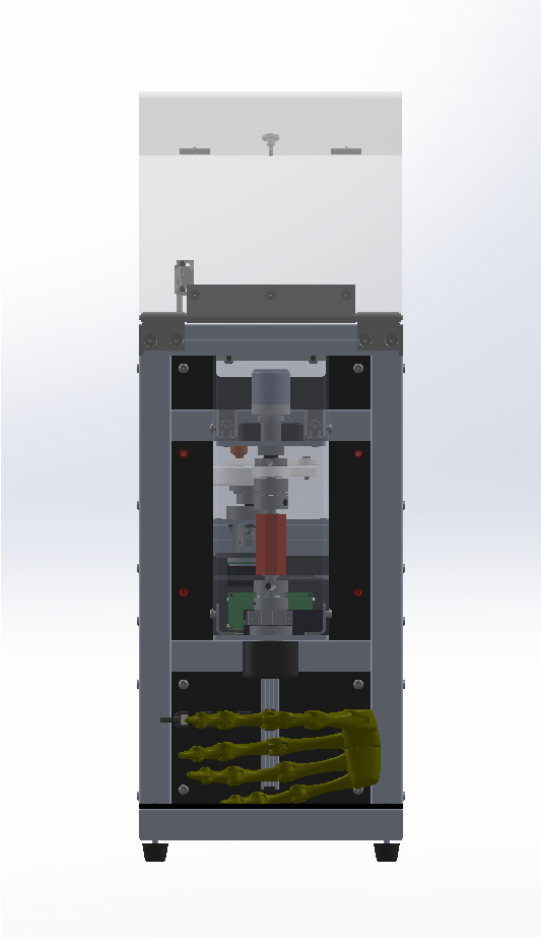
Fig. 66: Finger interface (CAD) : Inertial oscillating system measured by the torque meter.



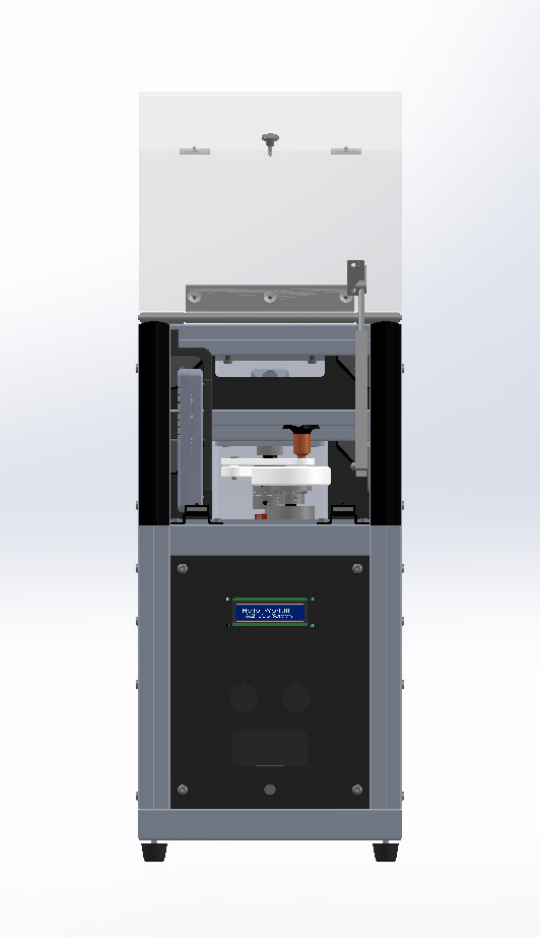
(a) Left view.



(b) Right view.



(c) Front view.



(d) Back view.

Fig. 67: Global prototype views (CAD) : left and right, front and back view.

B.3 Clinical aspects

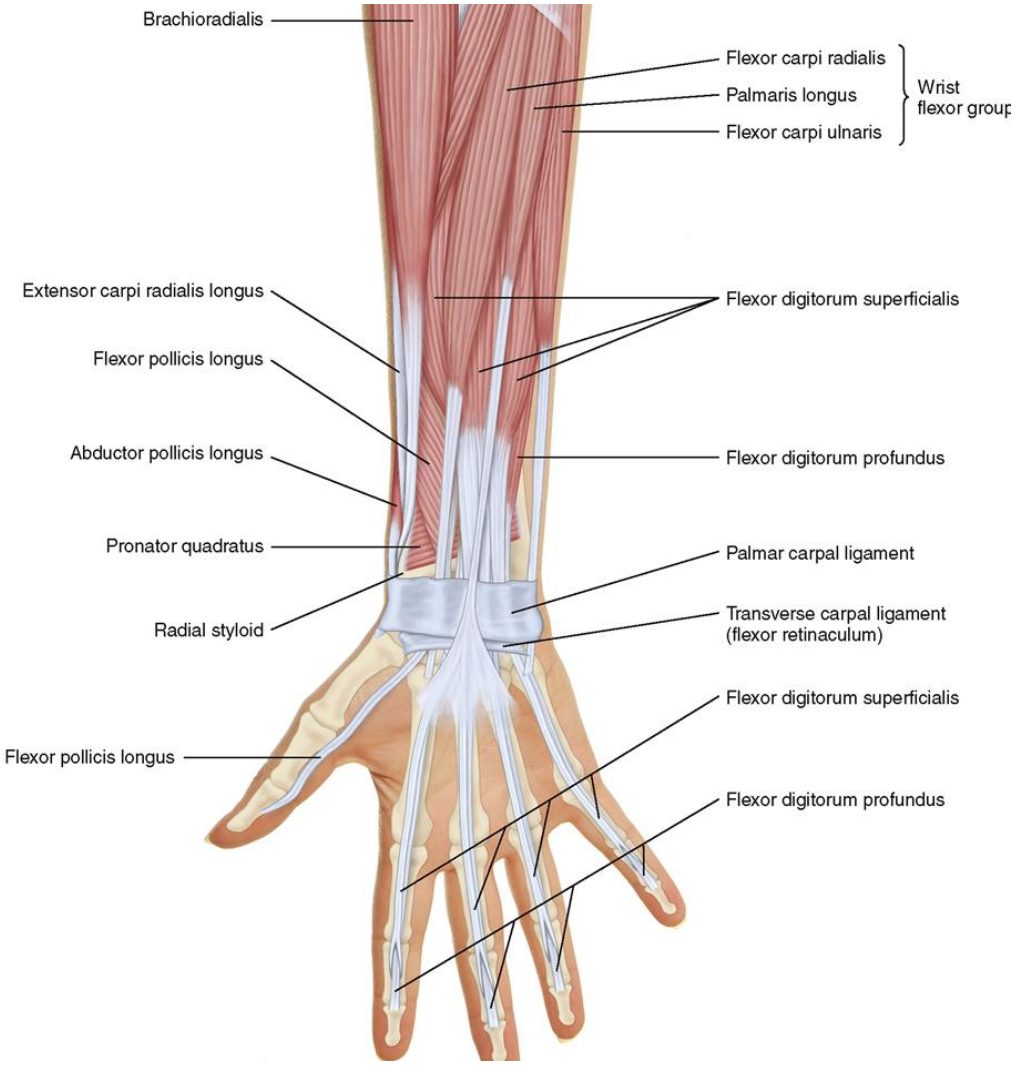


Fig. 68: Anterior view of muscles of the right wrist joint (a) Superficial view [58].

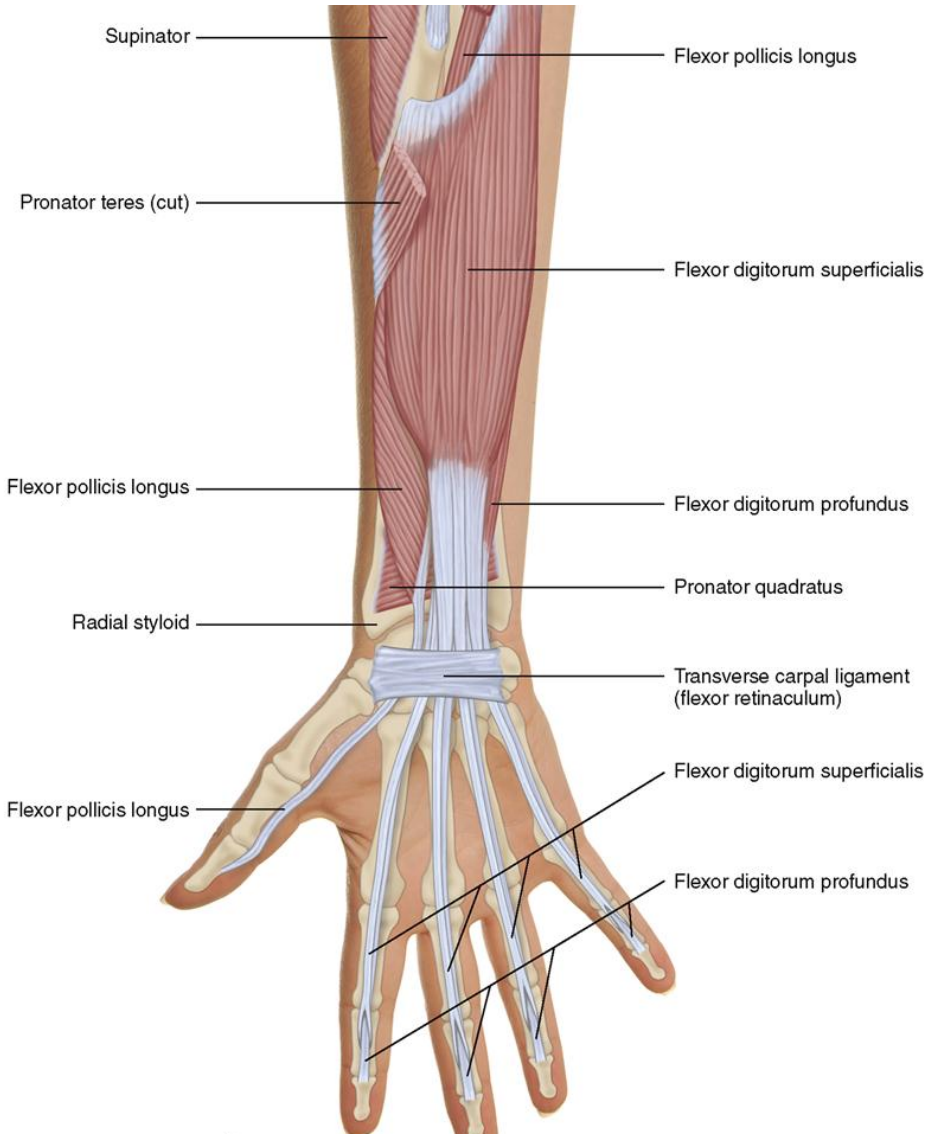


Fig. 69: Anterior view of muscles of the right wrist joint (b) Intermediate view [58].

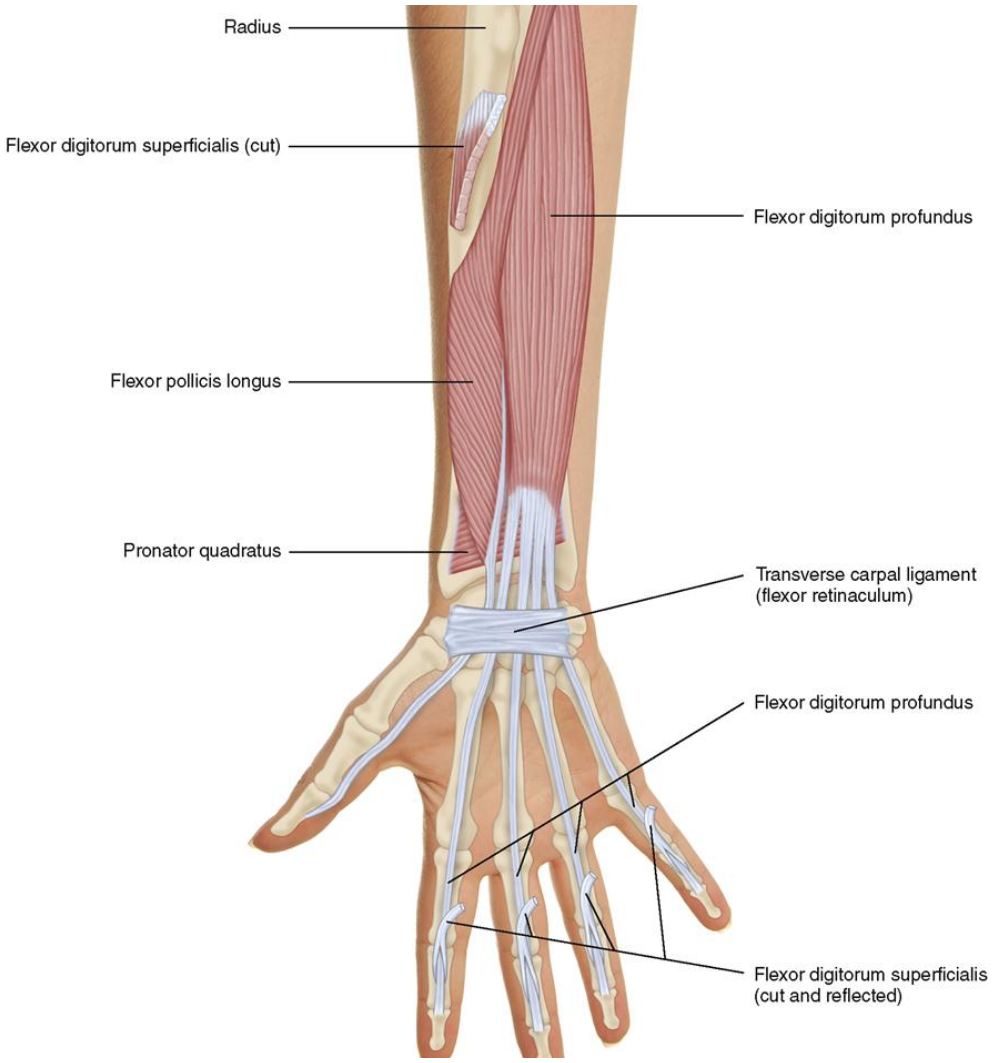


Fig. 70: Anterior view of muscles of the right wrist joint (c) Deep view [58].

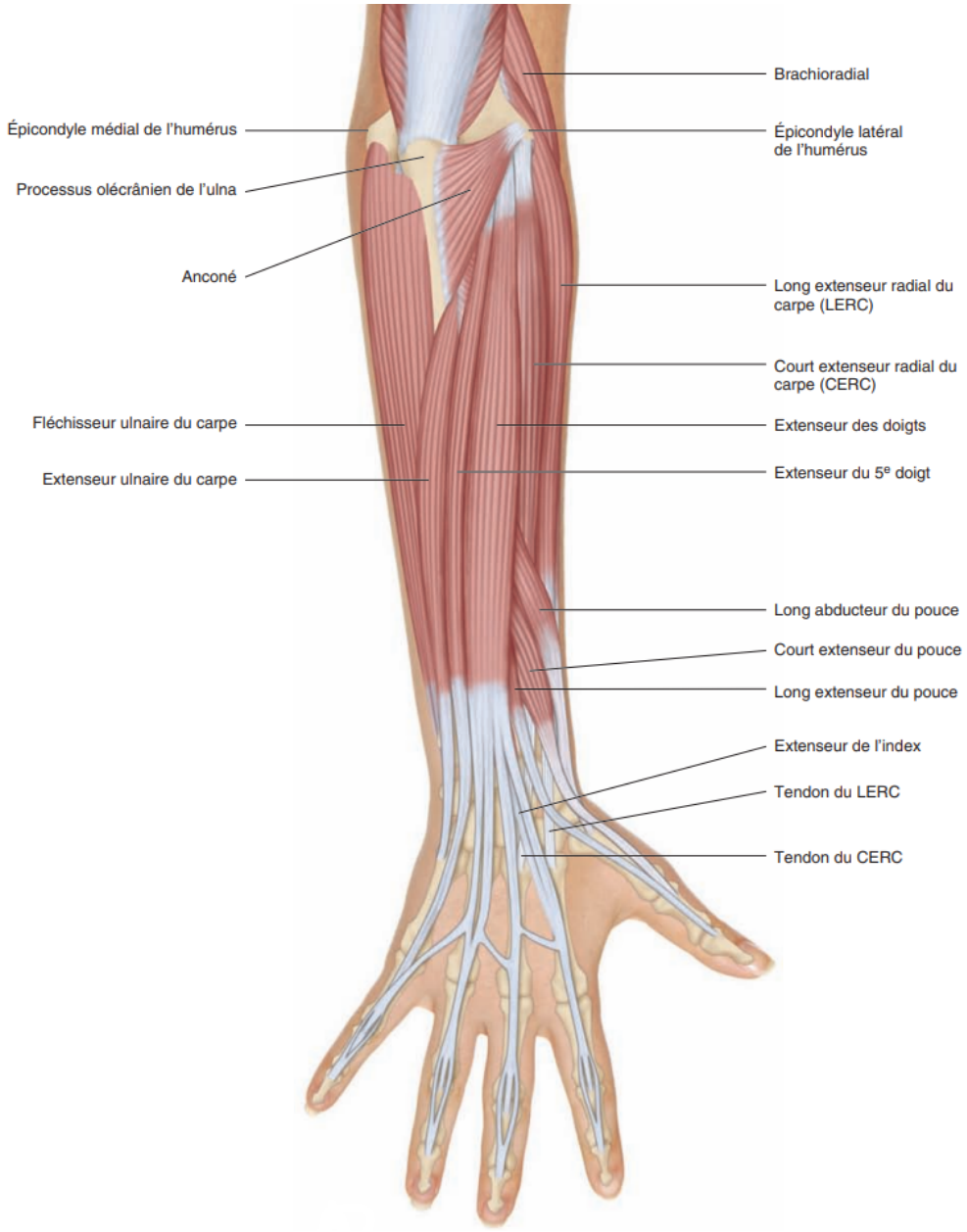


Fig. 71: Posterior view of muscles of the right wrist joint (a) Superficial view in french annotations [58].

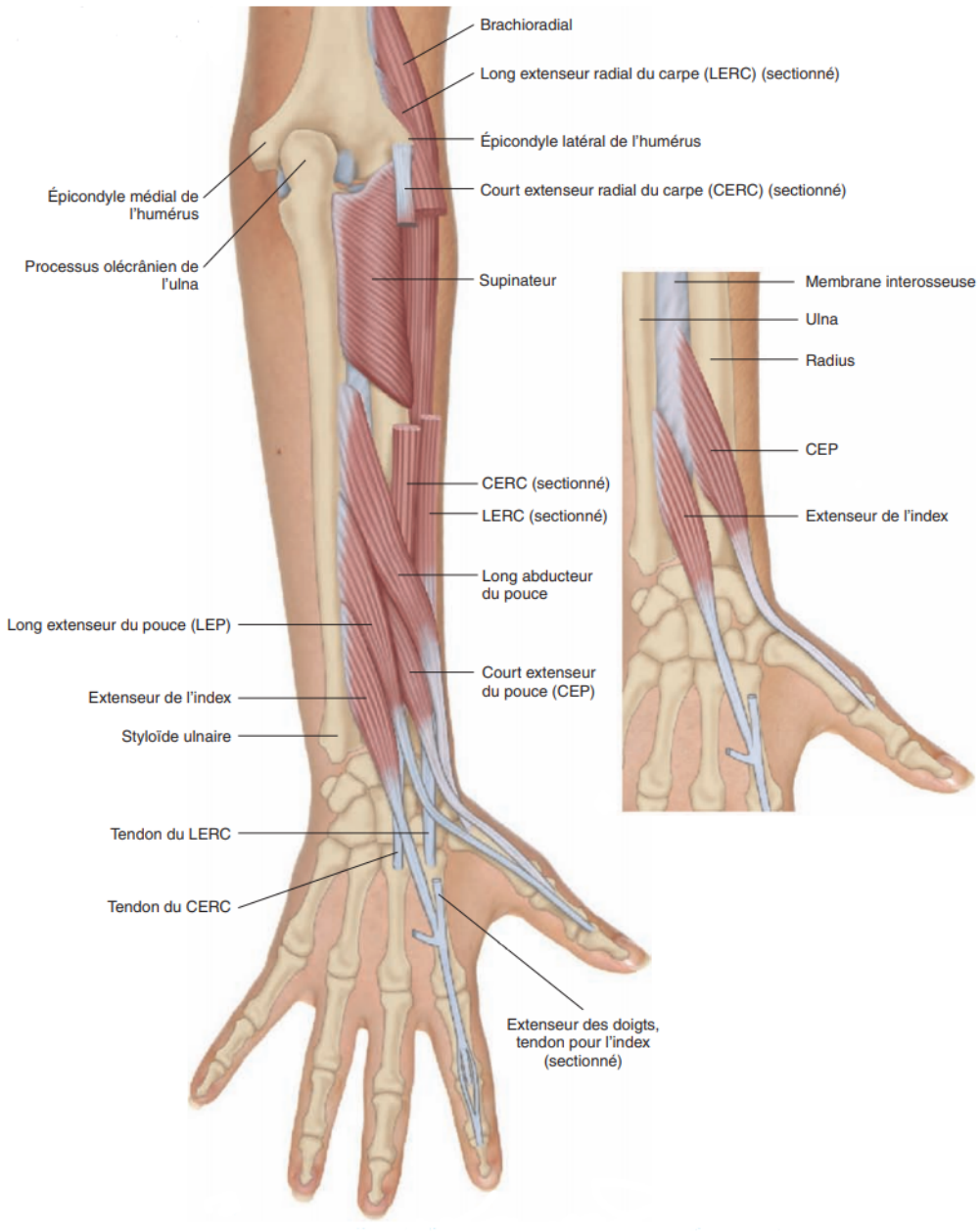


Fig. 72: Posterior view of muscles of the right wrist joint (b) Deep view in french annotations [58].

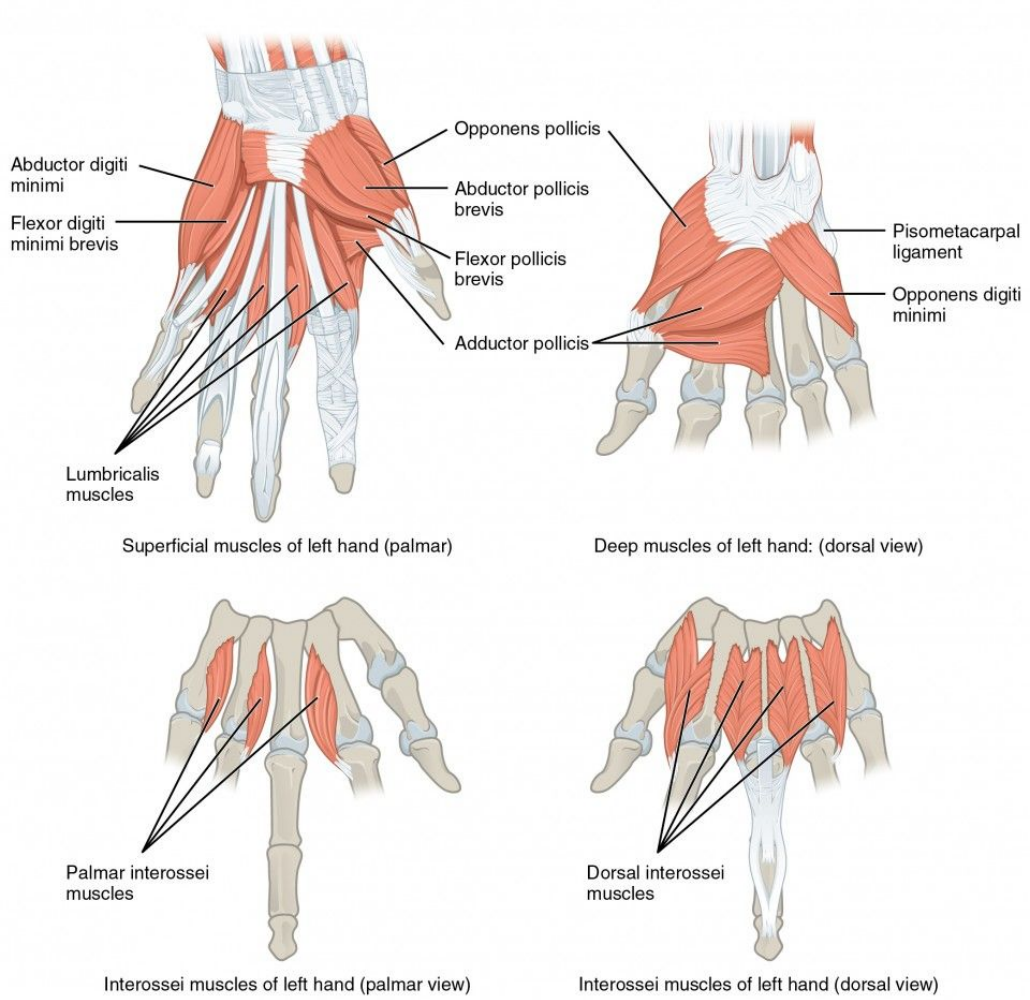


Fig. 73: Intrinsic muscles of the hand.

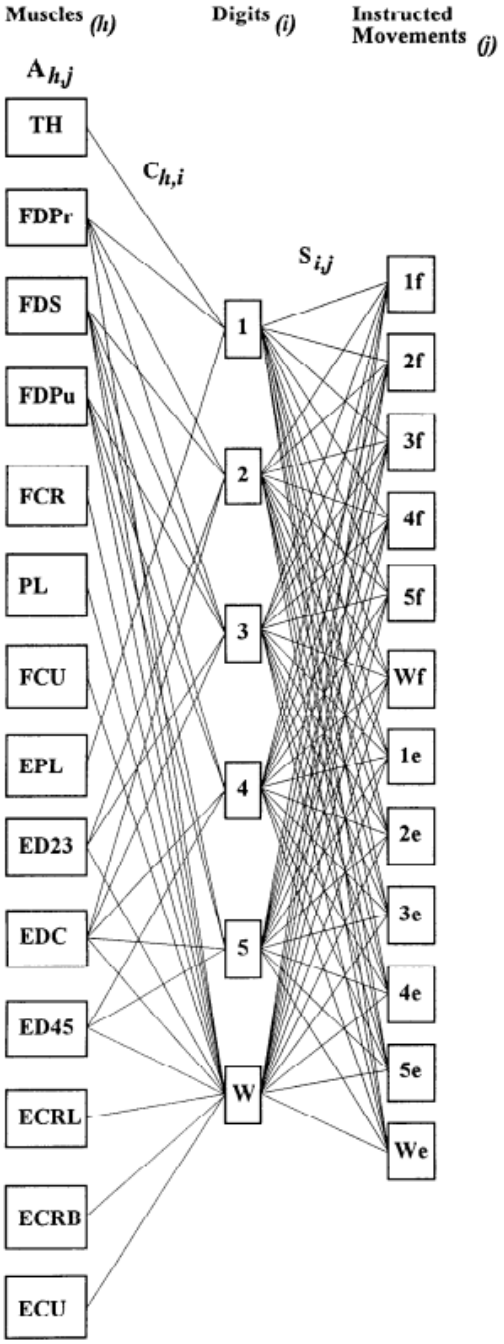


Fig. 74: Three-level connection model of muscles which links the digit motion during each finger movement [9]. The muscles abbreviations are successively : thenar ; flexor digitorium profundus, ulnar region (FDPu); flexor digitorum superficialis (FDS); flexor carpiradialis (FCR); palmaris longus (PL); flexor carpi ulnaris (FCU); extensor or digitorum communis (EDC); extensor digiti quarti et quinti (ED45); extensor carpi radialis longus (ECRL); extensor carpi radialis brevis (ECRB); and extensor carpi ulnaris (ECU). For the digits : 1-5 are the fingers and W is the wrist. For the movement, the numbers designate the digits in motion, "f" stands for flexion and "e" for extension.

Table 2: The Modified Ashworth Scale (Bohannon and Smith, 1987)

Grade	Description
0	No increase in muscle tone
1	Slight increase in muscle tone, manifested by a catch and release or by minimal resistance at the end of the ROM when the affected part(s) is moved in flexion or in extension
1+	Slight increase in muscle tone, manifested by a catch, followed by minimal resistance throughout the reminder (less than half) of the ROM
2	More marked increase in muscle tone throughout most of the ROM, but affected part(s) easily moved
3	Considerable increase in muscle tone, passive movement is difficult
4	Affected part(s) rigid in flexion or extension

Fig. 75: Modified Ashworth table [59].

Table 3
Tardieu scale

Velocities	
V1	As slow as possible, slower than the natural drop of the limb segment under gravity
V2	Speed of limb segment falling under gravity
V3	As fast as possible, faster than the rate of the natural drop of the limb segment under gravity
Scoring	
0	No resistance throughout the course of the passive movement
1	Slight resistance throughout the course of passive movement, no clear catch at a precise angle
2	Clear catch at a precise angle, interrupting the passive movement, followed by release
3	Fatigable clonus with less than 10 s when maintaining the pressure and appearing at the precise angle
4	Unfatigable clonus with more than 10 s when maintaining the pressure and appearing at a precise angle
5	Joint is immovable

Fig. 76: Modified Tardieu table [60].

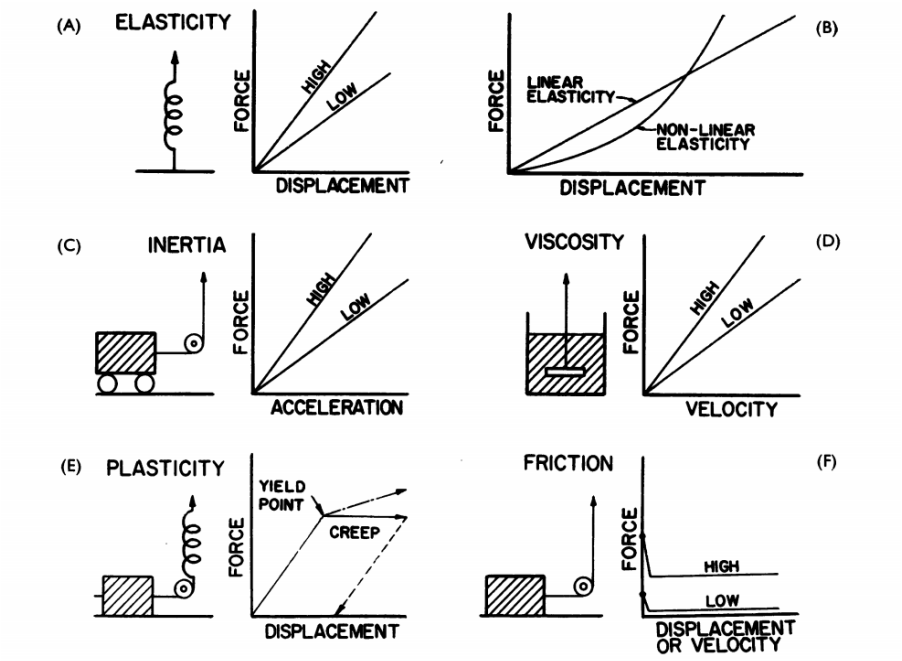


Fig. 3.—Force relationships in five types of stiffness.

A. Elastic stiffness exemplified by an ideal spring, showing a linear relation between force and displacement. A stiffer spring exhibits a greater stiffness (steeper slope).

B. Linear and non-linear elasticity in which stiffness (slope) increases with displacement.

C. Inertial stiffness exemplified by a mass moving on frictionless bearings, showing a linear relation between force and acceleration.

D. Viscous stiffness exemplified by a plate moving through an ideal viscous fluid, showing a linear relation between force and velocity. Increased viscosity results in greater viscous stiffness (steeper slope).

E. Plastic stiffness illustrated by a spring attached to a frictional element. The yielding behaviour is described in the text.

F. Frictional stiffness exemplified by two opposing surfaces. The force is independent of displacement or velocity and is greatest at rest.

Fig. 77: Forces relationships in five types of stiffness in Wright and Johns [42].

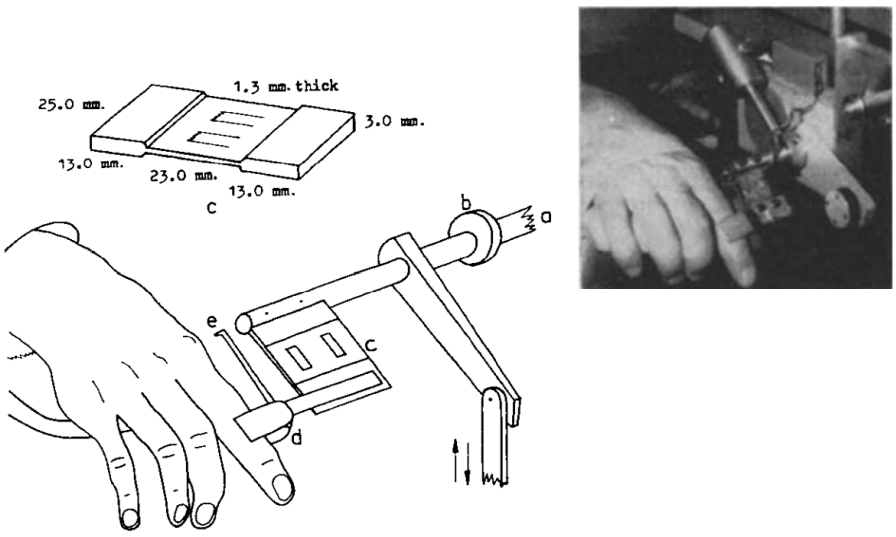


Fig. 78: Apparatus of Bäcklund and Tiselius [43].

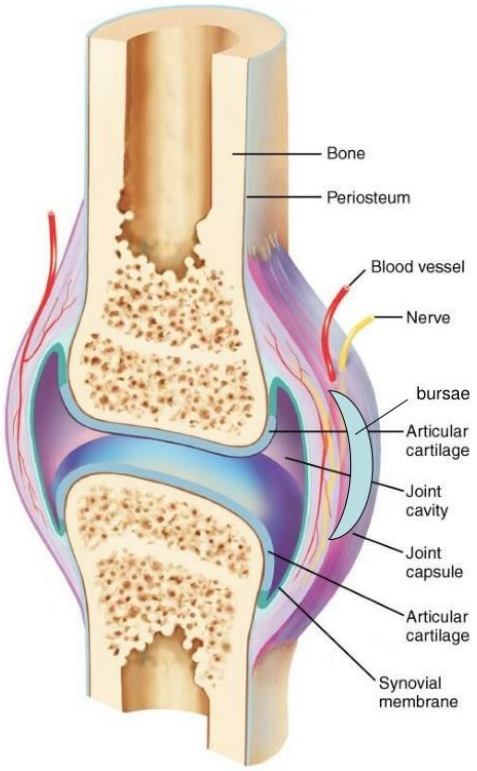


Fig. 79: Joint capsule complex structure [61].

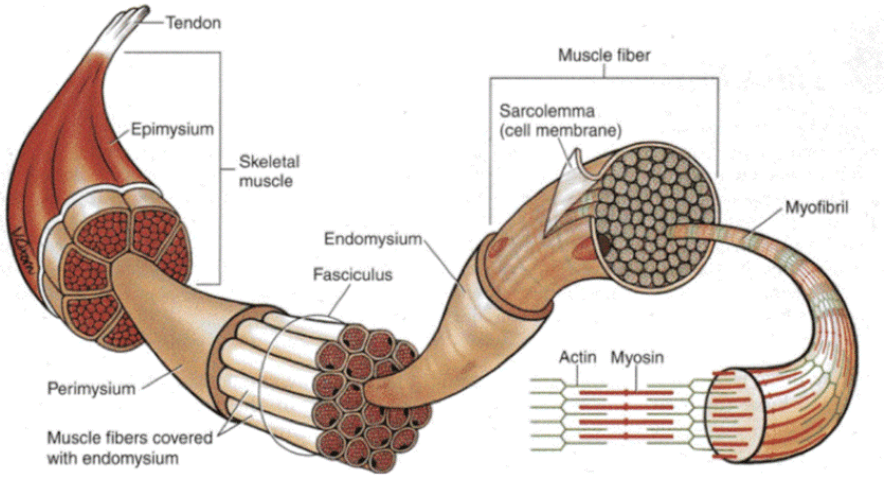
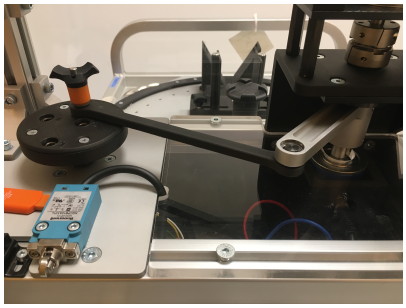
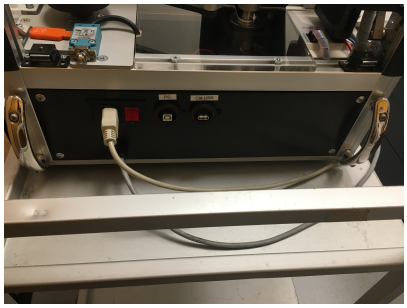


Fig. 80: Structure of a skeletal muscle [62].

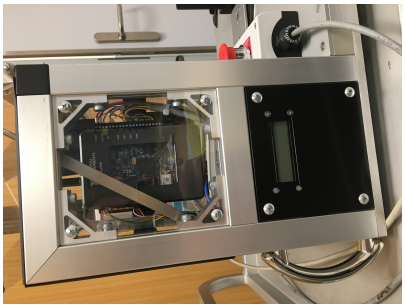
B.4 Wrist PMAS device



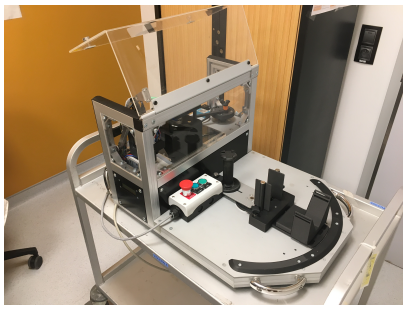
(a)



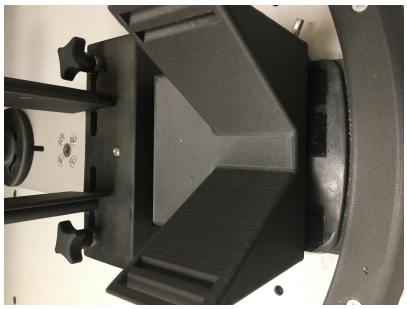
(b)



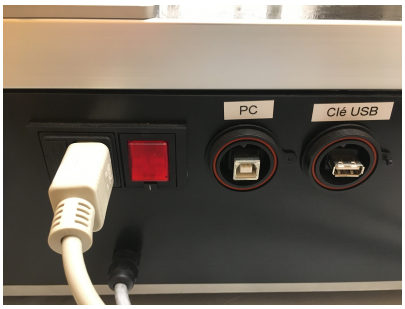
(c)



(d)



(e)

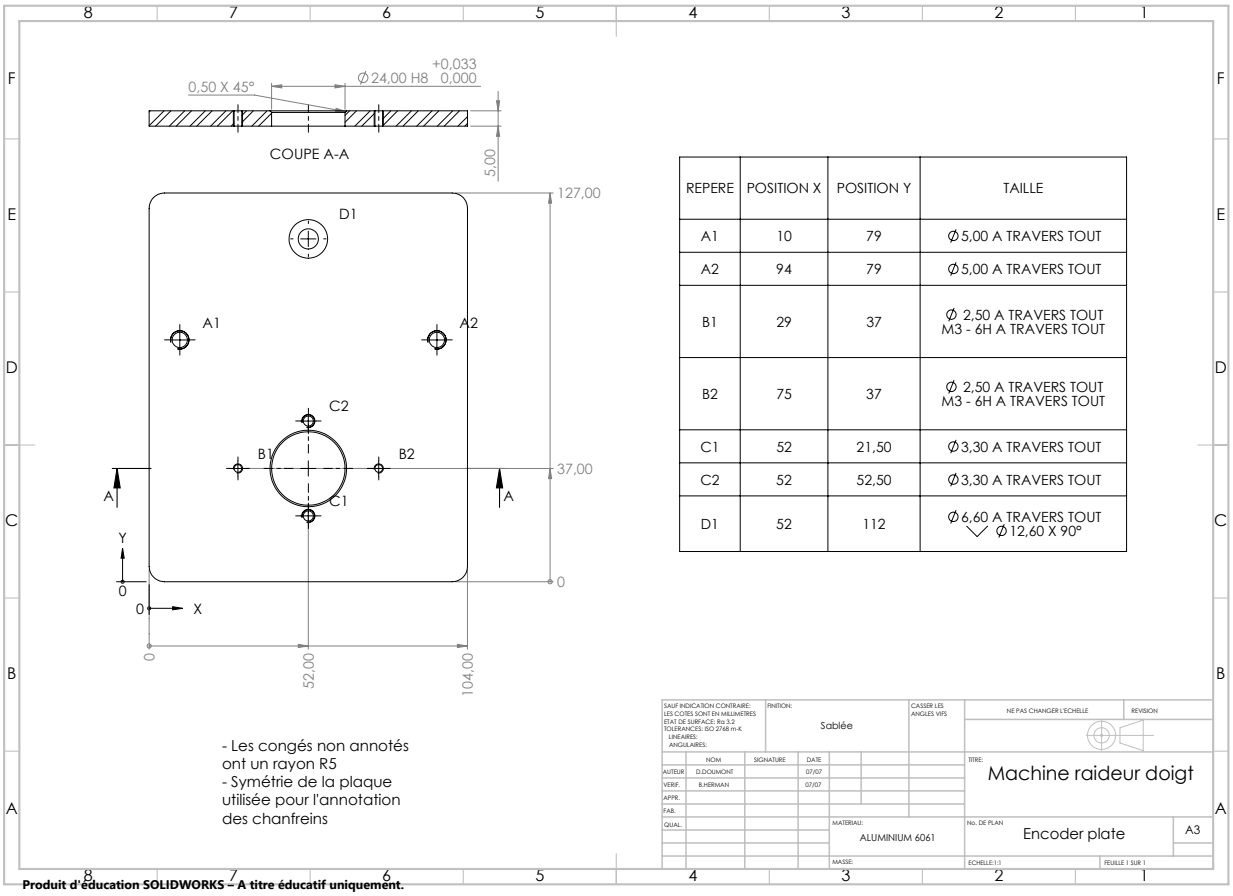


(f)

Fig. 81: Wrist EOD.

C Appendix : technical doc

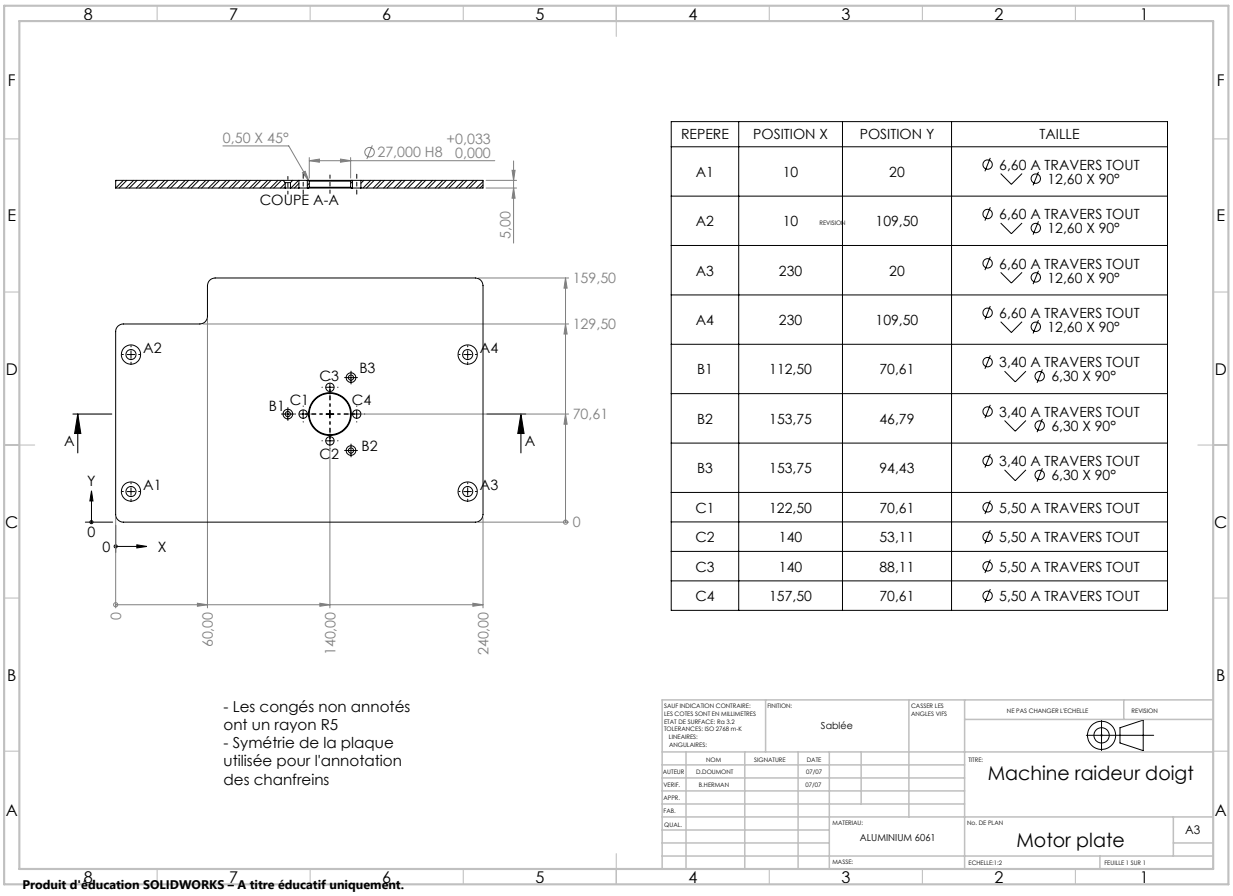
Drawings of machined pieces



REPERE	POSITION X	POSITION Y	TAILLE
A1	10	79	Ø5,00 A TRAVERS TOUT
A2	94	79	Ø5,00 A TRAVERS TOUT
B1	29	37	Ø 2,50 A TRAVERS TOUT M3 - 6H A TRAVERS TOUT
B2	75	37	Ø 2,50 A TRAVERS TOUT M3 - 6H A TRAVERS TOUT
C1	52	21,50	Ø3,30 A TRAVERS TOUT
C2	52	52,50	Ø3,30 A TRAVERS TOUT
D1	52	112	Ø6,60 A TRAVERS TOUT Ø12,60 X 90°

SAUF INDICATION CONTRAIRE: LES COTES SONT EN MILLIMETRES ETAT DE SURFACE: Ra 3.2 TOLERANCES: ISO 2768 m-K LINEAIRES: ANGULAIRES:	FINITION: Sablée	CASSER LES ANGLES VIFS	NE PAS CHANGER L'ECHELLE / REVISION
	NOM	SIGNATURE	DATE
AUTEUR	D.DOUMONT		07/07
VERIF.	B.HERMAN		07/07
APPR.			
FAB.			
QUAL.			
MATERIAU: ALUMINIUM 6061			TITRE: Machine raideur doigt
MASSE:			No. DE PLAN: Encoder plate / A3
			ECHELLE:1:1 / FEUILLE 1 SUR 1

Produit d'éducation SOLIDWORKS – A titre éducatif uniquement.



REPERE	POSITION X	POSITION Y	TAILLE
A1	10	20	Ø 6,60 A TRAVERS TOUT ⌵ Ø 12,60 X 90°
A2	10	109,50	Ø 6,60 A TRAVERS TOUT ⌵ Ø 12,60 X 90°
A3	230	20	Ø 6,60 A TRAVERS TOUT ⌵ Ø 12,60 X 90°
A4	230	109,50	Ø 6,60 A TRAVERS TOUT ⌵ Ø 12,60 X 90°
B1	112,50	70,61	Ø 3,40 A TRAVERS TOUT ⌵ Ø 6,30 X 90°
B2	153,75	46,79	Ø 3,40 A TRAVERS TOUT ⌵ Ø 6,30 X 90°
B3	153,75	94,43	Ø 3,40 A TRAVERS TOUT ⌵ Ø 6,30 X 90°
C1	122,50	70,61	Ø 5,50 A TRAVERS TOUT
C2	140	53,11	Ø 5,50 A TRAVERS TOUT
C3	140	88,11	Ø 5,50 A TRAVERS TOUT
C4	157,50	70,61	Ø 5,50 A TRAVERS TOUT

REVISION

- Les congés non annotés ont un rayon R5
- Symétrie de la plaque utilisée pour l'annotation des chanfreins

SAUF INDICATION CONTRAIRE:
LES COTES SONT EN MILLIMETRES
ETAT DE SURFACE: Ra 3.2
TOLERANCES: ISO 2768 m-K
LINEAIRES:
ANGULAIRES:

FINITION: Sablée

CASSER LES ANGLES VIFS

NE PAS CHANGER L'ECHELLE

REVISION

	NOM	SIGNATURE	DATE
AUTEUR	D.DOUMONT		07/07
VERIF.	B.HERMAN		07/07
APPR.			
FAB.			
QUAL.			

MATERIAU: ALUMINIUM 6061

MASSE:

TITRE: Machine raideur doigt

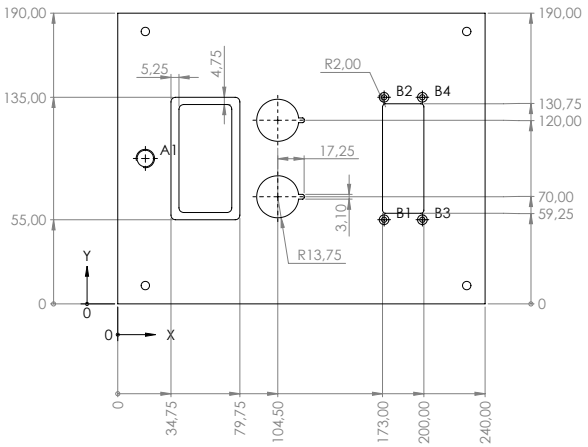
No. DE PLAN: Motor plate

A3

ECHELLE:1:2

FEUILLE 1 SUR 1

Produit d'éducation SOLIDWORKS - A titre éducatif uniquement.

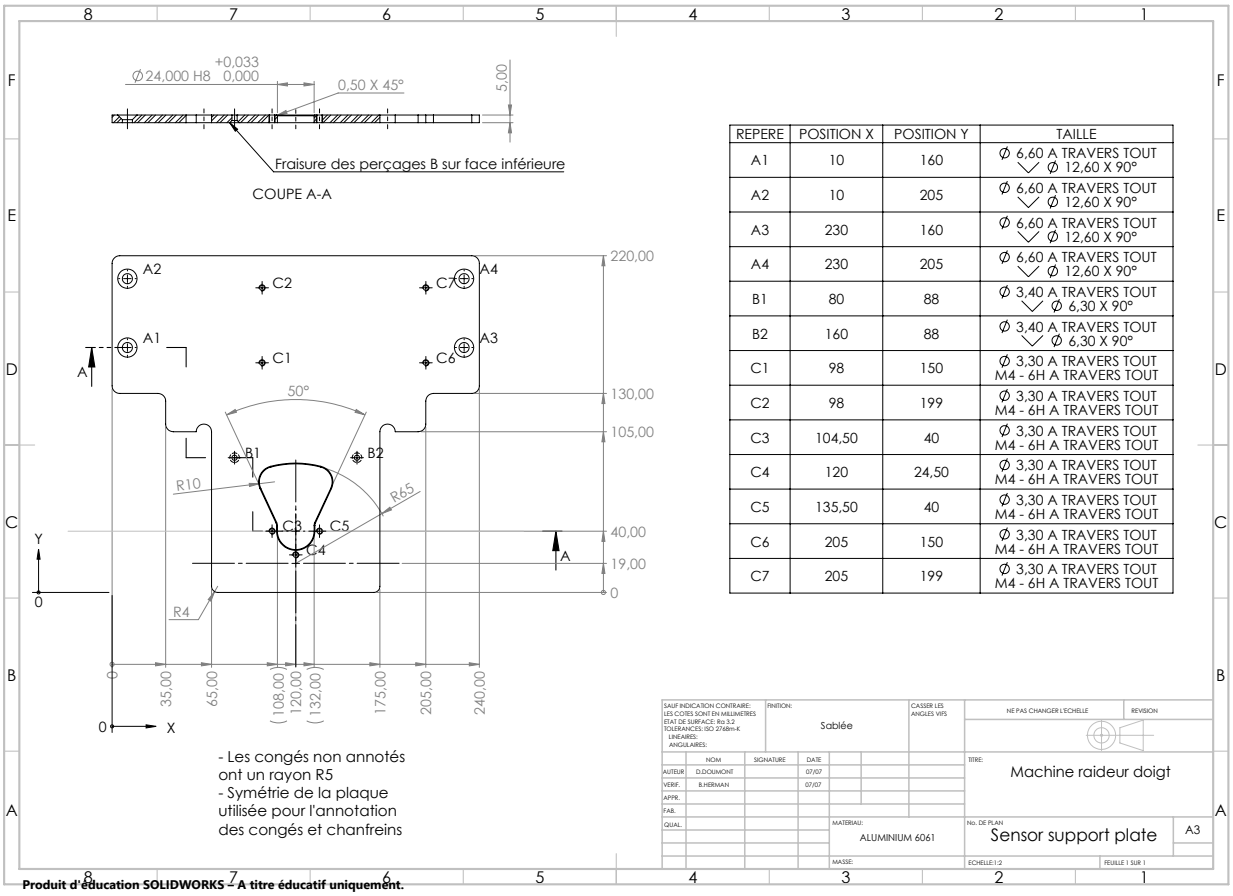


REPERE	POSITION X	POSITION Y	TAILLE
A1	18	95	Ø 10,80 A TRAVERS TOUT M12x1.25 - 6H A TRAVERS TOUT
B1	174	55	Ø 3,40 A TRAVERS TOUT ⌵ Ø 6,30 X 90°
B2	174	135	Ø 3,40 A TRAVERS TOUT ⌵ Ø 6,30 X 90°
B3	199	55	Ø 3,40 A TRAVERS TOUT ⌵ Ø 6,30 X 90°
B4	199	135	Ø 3,40 A TRAVERS TOUT ⌵ Ø 6,30 X 90°

- Symmétrie de la plaque utilisée pour l'alésage de connecteur USB
- Congés non annotés sont R3

SAUF INDICATION CONTRAIRE: LES COTES SONT EN MILLIMETRES ETAT DE SURFACE: TOLERANCES: LINEAIRES: ANGULAIRES:	FINITION:	CASSER LES ANGLES VIFS	NE PAS CHANGER L'ECHELLE	REVISION
	NOM	SIGNATURE	DATE	TITRE: Machine raideur doigt
AUTEUR	D.DOUMONT		15/07	
VERIF.				
APPR.				
FAB.				
QUAL.			MATÉRIAU: Polyacétale	No. DE PLAN: Panneau vertical arrière — A3
			MASSE:	ECHELLE:1:2 — FEUILLE 1 SUR 1

Produit d'éducation SOLIDWORKS - A titre éducatif uniquement.



REPERE	POSITION X	POSITION Y	TAILLE
A1	10	160	Ø 6,60 A TRAVERS TOUT ⌵ Ø 12,60 X 90°
A2	10	205	Ø 6,60 A TRAVERS TOUT ⌵ Ø 12,60 X 90°
A3	230	160	Ø 6,60 A TRAVERS TOUT ⌵ Ø 12,60 X 90°
A4	230	205	Ø 6,60 A TRAVERS TOUT ⌵ Ø 12,60 X 90°
B1	80	88	Ø 3,40 A TRAVERS TOUT ⌵ Ø 6,30 X 90°
B2	160	88	Ø 3,40 A TRAVERS TOUT ⌵ Ø 6,30 X 90°
C1	98	150	Ø 3,30 A TRAVERS TOUT M4 - 6H A TRAVERS TOUT
C2	98	199	Ø 3,30 A TRAVERS TOUT M4 - 6H A TRAVERS TOUT
C3	104,50	40	Ø 3,30 A TRAVERS TOUT M4 - 6H A TRAVERS TOUT
C4	120	24,50	Ø 3,30 A TRAVERS TOUT M4 - 6H A TRAVERS TOUT
C5	135,50	40	Ø 3,30 A TRAVERS TOUT M4 - 6H A TRAVERS TOUT
C6	205	150	Ø 3,30 A TRAVERS TOUT M4 - 6H A TRAVERS TOUT
C7	205	199	Ø 3,30 A TRAVERS TOUT M4 - 6H A TRAVERS TOUT

SAUF INDICATION CONTRAIRE: LES COTES SONT EN MILLIMETRES ETAT DE SURFACE: Ra 3.2 TOLERANCES: ISO 2768m-K LINEAIRES: ANGULAIRES:

FINITION: Sablée

CASSER LES ANGLES VIFS

NE PAS CHANGER L'ECHELLE

REVISION

	NOM	SIGNATURE	DATE
AUTEUR	D.DOUMONT		07/07
VERIF.	B.HERMAN		07/07
APPR.			
FAB.			
QUAL.			

TITRE: Machine raideur doigt

MATERIAU: ALUMINIUM 6061

No. DE PLAN: Sensor support plate

A3

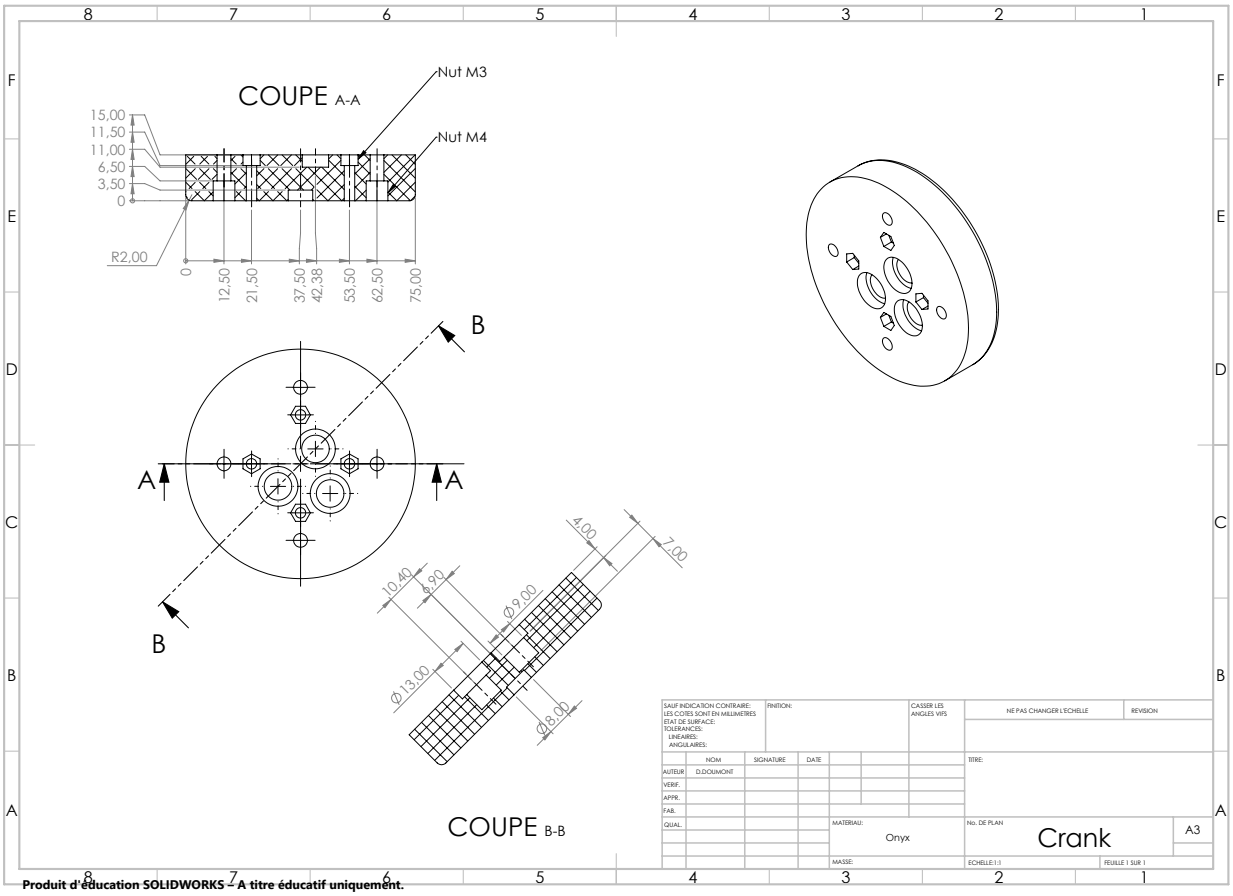
MASSE:

ECHELLE:1:2

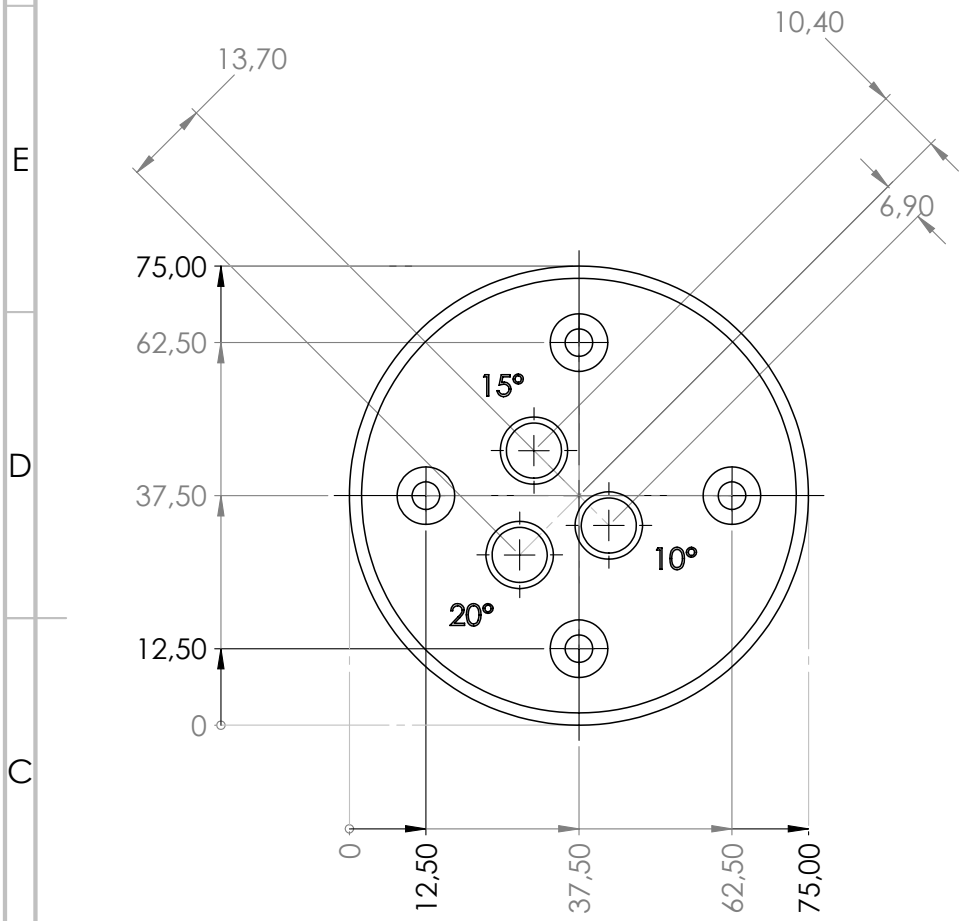
FEUILLE 1 SUR 1

Produit d'éducation SOLIDWORKS - A titre éducatif uniquement.

Drawings of 3d printed pieces

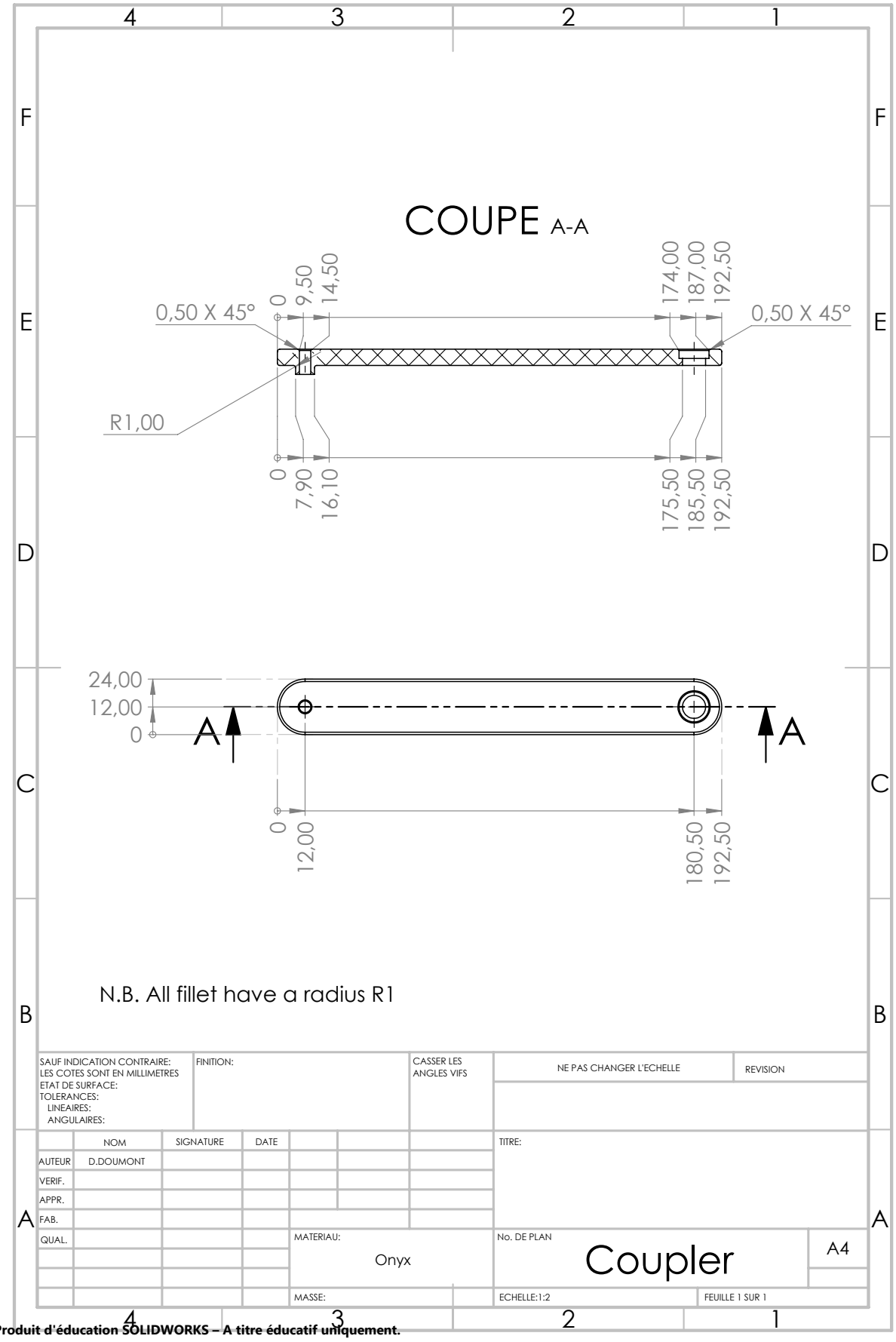


Produit d'éducation SOLIDWORKS - A titre éducatif uniquement.



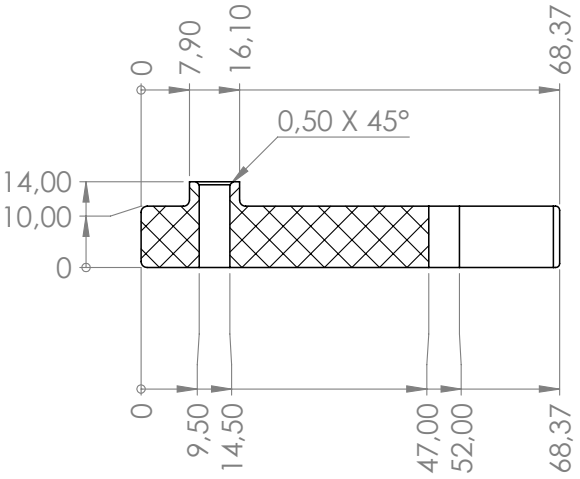
SAUF INDICATION CONTRAIRE: LES COTES SONT EN MILLIMETRES ETAT DE SURFACE: TOLERANCES: LINEAIRES: ANGULAIRES:	FINITION:		CASSER LES ANGLES VIFS	NE PAS CHANGER L'ECHELLE	REVISION		
	NOM	SIGNATURE	DATE	TITRE:			
AUTEUR	D.DOUMONT						
VERIF.							
APPR.							
FAB.							
QUAL.				MATERIAU: Onyx	No. DE PLAN Crank cap	A4	
				MASSE:	ECHELLE:1:2	FEUILLE 1 SUR 1	

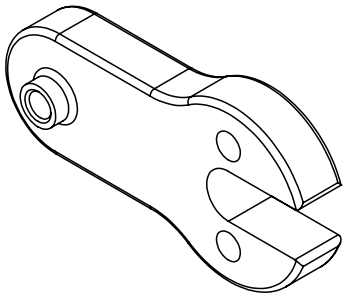
Produit d'éducation SOLIDWORKS – A titre éducatif uniquement.

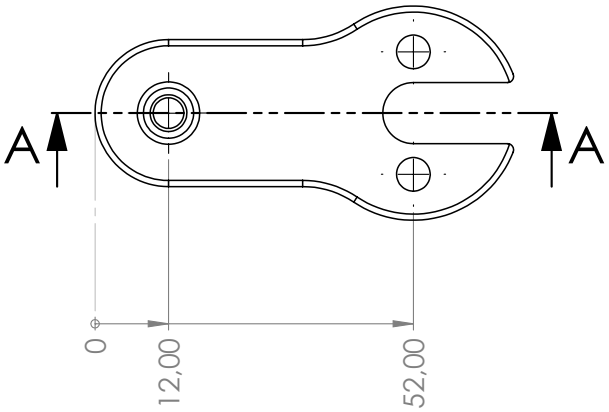


Produit d'éducation SOLIDWORKS – A titre éducatif uniquement.

COUPE A-A



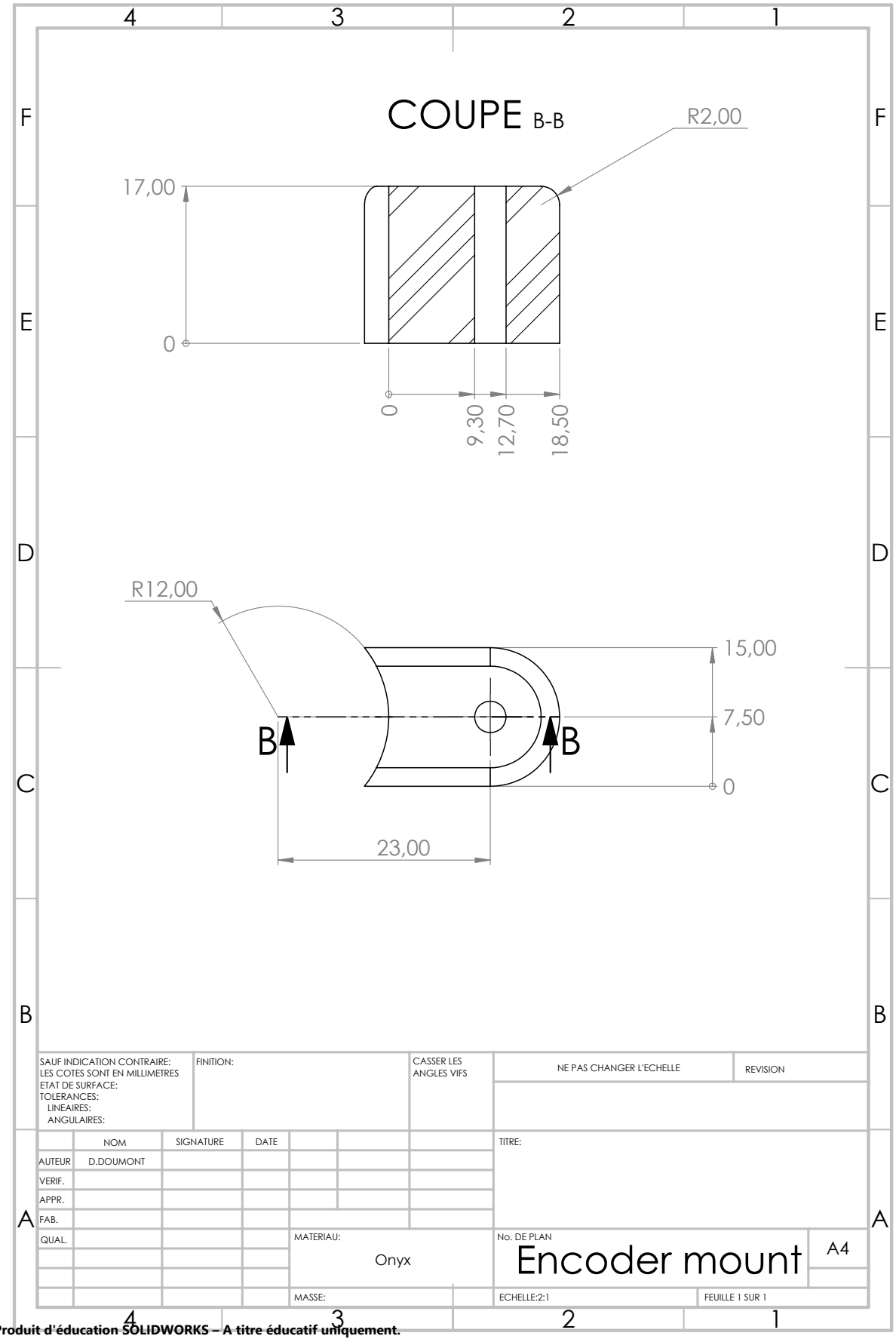




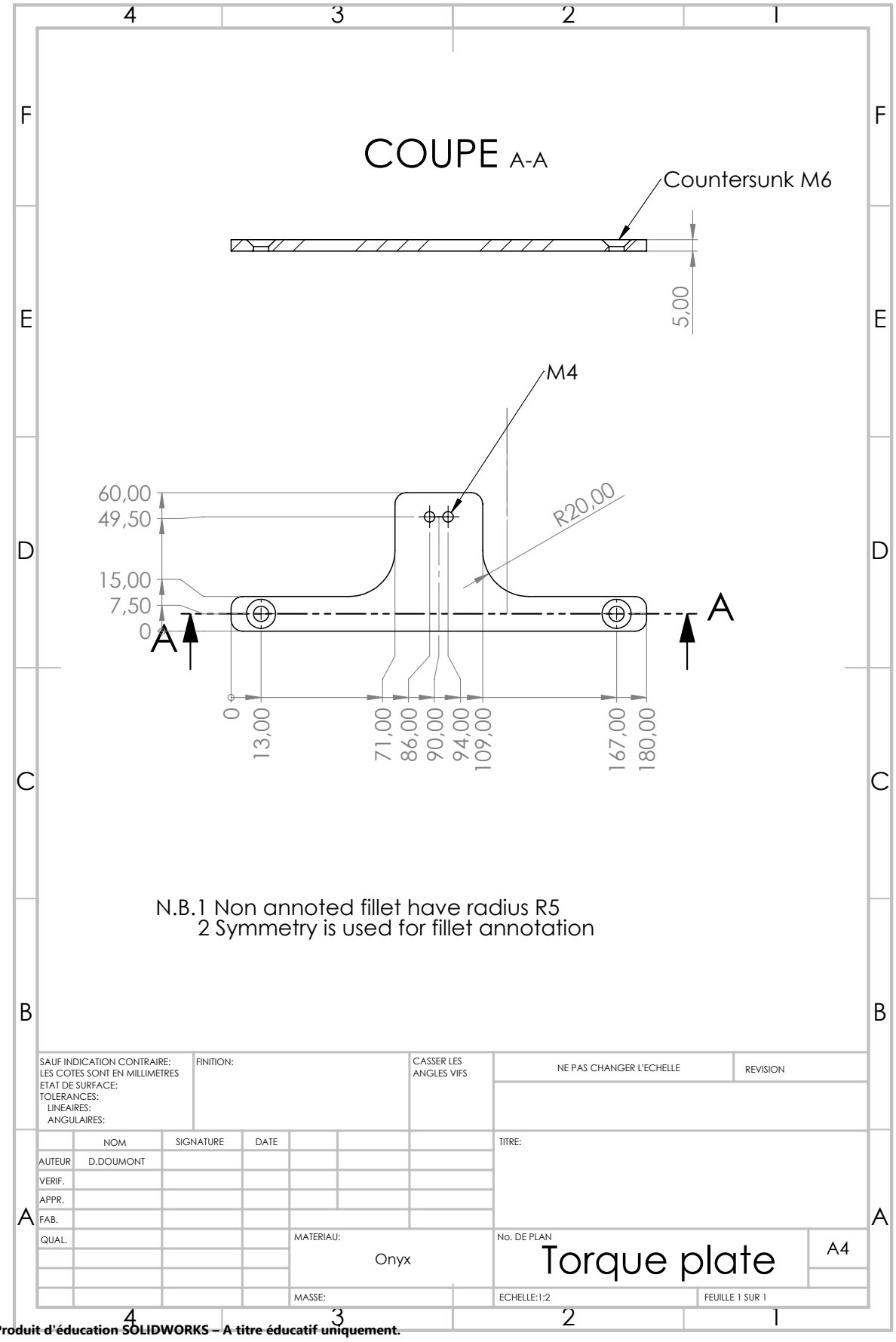
N.B. All fillet have a radius R1

SAUF INDICATION CONTRAIRE: LES COTES SONT EN MILLIMETRES ETAT DE SURFACE: TOLERANCES: LINEAIRES: ANGULAIRES:		FINITION:		CASSER LES ANGLES VIFS		NE PAS CHANGER L'ECHELLE	REVISION
	NOM	SIGNATURE	DATE				TITRE:
AUTEUR	D.DOUMONT						
VERIF.							
APPR.							
FAB.							
QUAL.				MATERIAU: Onyx		No. DE PLAN Follower	A4
				MASSE:		ECHELLE:1:1	FEUILLE 1 SUR 1

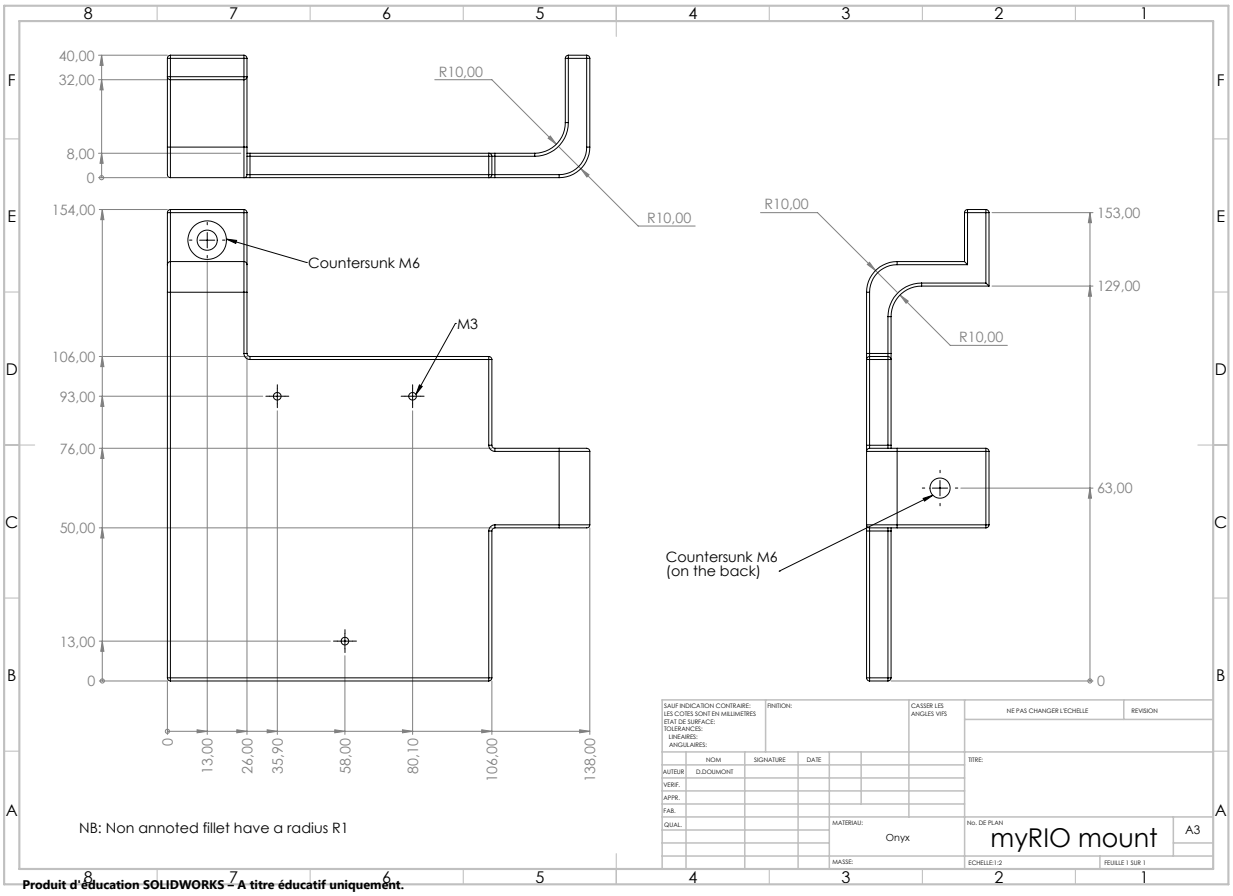
Produit d'éducation SOLIDWORKS – A titre éducatif uniquement.



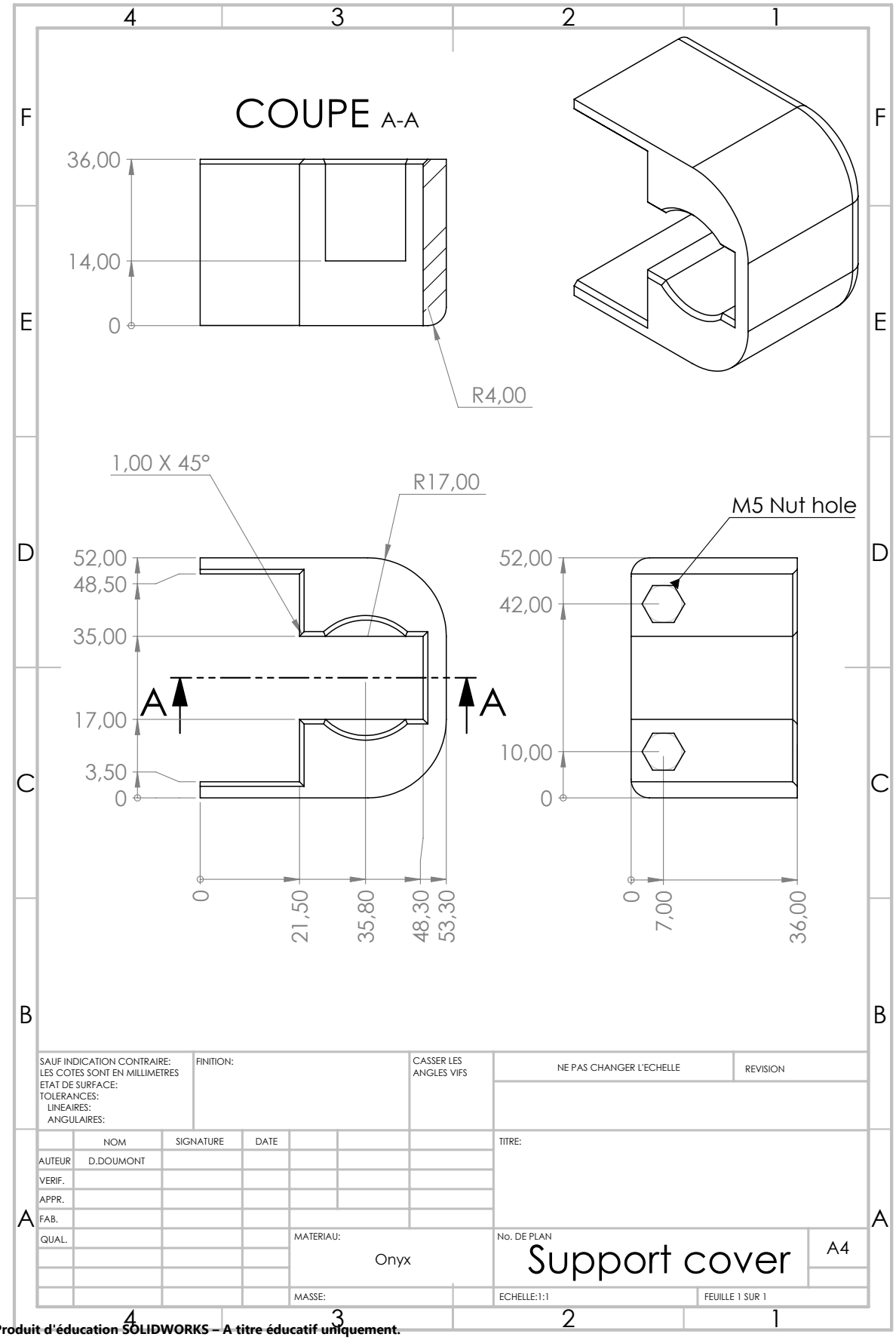
Produit d'éducation SOLIDWORKS – A titre éducatif uniquement.



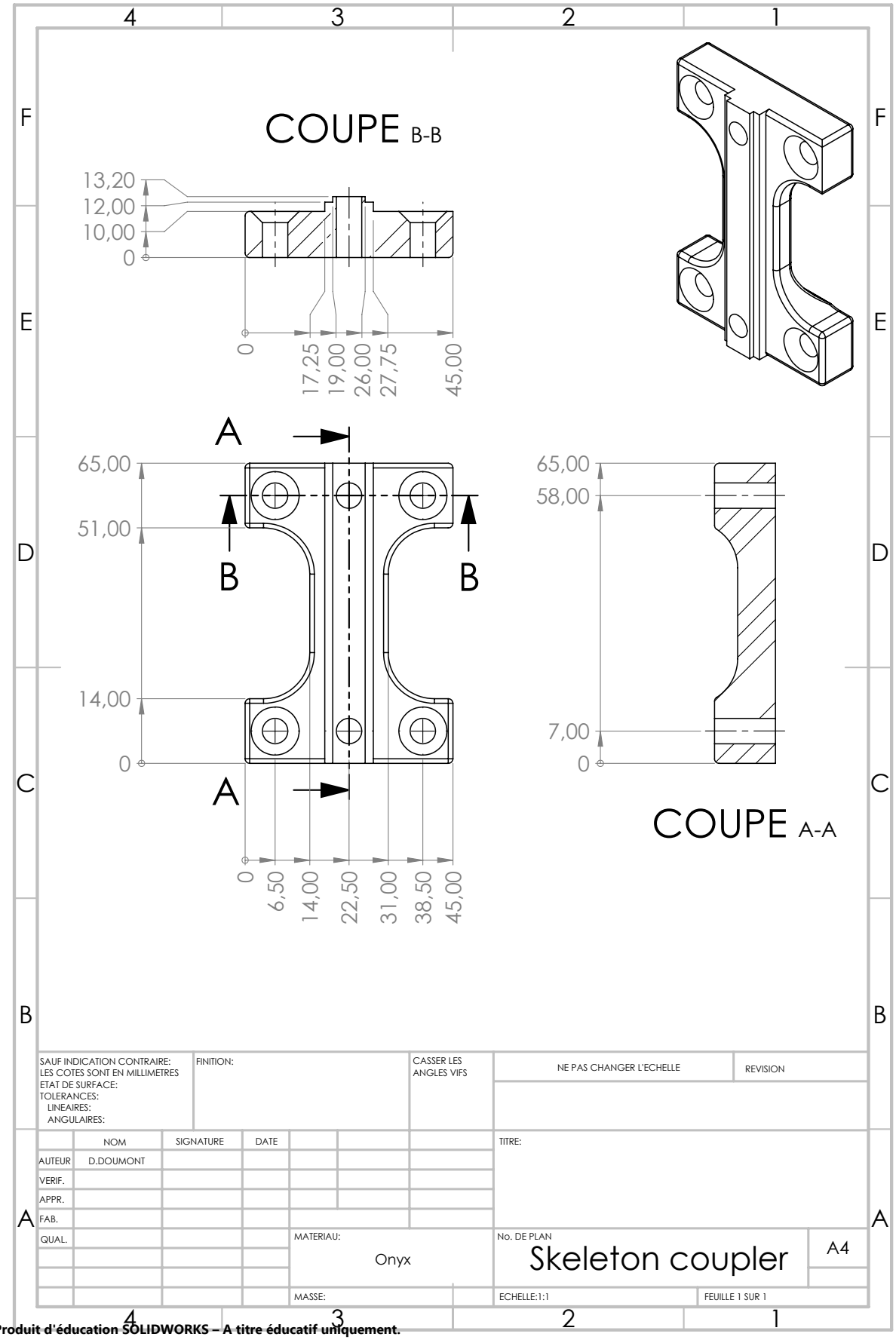
Produit d'éducation SOLIDWORKS – A titre éducatif uniquement.



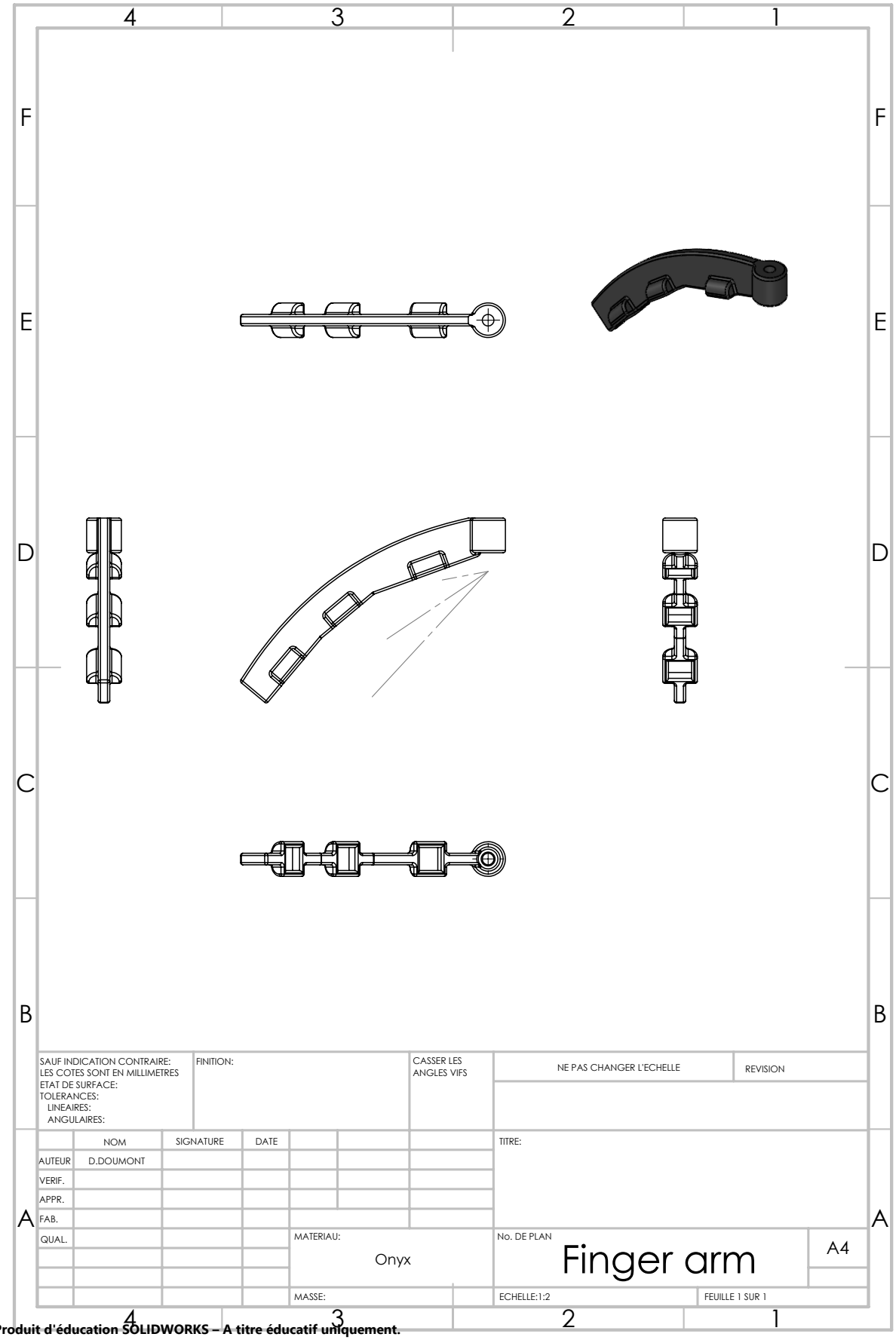
Produit d'éducation SOLIDWORKS – A titre éducatif uniquement.



Produit d'éducation SOLIDWORKS – A titre éducatif uniquement.



Produit d'éducation SOLIDWORKS – A titre éducatif uniquement.

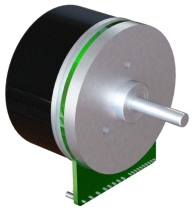


Produit d'éducation SOLIDWORKS – A titre éducatif uniquement.

Datasheets

Actuator sensing and control datasheet

Moteur Brushless
EC45flat 80W/MILE



Les avantages :
Moteur plat pour une meilleure intégration
Rotor ouvert pour plus de performance
Codeur 1024pts intégré

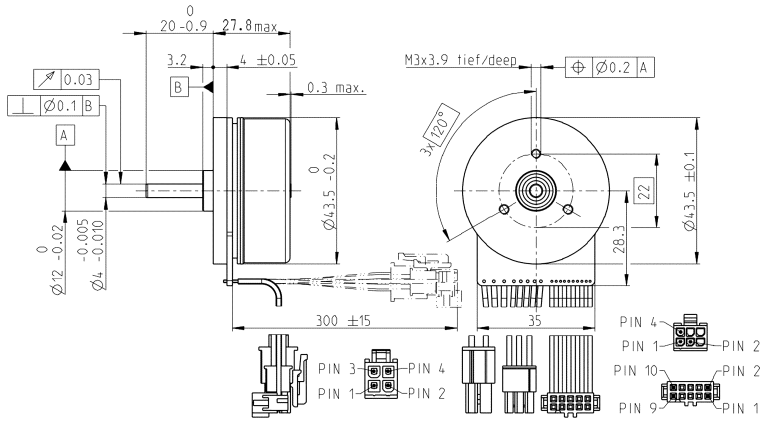
Les produits associés :

> Alimentation
DR-120-24
DRP-480S-24
> Cartes électroniques
EPOS2P 24/5
EPOS4 50/5
EPOS4 70/15
ESCON 50/5
ESCON 70/10
MAXPOS 50/5

maxon motor — 80 W - 175 W

Tension d'alimentation (Ua)	V	24
Vitesse au courant In	tr/mn	4560
Couple au courant In	mNm	167.00
Courant maximum permanent In	mA	3960
Vitesse à vide à Ua à +/- 10%	tr/mn	5600
Courant à vide à +/- 50%	mA	270
Courant de démarrage à Ua	mA	42000
Couple de démarrage à Ua	mNm	1 690.00
Constante de couple	mNm/A	40.40
Constante de vitesse	tr/mn/V	236
Pente vitesse/couple	tr/mn/mN	3
Vitesse limite	tr/mn	10000
Puissance utile maximum à Ua	W	248
Rendement maximum	%	84.9
Constante de temps	ms	6.35
Inertie	gcm²	181
Résistance aux bornes	Ohm	0.573
Inductance	mH	0.301
Résistance thermique	K/W	1.29
Résistance thermique	K/W	5.23
Cste Tps thermique Bobinage	s	34
Cste Tps thermique Boîtier	s	64.7
Tension de mesure	V	24
Puissance utile nominale	W	79,7
Puissance utile max permanente	W	175

Commutation	électronique
Nombre de phases	3
Paliers	Roulements à billes
Charge axiale maximum (dynamique)	7.2 N
Jeu axial minimum	0 mm
Jeu axial maximum	0.14 mm
Charge radiale maximum	15.1 N
à une distance de la face de :	5 mm
Force de chassage maximum (statique)	53 N
Si axe arrière tenu	1000 N
Température ambiante minimum de	-40 °C
Température ambiante maximum de	+100 °C
Température maximum du bobinage	125 °C
Poids	147.1 g



Sensors (AWG 24)
Pin 1 Hall sensor 1
Pin 2 Hall sensor 2
Pin 3 Hall sensor 3
Pin 4 GND
Pin 5 V_{Hall} 4.5...18 VDC
Pin 6 N.C.
Motor (AWG 22)
Pin 1 Motor winding 1
Pin 2 Motor winding 2
Pin 3 Motor winding 3
Pin 4 Not connected
Encoder (AWG 28)
Pin 1 N.C.
Pin 2 V_{cc}
Pin 3 GND
Pin 4 N.C.
Pin 5 Channel $\overline{A}$
Pin 6 Channel A
Pin 7 Channel $\overline{B}$
Pin 8 Channel B
Pin 9 Do not connect
Pin 10 Do not connect

43025-600 Molex
39-01-2040 Molex
DIN 41651/EN 60603-13

Editionjanvier 2021 / sous réserve de modifications

Carte technologie Brushless ESCON 50/5



Les avantages :
Carte d'asservissement de vitesse pour moteur DC et BLDC jusqu'à 250W - 4 E/S disponibles - Encombrement réduit - Carte configurable via USB et interface graphique !!! Livrée sans cable!!!

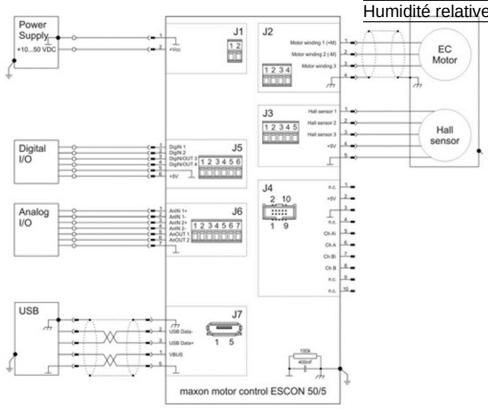
Les produits associés :

> Alimentation
DR-120-24
DRP-240-48
RS-150-24
> Potentiomètre
POTENTIOMETRE POT-

maxon motor — 4 Quadrant(s) - 250 W

Puissance max	250 W
Tension d'alimentation	10 à 50 V
Courant de sortie en pointe	15 A
Courant de sortie	5 A
Vitesse moteur maximum	150 000 tr/min
Programmation	Non
Mode de régulation	Courant, Vitesse
ENTREES :	.....
Fins de course	Non
Analogiques	2, 12 bit, +/-10V,
Consigne de vitesse	Pot. ext/int, PWM 53.6KHZ
Consigne de courant	5 A
Consigne de courant de	15 A
Enable/disable	Oui
Freinage électronique	Oui
Stop	Non
Sens	Oui
Codeur	A, A/, B, B/ - 1MHz
Tachy	Oui
Sélection régulation	RxI
Liaison série	Non
Liaison CAN	Non

SORTIES :	.....
Liaison USB	Mini USB
Image de la vitesse	Oui
Image du courant	Oui
Ready	Oui
Défaut	Oui
Tension auxiliaire	+5 VDC max. 10 mA
Alimentation sondes hall	+5 VDC max. 30 mA
Alimentation codeur	+5 VDC 70 mA
Tension auxiliaire entrées /	-10 à +10 VDC
REGLAGES :	.....
Offset	Oui
Vitesse max	Oui
Courant permanent max	5 A
Rampe d'accélération	Oui
Courant de pointe max	15 A
Gain du régulateur	Oui
PROTECTIONS :	.....
Inversion de polarité	Non
Surtension	Oui
Soustension	Oui
Suralimentation	Oui
Surcharge de courant	Limitation par réglage
Court-circuit moteur	Oui
Court-circuit sur entrées /	Oui
Court-circuit sur alim.	Oui
Thermique	Oui
Exploitation	-30° à +45°C
Stockage	-40° à +85°C
Humidité relative	20 à 80% non condensée



Edition mars 2016 / sous réserve de modifications

Motors Systems Solutions
Commander en ligne sur store.mdpmotor.fr
www.mdp.fr Tél. 04 72 019 019

FUTEK
ADVANCED SENSOR TECHNOLOGY, INC.

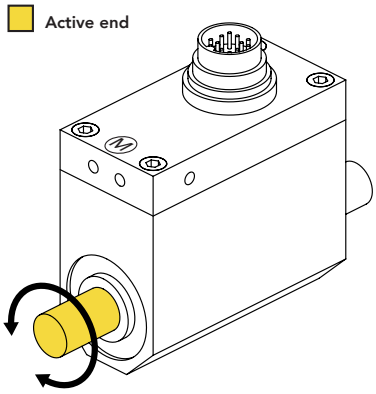
MODEL TRS605

Non-Contact Shaft-to-Shaft Rotary Torque Sensor with Encoder



FEATURES

- Utilizes strain gauge technology
- Angle speed feedback
- Compact size
- Can operate up to 7000 RPM



SPECIFICATIONS	
PERFORMANCE	
Nonlinearity	±0.2% of RO
Hysteresis	±0.1% of RO
Nonrepeatability	±0.2% of RO
Rotational Speed	7000 Max
ELECTRICAL	
Rated Output (RO)	±5 VDC
Excitation	11–26 VDC, 1 Watt
Connector	12 pin Binder Series #581 (09-0331-90-12)
MECHANICAL	
Safe Overload	150% of RO
Zero Balance	±1% of RO
Material	Aluminum (Housing), Steel Alloy (Shaft)
IP Rating	IP40
TEMPERATURE	
Operating Temperature	–13 to 176°F (–25 to 80°C)
Compensated Temperature	41 to 122°F (5 to 50°C)
Temperature Shift Zero	±0.01% of RO/°F (±0.02% of RO/°C)
Temperature Shift Span	±0.01% of RO/°F (±0.02% of RO/°C)
CALIBRATION	
Calibration Test Excitation	12 VDC
Calibration (standard)	Certificate of Conformance
Calibration (available)	5-pt CW & CCW
Shunt Calibration Value	With sensor fully connected apply 11–26 VDC to Pins A & K to generate 5 VDC nom output
ENCODER	
Output	Impulse (TTL)
Pulses per Revolution	2 × 360
Excitation	5 VDC, 40 mA max
Angle 1	Leading Pulse
Angle 2	Trailing Pulse (90°)
CONFORMITY	
RoHS	2014/30/EU
CE	Declaration of Conformity

Sensor Solution Source
Load · Torque · Pressure · Multi-Axis · Calibration · Instruments · Software

www.futek.com

CE RoHS ANSI Z540-1 ISO 17025 ISO 9001 ISO 13485 U.S. Manufacturer

Model TRS605

TORQUE CONNECTIONS

PIN	COLOR	DESCRIPTION
C	Green	+ Voltage Output
D	White	– Voltage Output
E	Black	Ground
F	Red	Power Supply

ANGLE CONNECTOR CODES

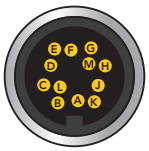
PIN	COLOR	DESCRIPTION
B	Blue	Signal (Angle 1)
E	Black	Ground
G	Brown	Signal (Angle 2)
H	Orange	Power

SHUNT CAL CONNECTOR CODES

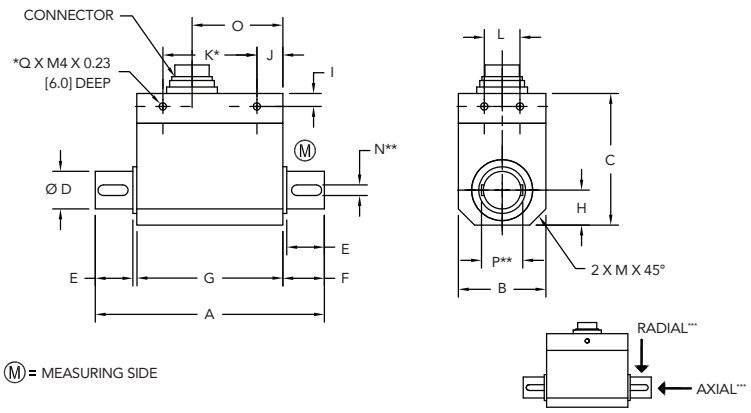
PIN	COLOR	DESCRIPTION
A	Yellow	Ground
K	Purple	Power

SHIELD CONNECTOR CODES

PIN	COLOR	DESCRIPTION
M	Floating	Shield



DIMENSIONS inches [mm]



Ⓜ = MEASURING SIDE

* ANTI-ROTATION HOLES. NOT TO BE USED TO SUPPORT LOAD.
** FEATHER KEYWAYS APPLY TO 20 AND 50 Nm PER DIN 6885, KEYWAYS COME PRE-INSTALLED

MASS MOMENT OF INERTIA (kg × cm²)

ITEM #	Measuring End	Drive End
FSH02052	0.0146	0.0147
FSH02053	0.0146	0.0147
FSH02054	0.015	0.015
FSH02055	0.015	0.015
FSH02056	0.9	1.02
FSH02057	0.91	1.04

CAPACITIES

ITEM #	Nm [in-lb]	Ø D	A	B	C	E	F	G	H	I	J	K*	L	M	N**	O	P**	Q*	*** Max Axial Force lb [N]	*** Max Radial Force lb [N]	Weight lb [kg]	Torsional Stiffness Nm/rad
FSH02052	1 [9]	0.394 [10] g6	3.62 [92]	1.10 [28]	2.04 [52]	0.63 [16]	0.67 [17]	2.28 [58]	0.55 [14]	0.19 [5]	0.43 [11]	-	0.31 [8]	0.31 [8]	N/A	1.46 [37]	N/A	6	4.5 [20]	1 [5]	0.7 [0.30]	317
FSH02053	2 [18]																		11 [50]	1 [5]		317
FSH02054	5 [44]																		11 [50]	2 [10]		855
FSH02055	10 [89]																		34 [150]	4.5 [20]		855
FSH02056	20 [177]	0.630 [16] g6	4.09 [104]	1.49 [38]	2.28 [58]	0.78 [20]	0.90 [23]	2.32 [59]	0.75 [19]	0.19 [5]	0.47 [12]	1.38 [35]	0.55 [14]	0.40 [10]	0.197 [5]	1.50 [38]	0.787 [20]	8	34 [150]	7 [30]	1.3 [0.60]	5450
FSH02057	50 [443]																		45 [200]	11 [50]		8190

CE RoHS ANSI Z540-1 ISO 17025 ISO 9001 ISO 13485 U.S. Manufacturer

AHS36B-BDAC004096 | AHS/AHM36

CODEURS ABSOLUS



illustration non contractuelle

Informations de commande

Type	Référence
AHS36B-BDAC004096	1075904

Autres modèles d'appareil et accessoires ➜ www.sick.com/AHS_AHM36

Caractéristiques techniques détaillées

Performance

Nombre de pas par tour (résolution max.)	4.096 (12 bit)
Limites d'erreur G	0,35° (à 20 °C) [1]
Différence de répétition standard σ_r	0,25° (à 20 °C) [2]

[1] Selon la norme DIN ISO 1319-1, position de la limite d'erreur supérieure et inférieure en fonction de la situation de montage, valeur indiquée se réfère à la position symétrique, c.à.d. différences vers le haut et vers le bas ont la même valeur.
[2] Selon la norme DIN ISO 55350-13 : 68,3 % des valeurs mesurées se situent au sein de la plage indiquée.

Interfaces

Interface de communication	SSI
Données de processus	Position
Durée d'initialisation	100 ms [1]
Temps de détermination de la position	125 µs
SSI	
Type de code	Gray
Séquence de code ajustable	CW/CCW (V/R) configurable par câble
Fréquence d'horloge	2 MHz [2]
Kit (réglage électronique)	Actif H (L = 0 - 3 V, H = 4,0 - U_s V)
CW/CCW (séquence d'étapes dans le sens de rotation)	Actif L (L = 0 - 1 V, H = 2,0 - Us V)

[1] Après ce temps, il est possible de lire des positions valides.
[2] Minimum, niveau LOW (Clock+) : 250 ns.

Caractéristiques électriques

Mode de raccordement	Connecteur mâle, M12, 8 pôles, universel
Tension d'alimentation	4,5 ... 32 V DC
Puissance absorbée	≤ 1,5 W (sans charge)

[1] Ce produit est un produit standard et non un composant de sécurité au sens de la directive machines. Calculé sur la base d'une charge nominale des composants, d'une température moyenne de 40 °C, d'une fréquence d'utilisation de 8760 h/a. Toutes les défaillances électroniques sont considérées comme des défaillances dangereuses. pour plus d'informations, voir le document n° 8015532.

Protection contre l'inversion de polarité	✓
MTTFd : temps moyen avant défaillance dangereuse	230 années (EN ISO 13849-1) [1]

[1] Ce produit est un produit standard et non un composant de sécurité au sens de la directive machines. Calculé sur la base d'une charge nominale des composants, d'une température moyenne de 40 °C, d'une fréquence d'utilisation de 8760 h/a. Toutes les défaillances électroniques sont considérées comme des défaillances dangereuses. pour plus d'informations, voir le document n° 8015532.

Caractéristiques mécaniques

Interface mécanique	Axe creux non traversant
Diamètre de l'axe	10 mm
Poids	0,12 kg [1]
Matériau, arbre	Acier inoxydable
Matériau, bride	Aluminium
Matériau, boîtier	Zinc
Couple de démarrage	0,5 Ncm
Couple de fonctionnement	< 0,5 Ncm
Mouvement admissible de l'arbre statique	± 0,3 mm (radial) ± 0,3 mm (axial)
Mouvement admissible de l'arbre dynamique	± 0,1 mm (radial) ± 0,1 mm (axial)
Moment d'inertie du rotor	15 gcm²
Durée de stockage	2,0 x 10^9 tours
Accélération angulaire	≤ 500.000 rad/s²
Vitesse de fonctionnement	≤ 9.000 min⁻¹ [2]

[1] Se rapportant aux appareils avec connecteur mâle.

[2] Tenir compte d'un autoréchauffement de 3,5 K pour 1.000 tr./min. lors de la détermination de la plage de températures de fonctionnement.

Caractéristiques ambiantes

CEM	Selon EN 61000-6-2 et EN 61000-6-3
Indice de protection	IP65 (selon CEI 60529)
Humidité relative admissible	90 % (condensation inadmissible)
Plage de température de fonctionnement	–20 °C ... +70 °C
Plage de température de stockage	–40 °C ... +100 °C, sans emballage
Résistance aux chocs	100 g, 6 ms (selon EN 60068-2-27)
Résistance aux vibrations	20 g, 10 Hz ... 2.000 Hz (selon EN 60068-2-6)

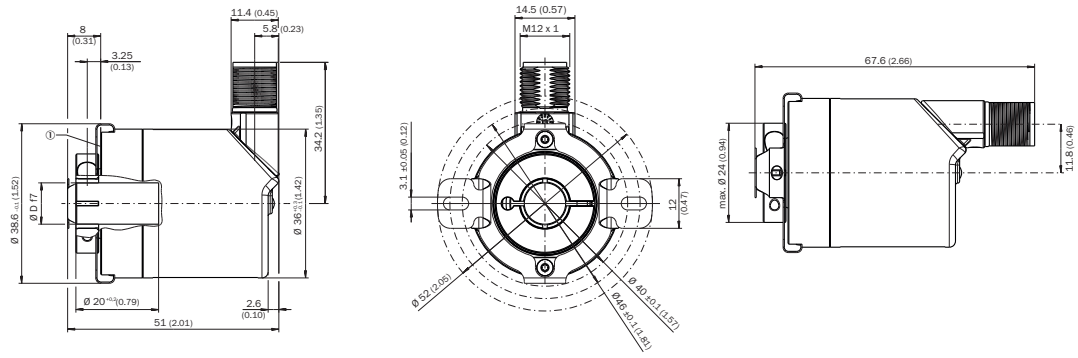
Classifications

ECl@ss 5.0	27270502
ECl@ss 5.1.4	27270502
ECl@ss 6.0	27270590
ECl@ss 6.2	27270590
ECl@ss 7.0	27270502
ECl@ss 8.0	27270502
ECl@ss 8.1	27270502
ECl@ss 9.0	27270502

ECl@ss 10.0	27270502
ECl@ss 11.0	27270502
ETIM 5.0	EC001486
ETIM 6.0	EC001486
ETIM 7.0	EC001486
UNSPSC 16.0901	41112113

Plan coté (Dimensions en mm (inch))

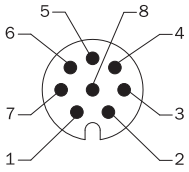
Axe creux non traversant, connecteur mâle



① Point de mesure pour la température de fonctionnement

Affectation des broches

Connecteur mâle M12, 8 pôles et câble 8 fils, SSI/Gray



Vue connecteur d'appareil M12 sur le codeur

PIN	Couleurs des fils (raccordement des câbles)	Signal	Explication
1	Marron	Données -	Signaux d'interface
2	Blanc	Données +	Signaux d'interface
3	Noir	V/R	Succession des étapes dans le sens de rotation
4	Rose	SET	Réglage électronique Signaux d'interface
5	Jaune	Clock +	Signaux d'interface
6	Violet	Clock -	Signaux d'interface
7	Bleu	GND	Raccord à la masse

PIN	Couleurs des fils (raccordement des câbles)	Signal	Explication
8	Rouge	U_S	Tension de service
		Écran	Écran relié au boîtier du côté du codeur. Relier côté commande à la terre.

Accessoires recommandés

Autres modèles d'appareil et accessoires ➜ www.sick.com/AHS_AHM36

	Description succincte	Type	Référence
Brides			
	• **Description:** Support de couple sur cercle de trou 63 mm	BEF-DS08	2072206
	• **Description:** Bras de couple standard, AHS/AHM36	BEF-DS16-AHX	2108615
Connecteurs et câbles			
	• **Mode de raccordement tête A:** Connecteur femelle, M12, 8 pôles, droit, Codage A • **Mode de raccordement tête B:** - • **Type de signal:** Incrémental, SSI • **Câble:** CAT5, CAT5e • **Description:** Incrémental, blindé, Tête A : connecteur femelle, M12, 8 pôles, droit, codage A, incrémental, SSI, blindé, pour un diamètre de câble de 4 mm à 8 mm Tête B : - température de fonctionnement : –40 °C à +85 °C, SSI • **Raccordement:** Raccord autodénudant rapide • **Section du conducteur admissible:** 0,14 mm² ... 0,34 mm²	DOS-1208-GA01	6045001
	• **Mode de raccordement tête A:** Câble • **Mode de raccordement tête B:** Extrémité de câble ouverte • **Type de signal:** SSI, incrémental, HIPERFACE® • **Câble:** 8 fils, PUR, sans halogène • **Description:** SSI, blindé, Incrémental, HIPERFACE®	LTG-2308-MWENC	6027529
	• **Mode de raccordement tête A:** Câble • **Mode de raccordement tête B:** Extrémité de câble ouverte • **Type de signal:** SSI, TTL, HTL, incrémental • **Câble:** 12 fils, résistant aux UV et à l'eau salée, PUR, sans halogène • **Description:** SSI, blindé, Tête A : câble Tête B : câble Câble : compatible chaîne porte-câble, PUR, sans halogène, blindé, résistant aux rayons UV et à l'eau salée, 4 x 2 x 0,25 mm² + 2 x 0,5 mm² + 2 x 0,14 mm², Ø 7,8 mm, TTL, HTL, Incrémental	LTG-2612-MW	6028516
	• **Mode de raccordement tête A:** Connecteur femelle, M12, 8 pôles, droit • **Mode de raccordement tête B:** Extrémité de câble ouverte • **Type de signal:** Incrémental, SSI • **Câble:** 2 m, 8 fils, PUR, sans halogène • **Description:** Incrémental, blindé, Tête A : connecteur femelle, M12, 8 pôles, droit Tête B : câble Câble : compatible chaîne porte-câble, PVC, blindé, 4 x 2 x 0,25 mm², Ø 7,0 mm, SSI • **Raccordement:** Extrémité de câble ouverte	DOL-1208-G02MAC1	6032866

	Description succincte	Type	Référence
	• **Mode de raccordement tête A:** Connecteur femelle, M12, 8 pôles, droit • **Mode de raccordement tête B:** Extrémité de câble ouverte • **Type de signal:** Incrémental, SSI • **Câble:** 5 m, 8 fils, PUR, sans halogène • **Description:** Incrémental, blindé, Tête A : connecteur femelle, M12, 8 pôles, droit Tête B : câble Câble : compatible chaîne porte-câble, PVC, blindé, 4 x 2 x 0,25 mm², Ø 7,0 mm, SSI • **Raccordement:** Extrémité de câble ouverte	DOL-1208-G05MAC1	6032867
	• **Mode de raccordement tête A:** Connecteur femelle, M12, 8 pôles, droit • **Mode de raccordement tête B:** Extrémité de câble ouverte • **Type de signal:** Incrémental, SSI • **Câble:** 10 m, 8 fils, PUR, sans halogène • **Description:** Incrémental, blindé, Tête A : connecteur femelle, M12, 8 pôles, droit Tête B : câble Câble : compatible chaîne porte-câble, PVC, blindé, 4 x 2 x 0,25 mm², Ø 7,0 mm, SSI • **Raccordement:** Extrémité de câble ouverte	DOL-1208-G10MAC1	6032868
	• **Mode de raccordement tête A:** Connecteur femelle, M12, 8 pôles, droit • **Mode de raccordement tête B:** Extrémité de câble ouverte • **Type de signal:** Incrémental, SSI • **Câble:** 20 m, 8 fils, PUR, sans halogène • **Description:** Incrémental, blindé, Tête A : connecteur femelle, M12, 8 pôles, droit Tête B : câble Câble : compatible chaîne porte-câble, PVC, blindé, 4 x 2 x 0,25 mm², Ø 7,0 mm, SSI • **Raccordement:** Extrémité de câble ouverte	DOL-1208-G20MAC1	6032869
	• **Mode de raccordement tête A:** Connecteur femelle, M12, 8 pôles, droit • **Mode de raccordement tête B:** Extrémité de câble ouverte • **Type de signal:** Incrémental, SSI • **Câble:** 25 m, 8 fils, PUR, sans halogène • **Description:** Incrémental, blindé, Tête A : connecteur femelle, M12, 8 pôles, droit Tête B : câble Câble : compatible chaîne porte-câble, PVC, blindé, 4 x 2 x 0,25 mm², Ø 7,0 mm, SSI • **Raccordement:** Extrémité de câble ouverte	DOL-1208-G25MAC1	6067859

Power supply unit - TRIO-PS/1AC/24DC/10 - 2866323

Please be informed that the data shown in this PDF Document is generated from our Online Catalog. Please find the complete data in the user's documentation. Our General Terms of Use for Downloads are valid (http://phoenixcontact.com/download)



Primary-switched TRIO POWER power supply for DIN rail mounting, input: 1-phase, output: 24 V DC/10 A

Product Description

TRIO POWER power supplies with standard functionality
TRIO POWER is particularly suited to standard machine production, thanks to 1- and 3-phase versions up to 960 W. The wide-range input and the international approval package enable worldwide use.
The robust metal housing, the high electric strength, and the wide temperature range ensure a high level of power supply reliability.

Why buy this product

- Use the third negative terminal block as a grounding terminal block and minimize installation costs
- Rugged design with metal housing and wide temperature range from -25 to +70°C
- Maximum operational reliability thanks to high MTBF (mean time between failures) of more than 500,000 hours and high dielectric strength of up to 300 V AC
- Compensation of voltage drops by means of output voltage that can be adjusted on the front



Key Commercial Data

Packing unit	1 pc
GTIN	4 046356 046657
Weight per Piece (excluding packing)	1400.0 g
Custom tariff number	85044030
Country of origin	China

Technical data

Dimensions

Width	60 mm
Height	130 mm
Depth	152.5 mm

Ambient conditions

Degree of protection	IP20
Ambient temperature (operation)	-25 °C ... 70 °C (> 55° C derating : 2.5%/K)

Power supply unit - TRIO-PS/1AC/24DC/10 - 2866323

Technical data

Ambient conditions

Ambient temperature (storage/transport)	-40 °C ... 85 °C
Max. permissible relative humidity (operation)	≤ 95 % (at 25 °C, non-condensing)
Noise immunity	EN 61000-6-2:2005

Input data

Nominal input voltage range	100 V AC ... 240 V AC
Input voltage range	85 V AC ... 264 V AC (Derating < 90 V AC: 2,5 % / V)
Dielectric strength maximum	300 V AC
AC frequency range	45 Hz ... 65 Hz
Discharge current to PE	< 3.5 mA
Inrush surge current	< 15 A
Power failure bypass	> 24 ms (120 V AC)
	> 24 ms (230 V AC)
Input fuse	6.3 A (slow-blow, internal)
Choice of suitable circuit breakers	10 A ... 16 A (Characteristics B, C, D, K)
Power factor (cos phi)	0.99
Type of protection	Transient surge protection
Protective circuit/component	Varistor

Output data

Nominal output voltage	24 V DC ±1 %
Setting range of the output voltage (U_{Set})	22.5 V DC ... 29.5 V DC (> 24 V DC, constant capacity restricted)
Nennausgangsstrom (I_N)	10 A (U_{OUT} = 24 V DC)
Derating	55 °C ... 70 °C (2.5%/K)
Connection in parallel	Yes, for redundancy and increased capacity
Connection in series	Yes
Max. capacitive load	Unlimited
Active current limitation	Approx. 14 A (for short-circuit)
Control deviation	< 1 % (change in load, static 10 % ... 90 %)
	< 2 % (change in load, dynamic 10 % ... 90 %)
	< 0.1 % (change in input voltage ±10 %)
Residual ripple	< 10 mV_{PP}
Output power	240 W
Typical response time	< 1 s
Peak switching voltages nominal load	< 50 mV_{PP}
Maximum power dissipation in no-load condition	6.7 W
Power loss nominal load max.	30 W

General

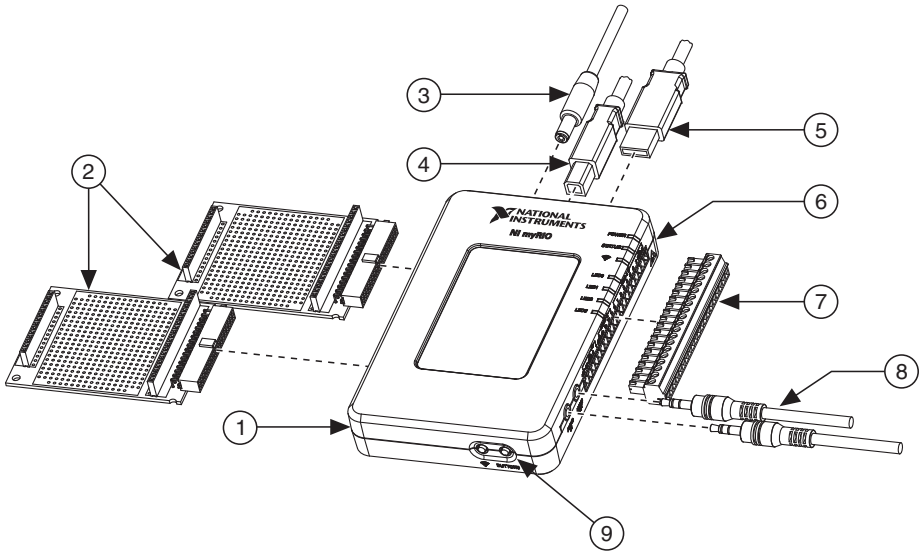
Net weight	1.4 kg
Operating voltage display	Green LED
Efficiency	89 % (for 230 V AC and nominal values)

USER GUIDE AND SPECIFICATIONS

NI myRIO-1900

The National Instruments myRIO-1900 is a portable reconfigurable I/O (RIO) device that students can use to design control, robotics, and mechatronics systems. This document contains pinouts, connectivity information, dimensions, mounting instructions, and specifications for the NI myRIO-1900.

Figure 1. NI myRIO-1900



1	NI myRIO-1900	6	LEDs
2	myRIO Expansion Port (MXP) Breakouts (One Included in Kit)	7	Mini System Port (MSP) Screw-Terminal Connector
3	Power Input Cable	8	Audio In/Out Cables (One Included in Kit)
4	USB Device Cable	9	Button0
5	USB Host Cable (Not Included in Kit)		

Cables and Accessories

Table 5. Accessories Available from NI

Accessory	Description	NI Part Number
Power supply	Power supply for NI myRIO-1900	723403-01
MXP breakouts	Set of five MXP breakout boards for NI myRIO-1900	782696-01
MSP connector	MSP replacement connector plug for NI myRIO-1900	765788-01
Panel mounting kit	Panel mounting kit for NI myRIO-1900	783091-01

Specifications

The following specifications are typical for the 0 to 40 °C operating tempreature range unless otherwise noted.

Processor

Processor type ..... Xilinx Z-7010

Processor speed ..... 667 MHz

Processor cores 2

Memory

Nonvolatile memory ..... 512 MB

DDR3 memory ..... 256 MB

- DDR3 clock frequency ..... 533 MHz
- DDR3 data bus width ..... 16 bits

For information about the lifespan of the nonvolatile memory and about best practices for using nonvolatile memory, go to `ni.com/info` and enter the Info Code `SSDBP`.

FPGA

FPGA type ..... Xilinx Z-7010

Wireless Characteristics

Radio mode ..... IEEE 802.11 b,g,n

Frequency band ..... ISM 2.4 GHz

Channel width ..... 20 MHz

Channels ..... USA 1 to 11, International 1 to 13

TX power ..... +10 dBm max (10 mW)

Outdoor range ..... Up to 150 m (line of sight)

Antenna directivity ..... Omnidirectional

Security ..... WPA, WPA2, WPA2-Enterprise

USB Ports

USB host port ..... USB 2.0 Hi-Speed

USB device port ..... USB 2.0 Hi-Speed

Analog Input

Aggregate sample rate ..... 500 kS/s

Resolution ..... 12 bits

Overvoltage protection ..... ±16 V

MXP connectors

- Configuration ..... Four single-ended channels per connector
- Input impedance ..... >500 kΩ acquiring at 500 kS/s
1 MΩ powered on and idle
4.7 kΩ powered off
- Recommended source impedance ..... 3 kΩ or less
- Nominal range ..... 0 V to +5 V
- Absolute accuracy ..... ±50 mV
- Bandwidth ..... >300 kHz

MSP connector

- Configuration ..... Two differential channels
- Input impedance ..... Up to 100 nA leakage powered on;
4.7 kΩ powered off
- Nominal range ..... ±10 V
- Working voltage
(signal + common mode) ..... ±10 V of AGND
- Absolute accuracy ..... ±200 mV
- Bandwidth ..... 20 kHz minimum, >50 kHz typical

Audio input

- Configuration ..... One stereo input consisting of two AC-coupled, single-ended channels
- Input impedance ..... 10 kΩ at DC
- Nominal range ..... ±2.5 V
- Bandwidth ..... 2 Hz to >20 kHz

Analog Output

Aggregate maximum update rates

- All AO channels on MXP connectors ..... 345 kS/s
- All AO channels on MSP connector and audio output channels ..... 345 kS/s

Resolution ..... 12 bits

Overload protection ..... ±16 V

Startup voltage ..... 0 V after FPGA initialization

MXP connectors

- Configuration ..... Two single-ended channels per connector
- Range ..... 0 V to +5 V
- Absolute accuracy ..... 50 mV
- Current drive ..... 3 mA
- Slew rate ..... 0.3 V/µs

MSP connector

- Configuration ..... Two single-ended channels
- Range ..... ±10 V
- Absolute accuracy ..... ±200 mV
- Current drive ..... 2 mA
- Slew rate ..... 2 V/µs

Audio output

- Configuration ..... One stereo output consisting of two AC-coupled, single-ended channels
- Output impedance ..... 100 Ω in series with 22 µF
- Bandwidth ..... 70 Hz to >50 kHz into 32 Ω load; 2 Hz to >50 kHz into high-impedance load

Digital I/O

Number of lines

- MXP connectors ..... 2 ports of 16 DIO lines (one port per connector); one UART.RX and one UART.TX line per connector
- MSP connector ..... 1 port of 8 DIO lines

Direction control ..... Each DIO line individually programmable as input or output

Logic level ..... 5 V compatible LVTTL input; 3.3 V LVTTL output

Input logic levels

Input low voltage, V_{IL} ..... 0 V min; 0.8 V max

Input high voltage, V_{IH} ..... 2.0 V min; 5.25 V max

Output logic levels

Output high voltage, V_{OH}
sourcing 4 mA ..... 2.4 V min; 3.465 V max

Output low voltage, V_{OL}
sinking 4 mA ..... 0 V min; 0.4 V max

Minimum pulse width..... 20 ns

Maximum frequencies for secondary digital functions

SPI ..... 4 MHz

PWM..... 100 kHz

Quadrature encoder input ..... 100 kHz

I^2C..... 400 kHz

UART lines

Maximum baud rate..... 230,400 bps

Data bits..... 5, 6, 7, 8

Stop bits 1, 2

Parity..... Odd, Even, Mark, Space

Flow control..... XON/XOFF

Accelerometer

Number of axes..... 3

Range ..... ±8 g

Resolution..... 12 bits

Sample rate ..... 800 S/s

Noise..... 3.9 mg_{rms} typical at 25 °C

Power Output

+5 V power output

Output voltage ..... 4.75 V to 5.25 V

Maximum current on each connector ..... 100 mA

+3.3 V power output

Output voltage ..... 3.0 V to 3.6 V

Maximum current on each connector ..... 150 mA

+15 power output

Output voltage.....+15 V to +16 V

Maximum current .....32 mA (16 mA during startup)

-15 V power output

Output voltage.....-15 V to -16 V

Maximum current .....32 mA (16 mA during startup)

Maximum combined power from +15 V and -15 V power output .....500 mW

Power Requirements

NI myRIO-1900 requires a power supply connected to the power connector.

Power supply voltage range.....6 to 16 VDC

Maximum power consumption .....14 W

Typical idle power consumption.....2.6 W

Environmental

To meet these specifications, you must operate the NI myRIO-1900 with the window facing away from the mounting surface and ensure that there is at least 1 in. of clearance in front of the window during use.

Ambient temperature near device (IEC 60068-2-1, IEC 600682-2).....0 to 40 °C

Storage temperature (IEC 60068-2-1, IEC 600682-2).....-20 to 70 °C

Operating humidity (IEC 60068-2-56) .....10 to 90% RH, noncondensing

Storage humidity (IEC 60068-2-56) .....10 to 90% RH, noncondensing

Maximum altitude.....2,000 m

Pollution Degree (IEC 60664) 2

Indoor use only.

Physical Characteristics

Weight .....193 g (6.8 oz)

Safety

Safety Standards

This product is designed to meet the requirements of the following standards of safety for electrical equipment for measurement, control, and laboratory use:

- IEC 61010-1, EN 61010-1
- UL 61010-1, CSA 61010-1

Mechanical datasheet

Ball Lock Pins

Spring Type / Push Type

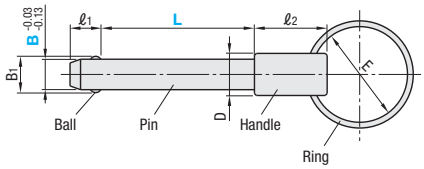
■**Features:** Locks with the spring force. Priced at approx. 1/3 of the Push Type.

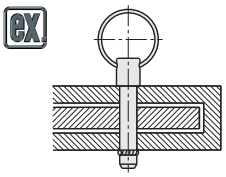
■**Ball Lock Pins**
- Spring Type



RoHS10

Type		Ball		Pin		Handle		Ring	
L Selectable	L Configurable	M Material	H Hardness	M Material	S Surface Treatment	M Material	S Surface Treatment	M Material	S Surface Treatment
BLPS	BLPF	EN 1.4125 Equiv.	HRC55~	EN 1.1191 Equiv.	Electroless Nickel Plating	EN 1.0736 Equiv.	Electroless Nickel Plating	JIS-SWRH	Nickel Plating





■**L Selectable**

Part Number Type	B	L Selection	B1	ℓ1	D	ℓ2	E	Unit Price L=25	L=30	L=40	L=50	L=60
BLPS	5	30	5.5	6	11	22	25	-		-	-	-
	6	25 30 40 50	7	7	11	22	25					-
	8	25 30 40 50	9.5	8	11	22	25					-
	10	25 30 40 50 60	12	9	16	27	25					
	12	60	14.5	10	16	27	25	-	-	-	-	
	16	60	19	14	19	32	25	-	-	-	-	

■**L Configurable**

Part Number Type	B	L 5mm Increment	B1	ℓ1	D	ℓ2	E	Unit Price
BLPF	5	10~30	5.5	6	11	22	25	
	6	15~50	7	7	11	22	25	
	8	20~100	9.5	8	11	22	25	
	10	25~100	12	9	16	27	25	
	12	30~100	14.5	10	16	27	25	
	16	50~100	19	14	19	32	25	

Ordering Example

Part Number	-	L
BLPS8	-	25
BLPF10	-	45

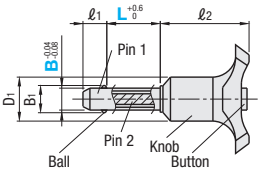
B	Mating Hole Recommended Dimensions	Resistance when Removed (N)	Pin Fracture Load (kN)	Mass (g)
5	$5^{+0.07}_{0}$	9	5	19~22
6	$6^{+0.07}_{0}$	9	7	21~28
8	$8^{+0.09}_{0}$	9	13	27~58
10	$10^{+0.09}_{0}$	20	20	59~105
12	$12^{+0.11}_{0}$	30	29	73~135
16	$16^{+0.11}_{0}$	50	51	159~237

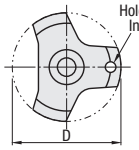
■**Ball Lock Pins**
- Push Type

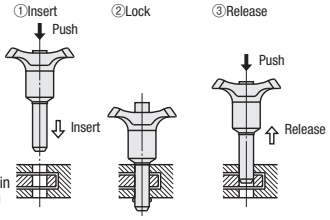


RoHS10

Type	Ball M Material	Ball H Hardness	Pin 1 M Material	Pin 2 M Material	Spring M Material	Knob M Material
BLP	EN 1.4125 Equiv.	55HRC~	EN 1.4542 Equiv.	EN 1.4305 Equiv.	EN 1.4568 Equiv.	Nylon 6 (Black, Orange)







①When the button is pushed, the ball lock is released. The pin can be inserted into a hole as the balls draw in the pin.
②When the button is released, the pin is locked as the balls extend outward from the pin.
③When the button is pushed again, the ball lock is released and the pin is pulled out.

Part Number Type	B	L	D	D1	B1	ℓ1	ℓ2	Mating Hole Recommended Dimensions	Shear Load (kN)	Mass (g)	Unit Price L=10~25	L=30~50	L=60, 80	L=100
BLP	5	10 15 20 25 30	38	16	5.5	6	31.5	$5^{+0.07}_{0}$	24	30~32			-	-
	6	10 15 20 25 30 40 50			7	7		$6^{+0.07}_{0}$	35	31~39			-	-
	8	20 25 30 40 50			9.5	8		$8^{+0.09}_{0}$	63	38~47			-	-
	10	25 30 40 50 60	43	23	12	9	36	$10^{+0.09}_{0}$	100	76~97				-
	12	40 50 60 80			14.5	10		$12^{+0.11}_{0}$	144	100~135	-			-
	16	60 80 100			19	14		$16^{+0.11}_{0}$	257	171~232	-	-		

Ordering Example

Part Number	-	L
BLP8	-	25

Disc Couplings For Servo Motors

Ultra High Torque Clamping (Single Disc)

Points of comparison between similar products | Max. Rotational Speed: 3,500~6,000rpm

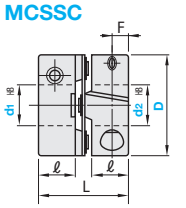


RoHS 10

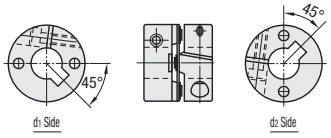
Type	Parts	M Material	S Surface Treatment	A Accessory
MCSSC MCSSCWK	Main Body	Aluminum Diecast	Electroless Nickel Plating	Hex Socket Head Cap Screw
	Disc	Stainless Steel	-	
	Screw	EN 1.7220 Equiv.	Black Oxide	

Tolerances for d1 and d2 are values before slit machining.
For keyway dimension, refer to the following.

Standad Bore
MCSSC



Keywayed Bore (d1·d2Both Sides)
MCSSCWK



Part Number Type	D	d1, d2 Selection (d1≤d2) Keywayed Bore Type is selectable for diameter 6 or larger	L	ℓ	A	F	Clamp Screw M	Clamp Screw Tightening Torque (N·m)	Unit Price MCSSC	Unit Price MCSSCWK
Clamping MCSSC MCSSCWK	16	*4 5 6	16.5	7	5	3	M2.5	1		
	20	*4 5 6 6.35 7 8	18.4	7.5	6.5	3.7				
	25	*5 6 6.35 7 8 9.53 10	21.6	9	8.5	4	M3	1.7		
	32	8 9.53 10 11 12 14	29	12.4	10	6	M4	2.5		
	40	8 9.53 10 11 12 14 15 16 18	35	15.5	13.1	7.8	M5	7		
	50	14 15 16 18 20 22 24	41	18	16.7	9	M6	12		

When d1, d2 is *4, *5, use with load torque 50% or less than shown in the table to prevent slipping.

Characteristic Values

Part Number Type	D	Allowable Torque (N·m)	Angular Misalignment (°)	Lateral Misalignment (mm)	Static Torsional Spring Constant (N·m/rad)	Max. Rotational Speed (r/min)	Moment of Inertia (kg·m²)	Allowable Axial Misalignment (mm)	Compensation Factor	Mass (g)
MCSSC MCSSCWK	16	0.9	1	-	650	6000	2.2×10^{-7}	±0.1	5~10	8
	20	1.3			950	5500	7.0×10^{-7}			13
	25	2.8			1300	5000	2.2×10^{-6}	±0.2		24
	32	5			1400	4000	5.6×10^{-6}			53
	40	9			3300	3800	1.5×10^{-5}			90
	50	16			4000	3500	3.9×10^{-5}	±0.3		180

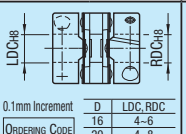
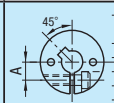
Single Disc Type cannot tolerate lateral misalignment.
The lateral, angular, and axial misalignment values shown are for each occurring individually. When multiple misalignments are occurring simultaneously, the allowable maximum value of each will be reduced to 1/2.
For the selection criteria and alignment procedures, see P.1061, 1062.

Ordering Example

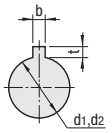
Part Number	-	Shaft Bore Dia. d1	-	Shaft Bore Dia. d2
MCSSC40	-	10	-	15
MCSSCWK32	-	8	-	10

Alterations

Part Number	-	Shaft Bore Dia. d1 (LDC)	-	Shaft Bore Dia. d2 (RDC)	-	
MCSSC40	-	LDC9.5	-	RDC10.5		
MCSSCWK40	-	8	-	10	-	KRH4

Alterations	Shaft Bore Dia.	Keyway Width	Keyway
Spec.	 0.1mm Increment. Ordering Code: LDC7.8, RDC9.3. D: 16 LDC, RDC 4~6; 20 4~8; 25 5~10; 32 6~14; 40 8~18; 50 14~24	Keyway Width (b) is changed as the table below. Ordering Code: KLH4 KRH4  Shaft Bore Dia. d1, d2: 8 (b) Reference Dia. 2, Tolerance ±0.0125, t Reference Dia. 1.0, Tolerance +0.1 0; 10 4 ±0.0150 1.8 +0.1 0; 12 5 2.3; 22 8 ±0.0180 3.3 +0.2 0. Cannot be combined with shaft bore change (LDC, RDC) alterations. Applicable to Keywayed Bore only.	 Shaft Dia. d1, d2 / LK, RK: 6~8 2; 8~10 3; 10~12 4; 12~17 5; 17~22 6; 22~24 8. Ordering Code: LK3 RK4. Keyway machining is available for Ø6 ~. For keyway dimensions, refer to the right table.
Code	LDC (Left Shaft) RDC (Right Shaft)	KLH (Left Shaft) KRH (Right Shaft)	LK (Left Shaft) RK (Right Shaft)

Keyway Dimension



Shaft Bore Dia. d1, d2	b Reference Dia.	b Tolerance	t Reference Dia.	t Tolerance	Key Nominal Dim. bxh
6~7.9	2	±0.0125	1.0	+0.1 0	2x2
8~10	3		1.4		3x3
10.1~12	4	±0.0150	1.8		4x4
12.1~17	5		2.3		5x5
17.1~22	6		2.8		6x6
22.1~24	8	±0.0180	3.3	+0.2 0	8x7

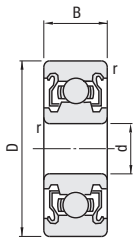
Small Ball Bearings
Double Shielded

This product can be used even when heavy load, high rotation speed, and high rotational accuracy are required. See **P990** for the C-VALUE Product of this item.

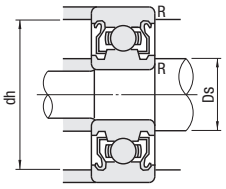


RoHS 10

B6□□ZZ
B6□□AZZ



(Installation Diagram)



Material: EN 1.3505 Equiv.
Bearing Accuracy JIS B 1514 Class 0

For details on the tolerance and allowable values of inner and outer rings, P.2243

Part Number	d	D	B	r (min)	Basic Load Rating Cr (Dynamic) N	Basic Load Rating Cor (Static) N	Allowable Rotational Speed rpm (Reference)	Relative Dimensions Ds (min)	Relative Dimensions dh (max)	Relative Dimensions R (max)	Mass (g) (Reference)	Unit Price
B682ZZ	2	5	2.3	0.08	169	50	85000	2.7	3.9	0.08	0.17	
B692ZZ		6	3.0	0.15	330	98	75000	3.0	4.8	0.15	0.38	
B602ZZ		7	3.5		385	127	60000	3.2	5.8		0.58	
B682AZZ	2.5	6	2.6	0.08	208	74	71000	3.7	4.9	0.08	0.29	
B692AZZ		7	3.5	0.15	385	127	63000	3.85	5.65	0.15	0.55	
B673ZZ	3	6	2.5	0.1	208	74	71000	3.6	5.4	0.08	0.2	
B683ZZ		7	3		390	130	63000	3.9	5.8	0.1	0.45	
B693ZZ		8	4	0.15	560	179	60000	4.2	6.8	0.15	0.83	
B603ZZ		9	5		570	187	56000		7.8		1.45	
B623ZZ		10	4		630	218	50000		8.8		1.66	
B633ZZ		13	5	0.2	1300	485	40000	4.6	11.4	0.2	3.33	
B674ZZ	4	7	2.5	0.1	222	88	60000		6.4	0.08	0.29	
B684ZZ		9	4		640	224	53000	5.0	7.8	0.1	1.01	
B694ZZ		11		0.15	715	276	48000	5.2	9.8	0.15	1.75	
B604ZZ		12		0.2	957	350		5.6	10.4	0.2	2.29	
B624ZZ		13	5		1300	485	40000		11.4		3.04	
B634ZZ		16		0.3	1340	523	36000	6	14	0.3	5.21	
B675ZZ	5	8	2.5	0.1	218	131	53000	5.8	7.4	0.1	0.34	
B685ZZ		11	5	0.15	715	281	45000	6.2	9.8	0.2	1.96	
B695ZZ		13	4	0.2	1080	430	43000	6.6	11.4		2.5	
B605ZZ		14	5		1330	505	40000		12.4		3.48	
B625ZZ		16		0.3	1730	670	36000	7	14	0.3	4.86	
B635ZZ		19	6		2336	835	32000		17		8.34	
B676ZZ	6	10	3	0.1	495	218	45000	7.04	9.3	0.1	0.68	
B686ZZ		13	5	0.15	1080	440	40000	7.0	11.8	0.15	2.69	
B696ZZ		15		0.2	1350	530		7.6	13.4	0.2	3.72	
B606ZZ		17	6	0.3	2190	835	38000	8	15	0.3	6.08	
B626ZZ		19			2340	885	32000		17		7.94	
B636ZZ		22	7		3333	1423	30000		20		14.5	
B678ZZ	8	12	3.5	0.1	543	274	40000	9.05	11.33	0.1	0.97	
B688ZZ		16	5	0.2	1610	710	36000	9.6	14.4	0.2	4.02	
B698ZZ		19	6	0.3	1990	865		10	17	0.3	7.18	
B608ZZ		22	7		3350	1400	34000		20		12	
B628ZZ		24	8		4000	1590	28000		22		17	
B638ZZ		28	9		4563	1983			26		30.3	

kgf=Nx0.101972

Ordering Example **Part Number** B626ZZ

Bearings with Housings

Short Double Bearings, Retained



RoHS10

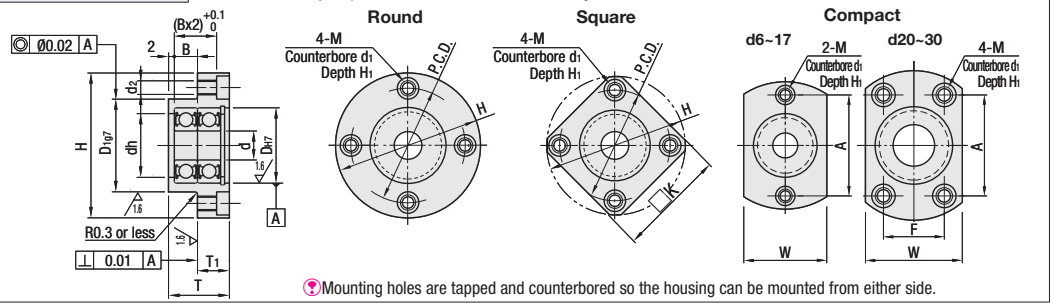
Type			Material		Surface Treatment
Round	Square	Compact	Bearing	Housing	Housing
BGREB	BGSEB	BGCEB	Steel	EN 1.1191 Equiv.	Black Oxide
BGRE	BGSE	BGCE			Electroless Nickel Plating
SBGRE	SBGSE	SBGCE	* Stainless Steel	EN 1.4301 Equiv.	-

Bearing Accuracy: JIS B 1514 Class 0

Easier to obtain required radial load ratings when space is limited.

* Bearings with Rubber Seals (VV and DD) are all made of steel.

The "(Bx2)" dimension for "Short Double Bearings, Retained" Type indicates the position where the retaining ring groove begins. Please note that considering the groove width tolerance and the retaining ring thickness tolerance, there may be up to max.0.3 of axial clearance on the bearings.



Mounting holes are tapped and counterbored so the housing can be mounted from either side.

Part Number			d	D_{H7}	Tolerance	B	H	W	T	T_1	dh	D_{1g7}	Tolerance	P.C.D.	K	A	F	M (Coarse) (d_2)	d_1	H_1
Type	Bearing No.	Seal																		
(Round) BGREB BGRE SBGRE	606	ZZ Double Shielded	6	17	+0.018 0	6	39	23	17	9	13	21	-0.007 -0.028	29	32	29	-	M5 (4.3)	8	4.4
	608		8	22	+0.021 0	7	45	29	19	12	18	27		35	36	35				
	6900		10	22		6	45	29	17	11	19	27		35	36	35				
	6000			26		8	50	34	21	13	22	32	-0.009 -0.034	40	39	40				
	6901		12	24		6	48	31	17	11	21	30	-0.007 -0.026	38	38	38				
(Square) BGSEB BGSE SBGSE	6001	*1 *2 VV Non-Contact Sealed Rubber Seal		28		8	52	36	21	13	24	34	-0.009 -0.034	42	40	42		M6 (5.2)	9.5	5.4
	6902		15	28		7	57	37	19	12	25	35		45	45	45				
	6002			32	+0.025 0	9	60	40	23	14	28	38		48	46	48				
	6903		17	30	+0.021 0	7	60	38	19	12	27	36		48	46	48				
	6003	*2 DD Contact Sealed Rubber Seal		35		10	66	44	26	16	31	42		54	50	54				
(Compact) BGCEB BGCE SBGCE	6904		20	37	+0.025 0	9	69	47	24	15	34	45		56	54	51	24	M8 (6.8)	11	6.5
	6004			42		12	77	54	30	18	36	50		64	59	56	32			
	6005		25	47		12	88	58	30	18	41	54	-0.010 -0.040	72	67	63	36	M10 (8.5)	14	8.6
	6006		30	55	+0.030 0	13	96	66	33	20	48	62		80	73	70	40			

Check for available sizes in the price list.

*1 No. 606 is not available for VV (Non-contact Sealed).

*2 Bearings with Rubber Seals are all made of steel.

Ordering Example

Part Number		
Type	Bearing	Seal
BGRE	6000	ZZ
BGSE	6003	VV

Alterations

Part Number - (NA)

BGRE6000VV - NA

Alteration	Bearings, Retaining Rings Not Assembled
Code	NA
Spec.	Bearings and retaining rings are shipped unassembled to the housing.

Bearing No.	Seal	Unit Price								
		Round			Square			Compact		
		BGREB	BGRE	SBGRE	BGSEB	BGSE	SBGSE	BGCEB	BGCE	SBGCE
606	ZZ (x1.0)									
608										
6900										
6000										
6901										
6001										
6902	VV (x1.1)									
6002										
6903										
6003	DD (x1.1)									
6904										
6004										
6005				-			-			-
6006				-			-			-

The price of sealed VV and DD are the price shown in the table multiplied by 1.1.

Bearing Spacers

Bearing Inner, Outer Rings

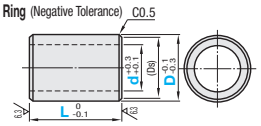


RoHS 10

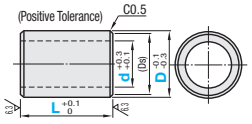
Applicable	L Dimension Tolerance		M Material	S Surface Treatment
	Negative Tolerance	Positive Tolerance		
For Inner Ring	CLBU	CLBP	Aluminum Alloy 5000 series	-
	CLBUB	CLBPB	EN 1.0038 Equiv.	Black Oxide
	CLBUM	CLBPM		Electroless Nickel Plating
	CLBUS	CLBPS	EN 1.4301 Equiv.	-

Applicable	L Dimension Tolerance		M Material	S Surface Treatment
	Negative Tolerance	Positive Tolerance		
For Outer Ring	CLBS	CLBT	EN AW-5052 Equiv.	-
	CLBSB	CLBTB	EN 1.0038 Equiv.	Black Oxide
	CLBSM	CLBTM		Electroless Nickel Plating
	CLBSS	CLBTS	EN 1.4301 Equiv.	-

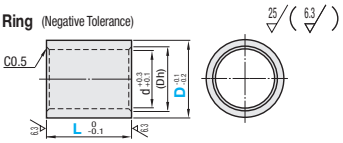
■For Inner Ring (Negative Tolerance) C0.5



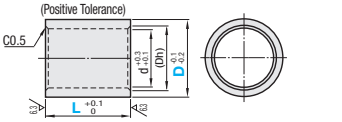
(Positive Tolerance) C0.5



■For Outer Ring (Negative Tolerance)



(Positive Tolerance)



* L= Less than 3, C0.2 or less

Part Number Type	d	D	L 0.1mm Increment	Ds	Applicable Bearing	Unit Price CLBU, CLBP L1.0~25.0	CLBU, CLBP 25.1~50.0	CLBU, CLBP 50.1~100.0	CLBUB, CLBPB L1.0~25.0	CLBUB, CLBPB 25.1~50.0	CLBUB, CLBPB 50.1~100.0	CLBUM, CLBPM L1.0~25.0	CLBUM, CLBPM 25.1~50.0	CLBUM, CLBPM 50.1~100.0	CLBUS, CLBPS L1.0~25.0	CLBUS, CLBPS 25.1~50.0	CLBUS, CLBPS 50.1~100.0
For Inner Ring (Negative Tolerance) CLBU CLBUB CLBUM CLBUS (Positive Tolerance) CLBP CLBPB CLBPM CLBPS	3	5	1.0~50.0	4	673ZZ, 693ZZ, 623ZZ			-			-			-			-
	4	7		6	674ZZ*, 694ZZ, 624ZZ			-			-			-			-
	5	8		7	675ZZ*, 695ZZ, 605ZZ, 625ZZ			-			-			-			-
	6	9		8	676ZZ, 696ZZ, 606ZZ, 626ZZ			-			-			-			-
	8	10		9	678ZZ	-	-	-			-			-	-	-	-
		11		10	678ZZ, 698ZZ, 608ZZ, 628ZZ			-			-			-			-
	10	12		11	6700ZZ	-	-	-			-			-	-	-	-
		13	1.0~100.0	12	6800ZZ												
		14		13	6900ZZ, 6000ZZ												
		17	2.0~100.0	16	6200ZZ, 6300ZZ												
	12	15	1.0~100.0	14	6701ZZ, 6801ZZ												
		16		15	6901ZZ, 6001ZZ												
		18	2.0~100.0	17	6201ZZ, 6301ZZ												
	15	18		17	6702ZZ, 6802ZZ												
		19		18	6902ZZ, 6002ZZ												
		21		20	6202ZZ												
		23		22	6302ZZ	-	-	-							-	-	-
	17	20		19	6803ZZ												
		22		21	6903ZZ, 6003ZZ												
		24		23	6203ZZ												
		26		25	6303ZZ	-	-	-							-	-	-
	20	23		22	6804ZZ												
		25		24	6904ZZ												
		27	2.0~100.0	26	6004ZZ, 6204ZZ												
		29		28	6304ZZ	-	-	-							-	-	-
	25	28		27	6805ZZ												
		29		28	6905ZZ												
		31		30	6005ZZ												
		33		32	6205ZZ												
		36		35	6305ZZ	-	-	-							-	-	-
	30	33		32	6806ZZ												
		35		34	6906ZZ												
		38		37	6006ZZ												
		40		39	6206ZZ												
		43		42	6306ZZ	-	-	-							-	-	-
	35	38	3.0~100.0	37	6807ZZ												
		42		41	6907ZZ												
		44		43	6007ZZ, 6207ZZ												
		46		45	6207ZZ	-	-	-							-	-	-
		48		47	6307ZZ	-	-	-							-	-	-
	40	43		42	6808ZZ												
		46		45	6908ZZ												
		49		48	6008ZZ, 6208ZZ												
		52		51	6208ZZ	-	-	-							-	-	-
		54		53	6308ZZ	-	-	-							-	-	-
	45	53		52	6009ZZ	-	-	-							-	-	-
		55		54	6209ZZ	-	-	-							-	-	-
	50	56		55	6010ZZ	-	-	-							-	-	-
		60		59	6210ZZ	-	-	-							-	-	-

When L=less than 3, *marked bearings cannot be used.

Rotary Shafts D Tolerance h9 (Cold-drawn) / h7 (Ground) / g6 (Ground)

Straight

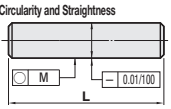
■Select from h9 (Cold-drawn), h7 (Ground) and g6 (Ground) for your applications.



	Type	D Tolerance	M Material	S Surface Treatment
①	SFMR	h9 (Cold-drawn)	EN 1.1191 Equiv.	Black Oxide
	PSFMR			Electroless Nickel Plating
	SSFMR		EN 1.4301 Equiv.	-
②	SFHR	h7 (Ground)	EN 1.1191 Equiv.	Black Oxide
	PSFHR			Electroless Nickel Plating
	SSFHR		EN 1.4301 Equiv.	-
③	SFR	g6 (Ground)	EN 1.1191 Equiv.	Black Oxide
	PSFR			Electroless Nickel Plating
	SSFR		EN 1.4301 Equiv.	-
	HFR		EN 1.7220 Equiv. H Hardness: 30 ~ 35HRC	Black Oxide
	PHFR			Electroless Nickel Plating

Surface roughness of D part for h9 (Cold-drawn) is 6.3. Surface roughness for h7 (Ground) and g6 (Ground) is 1.6.

■Circularity and Straightness



Straightness of size D2, D2.5 is 0.1/100.
Not applicable to h9 (Cold-drawn).

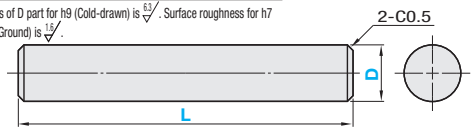
■Circularity of Part D

D over	D or Less	Circularity M
1	2.5	0.006
3	13	0.004
13	20	0.005
20	40	0.006
40	50	0.007

Not applicable to h9 (Cold-drawn).

■L Dimension Tolerance

Dimension over	Dimension or Less	Tolerance
14	30	±0.2
30	120	±0.3
120	400	±0.5
400	800	±0.8



①h9 (Cold-drawn)

Part Number Type	Dh9		L=0.1mm Increment
	3	0 -0.025	15.0 ~ 150.0
	4	0 -0.030	15.0 ~ 200.0
	5		15.0 ~ 250.0
	6		20.0 ~ 300.0
SFMR	8	0 -0.036	20.0 ~ 400.0
PSFMR	10		20.0 ~ 500.0
	12	0 -0.043	30.0 ~ 600.0
SSFMR (D6 is not available for SSFMR.)	15		30.0 ~ 700.0
	20	0 -0.052	40.0 ~ 800.0
	25		50.0 ~ 800.0
	30		60.0 ~ 800.0
	35	0 -0.062	70.0 ~ 800.0
	40		80.0 ~ 800.0
	50		100.0 ~ 800.0

②h7 (Ground)

Part Number Type	Dh7		L=0.1mm Increment
	3	0 -0.010	15.0 ~ 150.0
	4	0 -0.012	15.0 ~ 200.0
	5		15.0 ~ 250.0
	6		20.0 ~ 300.0
	8	0 -0.015	20.0 ~ 400.0
SFHR	10		20.0 ~ 500.0
	12	0 -0.018	30.0 ~ 600.0
PSFHR	15		30.0 ~ 700.0
	17		40.0 ~ 800.0
SSFHR	20	0 -0.021	40.0 ~ 800.0
	25		50.0 ~ 800.0
	30		60.0 ~ 800.0
	35	0 -0.025	70.0 ~ 800.0
	40		80.0 ~ 800.0
	50		100.0 ~ 800.0

③g6 (Ground)

Part Number Type	Dg6		L=0.1mm Increment
	2	-0.002 -0.008	15.0 ~ 50.0
	2.5		15.0 ~ 50.0
	3		15.0 ~ 150.0
	4	-0.004 -0.012	15.0 ~ 200.0
	5		15.0 ~ 250.0
SFR	6		20.0 ~ 300.0
	8	-0.005 -0.014	20.0 ~ 400.0
PSFR	10		20.0 ~ 500.0
	12	-0.006 -0.017	30.0 ~ 600.0
SSFR (D13, 16, 18 and 22 are not available for SSFR.)	13		30.0 ~ 600.0
	*15		30.0 ~ 700.0
	16		30.0 ~ 800.0
*HFR (Only * marked sizes are available.)	17		40.0 ~ 800.0
	18		40.0 ~ 800.0
	*20	-0.007 -0.020	40.0 ~ 800.0
*PHFR (Only * marked sizes are available.)	22		40.0 ~ 800.0
	*25		50.0 ~ 800.0
	*30		60.0 ~ 800.0
	*35	-0.009 -0.025	70.0 ~ 800.0
	*40		80.0 ~ 800.0
	*50		100.0 ~ 800.0

Ordering Example

Part Number	-	L
SFMR15	-	150
PSFHR20	-	300

Shaft Collar Clamp

2-Hole / 2-Tapped (Coarse)

■2-Hole
■2-Tapped (Coarse)



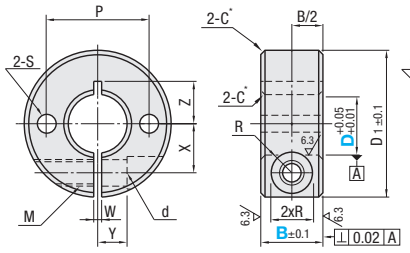
RoHS 10

Type		M Material	S Surface Treatment	A Accessory
2-Hole	2-Tapped			Hex Socket Head Cap Screw 1 pc.
SCSM	SCSW	EN 1.1191 Equiv.	Black Oxide Coating	M EN 1.7220 Equiv.
PSCSM	PSCSW		Electroless Nickel Plating	M EN 1.4301 Equiv.
SSCSM	SSCSW	EN 1.4301 Equiv.	-	

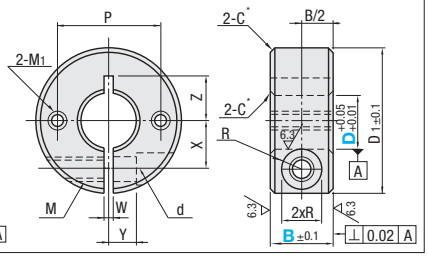
25/ (6.3/)

*D6 ~D25: C0.5
D30~D50: C1

2-Hole



2-Tapped (Coarse)



Part Number Type	D	B Selection	D1	M (Coarse)	d	R	W	X	Y	Z	P	S	2-Hole Unit Price SCSM	PSCSM	SSCSM	2-Tapped M1 (Coarse)	2-Tapped Unit Price SCSW	PSCSW	SSCSW
(2-Hole) SCSM PSCSM SSCSM (2-Tapped) SCSW PSCSW SSCSW	6	* 8	20	M3	3.4	3	1	6	4	6~6.5	12	3.5				M3			
		*10		M4	4.5	3.75					13								
	8	* 8	25	M3	3.4	3	1.5	8	5	7~9	14	4.5				M4			
		*10		M4	4.5	3.75					18								
		*12	30	M5	5.5	4.5		9		7~10		5.5				M5			
		15		M6	6.6	6					20					-	-	-	-
	10	* 8		M3	3.4	3				8~10						M5			
		*10		M4	4.5	3.75													
		*12		M5	5.5	4.5		10											
		15	35	M6	6.6	6			6	8~12	24	6.6				-	-	-	-
	12	* 8	30	M3	3.4	3			5	9~10	22	5.5				M5			
		*10		M4	4.5	3.75													
		*12		M5	5.5	4.5													
		*15	35	M6	6.6	6		11	6	9~12	24	6.6				M6			
	13	*10	30	M4	4.5	3.75		10	5	10	22	4.5				M4			
		*12	34	M5	5.5	4.5		11		10~12	23	5.5				M5			
		15	35	M6	6.6	6					24					-	-	-	-
	15	*10	34	M4	4.5	3.75		11.5	6	10~11	23	4.5				M4			
		*12	35	M5	5.5	4.5		12		11~13	26	5.5				M5			
		*15	40	M6	6.6	6		13	8		28	6.6				M6			
	16	*10	35	M5	5.5	4.5		12	6	11~12	24	4.5				M4			
		*12									26	5.5				M5			
		*15	40	M6	6.6	6		13	8	11~13	28	6.6				M6			
	18·20	*10		M5	5.5	4.5		14	7	13		4.5				M4			
		*12									30	5.5				M5			
		*15	45	M6	6.6	6		15	8	13~15	34	6.6				M6			
		20						16								-	-	-	-
		25																	
		30																	
	25	*12	45	M5	5.5	4.5		17	7	16	36	5.5				M5			
		*15	50	M6	6.6	6		18	10	16~18	38	6.6				M6			
		20	55					20		16~20	40					-	-	-	-
		25																	
		30																	
	30	*15								18~20	44					M6			
		20	60	M8	9	7		23		18~21	45	9			-	-			
		25													-				
		30																	
	35	15		M6	6.6	6	2		12	21	48	6.6				-	-	-	-
		20																	
		25																	
		30																	
	40	18	70	M8	9	7		26	13	23	56	9							
		30																	
	50	22	85	M10	11	9	3	32	16	28	68	11							
		30																	

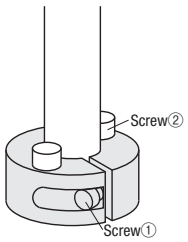
- Only * marked sizes are available for 2-Tapped Type.
- D18 is available for 2-Tapped Type only.

Ordering Example

Part Number	-	B
SCSM10	-	10

Example

Tips on Assembly
When using collars as shown in the diagram on the right, clamping the shaft with the screw ① after the collar is fully tightened to the plate with the screws ② is not possible.
The type shown on **P.285** that can be fully mounted first with the screws ② is recommended.



drylin® N low-profile guide systems | Product range

Guide rails and carriages – size 17



Complete Set

Order key

complete system ▶ Page 946

Type	Size	Options
NW -	22 -	17 - 30 - LLY

- drylin® N
- Guide carriages
- Type of carriage
- Rail width
- Carriage length
- Floating bearing in y-direction

Type of carriage:
- **02:** Carriage with threaded pin
- **22:** Double carriage with threaded pin

Options:
- **P:** Preload

Floating bearing:
- **LLY:** Floating y-direction
- **LLZ:** Floating z-direction
- **LLYZ:** Floating yz-direction

Guide rail – dimensions [mm]

Part No.	L max.	a	C4	C5: C6 Min.	C5: C6 max.	h	h1	K1[73]	Iy [mm⁴]	Iz [mm⁴]	Weight [g/m]
NS-01-17- □ [72]	2,000	17	60	20	49.5	5.5	0.9	Ø3.5	1,700	120	150
NS-01-17-UNGEBOHRT- □ [72]	2,000	17	–	–	–	5.5	0.9	–	1,700	120	150
NS-01-17-AR- □ [72]	2,000	17	60	20	49.5	5.5	0.9	Ø3.5	1,700	120	150

Guide carriage – dimensions [mm]

Part No.	H ±0.35	A	C	C2	K3 [74]	Sp	Dp	Weight [g]
NW-02-17	6.0	9.6	20	14	M3	2.5	5.0	1.7
NW-02-17-P	6.0	9.6	20	14	M3	2.5	5.0	1.7
NW-22-17-30	6.0	9.6	30	18	M3	2.5	5.0	2.4
NW-22-17-40	6.0	9.6	40	28	M3	2.5	5.0	2.6

[72] Please give the desired length in mm, hole pitches symmetrical C5=C6

[73] For cap screw with low head (i.e. DIN 7984, DIN 6912, DIN 84, EN ISO 1707)

[74] Metal thread

All elements can be ordered individually or as assembled systems

NS-01-17-1500: Guide rail, size 17, length 1,500 mm

NW-02-17-P-LLY: Guide carriage with threaded pin, size 17, pre-load, floating bearing in y-direction

NK-02-17-02-500-LLY: Complete system with two solid plastic guide carriages with threaded pins, size 17, floating bearing in y-direction and 500 mm guide rails with standard holes

DVB.6 - DVB.7 | Vibration-damping elements

Rubber and steel or stainless steel



VIBRATION-DAMPING BODY

Natural rubber NR, black colour.
Hardness 40, 55, 70 Shore A ±5.

STANDARD EXECUTIONS

- **DVB.6**: zinc-plated steel plate and threaded stud.
- **DVB.6-SST**: AISI 304 stainless steel plate and threaded stud.
- **DVB.7**: zinc-plated steel plate and boss, threaded blind hole.
- **DVB.7-SST**: AISI 304 stainless steel plate and boss, threaded blind hole.

FEATURES AND APPLICATIONS

DVB. vibration-damping elements have been designed to damp vibrations, shocks and noises produced by moving bodies or non-balanced vibrating masses of equipment and machines.
DVB elements are generally used as a bumper or as a limit stop for the absorption of vibrations.
Vibrations can cause:

- malfunctioning and reduction of the machine lifespan and/or of the adjacent ones;
- damage to operator's health;
- noise.

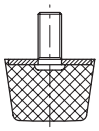
See Technical data and guidelines for the choice.

SPECIAL EXECUTIONS ON REQUEST

Natural rubber NR, hardness 40, 70 Shore A ±5 for the executions with AISI 304 stainless steel base.



DVB.6



DVB.7



elesa

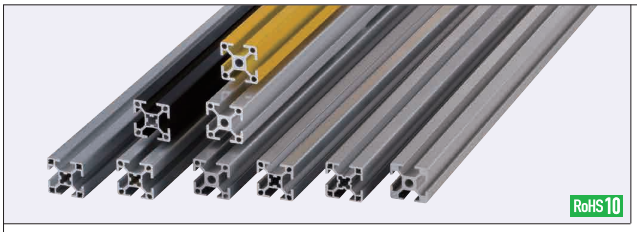
All rights reserved in accordance with the law. Always mention the source when reproducing our drawings.

December 2016

6 Series Aluminum Extrusions 30, 60 mm

1 Slot

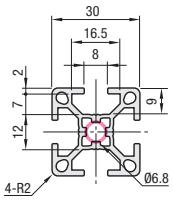
■**Features:** Standard extrusions for various use such as covers or frames.



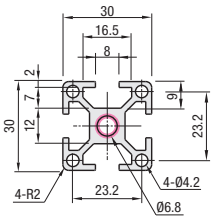
Type		Material	Surface Treatment
Configurable Length	Fixed Length		
NEFS6	KNEFS6	EN AW-6063-T5 Equiv.	Clear Anodize
GFS6	KGFS6	A6061SS-T6 Equiv.	
EFS6	KEFS6	EN AC-51400-T5 Equiv.	
HFS6	KHFS6		
NFSL6	KNFSL6	EN AW-6063-T5 Equiv.	
HFSL6	KHFSL6	EN AC-51400-T5 Equiv.	
NEFSB6	KNEFSB6	EN AW-6063-T5 Equiv.	Black Anodize
EFSB6	KEFSB6	EN AC-51400-T5 Equiv.	
HFSB6	KHFSB6		
HFSLB6	KHFSLB6		
CAF6	KCAF6		Clear Coating (Anodize + Clear Coating)
HFSY6	KHFSY6		Baked Paint (Yellow)

Cut surface and altered parts are not surface treated.
The color of HFSY6 is D22-80V (Japan Paint Manufacturers Association, Munsell Value Reference 2.5Y8/12).

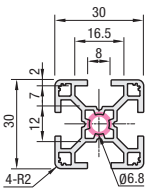
NEFS6-3030
NEFSB6-3030
(Black Anodize)
EFS6-3030
EFSB6-3030
(Black Anodize)



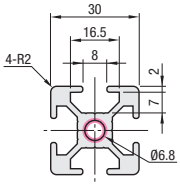
HFS6-3030
HFSB6-3030
(Black Anodize)
CAF6-3030
(Clear Coating)
HFSY6-3030
(Baked Paint, Yellow)



NFSL6-3030
HFSL6-3030
(Light Type)
HFSLB6-3030
(Light Type, Black Anodize)



GFS6-3030
(High Rigidity)



■Configurable Length Extrusions

Part Number		L 0.5mm Increment	Mass kg/m	Sectional Area mm²	Cross Sectional Moment of Inertia mm⁴ ℓx	ℓy	Unit Price Less than 300mm 1 ~ 9 pc(s).	Volume Discount Rate Less Than 300mm 10~49	50~160	Unit Price / m 300mm or More 1 ~ 9 pc(s).	Volume Discount Rate 300mm or More 10~49	50~160
NEFS6	3030	50~4000	0.8	296	2.85x10⁴	2.85x10⁴						
NEFSB6 (Black Anodize)												
EFS6												
EFSB6 (Black Anodize)												
HFS6		■Applicable to 6000mm depending on products. Refer to Information of Special Orders (P.103) and contact the person in charge of Special Orders at MISUMI QCT Center. ☤Some extrusions are not applicable.	0.9	333	2.83x10⁴	2.83x10⁴						
HFSB6 (Black Anodize)												
CAF6 (Clear Coating)												
HFSY6 (Baked Paint, Yellow)												
NFSL6			0.76	280	2.68x10⁴	2.68x10⁴						
HFSL6 (Light Type)												
HFSLB6 (Light Type, Black Anodize)												
GFS6 (High Rigidity)			1.02	377	3.47x10⁴	3.47x10⁴						

■Fixed Length Extrusions (1000mm)

☤Part numbers beginning with the character "K" indicate Fixed Length Extrusion.

Part Number		L mm	Sectional Area mm²	Cross Sectional Moment of Inertia mm⁴ Lx	Ly	Unit Price Qty. 1~19	Volume Discount Rate 20~120
KHFS6	3030	1000	333	2.83x10⁴	2.83x10⁴		

■Fixed Length Extrusions (Effective Length 4000mm ☞P.526)

☤Part numbers beginning with the character "K" indicate Fixed Length Extrusion.

Part Number		L mm	Sectional Area mm²	Cross Sectional Moment of Inertia mm⁴ ℓx	ℓy	Unit Price 1 ~ 9 pc(s).	Volume Discount Rate 10~20
KNEFS6	3030	4000 (Effective Length)	296	2.85x10⁴	2.85x10⁴		
KNEFSB6 (Black Anodize)							
KEFS6							
KEFSB6 (Black Anodize)							
KHFS6			333	2.83x10⁴	2.83x10⁴		
KHFSB6 (Black Anodize)							
KCAF6							
KHFSY6							
KNFSL6			280	2.68x10⁴	2.68x10⁴		
KHFSL6 (Light Type)							
KHFSLB6 (Light Type, Black Anodize)							
KGFS6 (High Rigidity)			377	3.47x10⁴	3.47x10⁴		

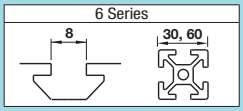
Ordering Example

Part Number	-	L
HFS6-3030	-	800
KHFS6-3030	-	1000
KHFS6-3030	-	4000

Alterations: Alterations are available for Configurable Length Extrusions. For details of alterations, see **P.755**.

Tabbed Brackets - For 1 Slot

For 6 Series (Slot Width 8mm) Aluminum Extrusions



Features: Tabbed Brackets to be connected by both L and Cross-Connections.

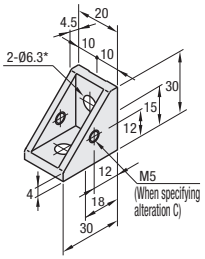
Tabbed Reversal Brackets

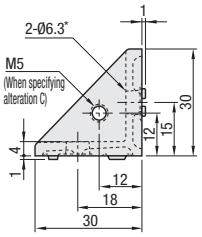


HBLFSN6
HBLFSN6-5 (For M5 Screw)
HBLFSNB6 (Black Anodize)
HBLFSNM6 (Electroless Nickel Plating)
CHBLFSN6 (Baked Paint, Silver)

Type	Material	Surface Treatment
①HBLFSN6	EN AC-46100 Equiv.	-
②HBLFSN6-5		-
③HBLFSNB6		Black Anodize
④HBLFSNM6		Electroless Nickel Plating
⑤CHBLFSN6		Baked Paint (Silver)

* Baked Paint (Silver) is color coordinated with Clear Coating Extrusions.





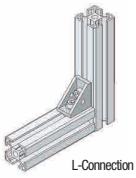
* Ø5.2 when HBLFSN6-5 is specified.

Part Number	Mass (g)	Applicable Screw, T Nut				Allowable Load (N)	Unit Price 1~99 pc(s).	Volume Discount Rate 100~200
		Screw	Quantity	T Nut	Quantity			
HBLFSN6	15	CBM6-12	2	HNTT6-6	2	1176		
HBLFSN6-5 (For M5 Screw)		CBM5-12		HNTT6-5				
HBLFSNB6* (Black Anodize)		CBM6-12		HNTT6-6				
HBLFSNM6 (Electroless Nickel Plating)								
CHBLFSN6 (Baked Paint, Silver)								

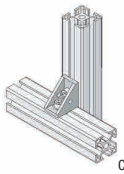
* For repairing black anodizing, refer to **P.846**.

Example

Can be installed in either direction.



L-Connection



Cross-Connection

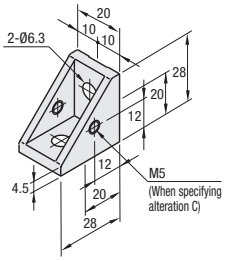
Features: Brackets with tabs to fit in slots of extrusions and stop rotating when tightening.

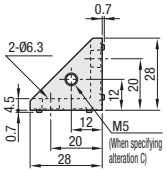
Tabbed Brackets



HBLFS6
HBLFSB6 (Cathodic Electrodeposition Paint: Black)

Type	Material	Surface Treatment
HBLFS6	EN AC-46100 Equiv.	-
HBLFSB6		Cathodic Electrodeposition Coating Black

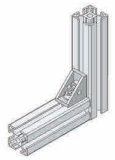




Part Number	Mass (g)	Applicable Screw, T Nut				Allowable Load (N)	Unit Price 1~99 pc(s).	Volume Discount Rate 100~200
		Screw	Quantity	T Nut	Quantity			
HBLFS6	13	CBM6-12	2	HNTT6-6	2	1176		
HBLFSB6 (Cathodic Electrodeposition Paint: Black)								

Example

Used for L-connections.

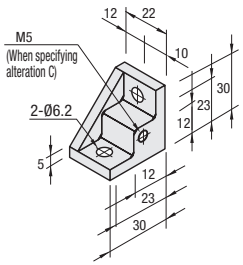


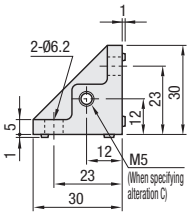
Features: One-Sided Tabbed Rib Brackets. Easy to work with wrenches.

One-Side Rib Brackets



HBLFSL6



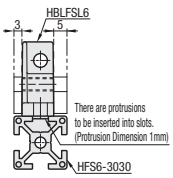


Material: EN AC-46100 Equiv.

Part Number	Mass (g)	Applicable Screw, T Nut				Allowable Load (N)	Unit Price 1~99 pc(s).	Volume Discount Rate 100~200
		Screw	Quantity	T Nut	Quantity			
HBLFSL6	17	CBM6-12	2	HNTT6-6	2	1176		

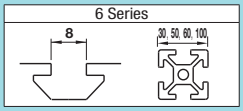
Example

Can be combined with both cover plates of 5mm and 3mm thickness.

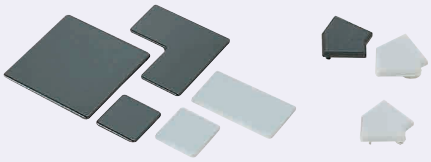


Extrusion End Caps

For 6 Series (Slot Width 8mm) Aluminum Extrusions



■**Features:** Standard caps for protecting extrusion end faces. Alterations for Aluminum Extrusions not necessary.

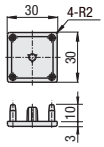


RoHS10

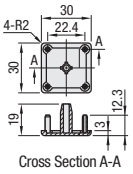
Type	Material
HFC	Polyamide
HFCL	Low Density Polyethylene

- Some products are not required to specify colors. In that case, color is black.
- The pin's shape and numbers of extrusion end caps may be changed to prevent caps from easily falling off.
- HFCL is not applicable to extrusions with Wrench Hole in Fixed Position (**P.761**), D Type Hole (**P.764**), or L Type Hole (**P.767**).

HFC6-3030

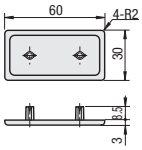


HFCL6-3030

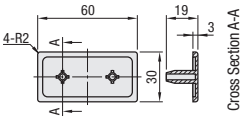


Cross Section A-A

HFC6-3060

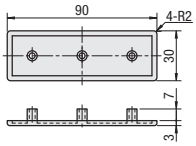


HFCL6-3060

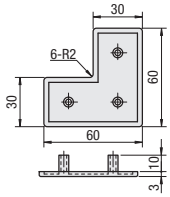


Cross Section A-A

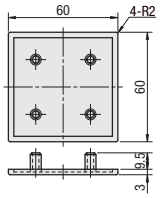
HFC6-3090



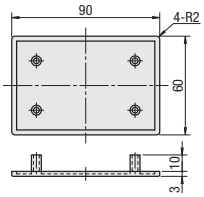
HFC6-606030



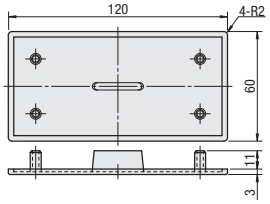
HFC6-6060



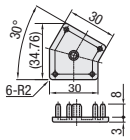
HFC6-6090



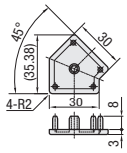
HFC6-60120



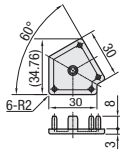
HFC30A6



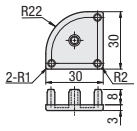
HFC45A6



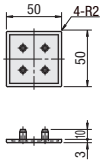
HFC60A6



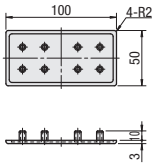
HFCR6-3030



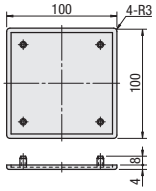
HFC6-5050



HFC6-50100



HFC6-100100

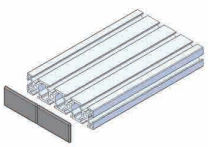


- HFC and HFCL can be used for each Aluminum Extrusion other than GFS/GNFS Series.
- For Aluminum Extrusions other than GFS Series, the same extrusion end caps as of HFS Series can be used. For caps for GFS Series, see **P.628**.

Part Number		Color	Unit Price	Volume Discount Rate		Applicable Extrusion
Type	No.		1 ~ 14 pc(s).	15~19	20~200	
HFC6	3030	B (Black)				6-3030
	3060					6-3060
	3090					6-3090
	606030					6-606030
	6060					6-6060
	6090					6-6090
	60120					6-60120
HFCL6	3030					6-3030
	3060					6-3060
HFC30A6		S (Light Gray)				30A6-30
HFC45A6						45A6-30
HFC60A6						60A6-30
HFCR6-3030						6-3030
HFC6	5050					6-5050
	50100					6-50100
	100100					6-100100

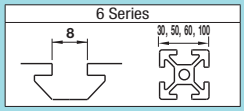
Part Number - Color
HFC30A6 - B

When using Aluminum Extrusion HFS6-30120, please use 2 pieces of HFC6-3060.



Pre-Assembly Insertion Nuts/Stoppers for Aluminum Extrusions - Standard

For 6 Series (Slot Width 8mm)



Tightening Torque P.526

Pre-Assembly Insertion Nuts

RoHS 10

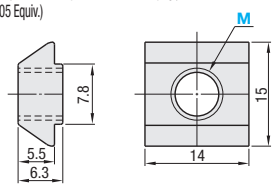


* Electrically conductive

Type	M Material	S Surface Treatment
①HNTT6	EN 1.0301 Equiv.	Trivalent Chromate
②PACK-HNTT6		
③HNTTV6	Thread Locking Adhesive Type, EN 1.0301 Equiv.	
④HNTTZ6	Thread Locking Resin Coating Type, EN 1.0301 Equiv.	
⑤HNTTSN6*	EN 1.4401 Equiv. (Sintered)	-
⑥PACK-HNTTSN6*		
⑦HNTTSS6	EN 1.4305 Equiv.	-

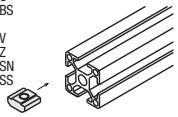
HNTT6 (EN 1.0301 Equiv.)
PACK-HNTT6 (EN 1.0301 Equiv., 100/pkg.)
HNTTV6 (Thread Locking Adhesive Type, EN 1.0301 Equiv.)
HNTTZ6 (Thread Locking Resin Coating Type, EN 1.0301 Equiv.)
HNTTSN6 (EN 1.4401 Equiv., Sintered)
PACK-HNTTSN6 (EN 1.4401 Equiv., Sintered, 100/pkg.)
HNTTSS6 (EN 1.4305 Equiv.)

Reference Tightening Torque (N · m)	
M	EN 1.0301 Equiv. EN 1.4401 Equiv. (Sintered) EN 1.4305 Equiv.
6	11.7



Example

· **Pre-Assembly Insertion Nuts**
Nuts are pre-inserted in the aluminum extrusion.
HNTU
HNTUV
HNTUZ
SHNTU
HNTTBS
HNTT
HNTTV
HNTTZ
HNTTSN
HNTTSS
HNTJ



Part Number	M	Unit Price	Volume Discount Rate		
		1 ~ 499 pc(s).	500~749	750~999	1000~1500
HNTT6 (EN 1.0301 Equiv.)	3 4 5 6				
HNTTV6 (Thread Locking, EN 1.0301 Equiv.)	6				
HNTTZ6 (Thread Locking, EN 1.0301 Equiv.)					
HNTTSN6 (EN 1.4401 Equiv., Sintered)	3 4 5 6				
HNTTSS6 (EN 1.4305 Equiv.)	6				

Part Number - M
HNTT6 - 6

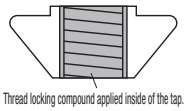
Bulk Packages

100 pcs. per package

Part Number	M	Unit Price (1 ~ 10 packages)	
		Package Price	Price per Pkg.
PACK-HNTT6 (EN 1.0301 Equiv.)	3 4 5 6		
PACK-HNTTSN6 (EN 1.4401 Equiv., Sintered)	3 4 5 6		

When ordering HNTT6 without specifying M, HNTT6-6 is selected automatically.

Thread Locking Type



Thread locking compound applied inside of the tap.

Nuts with thread locker applied on the inside of tap. Reduce loosening caused by vibration during transportation and operation of equipment.

Thread Locking Adhesive: A microencapsulated anaerobic adhesive prevents thread loosening. Note that it requires a hardening time (72 hours at room temperature 25°C). The adhesive property is lost once loosened.

Resin Coating: Resin is coated along the threads. Although the thread locking effect may be less than adhesive type, it can be used repeatedly without hardening time required.

Effect of Thread Locker (Reference)

Loosening torque values are for reference. Difference may occur depending on the clearances between screws and nuts.

	Characteristics	Loosening Torque after Tightening (1st time)	Remarks
Without Thread Locker	-	8.2N · m	-
Thread Locking Adhesive Type	• Prevents loosening effectively. • Thread locking properties are lost once loosened. •Requires a hardening time for adhesives (72 hours at room temperature 25°C) after tightening.	11.7N · m	Test Conditions: Measured value (HNTTV6-6) when a screw is loosened after drying for 72 hours at room temperature (25°C), after tightened at 11.7N · m.
Thread Locking Resin Coating Type	• Can be used repeatedly. (Thread locking effect decreases after repeated use.) • Thread locking effect is immediately seen right after tightening.	10.0N · m	Thread locking effect decreases after repeated use. Loosening Torque at 5 Repeats: 9.4N · m Measurement with HNTTZ6-6

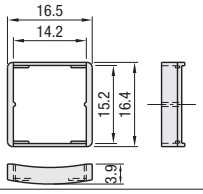
Pre-Assembly Insertion Stoppers

RoHS 10

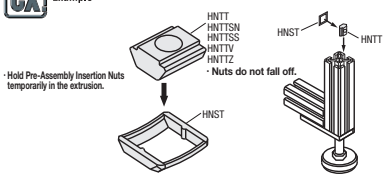


M Material: Polyamide

HNST6



Example



Part Number	Applicable Pre-Assembly Insertion Nut	Color	Unit Price 1 ~ 1500 pc(s).
HNST6	HNTT6 HNTTV6 HNTTZ6 HNTTSN6 HNTTSS6	Black	

Ordering Example: Part Number HNST6

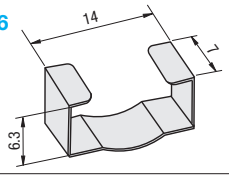
Pre-Assembly Insertion Metal Stoppers

RoHS 10

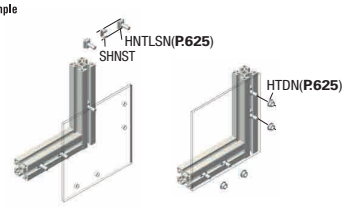


M Material: EN 1.4319 Equiv.

SHNST6



Example

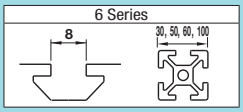


Part Number	Applicable Pre-Assembly Insertion Nut*	Unit Price 1 ~ 1500 pc(s).
SHNST6	HNTT6 HNTTV6 HNTTZ6 HNTTSN6 HNTTSS6	

Ordering Example: Part Number SHNST6

*Can also be used with Pre-Assembly Insertion Screws.

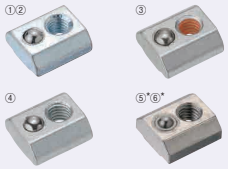
Pre-Assembly Insertion Nuts for Aluminum Extrusions with Temporary Holding Function For 6 Series (Slot Width 8mm)



Tightening Torque P.526

Pre-Assembly Insertion Spring Nuts

RoHS10

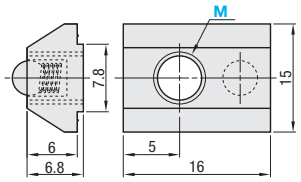


* Electrically conductive

Type	Material			
	Main Body	Ball	Spring	S Surface Treatment
①HNTU6 ②PACK-HNTU6 ③HNTUV6 ④HNTUZ6	EN 1.0301 Equiv.	EN 1.4301 Equiv.	JIS-SWP-A	Trivalent Chromate
⑤SHNTU6* ⑥PACK-SHNTU6*	EN 1.4301 Equiv. (Sintered)	EN 1.4301 Equiv.	SUS304-WP8	-

HNTU6 (EN 1.0301 Equiv.)
PACK-HNTU6 (EN 1.0301 Equiv., 100/pkg.)
HNTUV6 (Thread Locking Adhesive Type, EN 1.0301 Equiv.)
HNTUZ6 (Thread Locking Resin Coating Type, EN 1.0301 Equiv.)
SHNTU6 (EN 1.4301 Equiv., Sintered)
PACK-SHNTU6 (EN 1.4301 Equiv., Sintered, 100/pkg.)

Reference Tightening Torque (N · m)	
M	EN 1.0301 Equiv., EN 1.4301 Equiv. (Sintered)
6	11.7



Part Number	M	Unit Price	Volume Discount Rate		
		1 ~ 499 pc(s).	500~749	750~999	1000~1500
HNTU6 (EN 1.0301 Equiv.)	3 4 5 6				
HNTUV6 (Thread Locking, EN 1.0301 Equiv.)	6				
HNTUZ6 (Thread Locking, EN 1.0301 Equiv.)					
SHNTU6 (EN 1.4301 Equiv.)	3 4 5 6				

Ordering Example: Part Number HNTU6 - M 6

Bulk Packages

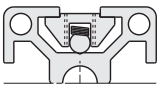
100 pcs. per package

Part Number	M	Unit Price (1 ~ 10 packages)	
		Package Price	Price per Pkg.
PACK-HNTU6 (EN 1.0301 Equiv.)	3 4 5 6		
PACK-SHNTU6 (EN 1.4301 Equiv.)			

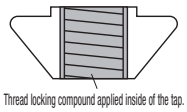
Example

- Does not fall even if the extrusion is placed vertically.

Built-in spring prevents slips. Moves easily in the slot when pressed slightly by hand.



Thread Locking Type



Thread locking compound applied inside of the tap.

Nuts with thread locker applied on the inside of tap. Reduce loosening caused by vibration during transportation and operation of equipment.
Thread Locking Adhesive: A microencapsulated anaerobic adhesive prevents thread loosening. Note that it requires a hardening time (72 hours at room temperature 25°C). The adhesive property is lost once loosened.
Resin Coating: Resin is coated along the threads. Although the thread locking effect may be less than adhesive type, it can be used repeatedly without hardening time required.

Effect of Thread Locker (Reference)

Loosening torque values are for reference. Difference may occur depending on the clearances between screws and nuts.

	Characteristics	Loosening Torque after Tightening (1st time)	Remarks
Without Thread Locker	-	8.2N · m	-
Thread Locking Adhesive Type	· Prevents loosening effectively. · Thread locking properties are lost once loosened. ·Requires a hardening time for adhesives (72 hours at room temperature 25°C) after tightening.	11.7N · m	Test Conditions: Measured value (HNTTV6-6) when a screw is loosened after drying for 72 hours at room temperature (25 °C), after tightened at 11.7N · m.
Thread Locking Resin Coating Type	· Can be used repeatedly. (Thread locking effect decreases after repeated use.) · Thread locking effect is immediately seen right after tightening.	10.0N · m	Thread locking effect decreases after repeated use. Loosening Torque at 5 Repeats: 9.4N · m Measurement with HNTTZ6-6

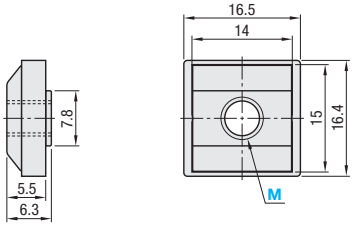
Stopper Integrated Nuts

RoHS10



Type	Material		
	Main Body	Stopper	S Surface Treatment
①HNTE6	EN 1.0301 Equiv.	Polypropylene	Trivalent Chromate
②SHNTE6	EN 1.4301 Equiv.		-

HNTE6
SHNTE6

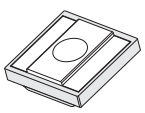


Reference Tightening Torque (N · m)	
M	EN 1.0301 Equiv. / EN 1.4301 Equiv.
6	11.7

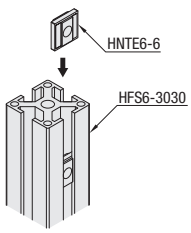
Part Number	M	Unit Price	Volume Discount Rate		
		1 ~ 499 pc(s).	500~749	750~999	1000~1500
HNTE6	3 4 5 6				
SHNTE6	3 4 5 6				

Ordering Example: Part Number HNTE6 - M 5

Example



Integrated Pre-Assembly Insertion Nuts and Stoppers.



The nuts do not slip off even if inserted into the vertically-placed extrusions.

Polyacetal Plates

Standard / Antistatic Grade

■Polyacetal (equal to Duracone®) is a general Engineered Plastic used for various industrial purposes. Antistatic Grade is made from non-carbon antistatic materials.For Finishing, Circular Sawing and Milling are available.

*For Details of color samples and features, see **P.951**

■Standard Type

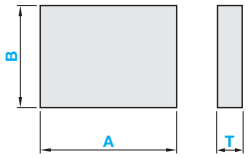


(?)Properties **P.953**

RoHS 10

(?)For Plastic Blocks, see **P.1024**.

Type	Ⓜ Grade	Color	Operating Ambient Temperature
PAA	Standard	White	-45~95°C
PABA		Black	
PACA	Antistatic	Ocher	Ambient Temperature: ~ 80°C



(?)A≥B

Ⓜ Material: Polyacetal

Dimension Tolerance of A and B

T	A·B Unit: mm	A, B Dimension Tolerance
5~30	~99	±0.5
	100~250	±0.75
	251~	±1.0
40~60	~300	0~+5

T Dimension Tolerance, Rate of Camber and Torsion

T	T Dimension Tolerance	Rates of Camber and Torsion per 1,000mm
5~10	+0.2~1.5	1.0% or Less
12	+0.3~2.0	
15~30		0.5% or Less
40, 50, 60	+0.5~3.0	

Finish	4 Sides		Upper-lower Surface	
	Drilling Method	Finish Symbol	Drilling Method	Finish Symbol
Circular Sawing	Circular Sawing	√	Material	~
Guaranteed Perpendicularity of Circular Saw Cuts (NT)	Circular Sawing	√	Material	~
4-side Milling (4F)	Milling	6.3	Material	~
6-surface Milling (6F)	Milling	6.3	Milling	6.3
Upper-lower Surface Milling (2F)	Circular Sawing	√	Milling	6.3

Precision Guarantee

Finish	Width Parallelism per 100mm	Perpendicularity of Reference Plane per 100mm
Guaranteed Perpendicularity of Circular Saw Cuts (NT)		
4-side Milling (4F)	0.1	0.1
6-surface Milling (6F)		

(?)Reference plane stickers are attached to 4-side milled plates.

Part Number: Type	Finish Selection	T Dimension Tolerance	A, B Dimension Tolerance	T Dimension Range by Material	A	B	T
PAA (Standard White) PABA (Standard Black) PACA (Antistatic Grade)	**Circular Sawing**				1mm Increment		Selectable
	-	Not available	Not available	PAA	20~500	20~400	5, 6, 8, 10, 12, 15, 20, 25, 30
					40~300	40~300	40, 50, 60
				PABA PACA	20~500	20~400	5, 6, 8, 10, 12, 15, 20, 25, 30
							6, 9, 12, 19, 25
	Guaranteed Perpendicularity of Circular Saw Cuts (NT)				0.5mm Increment		Selectable
	NT	Not available	T5, 6, 8, 9, 10 / T12, 15, 19, 20 / T25, 30 Q 0~+0.3 / 0~+0.4 / 0~+0.5 N ±0.2 / ±0.3 / ±0.4 M -0.3~0 / -0.4~0 / -0.5~0	PAA PABA	20~500	20~400	5, 6, 8, 10, 12, 15, 20, 25, 30
				PACA			6, 9, 12, 19, 25
	4-side Milling (4F)				0.1mm Increment		Selectable
	4F	Not available	Q 0~+0.2 N ±0.1 M -0.2~0	PAA PABA	10~400	10~200	5, 6, 8, 10, 12, 15, 20, 25, 30
				PACA			6, 9, 12, 19, 25
	6-surface Milling (6F)				0.1mm Increment		0.1mm Increment
	6F	Q 0~+0.2 N ±0.1 M -0.2~0	Q 0~+0.2 N ±0.1 M -0.2~0	PAA PABA	10~400	10~200	5~29
				PACA			5~24
	Upper-lower Surface Milling (2F)				1mm Increment		0.1mm Increment
	2F	Q 0~+0.2 N ±0.1 M -0.2~0	Not available	PAA PABA	20~400	20~250	5~29
				PACA			5~24

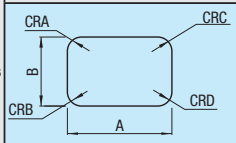
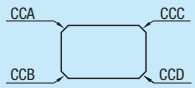
(?)T40, 50 and 60 may have steps on cut surfaces.

(?)For T0.5, 1.0, 1.5 and 2.0, see **P.973**.

Part Number	-	A	-	B	-	T
PAA	-	300	-	200	-	40
PAANTQ	-	200.5	-	100.5	-	10
PAA4FN	-	150.5	-	100.3	-	15
PAA6FMM	-	100.3	-	90.5	-	10.5
PAA2FQ	-	80	-	50	-	5

- Circular Sawing
- Guaranteed Perpendicularity of Circular Saw Cuts
- 4-surface Milling
- 6-surface Milling
- Upper-lower Surface Milling

Alterations Part Number - A - B - T - (CRA ··· etc.)
PAA - 300 - 200 - 10 - CRA10

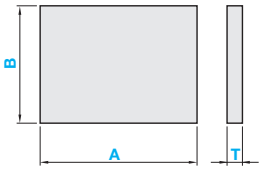
	Corner Radius	Corner Cut
Alterations		
Code	CRA, CRB, CRC, CRD	CCA, CCB, CCC, CCD
Spec.	Adds radius to any corner. R = 5mm Increment (?)10≤A(B)-R(2R) (?)5≤CRA, CRB, CRC, CRD≤100 Ordering Code (Ex.)Adds R10 at the corner of A and C. CRA10-CRC10 ⊗Not applicable to 4-side milling or 6-surface milling. ⊗Not applicable to T40, 50 and 60.	Cuts any corners. 5 ≤ Corner Cut ≤ 50 5mm Increment Ordering Code (Ex.) When the corners of A and D are cut by C5···› CCA5-CCD5 ⊗Not applicable to 4-side milling or 6-surface milling. ⊗Not applicable to T40, 50 and 60.

Acrylic Plates
Cast Plates

■MISUMI Acrylic Plates have two types: cast plates and extruded plates. 4-side(4F) Milling is now available for cast plates.
■Features of Cast Plates: Excels in heat resistance and mechanical strength. Extruded Plates: More inexpensive than cast plates. For details of extruded plates, see **P.967**. For details of cast plates and extruded plates, see **P.949.**

■Standard Type





(?)A≥B

• T Dimension Tolerance

T	T Dimension Tolerance
3	±0.5
4, 5	±0.6
6	±0.8
8	±0.9
10	±1.1
15	±1.5
20	±2.0
25	±2.5

•Dimension Tolerance of A and B ±1.0

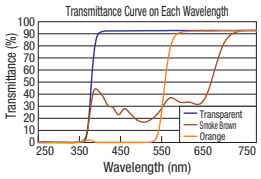
Type	Grade	Color	Light Transmittance	Operating Ambient Temperature
ACA	Standard	Transparent	93%	-30~80°C
ACBA	Standard	Smoke Brown	25%	
ACDA	Standard	Orange	43%	
ACTA	Antistatic	Transparent	79%	
ACBTA	Antistatic	Smoke Brown	32%	

Finish	4 Sides		Upper-lower Surface	
	Drilling Method	Finish Symbol	Drilling Method	Finish Symbol
Circular Sawing	Circular Sawing	√	Material	~
4-side Milling (4F)	Milling	6.3 ▽	Material	~

■ Standard Type

Part Number / Material	Finish Selection	A, B Dimension Tolerance	A	B	T
Standard Size	**Circular Sawing**		**1mm Increment**		**Selectable**
ACA (Standard, Transparent)	-	Not available	20~1200	20~1000	3, 4, 5, 6, 8, 10
			20~800	20~600	15, 20, 25
ACBA (Standard, Smoke Brown)			20~1200	20~1000	3, 4, 5, 6, 8, 10
ACDA (Standard, Orange) ACTA (Antistatic, Transparent) ACBTA (Antistatic, Smoke Brown)					3, 5
Large Size					
L-ACA (Standard, Transparent) L-ACBA (Standard, Smoke Brown) L-ACTA (Antistatic, Transparent) L-ACBTA (Antistatic, Smoke Brown)			1201~2000	20~1000	3, 5
4-side Milling	**4-side Milling**		**0.1mm Increment**		**Selectable**
ACA (Standard, Transparent)	4F	Q (0~+0.2) N (±0.1) M (-0.2~0)	10~400	10~200	5, 6, 8, 10, 15, 20, 25
ACBA (Standard, Smoke Brown)					5, 6, 8, 10
ACDA (Standard, Orange) ACTA (Antistatic, Transparent) ACBTA (Antistatic, Smoke Brown)					5

(?)For T0.5 ~ 2.0, see **P.973.**



(?)The above data are for reference, not guaranteed.

Ordering Example

■Standard Size

Part Number	-	A	-	B	-	T
ACTA	-	955	-	825	-	3

■Large Size

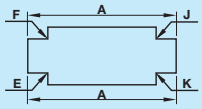
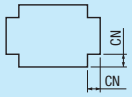
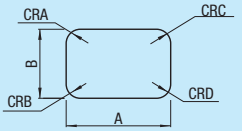
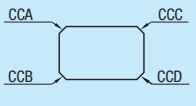
Part Number	-	A	-	B	-	T
L-ACA	-	1500	-	800	-	5

■4-side Milling

Part Number	-	A	-	B	-	T
ACA4FQ	-	300	-	200	-	15

Alterations

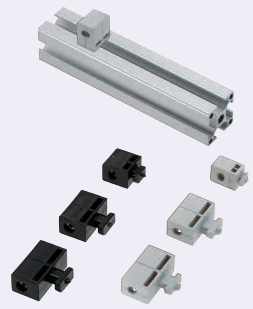
Part Number	-	A	-	B	-	T	-	(CRA··· etc)
ACA	-	100	-	80	-	3	-	CRA10-CRC10

Alterations	Notching for Blind Joints of Aluminum Extrusions	Relief at Four Corners	Corner Radius	Corner Cut
				
Code	F□, E□, J□, K□	CN	CRA, CRB, CRC, CRD	CCA, CCB, CCC, CCD
Spec.	Machines relief for blind joints of aluminum extrusions. (?)Margin against thermal expansion of the plate is not taken into account. (?)Longitudinal direction of notching is all on A dimension side. (?)Applicable to standard sizes only. ⊗ Not applicable to T=8. Ordering Code F S 6 — Extrusion Type; Joint Type; Notching Position (See the diagram above.) (?)Applicable to standard sizes only.	CN=1mm Increment Machines relief at four corners. (?)5≤CN≤50 (?)Applicable to standard sizes only. Ordering Code CN=25 ··· CN25 (?)Applicable to standard sizes only.	Adds radius to any corner. R = 5mm Increment (?)10≤A(B)-R(2R) (?)5≤CRA, CRB, CRC, CRD≤100 Ordering Code (Ex.)Adds R10 at the corner of A and C. CRA10-CRC10 (?)Applicable to standard sizes only.	Cuts any corners. 5 ≤ Corner Cut ≤ 50 5mm Increment Ordering Code (?)Applicable to standard sizes only. (Ex.)When the corners of A and D are cut by C5··· CCA5-CCD5

(?)For details of notching alterations for blind joint of aluminum frames, refer to **P.950.**
(?)Alterations are not available for Side Milling Plates.

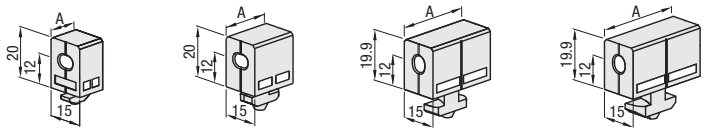
Panel Brackets - Plastic / Panel Clamping Brackets

■Panel Brackets - Plastic



Material: Polyamide RoHS10

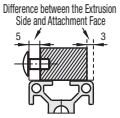
HCBR5 (Light Gray) **HCBRB5** (Black)
HCBR6 (Light Gray) **HCBR6S** (Light Gray) **HCBRB6** (Black) **HCBRB6S** (Black)
HCBR8 (Light Gray) **HCBRB8** (Black)
HCBR8-45 (Light Gray) **HCBRB8-45** (Black)



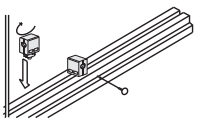
M5 insert nut is included inside. Use M5 screw with length 15 to attach panels.

Example

Since Plastic Type HCBR5 has an eccentric T-shaped stopping part, it can be used for both panels with thickness 5mm and 3mm.



■Plastic Type Mounting Method
Easy installation by inserting the T-shaped stopping part into the slot and turning 90.
Use mounting screws with L dimension 15 for plastic types.



Part Number		Mass	A	Difference between the Extrusion Side and Attachment Face	Unit Price	Volume Discount Rate
Type	No.				1 ~ 9 pc(s).	10
HCBR HCBRB	5	4.3	12	3 or 5		
	6	6.8	20	5		
	6S	6.0	24	3		
	8	10.9	30	5		
	8-45*	13.2	35	5		

* Select No. 8 for 45 Square Light type (HFSL8-45) series.

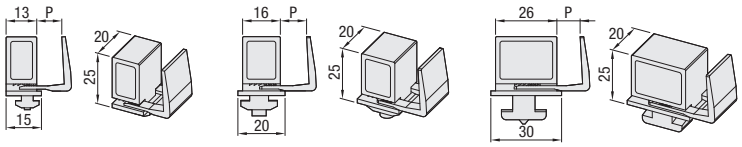
Ordering Example — Part Number: HCBR6

■Panel Clamping Brackets



Material: Polyamide RoHS10

HCBS5 **HCBS6** **HCBS8**



HCBS8 is commonly used for 8 Series and 8-45 Series. Panel thickness is adjustable by moving P part.

Part Number		Mass	P Applicable Panel Thickness	Unit Price	Volume Discount Rate
Type	No.			1 ~ 9 pc(s).	10
HCBS	5	2.6	3~5		
	6	3.9			
	8	6.3			

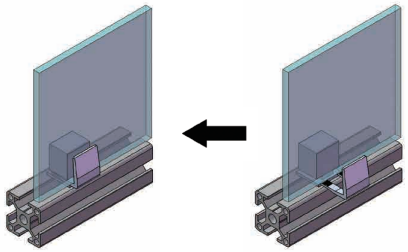
Ordering Example — Part Number: HCBS8

■How to Mount Panel Clamps

①Connection with Extrusion
Easy installation by inserting the T-shaped stopping part into the slot and turning 90.

②Connection with Panel
As shown on the right, insert a panel into P part and push the moving part against the panel. Hole machining on the panel is not necessary.

Example



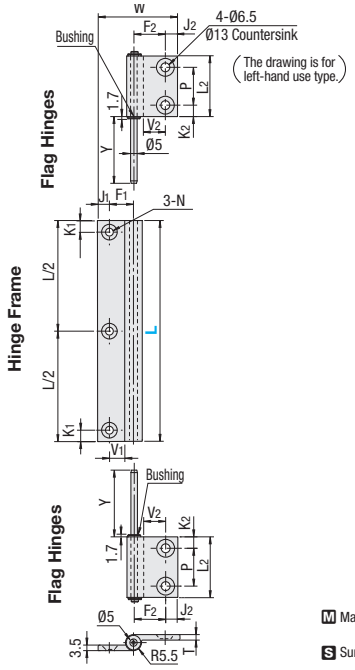
Aluminum Long Hinges

■Aluminum Long Hinges



RoHS 10

HHPV
(Left/Right Reversed Common)



M Material: EN AW-6063-T5 Equiv.
Bushing: Polyacetal (White)
S Surface Treatment: Anodize*

* No anodizing on ends of L specified part.

Part Number		Hinge Frame L	Allowable Load		W	L_2	P	K_1	K_2	J_1	J_2	F_1	F_2	V_1	V_2	N		T	Y	Screw / Nut (L Dimensions Less than 500mm)				Unit Price/m	2 Flag Hinges / 3 Counter-sinks
Type	No.	1mm Increment	kg	N												Through	Countersink			Screw	Quantity	Nut	Quantity	1 ~ 20 pc(s).	
HHPV	6-5	100~1000	10	98	55	40	25	7.5	7.5	8	10	16	21	10.5	15.5	5.5	11	3.5	43.5	Flat Head Screw 6-10	4	HNTT6-6	4		
																				Flat Head Screw 5-8	3	HNTT5-5	3		
	6-6				62															Flat Head Screw 6-10	7	HNTT6-6	7		
	8-6				71	50	30	8	10	10	14	21	26	15.5	20.5	6.8	13	4.5	38.5	Flat Head Screw 6-15	4	HNTT8-6	4		
																				Flat Head Screw 6-10	3	HNTT6-6	3		
	845-6										11.5		28.5		23					Flat Head Screw 6-15	4	HNTT8-6	4		
																				Flat Head Screw 6-10	3	HNTT6-6	3		

Ordering Example

Part Number	-	L
HHPV6-5	-	200

Example



Alterations

Part Number	-	L	-	(SET, SST)
HHPV8-6	-	250	-	SET

Alteration	Code	Spec.	Hinge	No.
Applicable Screw and Nut Set	SET	Applicable screws and nuts come in a set.	HHPV	6-5
				6-6
	SST (Stainless Steel)	When SST is specified, screws and nuts will be in stainless steel.		8-6
				845-6

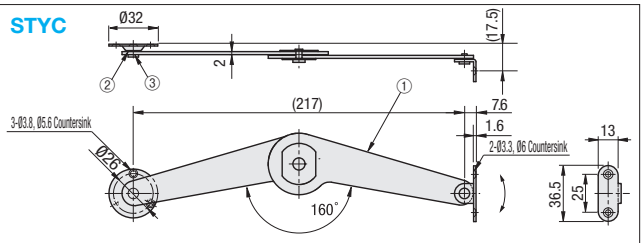
Locking Lid Stays / Rotary Door Stays / Spring Loaded Door Stays

■Locking Lid Stays



RoHS 10

STYC

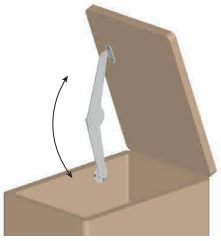


The latches click when open at 160° before being fixed by the catch mechanism.
The catch mechanism can be released when firmly pushed at the ends of the latches (e.g. with hands).
The latches do not have a locking and fixing mechanism.
The drawing is for left-hand use.

No.	Part Name	M Material	S Surface Treatment
①	Main Body	Steel	Chrome Plating
②	Washer	Polyamide	-
③	Rivet	Brass	Chrome Plating

Example

• STYC



Part Number Type	Right and Left	Mass (g)	Unit Price
STYC	L (For Left Side)	125	
	R (For Right Side)		

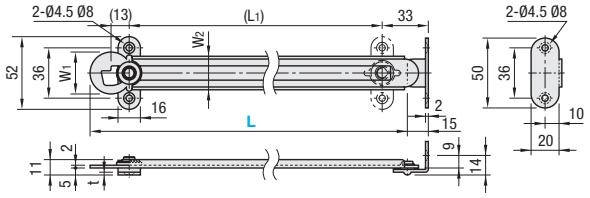
Ordering Example — Part Number: STYCR

■Rotary Door Stays



RoHS 10

STYR



The drawing is for right-hand use.

M Material: EN 1.4301 Equiv. Finish: Electrolytic Polishing

Example

① Stopper in Operation ② Stopper Switched ③ Stopper Released



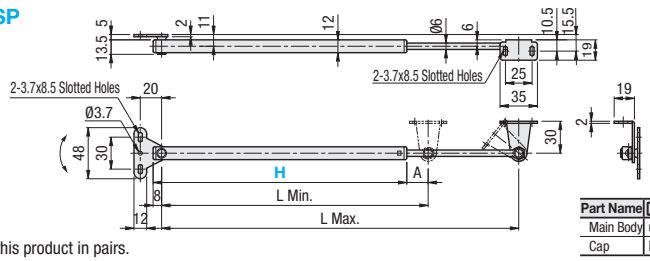
Part Number Type	Right and Left	L	(L1)	W1	W2	t	Mass (g)	Unit Price
STYR	L (For Left Side) R (For Right Side)	150	105	28	23	1.5	75	
	L (For Left Side) R (For Right Side)	198	153	28	23	1.5	85	
	L (For Left Side) R (For Right Side)	277	231	30	24	2	120	

Ordering Example — Part Number: STYRL150

■Spring Loaded Door Stays



STYSP



Use this product in pairs.

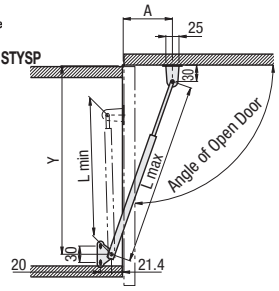
Part Name	M Material	Finish
Main Body	EN 1.4301 Equiv.	Brushed
Cap	Polyamide	-

Part Number Type	H	Max. Length L max.	Min. Length L min.	Stroke	A	Mass (g)	Reactive Force of Stay N (kgf) L Max	Reactive Force of Stay N (kgf) L Min	Unit Price
STYSP	170	222	172	50	10	145	31.4 (3.2)	68.6 (7.0)	
	238	335	250	85	20	185	37.2 (3.8)	83.3 (8.5)	
	269	380	280	100	19	205	35.3 (3.6)	83.3 (8.5)	

The main body and the bracket can be used on both right and left sides.

Example

App. Example: STYSP



■Features

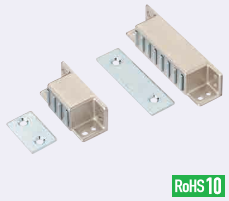
When the door/lid is opened or closed, it will automatically stop at the preset position by the action of the spring.
An extra stroke or action is not required.
The mounting example shows the distance from the rotation center of hinge.
When the door/lid is closed, L min dimension must be larger than the minimum dimension of contraction. (If L min is smaller, hinges or stays might be damaged.)

Ordering Example — Part Number: STYSP170

Type	Mass of Door (kg)	Angle of Open Door	L max	A	Y
STYSP170 (Two Latches, Right and Left)	2.4 or Less	90	222	58	235.9
	2.6 or Less	85		63	240.4
	3.0 or Less	75		75	251.5
STYSP238 (Two Latches, Right and Left)	2.9 or Less	90	335	90	334.5
	3.1 or Less	85		97	351.4
	3.6 or Less	75		115	368.1
STYSP269 (Two Latches, Right and Left)	3.1 or Less	90	380	103	386.9
	3.3 or Less	85		111	394.6
	3.9 or Less	75		131	413.7

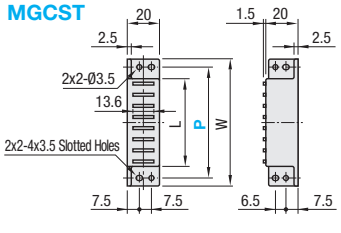
High Strength Magnetic Catches / Magnetic Catches

■High Strength Magnetic Catches



RoHS 10

MGCST



Part Name	Material	Surface Treatment
Main Body	Zinc Alloy	Nickel Plating
Catch Plate	EN 1.0330 Equiv.	Trivalent Chromate
Magnet	Ferrite	-

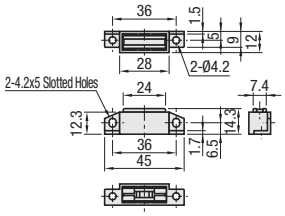
Part Number Type	P	W	L	A	S	Retention Force (kgf)	Mass (g)	Unit Price 1 ~ 9 pc (s).	Volume Discount Rate 10~49	50~200
MGCST	30	40	20	22	12	3	56			
	40	50	27	29	18	7	74			
	50	60	41	43	27	11	110			
	70	80	55	60	40	14	140			

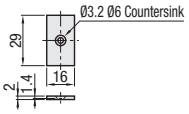
Ordering Example — Part Number: MGCST30

■Magnetic Catches Magnetic Force Selectable



MGCEJ





■Features

Magnetic catches enabling a retaining force to be selected with the same mounting pitch.

Part Name	Material	Surface Treatment
Main Body	Polypropylene	-
Catch Plate	EN 1.0330 Equiv.	Trivalent Chromate

💡10 pcs. per package. Order quantity should be noted.

Part Number Type	No.	Retention Force (kgf)	Mass (g)	Unit Price 1 ~ 9 pkg (s).	Volume Discount Rate 10~19	20~200
MGCEJ	1	1.4	10			
	2	3.4	10			
	3	8	10			

💡10 pcs. per package

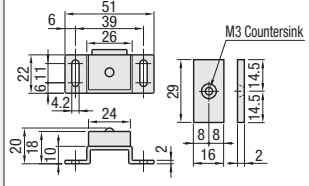
Ordering Example — Part Number: MGCEJ1

■Magnetic Catches



RoHS 10

HMEN-T
HMEN-T2



Part Name	Material	Surface Treatment
Housing	EN 1.4301 Equiv.	Dark Brown Paint
Magnet	Ferrite	-
Plate	EN 1.0330 Equiv.	Chrome Plating

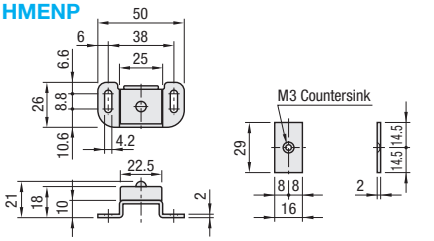
Part Number	Retention Force (kgf)	Mass (g)	Unit Price 1 ~ 9 pc (s).	Volume Discount Rate 10~50
HMEN-T	3	41		
HMEN-T2	1.5	41		

Ordering Example — Part Number: HMEN-T, HMENP

■Magnetic Catches



HMENP

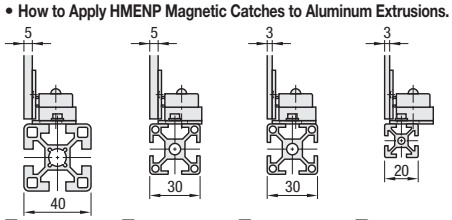


Part Name	Material	Surface Treatment
Housing	EN 1.4301 Equiv.	Dark Brown Paint
Magnet	Ferrite	-
Plate	EN 1.0330 Equiv.	Trivalent Chromate

Part Number	Holding Force (kgf)	Mass (g)	Unit Price 1 ~ 9 pc (s).	Volume Discount Rate 10~50
HMENP	2.8	39		

Example

• How to Apply HMENP Magnetic Catches to Aluminum Extrusions.



■When mounting a 5mm-thick panel to 40-Square Type.
■When mounting a 5mm-thick panel to 30-Square Type.
■When mounting a 3mm-thick panel to 30-Square Type.
■When mounting a 3mm-thick panel to 20-Square Type.

UNIVERSITÉ CATHOLIQUE DE LOUVAIN
École polytechnique de Louvain
Rue Archimède, 1 bte L6.11.01, 1348 Louvain-la-Neuve, Belgique | **www.uclouvain.be/epl**